THE UNIVERSITY
of EDINBURGH

River dynamics in the Himalayan foreland basin

Elizabeth H. Dingle

THE UNIVERSITY
of EDINBURGH

Thesis submitted in fulfillment of
the requirements for the degree of
Doctor of Philosophy
to the
University of Edinburgh — 2018

Declaration

I declare that this thesis has been composed solely by myself and that it has not been submitted, either in whole or in part, in any previous application for a degree. Except where otherwise acknowledged, the work presented is entirely my own.

Elizabeth H. Dingle

May 2018

Abstract

Rivers sourced in the Himalayan mountains support more than 10% of the global population, where the majority of these people live downstream of the mountain front on the alluvial Indo-Gangetic Plain. Many of these rivers however, are also the source of devastating floods. The tendency of these rivers to flood is directly related to their large-scale morphology. In general, rivers that drain the east Indo-Gangetic Plain have channels that are perched at a higher elevation relative to their floodplain, leading to more frequent channel avulsion and flooding. In contrast, those further west have channels that are incised into the floodplain and are historically less prone to flooding. Understanding the controls on these contrasting river forms is fundamental to determining the sensitivity of these systems to projected climate change and the growing water resource demands across the Plain.

This thesis examines controls on river morphology across the central portion of the Indo-Gangetic Plain drained by the Ganga River (the Ganga Plain). Specifically, the relative roles of basin subsidence, sediment grain size and sediment flux have been explored in the context of large-scale alluvial river morphology over a range of timescales. Furthermore, this thesis has developed and tested techniques that can be utilised to help quantify these variables at catchment-wide scales. This analysis has been achieved through combining new sediment grain size, pebble

lithology and cosmogenic radionuclide data with quantitative topographic and sedimentological analysis of the Ganga Plain.

In the first part of this thesis, I examine the contrast in channel morphology between the east and west Ganga Plain. Using topographic analysis, basin subsidence rates and sediment grain size data, I propose that higher subsidence rates in the east Ganga Plain are responsible for a deeper basin, with perched low-gradient rivers systems that are relatively insensitive to climatically driven changes in base-level. In contrast, lower basin subsidence rates in the west are associated with a shallower basin with entrenched river systems that are capable of recording climatically induced lowering of river base-level during the Holocene.

Through an analysis of fan geometry, sediment grain size and lithology, I then demonstrate that gravel flux from rivers draining the central Himalaya with contributing areas spanning three orders of magnitude is approximately constant. I show that the abrasion of gravel during fluvial transport can explain this observation, where gravel sourced from more than 100 km upstream is converted into sand by the time it reaches the Plain. I attribute the over-representation of quartzitic pebble lithologies in the Plain (relative to the proportion of the upstream catchment area likely to contribute quartzite pebbles) to the selective abrasion of weaker lithologies during transport in the mountainous catchment. This process places an upper limit on the amount of coarse sediment exported into the Indo-Gangetic Plain.

Finally, I consider the use of cosmogenic ^{10}Be derived erosion rates as a method to generate sediment flux estimates over timescales of 10^2-10^4 years. Cosmogenic radionuclide samples from modern channel and independently dated Holocene terrace and flood deposits in the Ganga River reveal a degree of natural variability in ^{10}Be concentrations close to the mountain front. This is explored using a numerical analysis of processes which are likely to drive variability in

catchment-averaged ^{10}Be concentrations. I propose that the observed variability is explained by the nature of stochastic inputs of sediment (e.g. the dominant erosional process, surface production rates, depth of landsliding, degree of mixing), and secondly, by the evacuation timescales of individual sediment deposits which buffers their impact on catchment-averaged concentrations. In landscapes dominated by high topographic relief, spatially variable climate and multiple geomorphic process domains, the use of ^{10}Be concentrations to generate sediment flux estimates may not be truly representative. The analysis presented here suggests that comparable mean catchment-averaged ^{10}Be concentrations can be derived through different erosional processes. For a given ^{10}Be concentration, volumetric sediment flux estimates may therefore differ.

Lay Summary

Rivers sourced in the Himalayan mountains support more than 10% of the global population, where the majority of these people live downstream of the mountains on the Indo-Gangetic Plain. Many of these rivers however, are also the source of devastating floods. The tendency of these rivers to flood is directly related to their large-scale morphology. In general, rivers that drain the east Indo-Gangetic Plain have channels that lie at a similar or slightly higher elevation relative to their floodplain, leading to more frequent channel switching and flooding. In contrast, rivers further west have channels that are incised into the floodplain and are historically more stable and less prone to flooding. Understanding the controls on these contrasting river forms is fundamental to determining the sensitivity of these systems to projected climate change and the growing water resource demands across the Plain.

In the first part of this thesis, I examine the contrast in dynamics and characteristics between rivers in the east and west Ganga Plain. Using topographic analysis, basin subsidence and sediment grain size data I propose that higher subsidence rates in the east Ganga Plain are responsible for low-gradient rivers systems that are relatively insensitive to climatically driven changes in water and sediment discharges from the Himalayan mountains. In contrast, lower basin subsidence rates in the west are associated with incised river systems that are capable of recording

climatically driven changes in channel gradient, formed by changing water and sediment discharges.

I then demonstrate that gravel flux from rivers draining the central Himalaya with contributing areas spanning three orders of magnitude is approximately constant. I show that the mechanical breakdown (abrasion) of gravel during fluvial transport can explain this observation, where gravel sourced from more than 100 km upstream is converted into sand by the time it reaches the Plain. I attribute the over-representation of quartzitic (very hard) pebble lithologies in the Plain (relative to the proportion of the upstream catchment area likely to contribute quartzite pebbles) to the selective abrasion of weaker lithologies during transport in the mountainous catchment. This process places an upper limit on the amount of coarse sediment exported into the Indo-Gangetic Plain.

Finally, I consider the use of cosmogenic radionuclide derived erosion rates as a method to generate sediment flux estimates over timescales of 10^2-10^4 years. The concentration of cosmogenic isotopes (such as ^{10}Be) recorded in modern river sediments reflects the time taken since the isotope was formed (by cosmic rays interacting with stable isotopes within the upper 1-2 m of the Earth's surface), and for that sediment to then be eroded from the landscape and transported to the sampling location. These erosion rates can then be converted into sediment flux estimates. Cosmogenic ^{10}Be samples from modern channel and independently dated Holocene terrace and flood deposits in the Ganga River reveal a degree of natural variability in ^{10}Be concentrations close to the mountain front. This degree of temporal variability is explained by the nature of the inputs of sediment, and by the evacuation timescales of sediment out of the catchment. These timescales buffer the impact of stochastic sediment inputs on catchment-averaged concentrations. I suggest that in landscapes dominated by high topographic relief, spatially variable climate and multiple geomorphic process domains, the use of ^{10}Be concentrations to generate sediment flux estimates may not be truly

representative. This is because comparable mean catchment ^{10}Be concentrations can be derived through dramatically different erosional processes which can generate much higher volumetric sediment fluxes than those inferred from the cosmogenic isotope concentration and erosion rate.

Acknowledgements

Wow what a ride! It might have taken me a little longer than most, but the past four and a bit years have flown by. The fact that I have enjoyed my PhD so much is a testament to the help, support and encouragement I have received from far too many people to mention here.

First and foremost, I would like to thank my supervisors Hugh Sinclair and Mikael Attal for their unwavering encouragement, 'honest' feedback and infectious enthusiasm both in Edinburgh and out in the field. When I started my PhD I was slightly unsure about returning to the Indo-Gangetic Plain, but it's been seven trips now and I've enjoyed every second (well, nearly) and much of this is down to Hugh and Mikael. I could not have asked for better guidance or company through my PhD, or indeed, the start of my research career (hopefully anyway!). I'd also like to thank Simon Mudd, the missing third of the Edinbugh LSD trio, who has always given me encouragement and feedback on various ideas and presentations as well as equipping me with command line based knowledge I would never have thought possible four years ago.

I've seen many people come and go from the Lower Lewis office during my PhD and I'd like to thank them ALL for putting up with my constant chatter, but there are a number of people who really deserve a special mention. First I'd like to thank my pal Fiona Clubb for her help, idea bouncing, friendship, for

letting me tag along on fieldwork and for letting me drag her out running in the dark (#WomenInScience). A big thanks also to Stuart, Dave and Boris for their coding (and often geology-related) help and to Baynes for general geomorphology idea bouncing and poor chat. Thanks to the rest of the 2013ish cohort - Donnie (whey) for his persistent shuffling, Luca for our shared love of green bananas and the Italian language, as well as John, Damon, Penny and the General with whom I've shared numerous drinks, squash/Bears games, grim bike rides (Delf) and trips out to the hills to help keep me sane. I can't forget to thank Alexis for helping me develop my loose tea addiction as well. You guys rock.

Most of my fieldwork wouldn't have been possible without the many field assistants and general help I've had. A special thank you to Jamie, DJ, Konark and Fred for being such brilliant geologists and great company. I also need to thank a number of people for all of the non-PhD fun I've had over the past four years which has helped keep my brain healthy, whether it's been biking, yoga, walking, climbing, sailing or just popping in for a cup of tea (namely the southside six, Jo and Maggie).

And last but not least, I almost certainly wouldn't have even got here without the love and support of my family and Ewan. Thank you for having an interest in what I'm doing (or at least pretending), your advice on how not to get foot-rot during the monsoon (cheers Dad) and for helping me ride through the tough times relatively unscathed.

Contents

List of Tables

List of Figures

Chapter 1

Introduction

1.1 Overview

Major river basins of the Himalayan mountains are often described as the 'water towers of Asia', irrigating the vast Indo-Gangetic Plain immediately downstream of the mountain front. These major river networks support approximately 10% of the global population who live on the Plain, yet the morphology and dynamics of rivers traversing it have traditionally received much less attention in the literature relative to their upstream headwaters within the Himalayan mountains. Perhaps one of the earliest recognitions of the importance of the morphology of the Indo-Gangetic Plain was noted by Arthur Geddes in 1960 [Geddes, 1960]:

'As the chief habitat of mankind at the dawn of civilisation in western, southern and eastern Asia, alluvial plains are of profound significance; while, with regard to re-development in the future, the extreme delicacy of the deposition and modelling brings difficulties in their irrigation if this is to prove beneficial, not harmful, to the intensive cultivation of their gently sloping surfaces associated with varied soils

and a changing water-table. To Europeans accustomed to their hilly, island-girt peninsula, the apparent flatness of the plains has made them extremely difficult to maps with accuracy. Partly in consequence, plains have tended to be almost ignored in geomorphology, instead of providing a central theme for physical study in world geography. Their populations of hundreds of millions, the unique part played by them in world civilization through history and protohistory, the newly acquired independence of their peoples and, as in the case of India-Pakistan, the frontier problems of water distribution arising from partition boundaries drawn across the plains: these are but a few of the elements that indicate the importance of alluvial morphology'. (pp. 253)

These river systems provide the fresh water and nutrient-rich soils which are essential for life across the Plain, but a number these rivers are also the source of devastating floods. The tendency for these rivers to flood is directly linked to their large-scale morphology. The Ganga Plain represents the portion of the Indo-Gangetic Plain drained by tributaries of the Ganga River, and is a large proportion of the current foreland basin to the Himalaya (Figure 1.1). The large-scale morphology of rivers across the Ganga Plain directly relates to factors such as the tectonics, climate and lithology of the upstream catchment (within the mountain range) in addition to factors associated with the actively subsiding foreland basin beneath the Plain, such as the spatial distribution and rates of subsidence. Understanding the interaction of these different processes across the timescales over which their impact is most significant is key to deciphering how the morphologies of these fluvial systems evolve across the Ganga Plain. Key drivers of river morphology in the Plain will control how sensitive the dynamics (such as flooding susceptibility) of these rivers are to projected climate-driven changes in monsoon intensity, reduced summer glacial melt-water discharges, and anthropogenic development (such as the construction of dams for hydro-power

and irrigation) across the Himalaya and its foreland basin . Systematic variations

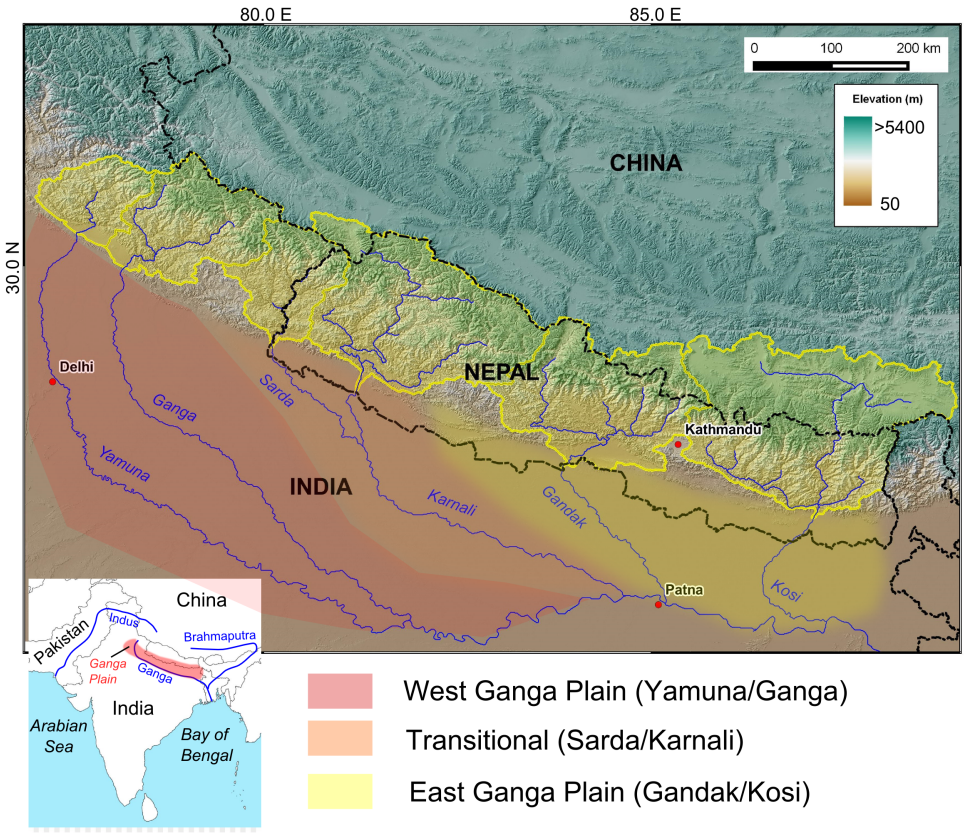

Figure 1.1: Overview of the Ganga basin and major tributaries. Catchment areas of each tributary upstream of the Himalayan mountain front are shaded and outlined in yellow. The west and east (and transitional) Ganga Plain are also shaded as shown on the key and labelled with the appropriate rivers at the bottom of the figure. A schematic of the wider Indus, Ganga and Brahmaputra River systems is also shown on the bottom left of the figure, where the Ganga Plain is shaded in red.

in the morphology of these river systems are recognised across the extent of the Ganga foreland basin [Sinha *et al.*, 2005]. Rivers of the east Ganga Plain are characterised by shallow aggrading channels that frequently flood and laterally migrate, whilst those in the west are characterised by degrading systems with incised channels and extensive areas of badland topography [Tandon *et al.*, 2006]. In the east Ganga Plain, numerous channel avulsions and random switching of the loci of fan lobe aggradation has resulted in a net westward migration of

>113 km of the Kosi River over the surface of its mega-fan during the last two centuries [Wells and Dorr, 1987; Chakraborty *et al.*, 2010]. During 2008, a single channel avulsion event resulted in a temporary eastward shift of the Kosi River by tens of kilometres where the channel breached its eastern levee resulting in extensive flooding [Chakraborty *et al.*, 2010; Sinha *et al.*, 2005, 2013, 2014b]. Palaeochannels are well preserved across much of the surface of the Kosi and Gandak fans [Sinha *et al.*, 2014a], reflecting the dynamic and mobile nature of these systems. In the west Ganga Plain, the Ganga River is described as a braided channel within a narrow incised valley with exposed cliffs extending 15-30 m above the modern channel in parts [Shukla *et al.*, 2001; Gibling *et al.*, 2005; Shukla *et al.*, 2012]. Numerous phases of incision and aggradation are documented within both the Yamuna and Ganga valleys where distinct geomorphic surfaces and facies associations are preserved in exposed valley walls [Shukla *et al.*, 2001; Gibling *et al.*, 2005; Tandon *et al.*, 2006].

The starting point of this thesis was to examine the controls behind these contrasting river morphologies across the Ganga Plain, which has long been recognised within the literature [Sinha *et al.*, 2005; Tandon *et al.*, 2006]. However, one of the main challenges when determining longer-term (millennial) controls on fluvial morphologies is to differentiate signals driven by shorter-term stochastic variations in climate or tectonic activity in the upstream catchment [Benda and Dunne, 1997a; Tucker and Slingerland, 1997; Leeder *et al.*, 1998]. Numerous modelling studies have simulated the effects of varying parameters such as sediment flux and basin subsidence over different time scales relative to the equilibrium time period of the basin, defined as the period required for streams within the basin to attain a steady-state profile [Paola *et al.*, 1992a; Heller and Paola, 1996; Robinson and Slingerland, 1998; Marr *et al.*, 2000]. In a system as large as the Ganga River, potential short-term (sub-millennial) controls on sediment flux and grain size could be linked to climatic changes in precipitation patterns, glacial discharge

and extreme storm events or earthquakes. In contrast, subsidence rates, which are controlled by topographic loading and the flexural response and subduction velocity of the underlying lithosphere [Sinclair and Naylor, 2012] are likely to vary at much longer millennial time scales. The main drivers of this thesis have been to 1) consider the role of basin subsidence on the longer term development and shaping of alluvial deposits in the foreland basin, 2) understand variations in modern sediment fluxes and sediment grain sizes delivered to the Plain, and 3) to understand how these processes interact to produce different channel morphologies and dynamics in one of the planet's largest river systems.

1.2 Approach

Many of the arguments presented in this thesis are built on new field-based evidence, derived from five of the main tributaries of the Ganga River (the Yamuna, Ganga, Sharda, Gandak and Kosi rivers). The portion of the foreland basin which the Ganga River drains (and henceforth, the Ganga Plain) presents the ideal natural laboratory to examine controls on large scale river morphology. Fieldwork across the Ganga Plain was built of three components; sediment grain size, gravel lithology and cosmogenic radionuclide data. Despite the large size of the basin, much of the work focuses in a relatively short reach along each river between ∼50 km upstream of the mountain front and the gravel-sand transition (∼10-40 km downstream of the mountain front). Here, the gravel-sand transition is defined as the point at which the channel bed composition switched from gravel-dominated, to sand-dominated. Further details on the study location are provided below. Using data from rivers of the Ganga Plain, a number of questions have been addressed to better understand the processes controlling the large-scale morphology

of rivers in foreland basins:

1. Can long-term rates of basin subsidence influence the large-scale morphology of modern rivers?

2. Which processes control the grain size of sediment exported into foreland basins, and does this influence downstream river morphology?

3. How can we better quantify the sediment flux from large mountainous catchments into foreland basins?

Below, I present a broad introduction to each of these three topics and outline the scope of the central chapters of this thesis.

1.3 Theoretical background

1.3.1 Subsidence and grain size

Sediment accumulation rates in subsiding foreland basins are driven by both the incoming sediment flux and basin subsidence rate [Paola *et al.*, 1992a; Allen *et al.*, 2013b]. Foreland basin sediment fill is thickest directly adjacent to or even partially beneath the associated thrust belt. The majority of this sediment is derived from erosion of the overlying or upstream fold-thrust belt [Jordan, 1981]. In general, vertical rates of sediment accumulation reduce with distance from the thrust belt. Along strike of the Himalayan thrust belt, rates of basin

subsidence are not uniform which can influence patterns of sediment deposition [e.g. Yin, 2006] across the Himalayan foreland basin. These spatially variable patterns in basin subsidence rates may alter vertical sedimentation rates, for a given sediment flux. Furthermore, the longer term preservation of sediment and development of stratigraphy in foreland basins depends on the spatial distribution of tectonic subsidence, which generates the total accommodation space available to deposit sediment within [Robinson and Slingerland, 1998; Marr *et al.*, 2000; Duller *et al.*, 2010; Whittaker *et al.*, 2011]. The quantity (sediment flux) and grain size distribution of sediment supplied to the basin, is also key in the preservation of material deposited within the basin.

Processes which are likely to influence sedimentation within foreland basins may also have a wider impact on fluvial systems draining the surface of the basin. Experimental modelling supports a positive correlation between sedimentation rate and avulsion frequency [Bryant *et al.*, 1995; Ashworth *et al.*, 2004], where both sediment flux and basin subsidence rates have independently been highlighted as principle drivers of vertical sedimentation rates in numerical experiments [Paola *et al.*, 1992a; Heller and Paola, 1992; Robinson and Slingerland, 1998]. Rivers in the east Ganga Plain, such as the Kosi River which discharges into Bihar State, have a long history of channel avulsion and flooding [Wells and Dorr, 1987; Chakraborty *et al.*, 2010]. The elevation of rivers such as the Kosi relative to their surrounding floodplain strongly influences their tendency to avulse [Slingerland and Smith, 2004]. Super-elevated channel beds sit higher than the adjacent floodplain, creating gradient advantages between the channel and topographic low points in the immediate floodplain [Jerolmack and Paola, 2007; Hajek and Edmonds, 2014; Ganti *et al.*, 2014]. Rivers will typically avulse down these steeper pathways of descent [Jerolmack and Paola, 2007]. Channel avulsion occurs when a triggering event such as a flood peak, sediment influx or tectonic uplift, forces a river across a stability threshold, also known as an avulsion threshold [Jones

and Schumm, 1999; Sinha *et al.*, 2014b]. Processes that may bring a river closer to their avulsion threshold are driven by those that alter the gradient of slope between the channel and the surrounding floodplain, or by factors that reduce the capacity of the existing channel [Jones and Schumm, 1999; Edmonds *et al.*, 2009]. Sedimentation rates will impact how quickly a channel bed will aggrade to an elevation at which channel avulsion is more likely [Ashworth *et al.*, 2004]. Patterns of aggradation in the Ganga Plain are likely to represent a more complicated balance of vertical sedimentation rate and basin subsidence rate, but may drive the development of certain morphological characteristics of modern fluvial systems.

In general, there is much uncertainty regarding how subsidence patterns control the geomorphological character or longitudinal profiles of rivers, such as those (transverse rivers) draining the Ganga Plain. Variations in sediment flux, input grain size distribution and basin subsidence rates have been predicted to be the most important mechanisms controlling downstream sediment fining trends over short (sub-millennial) and long (millennial) time scales (Fig. 1.2), respectively [Paola *et al.*, 1992a; Robinson and Slingerland, 1998; Marr *et al.*, 2000; Duller *et al.*, 2010]. Where higher amplitude subsidence regimes exist, greater rates of downstream grain size fining would be expected [Duller *et al.*, 2010]. Under the assumption that patterns and characteristics of sediment deposited within sedimentary basins are a function of tectonic subsidence, sediment flux and grain size, reconstructions of spatial distribution of subsidence, the initial grain size supply and sediment flux to the basin have been made (from grain size data collected from ancient fluvial successions) within the Spanish Pyrenees [Duller *et al.*, 2010; Whittaker *et al.*, 2011]. It therefore seems reasonable to expect downstream grain size fining rates to reflect the underlying basin subsidence rate. To determine basin subsidence histories across the Indo-Gangetic Plain, multiple well documented wells with good stratigraphic resolution are required [Allen and

Allen, 2013]. However, these types of data are not widely or freely available for this region. Patterns of sediment fining may therefore provide a useful tool in qualitatively assessing spatial patterns of basin subsidence rate.

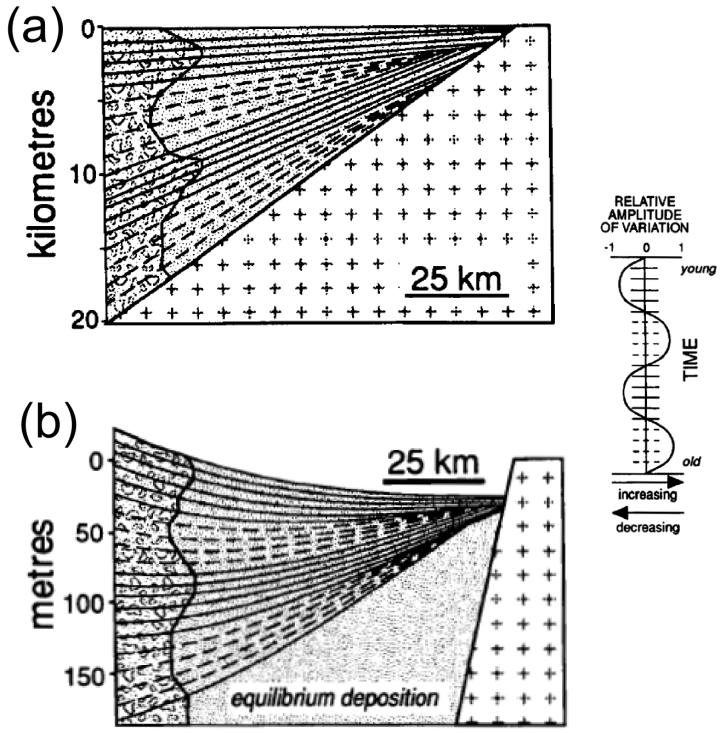

Figure 1.2: Cross-sections from hypothetical basins showing the variations in grain size in response to slow (a) and rapid (b) variations in basin subsidence rates (modified from Figure 2 and Figure 4 in Paola *et al.*, 1992a) derived from a coupled sediment-transport and grain size partitioning model. The sinusoidal form of the variation in subsidence rate is shown to the right of both sub-figures. The direction of transport is from left to right. In (a), the thin dashed and solid lines are isochrons drawn every 10^6 years, and every 10^4 years in (b). Gravel is shown in dark grey. The dashed lines in the hypothetical basins correspond to maxima in the modelled subsidence rates. The position of the gravel front is shown to be more sensitive to slower Myr scale subsidence forcing.

1.3.2 Sediment grain size and the gravel-sand transition

The role of sediment grain size in controlling large-scale river morphology is perhaps less well understood. At present, there are very few published data on modern fluvial grain size distributions across and downstream of the Himalayan mountain front. As such, there remains a notable gap in our understanding of how sediment grain sizes vary as a function of upstream processes and the possible impact on downstream channel morphology. Early qualitative observations extend back to the first mapping studies of the Indo-Gangetic Plain published in 1960 [Geddes, 1960], which suggested that the surface of the Plain is dominated by fine sediment grain sizes:

'Beyond the Himalaya foot and its five- to ten-mile belt of pebbly Bhabar [cobbles and pebbles]*, the Plain may be crossed without a single stone being seen'*(pp. 260)

Surprisingly little quantitative work on the grain size distribution of these river systems has subsequently occurred. Modern channel bed grain size analysis has been undertaken in detail for a number of small river systems in the east Ganga Plain [Dubille and Lavé, 2015], but there is a lack of comparable studies across major river systems of the Ganga Plain. Sediment grain size is commonly recognised as being strongly related to different river morphologies [e.g. Leopold, 1992; Montgomery and Buffington, 1997; Dade, 2000]. Morphological analysis on these small river systems in the east Ganga Plain suggested that channel bed gradients were responding to river transport capacity and sediment size distribution and supply rates [Dubille and Lavé, 2015]. Changes in channel planform, from braided to meandering, were observed across the gravel-sand transitions in these systems. These planform changes were attributed to the rapid reduction in bed grain size associated with the transition, suggesting that

an understanding of how sediment grain sizes vary with distance away from the mountain front (i.e. downstream fining rates and the position of the gravel-sand transition) are also important.

The degree of channel braiding is also influenced by channel slope, water discharge and also the availability of coarser bed load sediment relative to finer suspended sediment [Friend and Sinha, 1993]. Channel bed aggradation, initiated through a reduction in water discharge or increase in bed load sediment supply, may promote channel braiding. This in turn may also increase the likelihood of channel avulsion, if the channel aggrades to a position where the bed becomes super-elevated above the adjacent floodplain [Ashworth *et al.*, 2004; Slingerland and Smith, 2004; Jerolmack and Paola, 2007; Jerolmack and Mohrig, 2007; Hajek and Edmonds, 2014; Sinha *et al.*, 2014b]. It is therefore possible that channel morphology and pattern across the Ganga Plain may reflect spatial differences in sediment grain size delivered out of the mountain range. Factors that are likely to influence sediment grain size at the mountain front include the grain sizes represented in the sediment source material. Attal and Lavé [2006] observed downstream grain size coarsening on a stretch of the Marsyandi River (Nepal) as a result of different sediment sources and source grain size distributions (e.g. landslide and moraine material). It was suggested that sediment source exerted a major influence on the downstream evolution of sediment characteristics and bed load ratio, which in turn, could also influence river profile development through controlling bedrock incision rates [Attal and Lavé, 2006].

In general, the sediment grain size of river beds systematically decreases downstream [Sternberg, 1875]. Existing studies often attribute the downstream reduction of sediment grain sizes to size-selective sediment sorting, the deposition of suspended sediment from the water column, and the mechanical break-down (abrasion) of gravel [Paola *et al.*, 1992b,a; Wathen *et al.*, 1995; Ferguson *et al.*, 1996; Seal *et al.*, 1997; Rice and Church, 2001; Ferguson, 2003; Attal and Lavé,

2006; Fedele and Paola, 2007; Duller *et al.*, 2010; Venditti *et al.*, 2015; Lamb and Venditti, 2016]. Lateral inputs of sediment from tributaries or mass wasting deposits may interrupt this signal in some instances. For example, downstream grain size coarsening was observed on a reach of the Marsyandi River (Nepal) and was attributed to different sediment sources and source grain size distributions (e.g. landslide and moraine material) [Attal and Lavé, 2006]. Sediment sources may therefore exert a major influence on the downstream evolution of sediment characteristics [Attal and Lavé, 2006]. Inputs of sediment from tributaries are also likely to impact the grain size distributions of the parent channel, although downstream of the Himalayan mountain front these inputs are likely to be less significant where the relative size and flux of the foothill-fed tributaries joining the main trans-Himalayan rivers is small. The relative importance of processes such as selective transport and clast abrasion as sediment is transported to the mountain front and out into the Ganga Plain will also strongly dictate the grain size of sediment exported from the Himalaya.

Grain size across the gravel-sand transition

The gravel-sand transition is characterised by a rapid reduction in sediment grain size over a very short distance relative to the full length of the river [Sambrook Smith and Ferguson, 1995] (Fig. 1.3). In many instances it represents a longitudinal zone of a few hundred metres to several kilometres where the channel bed is predominantly sand, but large patches of gravels persist [Dubille and Lavé, 2015; Venditti *et al.*, 2015]. In a few instances, the length of the gravel-sand transition has been documented to cover more significant distances in excess of 175 km [Singer, 2008]. In general, the extent of these gravel patches reduces downstream. It is unique in that it is the only abrupt transition between different grain size fractions that occurs along a river system. The gravel-sand transition also represents a threshold between different types of river that exhibit

different dynamics and ecological habitats [Sambrook Smith and Ferguson, 1995]. Upstream of the transition, river beds and banks are composed of gravel and are typically only unstable at high flows, which can result in bank erosion and channel migration. In contrast, downstream of the gravel-sand transition the channel bed, banks and floodplain are composed of sand-sized and finer sediments. These channels are generally lower energy environments than gravel bed channels, but can still be highly mobile when transporting large sediment loads. The rate at which sand is deposited downstream of the transition contributes to elevated flood risk because higher deposition rates lead to greater rates of channel migration and switching [Ashworth *et al.*, 2004]. The formation and stability of the gravel-sand transition remains an important but not entirely understood phenomenon. Much of the early literature on downstream sediment fining focused on the role

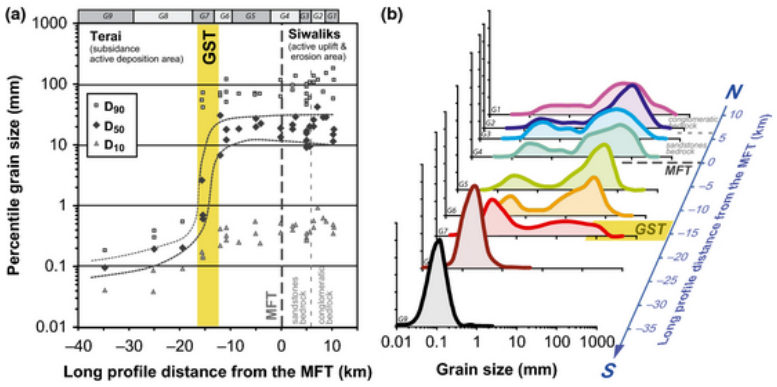

Figure 1.3: Grain size measurements in gravel and sand bars along the Churre River in Nepal (Figure 7 from Dubille and Lavé, 2015). Note the rapid reduction in all grain size fractions (D_{10}, D_{50} and D_{90}) across the gravel-sand transition (shown in yellow). In part (a), the Main Frontal Thrust (MFT) is equivalent to the Himalayan mountain front, and the direction of flow is right to left.

of sediment abrasion [e.g. Sternberg, 1875; Yatsu, 1955; Parker, 1991]. However, experiments examining abrasion rates of sediment showed that the magnitude of sediment fining across the gravel-sand transition is too great to be caused solely by abrasion. As such, the development of the gravel-sand transition has more commonly been attributed to size-selective sorting [e.g. Paola *et al.*, 1992b;

Wathen *et al.*, 1995; Ferguson *et al.*, 1996; Seal *et al.*, 1997; Parker and Cui, 1998]. More recently, interest in the gravel-sand transition has surged due to recognition that the transition may be sensitive to broader-scale environmental change. Changes in water and sediment discharge resulting from changes in climate (e.g. changes in glacial meltwater discharges, patterns of extreme weather) and anthropogenic activity (e.g. hydropower scheme development, in-channel engineering) may promote instability in the position of the gravel-sand transition. Migration of the gravel-sand transition may be indicators of these types of pressures, but its migration may also drive environmental change. An upstream retreat of the gravel-sand transition indicates sand deposition, which has detrimental effects on aquatic ecology in gravel reaches (e.g. suitability of salmon spawning sites). The rate at which sand is deposited immediately downstream of the transition may also contribute to elevated flood risk because higher deposition rates on the channel bed leads to greater rates of channel migration and switching, where the channel bed becomes perched above the adjacent floodplain [Ashworth *et al.*, 2004]. On the other hand, a downstream advance of the transition indicates gravel deposition, which also elevates flood risk in formerly sandy reaches where the channel becomes choked with coarser gravel [Chen and Petley, 2005]. A relatively new theory has also been proposed that suggests deposition of sediment from suspension drives the development of the gravel-sand transition [e.g. Venditti and Church, 2014; Venditti *et al.*, 2015; Lamb and Venditti, 2016].

Each of the three processes described above (abrasion, size selective sorting and suspension deposition) may be important in the development of gravel-sand transitions, but whether one process dominates over another is likely to depend on a variety of factors. For example, the local tectonic setting (subsidence), sedimentary characteristics such as the quantity and grain size of sediment, lithology and climatic conditions (influencing water discharge) may all influence the process through which gravel-sand transitions develop and result in transitions

with different characteristics. One of the most commonly observed characteristics associated with gravel-sand transitions is a reduction in channel bed gradient. In many cases there is a distinct break in channel slope associated with the gravel-sand transition [Sambrook Smith and Ferguson, 1995; Seal *et al.*, 1997]. Channel slope estimates from a range of studies, summarised in Sambrook Smith and Ferguson [1995], suggest a reduction in slope downstream of the transition by a factor of 1-11, which also results in a significant reduction in the sediment transport capacity of the system [Marr *et al.*, 2000]. Changes in channel planform from braided or wandering (upstream) to single-thread meandering (downstream) are also commonly, but not universally, observed at the gravel-sand transition [Parker and Cui, 1998; Labbe *et al.*, 2011; Dubille and Lavé, 2015]. Other variable characteristics include the abruptness of the gravel-sand transition [Singer, 2008] and the change in sediment grain size associated with the transition. Numerical modelling of depositional basins has also suggested that the position of the gravel front is related to spatial variations in basin subsidence rate [Paola *et al.*, 1992a; Robinson and Slingerland, 1998].

Immediately upstream of the transition, a strong bimodality of gravel and sand grain sizes is also commonly observed although the exact reasoning behind this is unclear [Paola and Seal, 1995; Wathen *et al.*, 1995; Smith and Ferguson, 1996]. Parker and Cui [1998] proposed that the frequency of particle motion will increase as grain size decreases downstream. If the grain is too coarse to entrain in suspension, it is less likely to undergo collision whilst stationary on the bed. For finer grains, there is a greater chance of entrainment into suspension which also reduces the probability of collision and abrasion. Peak abrasion rates are likely to occur on those intermediate sized grains which move via saltation and rolling during average flow conditions, and are only in suspension during larger flow events [Parker and Cui, 1998]. The gravel-sand transition has also be considered in terms of threshold transport and collision dynamics, where the viscous damping

of grain collisions sets a lower limit on gravel grain size [Jerolmack and Brzinski, 2010]. Sediment grain collisions are thought to be viscously damped below Stokes numbers of <105 [Jerolmack and Brzinski, 2010], where the Stokes number (St) is a function of:

$$St = \frac{(\rho_s - \rho)du_s}{9v\rho} = \frac{RDu_s}{9v} \tag{1.1}$$

where u_s and v are grain velocity and fluid velocity (respectively), ρ_s and ρ are sediment and water density (respectively), D is median grain diameter and R=(ρ_s-ρ)/ρ is the relative submerged density of a grain. Below this Stokes value, abrasion rates tend towards zero due to reduced kinetic energy transfer during grain collision. Jerolmack and Brzinski [2010] further examined how the commonly observed grain size biomodality upstream of the gravel-sand transition may be explained in terms of this viscous damping and the abrasion of gravel particles by sequential chipping (spallation), which produces discrete sand-sized particles which travel in suspension until all gravel has been extracted from the system [Marr *et al.*, 2000]. This combination of processes was also proposed as an explanation for the apparent 'grain size gap', where an absence of river bed sediments in the grain size fraction of 1-10 mm is commonly observed. This grain size gap has more recently been considered in a wider global context [Lamb and Venditti, 2016]. Lamb and Venditti [2016] proposed that the grain size gap relates to the ability of a river to transport sand as wash load where bed shear velocities drop below ∼0.1 m s^{-1}. Wash load is defined as fine suspended material which is not represented on the river bed in substantial quantities [Bagnold, 1966], and as such does not tend to dominate bed-material grain size distributions. Instead wash load is represented in either the finer end of the grain size distribution on the river bed, or coarser end of the grain size distribution of the suspended load, depending on the local bed shear velocity [Lamb and Venditti, 2016]. Downstream fining was modelled under the assumption that deposition of the coarsest fraction of the sediment load occurs where bed shear stresses fall below the threshold of motion for that grain size. The threshold for sediment motion is formulated as a critical Shields number

($\tau_c{}^*$) considered a function of particle Reynolds number (Re_p), bed shear velocity (u_*), fluid density (ρ), acceleration due to gravity (g), submerged specific density of sediment (R), particle diameter (D) and kinematic viscosity of the fluid (v) [Shields, 1936]:

$$\tau_c^* = u_*^2/RgD \tag{1.2}$$

$$Re_p = (RgD)^{1/2}D/v \tag{1.3}$$

$$u_* = \sqrt{\tau_b/\rho} \tag{1.4}$$

At small particle Reynolds numbers (where flow is less turbulent with fewer bursts of upward moving fluid), the transition from sediment being transported as bedload to being in suspension (or wash load) becomes increasingly difficult, due to effects relating to the viscous sublayer above the bed surface during particle re-entrainment [Niño *et al.*, 2003]. The particle Reynolds number is used to describe the ratio of inertial resistance to viscous resistance for a flowing fluid, where lower numbers (< 500) typically describe laminar flows, and higher numbers (>1000) describe turbulent flows. Based on this logic, particle re-suspension occurs at bed shear stresses that exceed those required for initial motion, indicating a regime of bed load transport at low particle Reynolds numbers [Niño *et al.*, 2003; Lamb and Venditti, 2016] (Figure 1.4). Lamb and Venditti [2016] further model the sediment size at the threshold of wash load (D_{10}) for the formative discharge event (e.g. bankfull) across a worldwide compilation of rivers, in which the coarsest grain sizes (D_{90}) are at the threshold of motion. At the threshold of initial motion, sediment grain sizes decrease smoothly with decreasing formative bed shear velocity. However, for particle sizes at the threshold for wash load entrainment, there is a dramatic drop from coarse sand to silt at bed shear velocity values of $\sim$0.1 m s^{-1} (Figure 1.5). Below bed shear velocity values of $\sim$0.1 m s^{-1}, the river loses the ability to transport sand as wash load due to Reynolds number effects. The median grain size (D_{50}) is taken as the geometric mean of the coarse

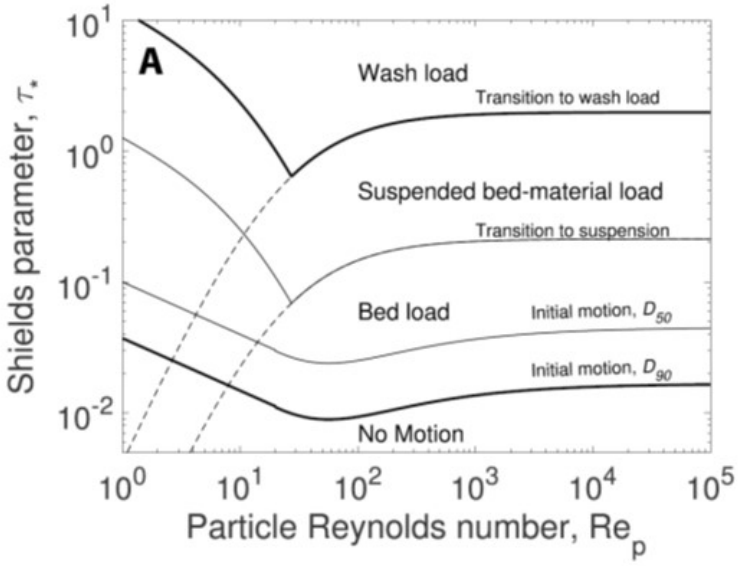

Figure 1.4: Modelled thresholds for initial motion for median particle diameter (D_{50}) and thresholds for incipient suspension/wash load. Dashed lines are predictions assuming that u_*/w_s is constant for all Re_p. Modified from Figure 2 in Lamb and Venditti [2016].

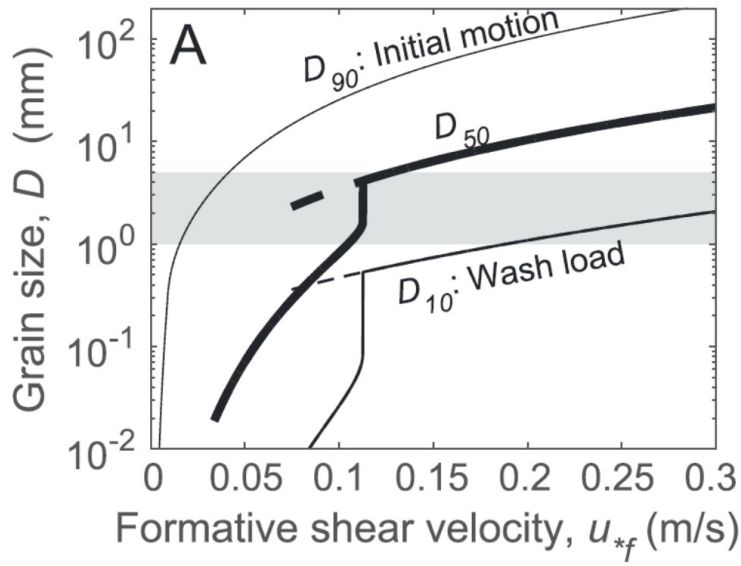

Figure 1.5: Modified from Figure 3 in Lamb and Venditti [2016]. Predictions at the formative (bankfull) bed shear velocity of grain size at initial motions (D_{90}), incipient was load (D_{10}), and median bed grain size (D_{50}). The region of multivalued solutions for wash load and D_{50} are shown with dashed lines, and the preferred solution by a solid line. The horizontal grey box denotes the inferred grain size gap ($1<D_{50}<5$ mm)

and wash load grain size fractions, and as such, also displays a dramatic decrease at bed shear velocity values of $\sim$0.1 m s^{-1} (Figure 1.5). Despite only a small reduction in bed shear velocity, the median grain size jumps from $\sim$5 mm to $\sim$1 mm [Lamb and Venditti, 2016]. While this new suspension deposition hypothesis presents a potentially very elegant solution, it has only been tested in one major river system and requires more complete testing across a wider range of river systems. It is not presently clear whether transitions previously attributed to size selective sorting or abrasion can be attributed to suspension deposition or whether there are domains under which different processes lead to a superficially similar phenomenon.

Stability of the gravel-sand transition

The stability of the gravel front (or gravel-sand transition) over different time scales has been most thoroughly tested through numerical modelling and experimental studies. A number of these studies have highlighted the potential role of sediment supply and subsidence rate on downstream fining trends in depositional basins [Parker and Cui, 1998; Robinson and Slingerland, 1998; Hoey and Bluck, 1999; Marr *et al.*, 2000], where the timescales over which these variables were perturbed was also found to dictate fining rates and position of the gravel-sand transition [Paola *et al.*, 1992a]. Over long geological timescales ($> 10^6$ years), sinusoidal variations in basin subsidence, gravel content and sediment flux have been modelled to drive phases of gravel front progradation and retreat. Using faster variations in the same forcing parameter (over timescales of 10^5 years), the effects of subsidence rate on the gravel-sand transition stability become more subdued [Paola *et al.*, 1992a; Marr *et al.*, 2000]. Conversely, over short geomorphic time scales the gravel-sand transition is thought to appear relatively stable in space [Cui and Parker, 1998].

Resistivity surveys and groundwater borehole data across the Gandak and Kosi alluvial fans in the east Ganga Plain suggest the presence of sub-surface gravel deposits considerably further downstream than the position of the modern gravel-sand transition [Sinha *et al.*, 2014a]. However, there are no dates or specific grain size details available for these cores and hence it is not possible to constrain when these systems were last capable of transporting gravel of a given grain size. Assuming a constant fan surface elevation, sedimentation rate of ∼1.5 mm yr^{-1} [Sinha *et al.*, 1996] and minimal sediment compaction, it could be inferred that these sub-surface gravel deposits are of the order of 10^4 years. Most of the proposed gravel deposits are at a depth of at least 25 m below the fan surface, implying a minimum age of ∼15,000-20,000 years, as a first-order estimate. In both systems, lower and upper fan successions were identified and attributed to a change in fluvial process from a relative stable and incised system characterised by narrow channel fills (lower succession), to a more mobile and avulsive system generating laterally stacked sand bodies (upper succession) [Sinha *et al.*, 2014a]. These observations suggest that the gravel-sand transition may have historically extended ∼40 km further downstream, and that large-scale changes or shifts in channel morphology have previously occurred.

1.3.3 Sediment flux and ^{10}Be concentrations

Current estimates of sediment flux out of the Himalayan mountains are based on a combination of suspended sediment gauging, cosmogenic radionuclide-derived fluxes, and volumetric estimates from the Bay of Begal [e.g. Goodbred and Kuehl, 1999; Andermann *et al.*, 2012; Lupker *et al.*, 2012]. Volumetric estimates from the Bay of Bengal typically average sediment delivery over long time-scales, and as such, likely buffer short-term tectonic and climatic perturbations within the Himalayan mountains [Jerolmack and Paola, 2010]. However, studies on the

Ganga dispersal system have suggested that there is a tight coupling between the source area, basin, coastal and marine depocentres. Changes in the strength of the Indian Summer Monsoon (which influences both water and sediment fluxes) are thought to be transferred as quickly as 1-2 kyr to the margin and deep-sea fan [Goodbred Jr., 2003]. This rapid source-sink signal propagation is attributed to the overwhelming control of the Indian Summer Monsoon on regional hydrology, and hence sediment production and transport. Peak monsoonal flows generate large fluvial capacity to mobilise and transport sediment out of the Himalayan mountains. Given the vast majority of water and sediment discharge occurs during only a few months of the year, the annual mean discharge of the system is likely to significantly underestimate what the river is capable of transporting during peak monsoonal flow [Goodbred Jr., 2003].

Suspended sediment gauging allows for much higher temporal resolution sediment flux estimates, and can be used to document seasonal changes in sediment flux associated with the Indian Summer Monsoon. Suspended sediment gauging records are not widely available across the Himalaya, and often are temporally incomplete. Sediment flux estimates derived purely from suspended load measurements also neglect the role of bed load, which is likely to make up a more substantial component of the sediment load during peak discharge events or sediment-laden floods [Pratt-Sitaula *et al.*, 2007]. Generating sediment flux estimates from point measurements of suspended sediment concentration at the channel margin relies on detailed knowledge of the cross-sectional flow velocity distribution of the channel, and the stage-discharge relationship at that locality [Meade and Stevens, 1990; Horowitz *et al.*, 1990]. A single daily measurement may also fail to capture variability in discharge and sediment flux associated with diurnal glacial melt-water cycles or fluctuations generated by short-lived rainfall events [Horowitz *et al.*, 1990; Singh *et al.*, 2005; Gitto *et al.*, 2017]. The development of

detrital cosmogenic radionuclide (CRN) analysis over the last 20 years now permits catchment-averaged denudation rates to be determined over time scales of 10^2-10^3 years [Vance *et al.*, 2003; Gabet *et al.*, 2008; Lupker *et al.*, 2012; Scherler *et al.*, 2014]. These rates of average landscape lowering can be converted into sediment flux estimates [e.g. Lupker *et al.*, 2012], but few studies have evaluated the application of this technique in determining sediment flux estimates in great detail.

Unlike sediment gauging, CRN analysis measures concentrations of cosmogenically derived isotopes (such as ^{10}Be) that have accumulated in the top layer of the earth's surface. The concentration of the isotope recorded in modern river sediments reflects the time taken since the isotope was formed (in-situ) within the upper 1-2 m of the Earth's surface, eroded from the landscape and transported to the sampling location. From this, catchment averaged denudation or erosion rates can be calculated, and converted into cosmogenic derived sediment fluxes (φ_{cosmo}) where basin surface areas are known, using the equation:

$$\varphi_{\text{cosmo}} = \epsilon \rho S \tag{1.5}$$

where ϵ is the basin-averaged erosion rate (cm yr^{-1}), ρ is the density of the eroded material (g cm^{-3}) and S is the basin surface area [Lupker *et al.*, 2012]. By using catchment-averaged erosion rates, and assuming negligible storage within the mountain catchment, both suspended and bedload portions of total sediment flux should be accounted for, and thus improves on one of the limitations associated with modern gauged sediment data. The published CRN data give an indication of how the total sediment flux delivered to the foreland basin varies spatially between the major river systems that drain the Himalaya (Fig. 1.6). Sediment fluxes calculated from ^{10}Be concentrations measured from the modern river sediment reveal marginally lower fluxes at the western end of the Ganga basin. However, estimates vary by up to a factor of three between sampling years of a single river,

highlighting the difficulty in accurately quantifying sediment flux to the foreland basin using this approach [Lupker *et al.*, 2012]. The sediment supplied to rivers

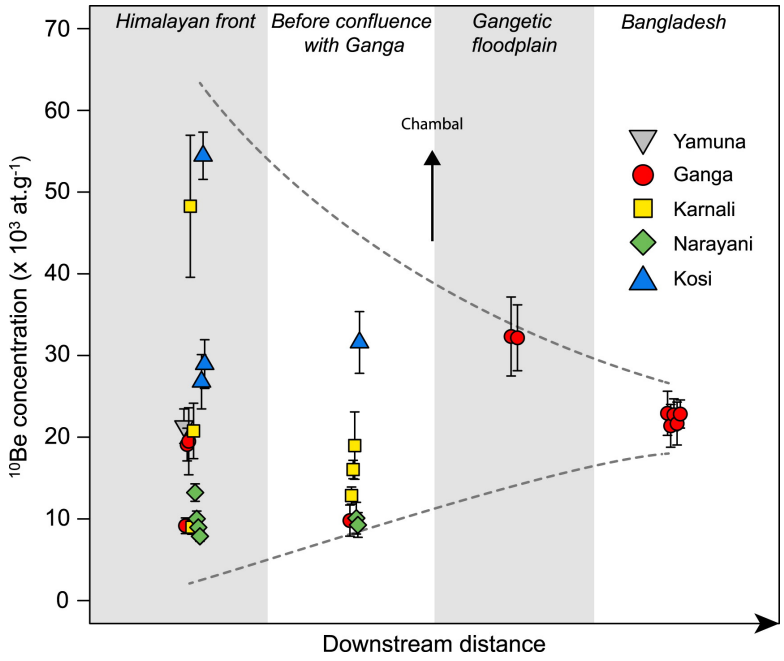

Figure 1.6: Variability in ^{10}Be concentrations sampled across tributaries in the Ganga basin downstream of the mountain front (from Figure 2 in Lupker *et al.*, 2012), which are used to calculated sediment flux.

draining the Ganga Plain is an integrated signal of upstream factors that control patterns of Himalayan landscape evolution (tectonics, climate and lithology). For example, in regions of elevated monsoon intensity it would be expected for more frequent landslides or debris flows to occur [Bookhagen *et al.*, 2005; Hobley *et al.*, 2010] generating large pulses of low ^{10}Be concentration sediments that are eventually exported to the Ganga Plain. Cosmogenic ^{10}Be concentrations sampled at the mountain outlet may be influenced by the presence or absence of discrete sediment pulses generated by such events, and the degree to which these low ^{10}Be concentration inputs are mixed into river sediments by the time they reach the mountain outlet.

In order to covert measured CRN concentrations into catchment-averaged erosion

rates, a number of assumptions are required [Dunai, 2010]. These include factors that are likely to influence CRN production rate across the catchment, such as glacier cover within the catchment, where it is typically assumed that beneath an ice thickness of a few metres CRN production rates are effectively zero [Mudd *et al.*, 2016]. The distribution of quartz-rich lithologies across the catchment (which contributes to the sediment from which quartz grains can be extracted and sampled if using ^{10}Be isotopes) must also be taken into account and is commonly corrected for where the lithology of the catchment is mixed (e.g. Vance *et al.*, 2003). Furthermore, intermediate sediment storage and recycling within the catchment may also perturb CRN concentrations, where sediment may reside on floodplains for several thousand years following erosion from the landscape and accumulate further cosmogenic radionuclides [Von Blanckenburg, 2005]. Following remobilisation and transport to the catchment outlet, this sediment may have a much higher CRN concentration which may be interpreted as lower catchment-averaged erosion rates. In large (>1000 km^2) tectonically active catchments, it is also commonly assumed that the effects of stochastic inputs of low CRN concentration sediment (generated by the mass wasting of hillslopes) is buffered, such that reliable estimates of long-term (millenial) erosion rates can be made [Niemi *et al.*, 2005]. In smaller catchments, these inputs of low CRN concentration sediment drive notable temporal variability in catchment-averaged CRN concentrations and subsequent erosion rate estimates [Niemi *et al.*, 2005; Von Blanckenburg, 2005; Yanites *et al.*, 2009; West *et al.*, 2014].

In many respects, a number of these assumptions are relatively straight-forward to quantify for rivers draining the Ganga basin where the lithology of the Himalayan mountains is dominated by quartz-rich lithologies [Vance *et al.*, 2003; Lupker *et al.*, 2012], where glacier extent is relatively well mapped by the Global Land Ice Measurements from Space (GLIMS) database [Armstrong *et al.*, 2005] and catchment areas are in excess of 10,000 km^2. Aspects which are perhaps more

difficult to quantify include the volume and timescales of sediment storage within the mountainous portion of the catchment, although first-order estimates of valley fill do exist for much of the Himalaya [Blöthe and Korup, 2013]. Assumptions concerning whether these systems are also in isotopic steady-state (where CRN production is equal to CRN export) may also influence CRN concentrations recorded at the outlet, where landscapes may also take several thousands of year to redevelop a CRN concentration profile in the upper few metres of the Earth's surface following episodes of mass wasting which can erode several metres of material from the landscape [Niemi *et al.*, 2005]. A number of recent studies have also suggested that the grain size fraction of sediment used for CRN analysis may bias results (e.g. Puchol *et al.*, 2014; Schildgen *et al.*, 2016; Lupker *et al.*, 2017) although no systematic grain size signal was documented in Lupker *et al.* [2012] which considered CRN concentrations measured from multiple sand grain size fractions in a small number of samples from the Ganga basin.

Until we have a better understanding of the controls on the variability in ^{10}Be concentrations, it remains difficult to quantify spatial variations in millennial-scale sediment supply rate from Himalayan catchments. Similarly, longer term erosion rates estimated from bedrock mineral cooling ages of the Greater Himalaya Sequence along the strike of the range do not suggest a significant west to east variation in erosion rates, although rates further east are marginally ($\sim$0.5 mm yr^{-1}) higher [Thiede and Ehlers, 2013]. Denudation rates over the past 4 Myr vary between $\sim$1-2.5 mm yr^{-1} across the Greater Himalayan Sequence within the Ganga basin, but there are large uncertainties with these data [Thiede and Ehlers, 2013]. Furthermore, erosion rates in the Greater Himalaya are thought to be relatively high in comparison to the Lesser Himalaya [Lavé and Avouac, 2001], and as such, denudation rates derived from thermochronology studies in this region do not represent catchment averaged rates. The timescales over which these denudation rates have been averaged over may also be too large to reflect spatial patterns in

modern or sub-millennial sediment fluxes to the Ganga Plain, and should not be interpreted as comparable rates to those derived from ^{10}Be concentrations.

1.4 Study Area

The Himalayan foreland basin formed as a result of the ongoing collision between the Indian and Eurasian plates, where crustal thickening generates high topography that is supported by the flexural rigidity of the underlying lithosphere [Lyon-Caen and Molnar, 1985; Flemings and Jordan, 1989; Burbank and Beck, 1991; Burbank, 1992; Brozovic and Burbank, 2000]. Along the strike of the mountain range, variations in lithospheric rigidity and basement faulting are believed to have modulated both basin width and large-scale patterns of subsidence [Burbank *et al.*, 1996]. The Himalayan orogen is split into four major structural units that run broadly parallel from west to east (Figure 1.7). These units are from south to north: the Neogene Siwalik Group, the Proterozoic Lesser Himalayan Sequence, the Proterozoic-Ordovician Greater Himalayan Crystalline Complex and the Proterozoic to Eocene Tethyan Himalayan Sequence [Yin, 2006]. These lithological units are bound by major faults, the most active of which is the Main Frontal Thrust (MFT). The MFT is the most southerly structure, situated between the Siwalik Group and the foreland basin, and absorbs approximately 80% of the $\sim$21$\pm$1.5 mm yr^{-1} convergence between India and south Tibet in central Nepal [Lavé and Avouac, 2000].

Sediment generated by the erosion of the Himalayan mountain range accumulates in the foreland basin. The thickness of the basin fill reduces progressively with distance from the mountain front, consistent with asymmetric subsidence caused by thrusting of the overlying orogen [Burbank and Beck, 1991; Burbank, 1992;

Yin, 2006]. The basin fill is dominated by the Neogene Siwalik Group and the pre-Miocene Rawalpindi Group [Burbank *et al.*, 1996]. The Siwalik Group comprises thick molasse deposits formed by the erosional products of the Lesser and Higher Himalaya [e.g. Kumar *et al.*, 2004]. Thin-skinned tectonics associated with the MFT have incorporated these poorly consolidated molasse deposits in the hanging wall of frontal structures, forming the Siwalik Hills which represent the youngest and southernmost topography of the Himalaya [Mugnier *et al.*, 1999]. The foredeep basin [*sensu* DeCelles and Giles, 1996] lies immediately south of the Siwalik Hills, forming the Indo-Gangetic Plain. Immediately inboard of the thrust front are several wedge-top basins, locally termed Duns, that act to buffer the sediment delivery to the foredeep [Densmore *et al.*, 2016]. In comparison to the confined bedrock channel both upstream and downstream of the Dun, the laterally unconfined and lower gradient surface of these Dun valleys has promoted sediment deposition during periods of heightened sediment export from the mountains, producing a thick alluvial valley fill. Dun valleys of direct relevance to this study are the Chitwan and Dehra Dun valleys where the Gandak, Ganga and Yamuna rivers flow through prior to passing the MFT and exiting onto the Plain (Figure 1.7). The Ganga Plain forms the central third of the Indo-Gangetic Plain and covers an area of 250,000 km^2, whilst the drainage area of the entire Ganga basin is in excess of 1,060,000 km^2 [Singh, 1996]. The hydrology of rivers draining the basin is dominated by the Indian Summer Monsoon (ISM), when over 85% of the annual rainfall falls between June and September [Sinha and Friend, 1994; Tandon *et al.*, 2006], producing broad peaked annual hydrographs. Along strike gradients in precipitation have been identified using passive microwave data [Bookhagen *et al.*, 2005; Anders *et al.*, 2006] where catchments in the east typically experience more Indian summer monsoon precipitation than those in the west. A strong north-south precipitation gradient has also been identified as a result of orographic enhancement of precipitation, where the heaviest rainfall is induced by the first significant topography encountered by southerly air masses originating

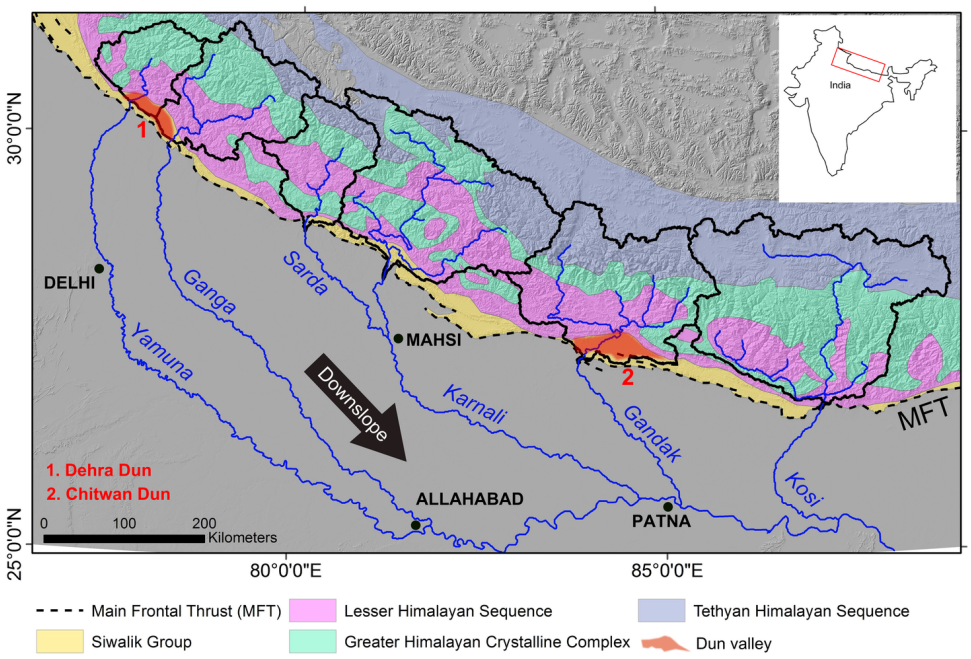

Figure 1.7: Location of major Dun valleys and geological units (from Yin, 2006) in the Ganga basin on a 90 m Shuttle Radar Topography Mission (SRTM) derived Digital Elevation Model (DEM).

from the Bay of Bengal [Bookhagen *et al.*, 2005; Bookhagen and Burbank, 2006; Anders *et al.*, 2006]. Apatite fission track ages from across the entire Himalaya do not reveal any systematic change in exhumation rates along the strike of the range [Thiede and Ehlers, 2013].

Sediment carried into the foreland basin that is not immediately deposited, typically sand and finer material, can continue downstream via the Ganga, Brahmaputra and Indus rivers and eventually to the sea where it accumulates in the Bengal and Indus fans. This fraction represents up to ∼90% of the total sediment load exported from the Himalaya [Lupker *et al.*, 2011]. Sediment trapped within the foreland basin is deposited across vast alluvial fans that are separated by broad interfan or interfluve areas that are drained by foothill or Plain fed rivers [Jain and Sinha, 2003; Sinha *et al.*, 2005]. These interfan parts of the basin are filled primarily with sediments eroded from the frontal Siwalik range, and sediments derived and reworked locally from the Plain [Sinha *et al.*, 2005]. The rivers feeding the Plain can be divided into mountain, foothill and Plain-fed [Sinha and Friend, 1994]. Mountain-fed rivers originate from large source areas within the Himalayan orogen, typically with a glacial source. Foothill or piedmont rivers have relatively small catchment areas of 20-2500 km^2 [Dubille and Lavé, 2015] and drain the interfluve region between alluvial fans created by sediment deposition of the much larger mountain fed rivers. Plain-fed rivers repetitively rework sediment deposited by the mountain and foothill fed rivers [Sinha *et al.*, 2005]. Grain size measurements in central Nepal across a number of interfan or foothill fed channels have documented a rapid gravel-sand transition occurring ∼8-20 km downstream of the mountain front [Dubille and Lavé, 2015]. This same rapid transition is consistent with vertical grain size measurements taken from the Siwalik molasse exposed in the frontal Himalayan fold belts [Dubille and Lavé, 2015].

1.5 Thesis Outline

The central chapters of this thesis (Chapters 3-5) are written in the form of research papers that have either already been, or will shortly be, submitted to journals. As such, each of these chapters serve as stand-alone documents covering separate topics, but each contributing to addressing the overarching aim of this thesis. The contributions I have made to each of these documents is clearly outlined at the start of each chapter, and the published versions of Chapters 3 and 4 are available in Appendix A and Appendix B, respectively. A resubmitted version of the manuscript presented in Chapter 5 is also available in Appendix C. The content of these chapters is outlined in more detail below.

Chapter 2 introduces a new basin-scale approach to quantifying patterns of channel incision and aggradation across the Ganga Plain using a swath profile tool. The application of this swath profile tool highlights the contrast in channel morphology between the west and east Ganga Plain, where in the west channel are entrenched by up to 30 m in broad ∼40 km wide valleys and in the east, channels may be super-elevated by as much as 10 m above their adjacent floodplain. Possible controls behind these observations are explored in terms of analysis of new basin subsidence rate estimates and sediment grain size data. Subsidence velocity estimates are derived from the gradient of the crystalline basement beneath the mountain front and known horizontal convergence velocities. The geometry and surface elevation of the foreland basin is assumed constant over the timescales which these subsidence velocity estimates are calculated. Tectonically-driven subsidence across the foreland basin can be separated into horizontal and vertical components, where the horizontal component can be independently acquired from GPS measurements of horizontal convergence velocities across the Himalayan orogen to calculate the true vertical component. Sediment grain size fining

rates between the mountain front and gravel-sand transition along major rivers of the Ganga Plain are also used as a proxy for subsidence rates. By integrating these results, it is proposed that higher subsidence rates are responsible for a deeper basin in the east with perched, lower gradient river systems that are relatively insensitive to climatically driven changes in base-level. In contrast, lower subsidence rates in the west are associated with higher elevation basin topography, and entrenched river systems recording climatically induced lowering of river base-levels during the early Holocene. This work was published in the *American Journal of Science* in 2016.

Chapter 3 builds on an intriguing observation in **Chapter 2** where the position of the gravel-sand transition in large trans-Himalayan rivers in the east Ganga Plain (Gandak and Kosi) is at a comparable distance to those noted by Dubille and Lavé [2015] in a number of small foothill-fed catchments in the Gandak-Kosi interfan region. Sediment transport models suggest that for a constant subsidence rate, the position of the gravel-sand transition in rivers is controlled by the sediment flux, water discharge and gravel fraction. Given the order of magnitude differences in catchment area between these two scales of system, it seems unlikely that sediment flux or water discharge are a dominant control on the position of the gravel-sand transition. Instead, differences in the amount of gravel exported by trans-Himalayan and foothill-fed river systems is explored. Using a mass-balance model, the quantity of gravel trapped upstream of the gravel-sand transition is calculated for rivers across the east Ganga Plain. This quantity is explained using an abrasion model, indicating that most gravel exported from the Himalayan mountains into the east Ganga Plain originates <100 km upstream of the mountain front, which is supported by new gravel lithology data from exposed gravel bars downstream of the mountain front. This work was published in

Nature in 2017.

In **Chapter 4** I present new cosmogenic radionuclide (CRN) samples from the Ganga River to examine the use of cosmogenic radionuclide analysis as a tool to estimate sediment flux in large and tectonically active catchments. It is commonly assumed that the effects of stochastic inputs of sediment (which typically deliver large quantities of low CRN concentration sediment into the fluvial network) are buffered in catchment areas larger than ∼1,000 km^2 (e.g. Niemi *et al.*, 2005). My observations combined with those in Lupker *et al.* [2012] suggest there is a notable degree of variation in CRN concentration measured at the Himalayan mountain front. Interestingly, this degree of natural variability appears insensitive to regional changes in climate experienced across the Himalaya during the early Holocene. Potential drivers of this degree of 'background' variability are then explored. It is proposed that the observed variability is driven by 1) the nature of the stochastic inputs of sediment (e.g. the type of hillslope process, surface CRN production rates, degree of mixing), and 2) the evacuation timescales of these sediment deposits. In landscapes dominated by high topographic relief, spatially variable climate and geomorphic process domains, it is suggested that the use of ^{10}Be concentrations to generate sediment flux estimates may not be truly representative, as comparable mean catchment CRN concentrations can be derived through dramatically different erosional processes. For a given CRN concentration, volumetric sediment flux estimates may vary considerably and under certain conditions, CRN concentrations may under-estimate actual erosion rates and hence sediment flux.

In **Chapter 5**, findings from the preceding three chapters are integrated into a single discussion in the context of the research questions outlined in Section 1.2. The wider implication and outcomes from this work are then also discussed,

highlighting how these findings further our understanding of processes influencing large-scale alluvial river morphology and considers remaining gaps in our knowledge and revenues for future research. This is then followed by a short summary or conclusion section (**Chapter 6**), emphasising the key findings from this thesis.

Chapter 2

Subsidence control on river morphology and grain size across the Ganga Plain

The work presented in this chapter was published in the American Journal of Science:

Dingle, E.H., Sinclair, H.D., Attal, M., Milodowski, D.T., and Singh, V. (2016) Subsidence control on river morphology and grain size across the Ganga Plain, *American Journal of Science*, Vol. 316, p778-812, doi: 10.2475/08.2016.03

The published format of this paper is presented in Appendix A. This research was conducted in collaboration with the named co-authors, who helped edit the final manuscript and write the swath code. E.H.D and M.A collected grain size data and V.S provided digitised depth-to-basement data. E.H.D performed the application and analysis of the swath tool (which D.T.M coded) and subsidence

and grain size data. E.H.D created the figures. E.H.D largely wrote the manuscript with discussions and contributions from H.D.S, M.A, and D.T.M.

2.1 Abstract

The Ganga Plain represents a large proportion of the current foreland basin to the Himalaya. The Himalayan-sourced waters irrigate the Plain via major river networks that support approximately 10% of the global population. However, some of these rivers are also the source of devastating floods. The tendency for some of these rivers to flood is directly linked to their large scale morphology. In general, the rivers that drain the east Ganga Plain have channels that are perched at a higher elevation relative to their floodplain, leading to more frequent channel avulsion and flooding. In contrast, those further west have channels that are incised into the floodplain and are historically less prone to flooding. Understanding the controls on these contrasting river forms is fundamental to determining the sensitivity of these systems to projected climate change and the growing water resource demands across the Plain. Here, we present a new basin scale approach to quantifying floodplain and channel topography that identifies areas where channels are super-elevated or entrenched relative to their adjacent floodplain. We explore the probable controls on these observations through an analysis of basin subsidence rates, sediment grain size data and sediment supply from the main river systems that traverse the Plain (Yamuna, Ganga, Karnali, Gandak and Kosi rivers). Subsidence rates are approximated by combining basement profiles derived from seismic data with known convergence velocities; results suggest a more slowly subsiding basin in

the west than the east. Grain size fining rates are also used as a proxy for relative subsidence rates along the strike of the basin; the results also indicate higher fining rates (and hence subsidence rates for given sediment supply) in the east. By integrating these observations, we propose that higher subsidence rates are responsible for a deeper basin in the east with perched, low gradient river systems that are relatively insensitive to climatically driven changes in base-level. In contrast, the lower subsidence rates in the west are associated with a higher elevation basin topography, and entrenched river systems recording climatically induced lowering of river base-levels during the Holocene.

2.2 Introduction

Many of the rivers of the Ganga Plain are prone to abrupt switching of channel courses (avulsion) causing devastating floods over some of the most densely populated regions on the globe. The Kosi River that drains central Nepal and discharges onto the Ganga Plain of Bihar State has a well-documented history of frequent channel avulsion and flooding [Wells and Dorr, 1987]. During 2008, a single channel avulsion event resulted in a temporary eastward shift of the Kosi River by tens of kilometres where the channel breached its eastern levee resulting in extensive flooding [Chakraborty *et al.*, 2010; Sinha *et al.*, 2005, 2013, 2014b]. Similarly, levee failures and channel avulsion resulted in catastrophic flooding of the Indus Plain of Pakistan in 2010 and the displacement of at least 10 million people [Syvitski and Brakenridge, 2013]. The nature and frequency of channel avulsion is also a first-order control on alluvial stratigraphy, defining the geometric distributions of channel and floodplain deposits [Bridge and Leeder, 1979; Slingerland and Smith, 2004]. In the Ganga Plain, the distribution of Quaternary channel sands and floodplain muds determines groundwater pathways and

associated arsenic pollution [Shah, 2007]. Given the significance of floodwaters and groundwater pathways in the Ganga Plain, documenting and understanding variations in the morphology of river channel and floodplain systems represents a research priority, particularly in light of changes in monsoon intensity, glacial meltwater discharge and the water demands of a growing population [Fleitmann *et al.*, 2007; Immerzeel *et al.*, 2010].

Systematic variations in the large-scale morphology of the river systems are recognised across the extent of the Ganga foreland basin (Figure 2.1) [Sinha *et al.*, 2005]. Rivers of the east Ganga Plain are characterised by shallow aggrading channels that frequently avulse and flood, whilst those in the west are characterised by degrading systems with incised channels and extensive areas of badland topography. In the east Ganga Plain, numerous channel avulsions and random switching of the loci of fan lobe aggradation has resulted in a net westward migration of >113 km of the Kosi River over the surface of its mega-fan during the last two centuries [Wells and Dorr, 1987; Chakraborty *et al.*, 2010]. Palaeochannels are well preserved across much of the surface of the Kosi and Gandak fans [Sinha *et al.*, 2014b], reflecting the dynamic and mobile nature of these systems. In the west Ganga Plain, the Ganga River is described as a braided channel within a narrow incised valley with exposed cliffs extending 15-30 m above the modern channel in parts [Shukla *et al.*, 2001; Gibling *et al.*, 2005; Shukla *et al.*, 2012], Numerous phases of incision and aggradation are documented within both the Yamuna and Ganga valleys where distinct geomorphic surfaces and facies associations are preserved in exposed valley walls [Shukla *et al.*, 2001, 2012; Gibling *et al.*, 2005; Tandon *et al.*, 2006]. In order to understand the controls on the variations in river morphology along the Ganga Plain, we need to consider a range of possible scenarios. As rivers exit mountain ranges, they commonly evolve into broad alluvial systems where river morphology (channel pattern, geometry, gradient) is typically determined by water and sediment discharges, sediment

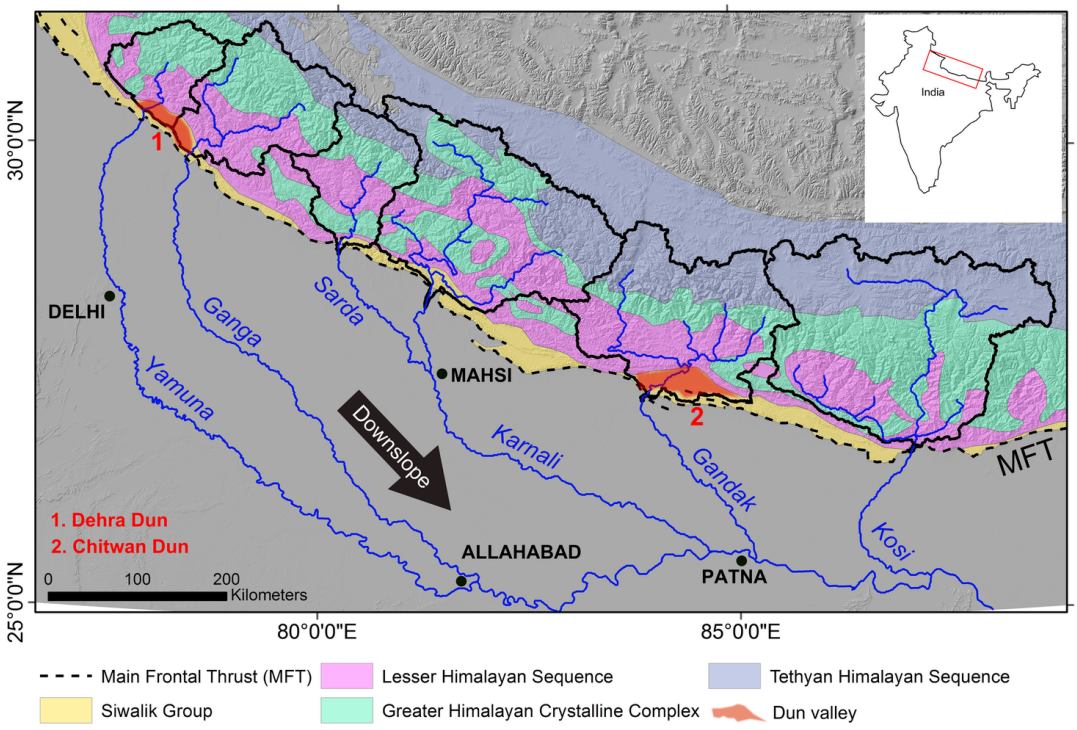

Figure 2.1: Study catchments, location of major Dun and geology (from Yin, 2006) in the Ganga basin on a 90 m Shuttle Radar Topography Mission (SRTM) derived Digital Elevation Model (DEM).

grain sizes, basin subsidence rates and vegetative patterns (Figure 2.2) [van den Berg, 1995; Dade and Friend, 1998; Dade, 2000; Duller *et al.*, 2010; Marr *et al.*, 2000; Allen *et al.*, 2013b]. In addition, first-order predictions from various studies (for example Paola *et al.*, 1992a; Robinson and Slingerland, 1998; Duller *et al.*, 2010; Allen *et al.*, 2013b) are that downstream grain size trends are also controlled by sediment supply and subsidence rate, with increased sediment supply reducing fining rates, and increased basin subsidence increasing fining rates as a result of enhanced rates of deposition or aggradation promoting selective deposition in the proximal region of the basin. Grain size fining trends impact the location of the gravel-sand transition [Dubille and Lavé, 2015], and variations in river morphology [Dade and Friend, 1998]. This paper initially quantifies the basin-wide variability

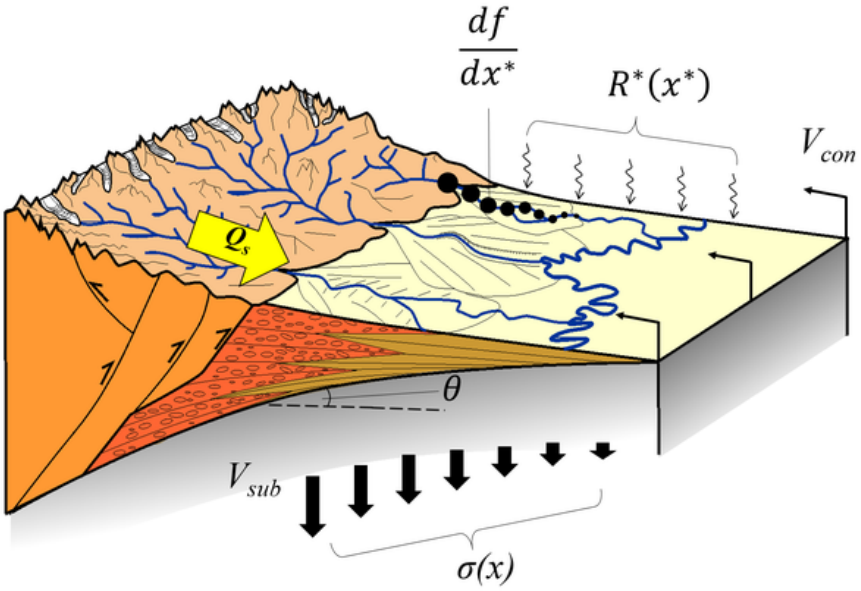

Figure 2.2: Major controls on large scale channel morphology across the Ganga Plain. These controls include sediment flux, Q_s to the basin; the distribution of tectonic subsidence, $\sigma(x)$, across the basin; the spatial distribution of sediment deposition down-system, $R^*(x^*)$; sediment grain size fining rate, $\frac{df}{dx*}$; and basin subsidence velocity, V_{sub}, which is a product of the horizontal convergence velocity across the Himalaya, V_{con}, and dip of the basement beneath the mountain front, θ.

in incision and aggradation of the river systems across the Ganga Plain from

digital topography using a swath based technique to map relative elevation of channels above or below their floodplains. The implications are that the lateral variations in incision versus aggradation should be recorded in the underlying basin stratigraphy, and that the relative contributions of sediment derived from the western and eastern Himalaya to the Ganges-Brahmaputra Delta are likely to be affected by the relative efficiency of sediment transport and bypass across the Ganga Plain. In addition to quantifying the relief along the valleys of the rivers, we also generate new basin-wide data on subsidence rates and grain size fining rates from the proximal foreland basin near to the mountain front. We finally discuss and analyse these data in context of the observed patterns in incision and aggradation of the river systems across the Ganga Plain.

A challenge when determining longer-term (millennial) controls on fluvial morphologies is to differentiate signals driven by shorter-term stochastic variations in climate or tectonic activity in the upstream catchment [Benda and Dunne, 1997a; Tucker and Slingerland, 1997; Leeder *et al.*, 1998]. Forward models have simulated the effects of varying parameters such as sediment flux and basin subsidence over different timescales relative to the equilibrium time period of the basin, defined as the period required for streams within the basin to attain a steady-state profile [Paola *et al.*, 1992a; Heller and Paola, 1996; Robinson and Slingerland, 1998; Marr *et al.*, 2000]. In a system as large as the Ganga Plain, potential short-term ($<10^4$ years) controls on sediment flux and grain size could be linked to climatic changes in precipitation patterns, glacial discharge and extreme storm events or earthquakes. In contrast, subsidence rates, which are controlled by topographic loading and the flexural response and subduction velocity of the underlying lithosphere [Sinclair and Naylor, 2012] are unlikely to vary at these timescales. Below, we discuss current knowledge and data available on the potential controlling parameters on the large-scale morphology of rivers across the Ganga Plain: sediment flux, basin subsidence and sediment grain size of rivers across the Ganga Plain.

2.2.1 Current constraints on sediment flux, basin subsidence and sediment grain size across the Ganga Plain

Our current understanding of sediment flux into the Ganga foreland basin is based principally on suspended sediment data from gauging station networks, but the spatial coverage of these data is restricted [Blöthe and Korup, 2013]. Advances in detrital cosmogenic radionuclide (CRN) analysis have allowed ^{10}Be concentrations to be measured in modern river sediments, allowing approximation of average denudation rates from the source catchments over timescales of thousands of years [Vance *et al.*, 2003; Lupker *et al.*, 2012; Godard *et al.*, 2014]. The published CRN data give an indication of how sediment flux delivered to the foreland basin varies spatially between the major river systems that drain the Himalaya. The mean erosion rates of ∼1 mm/yr derived from these data can be used to infer the timescales over which the rates are averaged, <1000 years in this case based on the reduction in CRN production rates with depth. Sediment fluxes calculated from ^{10}Be concentrations measured from the modern river sediment reveal marginally lower fluxes at the western end of the Ganga basin (Figure 2.3, 3.1). However, estimates vary by up to a factor of three between sampling years of a single river, highlighting the difficulty in accurately quantifying sediment flux to the foreland basin using this approach [Lupker *et al.*, 2012]. Until there is a better understanding of the controls on the variability in ^{10}Be concentrations, it remains difficult to quantify spatial variations in millennial-scale sediment supply rate from Himalayan catchments. Similarly, longer term erosion rates estimated from bedrock mineral cooling ages of the Greater Himalaya Sequence along the strike of the range do not suggest a significant west to east variation in erosion rates, although rates further east are marginally (∼0.5 mm/yr) higher [Thiede and Ehlers, 2013]. Denudation rates over the past 4 Myr vary between ∼1-2.5 mm/yr across the Greater Himalayan Sequence within the Ganga basin,

but there are large uncertainties with these data [Thiede and Ehlers, 2013]. Furthermore, erosion rates in the Greater Himalaya are thought to be relatively high in comparison to the Lesser Himalaya [Lavé and Avouac, 2001], and as such, denudation rates derived from thermochronology studies in this region do not represent catchment averaged rates. The timescales over which these denudation rates have been averaged may also be too large to reflect spatial patterns in modern or sub-millennial sediment fluxes to the Ganga Plain, and should not be interpreted as comparable rates to those derived from ^{10}Be concentrations.

Basin subsidence histories across the Indo-Gangetic Plain requires multiple,

Table 2.1: Sediment flux estimates summarized from Blöthe and Korup [2013]

River name	Sediment flux (Mt yr^{-1}) at mountain front	Source
Yamuna	13±5	Lupker et al., 2012*
	64	Jha et al., 1993***
Ganga	139±37	Lupker et al., 2012*
	67±17	Vance et al., 2003*
	65±23	Vance et al., 2003*
	100	Wasson, 2003***
Karnali	34±8	Lupker et al., 2012*
	295±77	Lupker et al., 2012*
	127±38	Lupker et al., 2012*
	71	Ghimire and Uprety, 1990***
	353	Andermann et al., 2012**
Gandak	110±35	Lupker et al., 2012*
	145±49	Lupker et al., 2012*
	162±53	Lupker et al., 2012*
	184±60	Lupker et al., 2012*
	82	Sinha and Friend, 1994***
	299	Andermann et al., 2012**
	128	Ghimire and Uprety, 1990***
Kosi	141±32	Lupker et al., 2012*
	69±14	Lupker et al., 2012*
	131±28	Lupker et al., 2012*
	155	Ghimire and Uprety, 1990***
	43	Sinha and Friend, 1994***
	242	Andermann et al., 2012**

*Sediment flux derived from ^{10}Be concentration in sand

**Based on a mean daily suspended sediment flux (1973-2006)

***Suspended sediment concentration

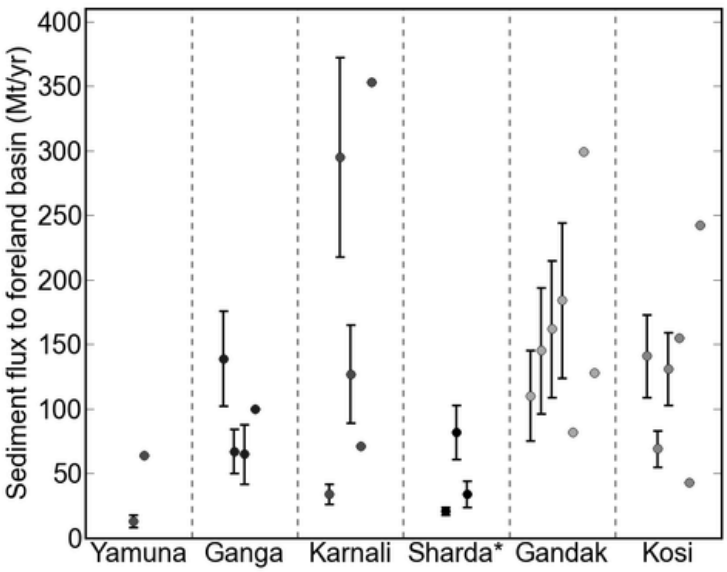

Figure 2.3: Sediment flux estimates derived from cosmogenic ^{10}Be concentrations (and errors) and suspended sediment concentrations. (*) Where no data were available for the Sharda catchment, catchment-averaged erosion rates derived from the adjacent Karnali catchment (from Lupker *et al.*, 2012) were used to calculate sediment flux estimates.

well documented wells with good stratigraphic resolution [Allen and Allen, 2013], but these types of data are not available for this region [Burbank *et al.*, 1996]. Therefore, for this study, we calculate the tectonic forcing of subsidence using the depth to the crystalline basement that underlies the Siwalik succession derived from the Seismotectonic Atlas of India, prepared by the Geological Survey of India [Narula *et al.*, 2000], integrated with the local convergence velocities [Sinclair and Naylor, 2012].

Grain size data from the principal Himalayan rivers are not available, and are therefore a key component of the new data presented in this study. We note that detailed downstream grain size fining trends have been analysed from smaller Himalayan rivers [Dubille and Lavé, 2015] that drain the foothills termed Piedmont Rivers [Sinha and Friend, 1994]. The grain size data show a clear transition from gravel to sand in the rivers at approximately 8-20 km from the

mountain front. Given the order of magnitude increase in catchment size and likely sediment supply from the larger rivers that drain the high mountains of the Himalaya, it is reasonable to predict an increase in distance from the mountain front to the gravel-sand transition for the main rivers presented here.

2.3 Regional context

The Himalayan foreland basin formed as a result of the ongoing collision between the Indian and Eurasian plates, where crustal thickening generates high topography that is supported by the flexural rigidity of the underlying lithosphere [Lyon-Caen and Molnar, 1985; Flemings and Jordan, 1989; Burbank and Beck, 1991; Burbank, 1992; Brozovic and Burbank, 2000]. Along the strike of the mountain range, variations in lithospheric rigidity and basement faulting are believed to have modulated both basin width and large-scale patterns of subsidence [Burbank *et al.*, 1996]. The Himalayan orogen is split into four major structural units that run broadly parallel from west to east (Figure 2.1). These units are from south to north: the Neogene Siwalik Group, the Proterozoic Lesser Himalayan Sequence, the Proterozoic-Ordovician Greater Himalayan Crystalline Complex and the Proterozoic to Eocene Tethyan Himalayan Sequence [Yin, 2006]. These lithological units are bound by major faults, the most active of which is the Main Frontal Thrust (MFT). The MFT is the most southerly structure, situated between the Siwalik Group and the foreland basin, and absorbs approximately 80% of the $\sim$21$\pm$1.5 mm/yr convergence) between India and south Tibet in central Nepal [Lavé and Avouac, 2000].

Sediment generated by the erosion of the Himalayan mountain range accumulates in the foreland basin. The thickness of the basin fill reduces progressively with distance from the mountain front, consistent with asymmetric subsidence caused

by thrusting of the overlying orogen [Burbank and Beck, 1991; Burbank, 1992; Yin, 2006]. The basin fill is dominated by the Neogene Siwalik Group and the pre-Miocene Rawalpindi Group [Burbank *et al.*, 1996]. The Siwalik Group comprises thick molasse deposits formed by the erosional products of the Lesser and Higher Himalaya (for example Kumar *et al.*, 2004). Thin-skinned tectonics associated with the MFT have incorporated these poorly consolidated molasse deposits in the hanging wall of frontal structures, forming the Siwalik Hills which represent the youngest and southernmost topography of the Himalaya [Mugnier *et al.*, 1999]. The foredeep basin (*sensu* DeCelles and Giles, 1996) lies immediately south of the Siwalik Hills, forming the Indo-Gangetic Plain. Immediately inboard of the thrust front are several wedge-top basins, locally termed Duns that act to buffer the sediment delivery to the foredeep [Densmore *et al.*, 2016]. In comparison to the confined bedrock channel both upstream and downstream of the Dun, the laterally unconfined and lower gradient surface of these Dun valleys has promoted sediment deposition during periods of heightened sediment export from the mountains, producing a thick alluvial valley fill. Dun valleys of direct relevance to this study are the Chitwan and Dehra Dun valleys where the Gandak, Ganga and Yamuna rivers flow through prior to passing the MFT and exiting onto the Plain (Figure 2.1).

The Ganga Plain (and henceforth Plain) forms the central third of the Indo-Gangetic Plain and covers an area of 250,000 km^2, whilst the drainage area of the entire Ganga basin is in excess of 1,060,000 km^2 [Singh, 1996]. The hydrology of rivers draining the basin is dominated by the Indian Summer Monsoon (ISM), when over 85% of the annual rainfall falls between June and September [Sinha and Friend, 1994; Tandon *et al.*, 2006], producing broad peaked annual hydrographs. Along strike gradients in precipitation have been identified using passive microwave data [Bookhagen *et al.*, 2005; Anders *et al.*, 2006] where catchments in the east typically experience more Indian summer

monsoon precipitation than those in the west. A strong north-south precipitation gradient has also been identified as a result of orographic enhancement of precipitation, where the heaviest rainfall is induced by the first significant topography encountered by southerly air masses originating from the Bay of Bengal [Bookhagen *et al.*, 2005; Bookhagen and Burbank, 2006; Anders *et al.*, 2006]. Apatite fission track ages from across the entire Himalaya do not reveal any systematic change in exhumation rates along the strike of the range [Thiede and Ehlers, 2013].

Sediment carried into the foreland basin that is not immediately deposited, typically sand and finer material, can continue downstream via the Ganga, Brahmaputra and Indus rivers ultimately reaching the sea where it accumulates in the Bengal and Indus fans. This fraction represents up to ∼90% of the total sediment load exported from the Himalaya [Lupker *et al.*, 2011]. Sediment trapped within the foreland basin is deposited across vast alluvial fans that are separated by broad interfan or interfluve areas that are drained by foothill or Plain fed rivers [Jain and Sinha, 2003; Sinha *et al.*, 2005]. These interfan parts of the basin are filled primarily with sediments eroded from the frontal Siwalik range, and sediments derived and reworked locally from the Plain [Sinha *et al.*, 2005].

The rivers feeding the Plain can be divided into mountain, foothill and Plain fed [Sinha and Friend, 1994]. Mountain-fed rivers originate from large source areas within the Himalayan orogen, typically with a glacial source. Foothill or piedmont rivers have relatively small catchment areas of 20-2500 km^2 [Dubille and Lavé, 2015] and drain the interfluve region between alluvial fans created by sediment deposition of the much larger mountain fed rivers. Plain fed rivers repetitively rework sediment deposited by the mountain and foothill fed rivers [Sinha *et al.*, 2005]. Grain size measurements in central Nepal across a number of interfan or foothill fed channels have documented a rapid gravel-sand transition occurring ∼8-20 km downstream of the mountain front [Dubille and Lavé, 2015]. This same

rapid transition is consistent with vertical grain size measurements taken from the Siwalik molasse exposed in the frontal Himalayan folds [Dubille and Lavé, 2015]. Grain size fining rates have not been documented for the mountain fed rivers.

2.4 Methods

2.4.1 Topographic analysis

Effective mapping of channel elevations relative to their adjacent alluvial fan surface reveals spatial variations in both aggradation and incision of active fluvial systems. Existing approaches to identify regions where channels are perched above their adjacent floodplain, or ′super-elevated′ [Bryant *et al.*, 1995], are typically limited to linear elevation transects across target alluvial fans using digital elevation models (DEMs) (for example Sinha *et al.*, 2005; Chakraborty *et al.*, 2010; Chakraborty and Ghosh, 2010). A number of limitations arise from this approach: (i) the approach is limited in its spatial resolution as each transect only records elevation across a small portion of the fan, which may not necessarily be coincident with areas of highest avulsion risk; (ii) the orientation of the transects does not directly reflect the geometry of either the channel or fan system; (iii) differentiating data noise from geomorphic features such as channel levees that are often comparable in amplitude [Chakraborty *et al.*, 2010], requiring significant degrees of smoothing to pick out first order features of the alluvial fan system [Chakraborty and Ghosh, 2010]. Sinha *et al.* [2014b] addressed the first of these issues by taking a series of profiles following parallel linear transects at 2 km spacing down the Kosi fan, permitting an assessment of changes in channel super-elevation along the length of the alluvial fan; however, the spatial resolution is still limited to the transects themselves, and suffers from the same problems relating to transect orientation and noise outlined above. Noise reduction could

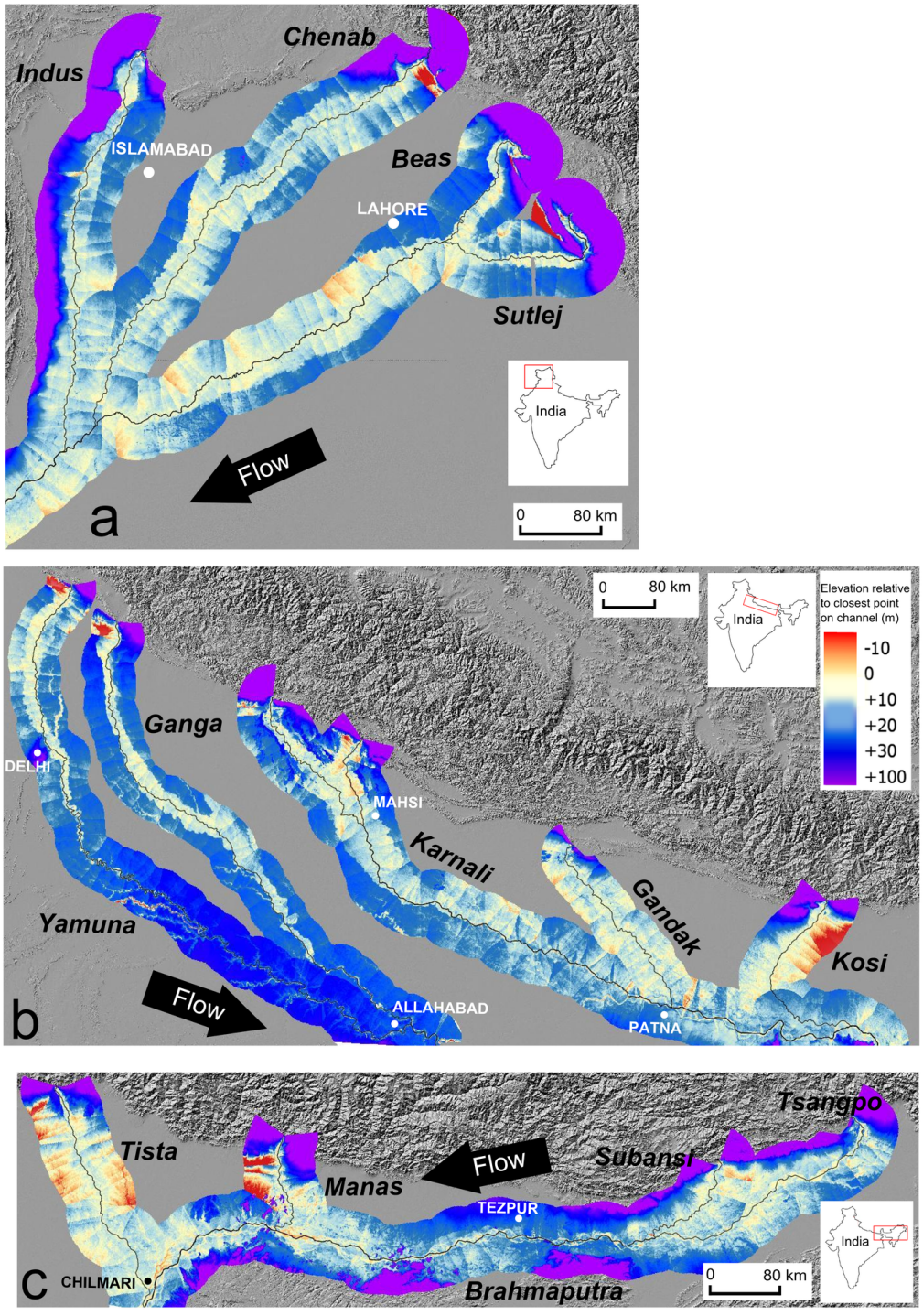

Figure 2.4: Valley topography from swath profile analysis for the three major river basins across the Himalayan foreland basin from west to east; (A) Indus (B) Ganga and (C) Brahmaputra.

potentially be achieved using swath profiles which provide a means of increasing the signal-noise ratio, and should highlight characteristics of the along-profile topography [Telbisz *et al.*, 2013; Hergarten *et al.*, 2014]. More recent generalised swath profile methods permit the use of arbitrary, non-linear baselines, such as river courses, enabling the unbiased characterisation of river valley morphology, but averaging along the length of a stream reach, reducing resolution [Hergarten *et al.*, 2014].

We present a new, spatially distributed method to map patterns of fluvial incision and aggradation across alluvial fan systems that addresses the above issues. The premise of this method is that when a channel is elevated relative to its floodplain or adjacent fan surface, the adjacent surface will lie below the elevation of the channel; when incised, the adjacent surface will have a higher elevation relative to the channel. Therefore, by mapping every location within the DEM to the closest point in the channel, it is possible to assess the relative elevation of the channel compared to the rest of the fan. In order to produce maps of channel super-elevation, we use a swath-based method, similar to that developed by Hergarten *et al.* [2014] to construct generalised swath profiles using curvi-linear baselines.

The first step in our procedure is to extract the trunk channel on the alluvial fan from the DEM. For this work, river networks were extracted from a 90 m resolution Shuttle Radar Topography Mission (SRTM) DEM using ESRI ArcMap v10.1, using a steepest-descent flow routing algorithm. Channel elevations along these river networks represent the elevation of the water surface in 2000, the time of the SRTM data capture. The root mean squared error (RMSE) of these data in mountainous regions is ± 7.75 m, while in less mountainous regions, the RMSE of the SRTM is ± 14.48 m [Amans *et al.*, 2013]. Given that the flow stage will be highly variable through the year, there may be a small impact on these results, although this is likely to be within the RMSE error of the DEM. As such, the use

of these data should provisionally be limited to the interpretation of very large scale patterns or where relief exceeds the RMSE of the data (∼±10-15 m).

These trunk channels are subsequently used as a baseline along which we generate an 80 km wide swath. This swath determines the region in which we map the relative super-elevation of the trunk channel, and in other applications can be modified for other river systems as required. Within this neighbourhood, we iterate through every pixel, p_i, and map it to the nearest point in the trunk channel baseline, following Hergarten *et al.* [2014]; DEM pixels for which the closest point on the baseline is at either of the termini are excluded. The elevation difference between the fan surface and the nearest point on the trunk channel is then calculated, with the resultant swath revealing spatial variations in the elevation of the fan surface relative to the closest point in the active channel (Figure 2.4). Negative values indicate areas of the fan that are lower in elevation to the closest point in the trunk channel (the channel is perched above the neighbouring fan surface); these areas are shaded red on the swath in Figure 2.4. Conversely, where the trunk channel is entrenched, elevations on the neighbouring fan surface are greater than the closest point in the trunk channel; the more entrenched portions of the swath are coloured in blue on Figure 2.4. Areas of the swath which are at a similar elevation to the channel are shaded in yellow, and areas more than 100 m above the channel are in purple, which typically represents mountainous topography.

Channel lengths extending from the Himalayan mountain front (defined as the most southerly area of notable relief) to the Ganga trunk stream were extracted for each river. Longitudinal profiles of each river were also extracted from the DEM from which slope values averaged over a 10 km moving window were then calculated. Normalised channel steepness (k_{sn}) was also calculated at the fan apex using a reference concavity of 0.5, to allow comparison of channel gradients independently of upstream catchment area [Wobus *et al.*, 2006; Allen *et al.*, 2013a].

Similar profiles were constructed from the surface of the adjacent floodplains, or valley tops where channels were entrenched in the west Ganga Plain. These profiles followed transects that were broadly parallel to the channel.

2.4.2 Basin subsidence

The distribution of sediment deposition, or the spatial apportioning of sediment sorting, at a given distance (x) can be expressed as:

$$R(x) = \frac{r}{q_s} \tag{2.1}$$

where r is the rate of sediment deposition, and q_s is sediment flux (Paola and Seal, 1995). R can be made non-dimensional such that:

$$R^*(x^*) = C_0 \frac{r(x)}{q_s(x)} L \tag{2.2}$$

where R^* is the non-dimensional function that describes the distribution of deposition, C_0 is the volumetric sediment concentration on the bed, r is the rate of sediment deposition, q_s is the sediment flux, and L is the length of the depositional stream [Paola and Seal, 1995]. Assuming that the rate of sediment deposition is controlled by the rate of tectonic subsidence, defined as $\sigma(x)$, $R^*(x^*)$ can also be expressed as:

$$R^*(x^*) = (1 - \lambda_p) L \frac{\sigma(x)}{q_s(x)} \tag{2.3}$$

where L is the length of the depositional stream, q_s (x) is the rate of decay in sediment flux downstream (L t^{-1}), λ_p is the sediment porosity and x^* is the normalised longitudinal location along a deposition system of length L [Duller *et al.*, 2010]. If R^* determines how sediment sorting is apportioned spatially,

most sorting will occur at the upstream end of the system where the greatest proportion of sediment is deposited [Duller *et al.*, 2010]. The rate of down-system grain size fining can also be described by the fractional Exner sediment mass balance [Paola and Seal, 1995], also incorporating tectonic subsidence through the R^* function:

$$\frac{df}{dx} = f[\, R^*(1 - \frac{1}{J})] \, - \frac{1}{J}\frac{dJ}{dx^*} \tag{2.4}$$

where f is the fraction of a given sediment size in the deposit and $J = p/f$, where p is the fraction of a given sediment size in the transporting system [Duller *et al.*, 2010]. This predicts a correlation between subsidence rates, sediment grain size fining rate and hence river morphology.

The methodology for calculating the tectonic forcing of subsidence of the surface near the mountain front uses new maps of the depth to crystalline basement derived from seismic data combined with known shortening rates [Stevens and Avouac, 2015]. The approach doesn't use the depth to basement, but instead utilises the gradient of the basement nearest to the mountain front [Sinclair and Naylor, 2012]. By reconstructing the gradient of the basement of the subducting slab (θ) and combining it with known convergence velocities (V_{con}) between the Ganga Plain and the Himalaya [Stevens and Avouac, 2015], we can derive the vertical velocity which determines the modern subsidence velocity at the surface (V_{sub}) at point x using:

$$V_{sub}(x) = V_{con} tan\theta(x) \tag{2.5}$$

This tectonic forcing of surface lowering (subsidence) at the mountain front remains steady as long as the following remain constant: 1) the mean distribution and magnitude of topography; 2) the density structure of the mountain range; 3) the convergence velocity between the subducting lithosphere and the distributed load of the range, and 4) the gradient of the subducting lithosphere. Within these parameters, the most likely to vary at a high spatial and temporal scale is the distribution of topography, as thrust units are accreted at the front of the

range. Analogue and numerical experiments from thrust wedges indicate that fluctuations in frontal accretion versus internal thickening of the wedge can result in punctuated topographic growth at a timescale characterised by the length of accreted thrust sheets divided by the convergence velocity [Hoth *et al.*, 2007; Naylor and Sinclair, 2007]. For the Himalayas, typical spacing of thrust units are approximately 12 km, which when divided by a mean convergence velocity of 18 km/Myr yields a timescale of probable topographic variations of 0.66 Myr.

Additionally, the rate of stratigraphic onlap of the Siwalik Group onto the basement of the foredeep is 19±5 km/Myr which is comparable to the convergence velocity, suggesting these parameters have been in steady state for the recent history of the thrust wedge and foreland basin system [Lyon-Caen and Molnar, 1985; Mugnier and Huyghe, 2006]. Based on these arguments, it is not envisaged that the tectonic forcing of subsidence has varied significantly for at least the last 100,000 years. For this study, the time interval of interest is the period over which the present morphology of the river systems of the Ganga Plains is defined; this interval may be approximated by the topographic relief of the fluvial system divided by the sediment accumulation rates. In this case, the local relief of the incised and super-elevated channel systems is up to 30 m. Holocene sedimentation rates for the proximal basin are of the order of 1 mm/yr [Sinha *et al.*, 1996]. Based on these rates, it is proposed that the time interval of interest in determining the basin surface morphology is approximately 30,000 years. Consequently, there is no reason to consider that subsidence rates have varied at any given location in the basin during the development of the present-fluvial morphology across the Ganga Plain.

The long-term ($>10^6$ yr) and recent convergent velocity between the subducting plate and the Himalayan topography can be approximated from the stratigraphy of the foreland basin, and modern GPS data respectively. As outlined above, stratigraphic sequences observed in deep well and seismic data imply convergence

rates of between ∼10-20 mm/yr over the past 15 to 20 Ma from these data [Lyon-Caen and Molnar, 1985]. Contemporary GPS data [Feldl and Bilham, 2006; Stevens and Avouac, 2015] have demonstrated along strike differences in modern India-Tibet convergence rates. Rates in the eastern Himalayan arc are typically 18-20 mm/yr compared to 12-15 mm/yr in the west. The tectonic displacement of fluvial terrace surfaces in central Nepal [Lavé and Avouac, 2000] and northwest India [Wesnousky *et al.*, 1999] further support a systematic east to west decrease in convergence rates with estimates of 21.5±1.5 mm/yr and 11.9±3.1 mm/yr, respectively.

Models calibrated against gravity data have also indicated that the flexural rigidity of the Ganga Basin varies along strike of the basin [Lyon-Caen and Molnar, 1985; Jordan and Watts, 2005]. Jordan and Watts [2005] demonstrated that the central Himalayan foreland basin, which relates to the west Ganga Plain, has a higher effective elastic thickness (∼70 km) compared to regions in the east and west (∼30-50 km).

The gradient of the basement beneath the proximal foreland basin (θ) is measured using the depth to basement plots of the Ganga basin derived from depth converted reflection seismic data (Figure 2.5 A). The dip of the basement beneath the mountain front has been calculated using the average gradient of the first 30 km of each profile basin-ward of the mountain front, thus reflecting a control on basin subsidence velocities of the proximal basin. Six cross-sections of the foreland basin have been generated from these plots and second order polynomial equations and curves have been fitted through the data to extend the cross section to a point beneath the mountain front to account for increasing rates of subsidence close to the mountain front [Sinclair and Naylor, 2012]. A range of V_{sub} values have been calculated along the course of each river using variable V_{con} values to assess the impact on V_{sub} estimates. The variable convergence rate estimates used are based on Stevens and Avouac [2015] with values of 13.3±1.7 mm/yr for the Yamuna

and Ganga, 18.5±1.8 mm/yr for the Sharda and Karnali and 20.2±1.1 mm/yr for the Kosi and Gandak. Previously mentioned convergence rate estimates from Wesnousky *et al.* [1999] and Lavé and Avouac [2000] have also been included in this analysis.

2.4.3 Grain size

Extensive coarse gravel bars dominate the bed of the major rivers of the Ganga Plain as they exit the mountain front. During the low-flow season (October-May), a considerable portion of the channel bed is accessible. If it is assumed that equal mobility conditions [Parker and Toro-Escobar, 2002] are attained during monsoon flows, allowing full reworking of gravel bar material, then the gravel deposits visible during this period should represent bedload transported and deposited during the preceding monsoon [Attal and Lavé, 2006]. Equal mobility implies that the grain size distribution of the annual transported yield is finer than that of the gravel in the armoured surface exposed at low flow, and similar to that beneath the armoured layer in the subsurface [Parker and Toro-Escobar, 2002]. Grain size measurements were taken from ∼30 to 50 km upstream of the mountain front down to the gravel-sand transition of each of the Kosi, Gandak, Sharda, Ganga and Yamuna rivers. Ideally, measurements would have been carried out at regular intervals but sampling was restricted by access and in-channel structures. Where large engineered dams (barrages) have been constructed to divert water into channels for irrigation were present, samples were taken at least 1-2 km upstream or downstream of the structure to minimise localised hydrodynamic and trapping effects, this being the distance over which the influence of the barrage appeared to dissipate.

Grain size measurements were taken of both the surface and subsurface material using photographic and volumetric analysis, respectively, to account for the effects

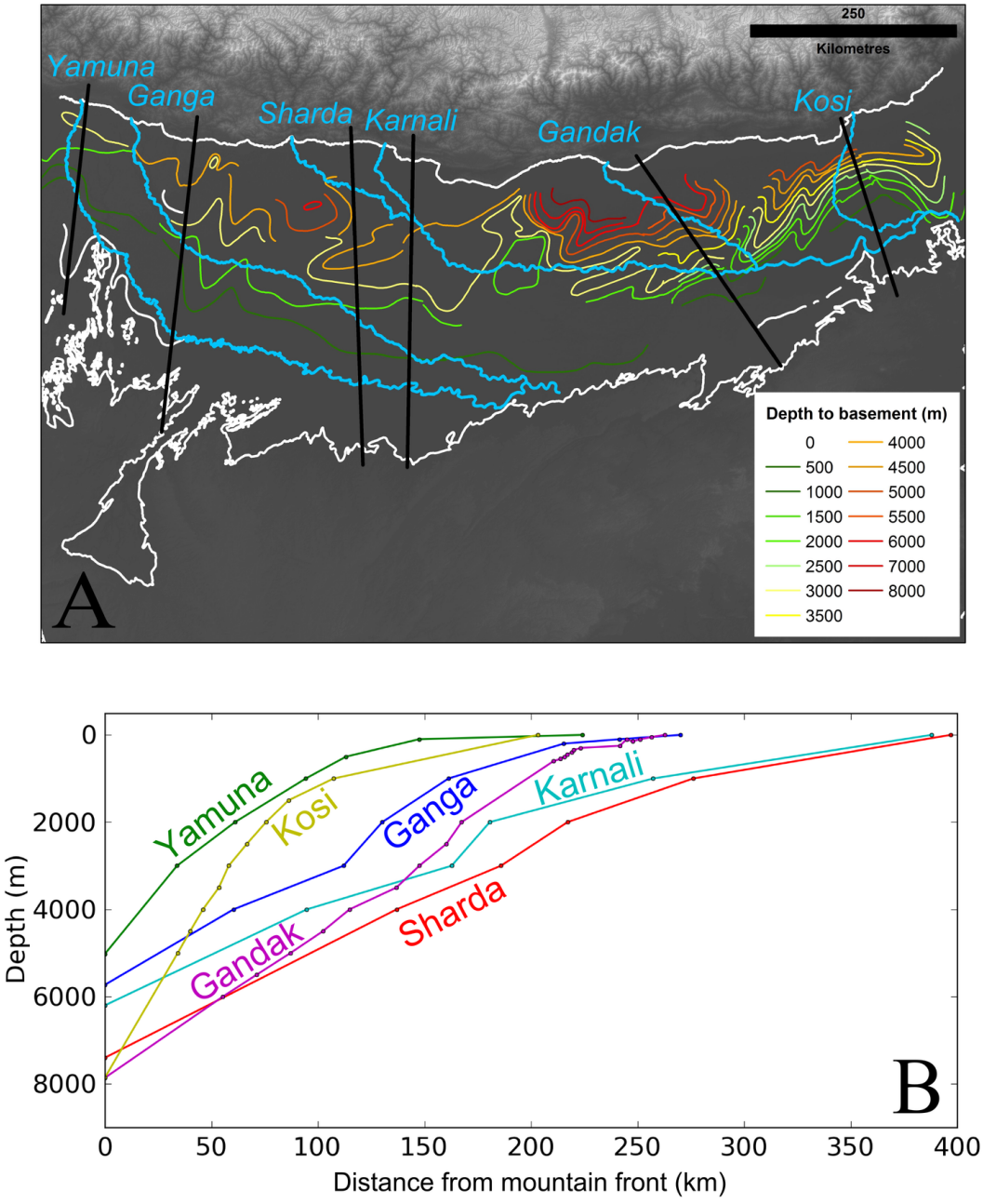

Figure 2.5: (A) Depth to basement contours across the Ganga basin showing positions of basin cross sections (black line) for each river and (B) basin profiles constructed using depth to basement contours in proximity of the Yamuna, Ganga, Sharda, Karnali, Gandak and Kosi rivers. Data sources: 90 m SRTM DEM and Geological Survey of India.

of surface coarsening [Dietrich *et al.*, 1989; Parker, 1990]. Samples were restricted to parts of the bar which appeared recently reworked with imbricated and sub-rounded to rounded gravel (clearly fluvial in origin). Gravel size variations were observed down the length of the gravel bars so sites were chosen in the centre of the coarsest fraction for consistency. At each site, 5 to 10 photos were taken of the channel bed to use for photo counting. Particle sizes were measured from each photo by overlaying a regular numeric square grid with 100 nodes, and measuring the intermediate b-axis of each pebble beneath the nodes [Attal and Lavé, 2006; Whittaker *et al.*, 2011]. Due to the coarse nature of much of the gravel bars, larger pebbles were often covered by multiple grid intersections. Consistent with the sampling method of Attal *et al.* [2015], pebbles covering n grid intersections were counted n times. This premise is based on Kellerhals and Bray [1971] analysis using a voidless cube model, although it is noted that this method results in over estimation of D_{84} values [Attal *et al.*, 2015]. Results from each photo at a given site were combined to create a single grain size distribution at each sampling location.

Volumetric subsurface measurements were taken using techniques documented by a number of studies [Attal and Lavé, 2006; Whittaker *et al.*, 2010; Dubille and Lavé, 2015]. Surface material was first removed from the site location (to a depth equal to the size of the largest pebble) and 100-300 kg of material was excavated and sieved through a series of 1, 2 and 4 cm square mesh sieves. Pebbles larger than 8 cm were individually weighed, and the weight of each fraction was recorded. For pebbles with b-axis greater than 8 cm, a representative diameter was calculated by assuming that the pebble was roughly spherical and had a density of 2650 kg m^{-3} [Whittaker *et al.*, 2010]. A well-mixed representative sample of $\sim$1 kg of the fraction $<$ 1 cm was sieved using a 1 mm sieve, from which a ratio was calculated and applied to the whole $<$1 cm fraction.

The presence of boulders on some gravel bars meant that the recommendation

that the largest clast represents $< 5\%$ of the sample mass was not always fulfilled [Church *et al.*, 1987]. For both surface and subsurface measurements, the effects of excessively large pebbles on D_{84} and D_{50} measurements was assessed using the same method outlined in Attal *et al.* [2015]. This process involves the removal of the largest clast from the distribution and recalculating the D_{84} and D_{50} values. This process was then repeated but with the addition of a large clast, similar in mass to the largest clast recorded within that sample. The recalculated D_{84} and D_{50} values with the removal or addition of the largest clast are plotted as upper and lower error bars on subsurface volumetric samples. Due to the large number of measurements obtained for each surface sample, following the same procedure on surface grain size distributions produced minimal variation ($< 5\%$) in D_{84} and D_{50} values. Instead, a more conservative approach was taken, as outlined in Whittaker *et al.* [2011], where an error margin of $\pm 15\%$ was applied to account for subjective bias when measuring the intermediate axis of each pebble beneath the grid node. This margin of 15% was estimated by Whittaker *et al.* [2011] based on the differences in grain size distribution from repeat sampling of the same photo.

The position of the gravel-sand transition was also mapped for each river, by noting the point at which exposed deposits were near exclusively sand ($> 95\%$). In some instances, small patches of gravels were present but represented a very small proportion ($\sim$ 1-5 %) of the bed fraction based on visual observations.

Downstream fining rates of the gravel fraction along each river were calculated using Sternberg's exponential function of the form:

$$D_x = D_0 e^{-\alpha x} \tag{2.6}$$

where D_0 is the predicted input or initial characteristic grain size in the system (such as D_{84}), α is the downstream fining exponent and x is the distance downstream [Sternberg, 1875]. Linear functions have also been fitted to account

for alternative fining patterns observed in the literature [Rice, 1999; Whittaker *et al.*, 2011] :

$$D_x = D_0 - \beta x \tag{2.7}$$

where β is the dimensionless fining rate (grain size reduction/km). The two key processes that are commonly seen to control downstream fining rates in fluvial systems are (1) the selective transport and deposition of particles and (2) abrasion of particles where larger particles are broken down by mechanical processes [Paola *et al.*, 1992b,a; Ferguson *et al.*, 1996; Rice and Church, 2001; Attal and Lavé, 2006; Fedele and Paola, 2007; Duller *et al.*, 2010]. The effect of pebble abrasion is considered negligible in this instance, as the lithology of gravel bars in all rivers was dominantly quartzite, suggesting that grain size fining by abrasion is likely to be similar across all systems. Any differences in grain size fining will likely reflect spatial variations in the grain size distribution of sediment delivered to the Plain from the Himalaya, sediment flux, the spatial distribution of basin subsidence, and local hydraulic and topographic effects [Paola *et al.*, 1992a; Robinson and Slingerland, 1998; Fedele and Paola, 2007; Duller *et al.*, 2010; Whittaker *et al.*, 2011].

2.5 Results

2.5.1 Topographic analysis

Along the strike of the mountain front, results of the swath profile analysis are consistent with previous findings [Gibling *et al.*, 2005; Sinha *et al.*, 2005; Sinha, 2005] where the degree of channel entrenchment was found to increase from east to west (Figure 2.4). In the far west of the Ganga Plain, both the Yamuna and Ganga rivers are clearly entrenched within well-defined broad valleys that are

incised into the surface of their respective alluvial fans. These incised valleys narrow with distance downstream of the mountain front from ∼20 km to < 1 km at a point immediately upstream of the Ganga and Yamuna confluence at Allahabad (Figure 2.4 B). Close to the mountain front, the valley sides are ∼30 m high and reduce to 10-20 m by ∼80 km downstream. Lateral incision into valley walls by large meander loops are clearly preserved in the lower half of the Ganga River. The Sharda and Karnali rivers converge at Mahsi, ∼100 km downstream of the mountain front, to form the Karnali system which is also known as the Ghaghara River in India (Figure 2.4 B). Both tributaries of the Karnali River flow down a well-defined incised valley up to 40 km in width. Downstream of the Sharda and Karnali confluence, the river course turns more sharply to the east and the incised valley loses definition as the degree of entrenchment into the fan surface is reduced. Much of the surrounding floodplain is of a comparable elevation (within 10 m) to the active channel here. Further east, the Gandak and Kosi rivers show minimal signs of entrenchment on the surface of their respective alluvial fans. Much of the surrounding floodplain is of a similar or lower elevation, most notably on the Kosi River [Chakraborty *et al.*, 2010; Sinha *et al.*, 2013, 2014b].

The Kosi channel currently occupies the western margin of its alluvial fan where the channel bed is marginally elevated with respect to the surface of the central area of the fan. This pattern is most apparent in the upper ∼80 km of the fan where much of the floodplain on the east bank is relatively lower in elevation, in some cases by up to nearly 10 m, than the active channel (Figure 2.4 A). Whilst still within the RMSE of the DEM, this observation appear consistent with independent observations. In 2008 the Kosi River breached its eastern embankment at Kusaha, Nepal [Sinha, 2009; Chakraborty *et al.*, 2010]. Much of the avulsion belt occupied the depressed area identified as lower in elevation in the SRTM data that were captured several years earlier in 2000. For the

remaining length of the fan, the Kosi channel sits at a very similar elevation to that of the fan surface. This west to east gradient also extends beyond the Ganga Basin into the wider Indo Gangetic Plain. East of the Ganga Plain, tributaries of the Brahmaputra River appear similar in nature to the Gandak and Kosi rivers where channels are either at a similar elevation or marginally super-elevated relative to their surrounding floodplain (Figure 2.4 C). Further west, rivers in the Indus basin show similar characteristics to those in the west Ganga Plain where active channels are laterally constrained in broad incised valleys (Figure 2.4 A). Unlike the Ganga Plain however, these valleys widen with distance downstream and the degree of entrenchment appears lower at 10-20 m. This is interpreted as a contrast in dominant controls on channel morphology between the Indus and Ganga basins. Longitudinal river profiles and 10 km averaged slope values extracted from SRTM data show that the Yamuna, Sharda and Karnali rivers exhibit elevated slope values relative to rivers further east within the first 40 km downstream of the mountain front (Figure 2.6). The Ganga however appears to exit the mountain front with a marginally lower gradient than the other west and central Ganga Plain rivers. In the east Ganga Plain the Gandak and Kosi rivers are lower in gradient, with maximum values of ∼0.0015 m/m in the first 10 km, rapidly decreasing to ∼0.0005 m/m by 20 km downstream of the mountain front. The Kosi maintains a more consistent and initially lower gradient down the length of its fan, attaining a maximum value of ∼0.001 m/m. By 40 km downstream, all of the channel gradients converge at ∼0.0005 m/m and fluctuate between 0-0.001 m/m for the remainder of the profile (Figure 2.6). By normalising channel gradient for upstream catchment area (k_{sn}), similar patterns are displayed where systems in the west and central Ganga Plain are typically steeper at the fan apex, with k_{sn} values of 200-300 (Figure 2.6). Whilst both 10 km averaged slope and k_{sn} values appear to be influenced by some noise along the first 10 km of the Gandak

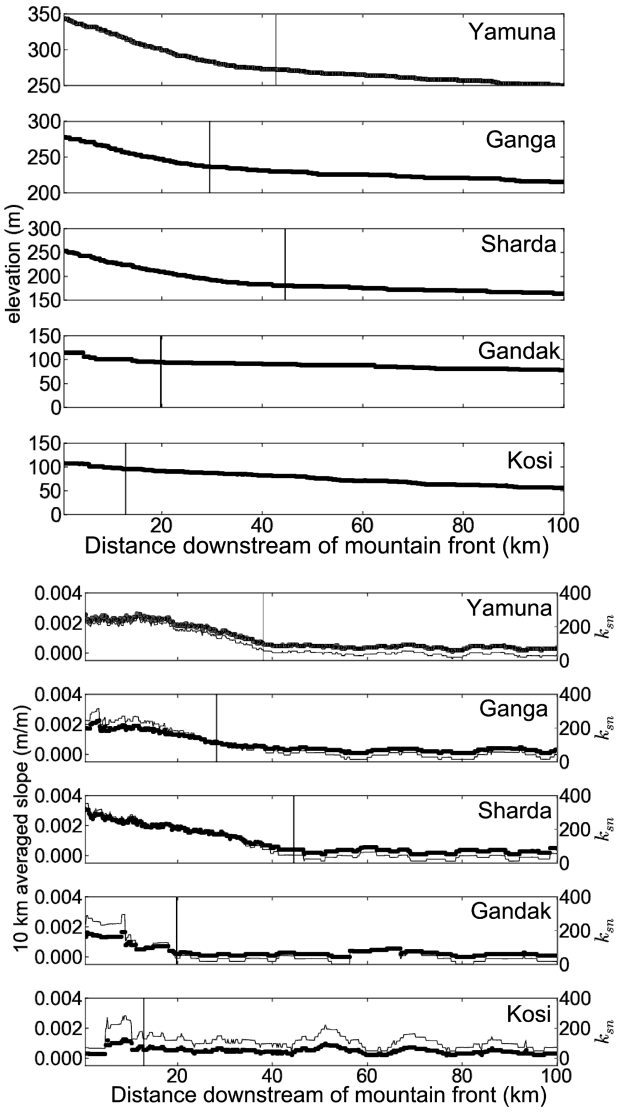

Figure 2.6: Longitudinal profiles, 10 km averaged slope and normalised channel steepness (k_{sn}) values for major tributaries of the Ganga basin. k_{sn} values are shown by the thinner black line on the slope plots. Vertical lines represent the position of the mapped gravel-sand transition.

and Kosi profiles, k_{sn} values in the east Ganga Plain appear slightly lower (150-250). With the exception of noise in the Gandak profile, there were no evident knickpoints that were larger in magnitude than the RMSE (∼15 m) of the data.

Comparing the average gradient of the Ganga and Kosi channels to their adjacent fan surfaces, it can be seen that the Ganga fan surface is steeper than the active channel (Figure 2.7). This is more pronounced at the fan apex where the degree of channel entrenchment is also greatest. In contrast, the surface gradient of the Kosi fan is comparable to the gradient of the active channel, and an absence of significant channel entrenchment is also clearly highlighted.

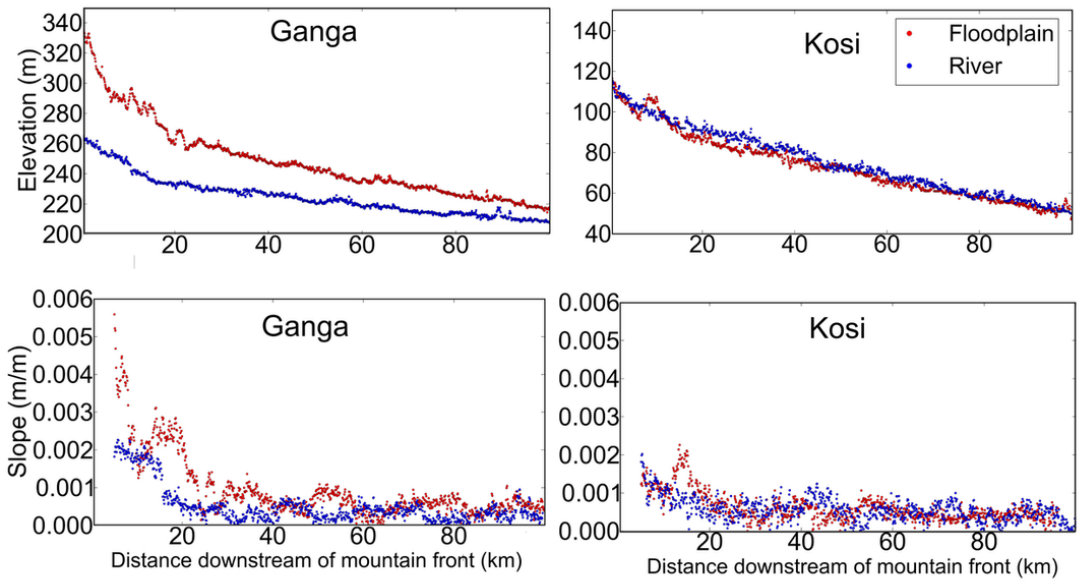

Figure 2.7: Absolute elevation and 10 km averaged slope values of the modern Ganga and Kosi channels and their adjacent fan surfaces at the fan apex. Fan surface profiles followed transects that were broadly parallel to the channel, either from the top of the valley side where channels were entrenched or within ∼5 km of the modern channel.

2.5.2 Basin subsidence

The depth to basement plots (Figure 2.5 B) demonstrate an along strike variation in the geometry of the Ganga basin, as has also been recognised previously by Singh [1996]. In the east Ganga Plain, the basin is deeper (5000-6000 m) and relatively narrow at ∼200 km. The basement has a steep or even convex, distal edge. Further west, the basin widens beneath the Sharda and Karnali rivers. Generally, the basin is shallower here but there are isolated basement lows such as on the Sharda section where the basin reaches 6000 m near to the mountain front. In the far west, the basin is notably shallower at 3000-4000 m and again narrows to ∼200 km wide. These variations in depth to basement at the mountain front broadly correlate with the variations in flexural rigidity of the downgoing lithosphere [Jordan and Watts, 2005], with lower rigidities correlating with greater basin depth at the mountain front.

Results indicate that the highest average subsidence velocities (V_{sub}) at the mountain front are located in the east of the region near the Kosi fan, with rates of 1.6±0.6 mm/yr. Further west average subsidence rates decrease to 1.4±0.4 mm/yr beneath the Gandak, 0.4±0.2 mm/yr beneath the Karnali, 0.8±0.2 mm/yr beneath the Ganga, and 0.3±0.4 mm/yr beneath the Yamuna. V_{sub} estimates are generally comparable across all but the Kosi and Gandak systems which are notably higher. When these calculated subsidence estimates are compared to documented short term sedimentation rates across the Ganga Plain, values are comparable. An average sedimentation rate of ∼0.08 (± 0.19) mm/yr for the entire Ganga floodplain has been calculated from chemical mass balance equations [Lupker *et al.*, 2011]. Sedimentation rates would be expected to increase exponentially from the cratonic to orogenic margin of the basin however [Flemings and Jordan, 1989], which is consistent with sedimentation rates documented closer to the mountain front. Sedimentation rates of 0.62-1.45 mm/yr have

been calculated from radiocarbon dating of organic material in northern Bihar upstream of the axial Ganga channel between the Kosi and Gandak rivers, averaged over a time period of 700-2500 yr [Sinha *et al.*, 1996]. The comparison of calculated long term subsidence rates of 1.6±0.6 mm/yr beneath the Kosi fan with the short term sedimentation rates of 0.62-1.45 mm/yr suggest the system is broadly in balance, with subsidence slightly outpacing sediment accumulation in this part of the basin.

2.5.3 Grain size

Grain size distributions from sites closest to the mountain front have been compared across each of the sampled channels and are found to be comparable between systems (Figure 2.8). Subsurface grain sizes documented close to the mountain front on the Yamuna are generally finer than other sites, where a D_{84} value of 66 mm was recorded compared to values ranging between 146-248 mm for the Kosi, Sharda and Ganga. This is attributed to the upstream barrage near Faizabad (∼3 km upstream). Compared to similar barrages located close to the mountain front on the Ganga, Sharda and Gandak rivers, a much larger proportion of flow is diverted into extensive canal networks at the Yamuna barrage, resulting in severely reduced flows downstream in the natural channel. During low flow conditions, parts of the Yamuna channel are entirely dry. It seems reasonable to interpret that a greater proportion of coarser material is trapped upstream or very close to the barrage, where there is insufficient discharge to rework or mobilise the coarsest fraction. The D_{84} of the subsurface Gandak sample was also found to be relatively fine (83 mm) compared to the Kosi, Sharda and Ganga samples, which is likely a function of the upstream Chitwan Dun. The coarse fraction of the sediment load is likely to be deposited at the upstream edge of the Dun, where bedrock channels emerge onto the low gradient alluvial surface

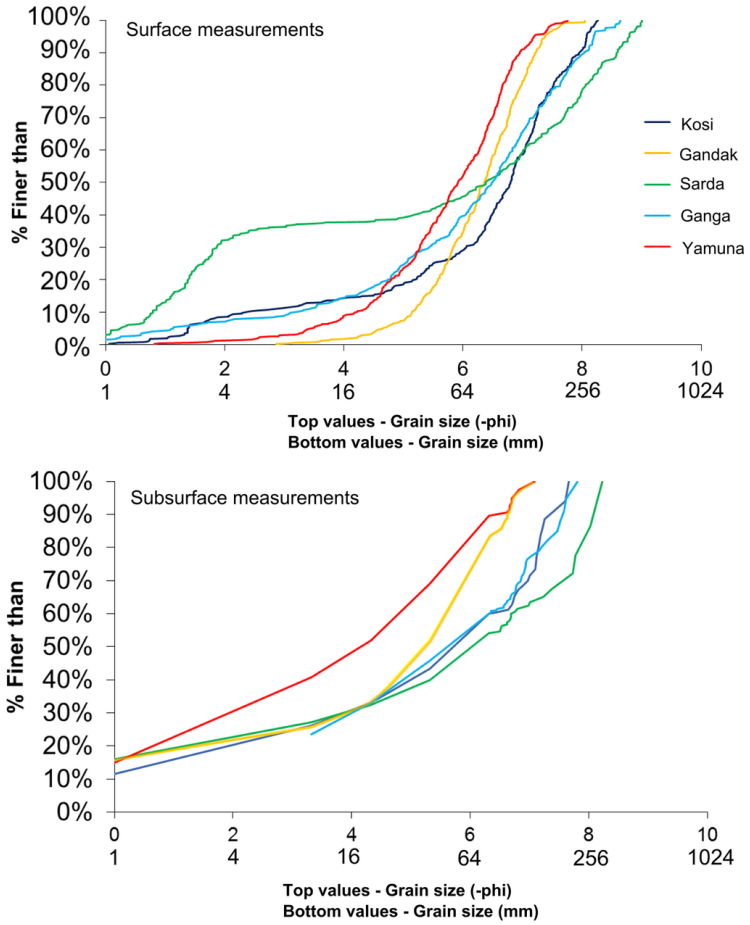

Figure 2.8: Surface and subsurface grain size distributions of gravel bar sediment at the mountain outlet of each river.

of the Dun. This is consistent with grain size measurements taken within the Dun which show an overall fining and narrowing of the grain size distributions (Figure 2.9), where the main source of sediment into the channel is restricted to seasonal inputs by ephemeral channels draining the surface of piedmont alluvial fans comprised of Upper Siwalik Group conglomerates [Kimura, 1999; Densmore *et al.*, 2016]. Hillslope processes are largely absent in these piedmont catchments where the primary source of sediment is from recycled Siwalik deposits, resulting in a much narrower input grain size distribution into the main Gandak channel. Subsurface D_{84} and D_{50} values measured on the Gandak within the Chitwan Dun vary by ∼50 mm, compared to values of 100-200 mm upstream of the Dun (Figure 2.9). In general, there is a strong correlation between subsurface and surface grain

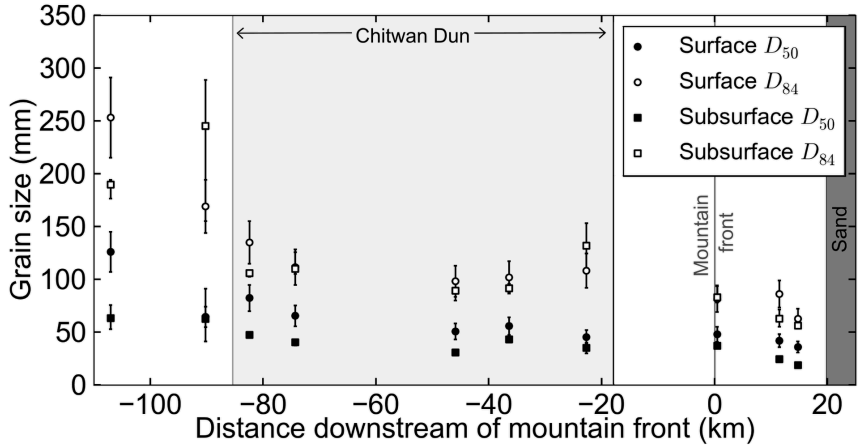

Figure 2.9: D_{84} and D_{50} values along the Gandak River. A notable fining and overall narrowing of the grain size distribution is visible as the channel enters the Chitwan Dun, resulting in a much narrower grain size distribution being transported in the Ganga Plain.

size measurements in terms of relative change between values down each profile. Whilst there is a clear surface coarsening visible, local changes in subsurface grain size are also reflected in surface grain size measurements, adding confidence to this sampling approach. This trend is more apparent in the coarser (D_{84}) fraction of the sediment load (Figure 2.10). The position of the gravel-sand transition and downstream fining rates in each channel shows a considerable west to east

variation (Figure 2.11), irrespective of the grain size distribution of the supplied sediment (Figure 2.8). The mapped position of the gravel-sand transition relative

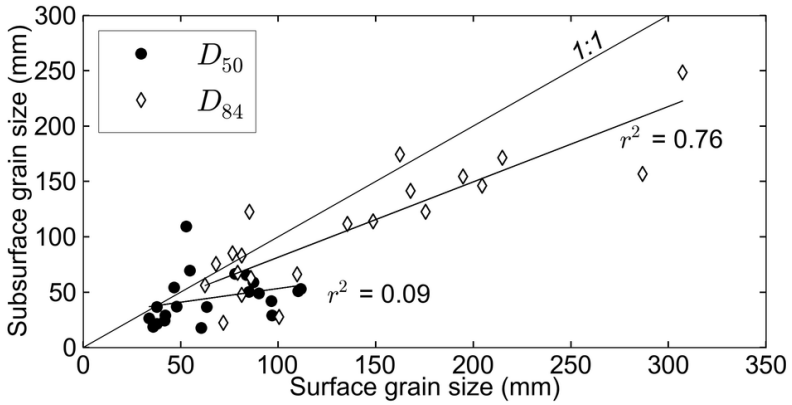

Figure 2.10: Comparison of surface and subsurface measrements for the D_{84} (diamonds) and D_{50} (circles) values at each site across the Ganga Plain. There is a much stronger correlation between surface and subsurface values in the D_{84} values than D_{50}.

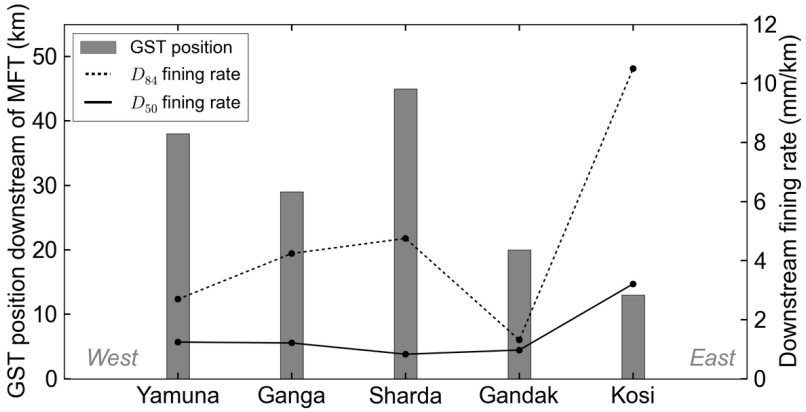

Figure 2.11: Downstream distance from the mountain front (MFT) to the gravel-sand transition (GST) and linear model fining rates on averaged surface and subsurface D_{84} (dashed line) and D_{50} (solid line) grain sizes.

to the mountain front on each river suggests that gravel progrades further into the basin for rivers in the central and west Ganga Plain (Figure 2.11). For the Gandak and Kosi rivers in the east Ganga Plain, the gravel-sand transition was documented within 20 km downstream of the mountain front. The gravel-sand

transition observed at the Yamuna, Ganga and Sharda rivers was notably further downstream at ∼38, 28 and 45 km respectively. The gravel-sand transition was also not found to be an abrupt transition; in most instances a zone of ∼2-5 km was noted where the bed was predominantly sand but large patches (up to 25% of the total bed fraction) of gravels were present, although these patches reduced in extent downstream. The position of the gravel-sand transition relative to long channel profiles (Figure 2.6) is coincident with a break in channel slope, where a steeper channel gradient exists upstream of the transition. This break in slope is less apparent in the east Ganga Plain on the Gandak and Kosi profiles, which may be explained by the noise in the DEM from which the long channel profiles were extracted. It seems more probable that any change in gradient associated with the gravel-sand transition is not as pronounced in the east Ganga Plain due to the gradients of these channels being lower overall. Upstream of the gravel-sand transition on the Sharda, Ganga and Yamuna, channel gradient and the absolute elevation of channels exiting the mountain front are also greater than for the Gandak and Kosi (Figure 2.12). Fining rates were generally comparable across the Yamuna, Ganga and Sharda rivers (Table 2.2 and Figure 2.13). For each site, r^2 values determined using each model were also near identical suggesting that the rate of exponential decay is very low (Table 2.2). Using the linear decay model, fining rates of 1.31-4.75 mm/km were observed for D_{84} values across the Yamuna, Ganga, Sharda and Gandak channels whilst a rate of 10.5 mm/km was obtained for the Kosi (Figure 2.11). This same increase in fining rate is also apparent in the D_{50} fraction, where rates increase from 0.83-1.24 mm/km across systems in the west and central Plain, to 3.21 mm/km along the Kosi. Comparable spatial differences in fining exponents (α) obtained from the exponential model were also found and are presented in Table 2.2. The relatively low fining exponent on the D_{84} fraction of the Gandak is likely to reflect upstream deposition of the coarsest fraction of the sediment load within the Chitwan Dun. As previously discussed, the grain size distribution exiting the Dun is much narrower (that is the D_{84} and

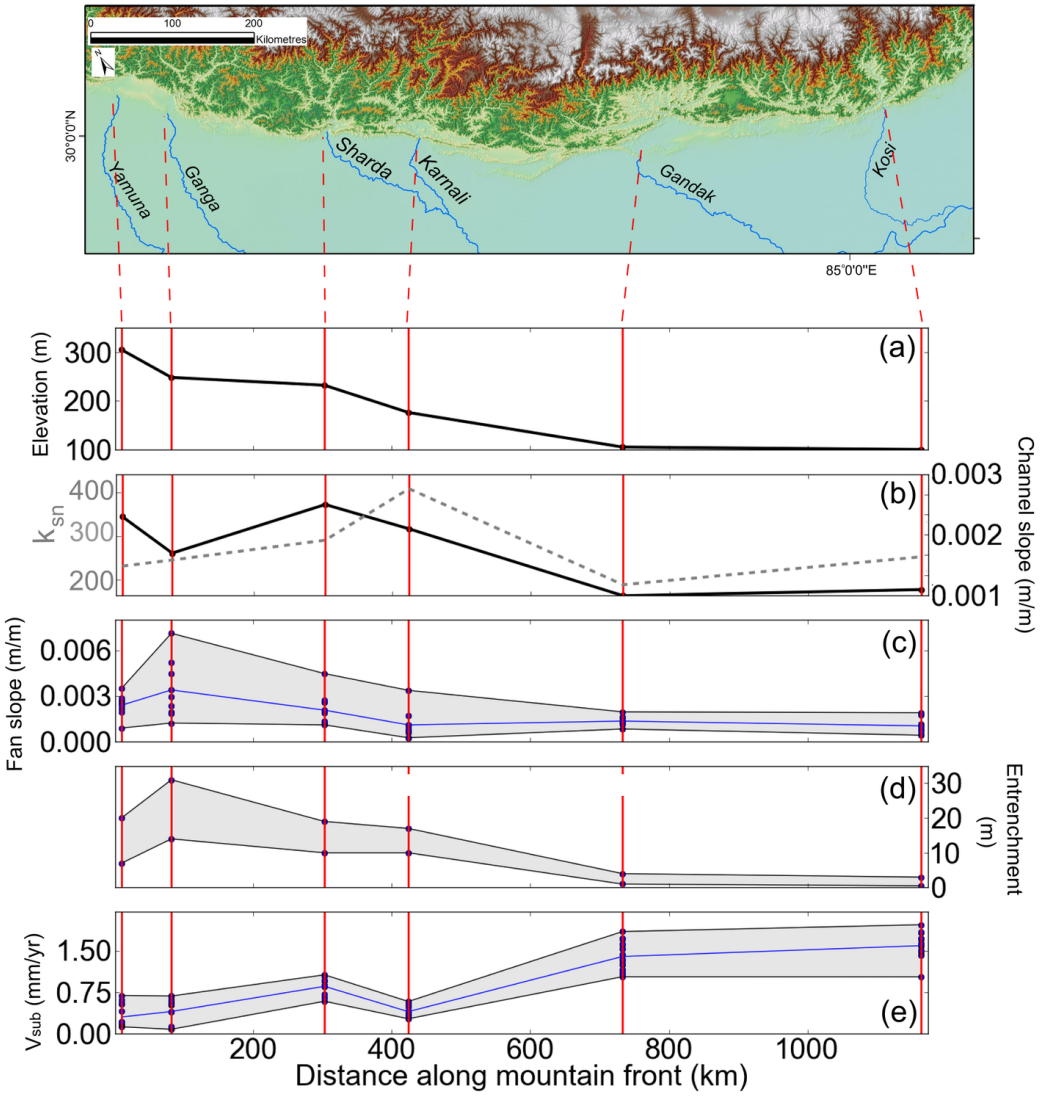

Figure 2.12: Lateral variations in (A) outlet elevation, (B) 10 km average channel gradient and normalised channel steepness (k_{sn}) at the fan apex and (C) proximal fan apex slopes, (D) channel entrenchment at the fan apex and (E) calculated subsidence velocity (V_{sub}) beneath the proximal foreland basin across the Ganga Plain.

D_{50} values are quite similar) on the Gandak relative to other systems (Figure 2.9). The D_{84} and D_{50} values are also lower than comparable sites at the mountain front in other systems.

Table 2.2: D_{50} and D_{84} grain size fining rate data using both exponential and linear equations

	Exponential fit				*Linear fit*			
River	D_{84} α (km^{-1})	r^2	D_{50} α (km^{-1})	r^2	D_{84} β (mm/km)	r^2	D_{50} β (mm/km)	r^2
Yamuna	0.024	0.53	0.025	0.31	2.69	0.54	1.24	0.40
Ganga	0.032	0.81	0.022	0.20	4.24	0.80	1.21	0.15
Sharda	0.033	0.59	0.016	0.19	4.75	0.57	0.83	0.22
Gandak	0.019	0.52	0.031	0.36	1.31	0.50	0.97	0.38
Kosi	0.062	0.37	0.052	0.18	10.5	0.36	3.21	0.18

2.6 Discussion

Topographic analysis of the west Ganga Plain has highlighted the degree of channel entrenchment in the surface of the Yamuna and Ganga fans, compared to the relatively subdued surfaces of the Gandak and Kosi fans further east. Subsidence velocity estimates and downstream grain size fining rates have been found to be highest in the east Ganga Plain, where fan gradients are typically less steep and the gravel-sand transition is found closer to the mountain front. In the west Ganga Plain, the basement depth of the basin is notably lower than the east Ganga Plain, which when combined with known convergence velocities, suggests that the west Ganga Plain is subsiding less rapidly. Assuming basement gradient and convergence velocity yield a reasonable proxy for recent subsidence rates, then clear along strike variations in subsidence rate exist across the Ganga basin. These variations arise from differences in the elastic thickness of the underlying

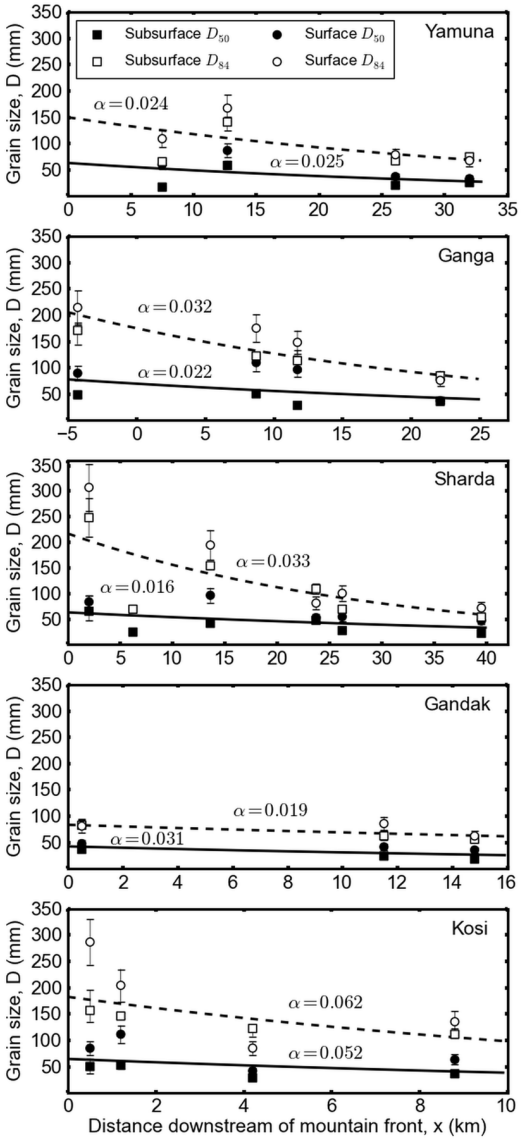

Figure 2.13: Evolution of sediment grain size on gravel bars. Downstream fining exponents (α) for surface and subsurface averaged $D_{84}$and D_{50} values downstream of the mountain front for the Yamuna, Ganga, Sharda, Gandak and Kosi rivers. Error bars were calculated for surface samples by applying a $\pm 15\%$ error margin to account for subjective bias. Error margins on subsurface samples reflect the effects of the addition and removal of large clasts from the sample on D_{84} and D_{50} measurements. It should be noted that the scale of the horizontal axis is changing between plots.

lithosphere [Lyon-Caen and Molnar, 1983, 1985; Jordan and Watts, 2005; Jackson *et al.*, 2008] and/or local inherited morphological variations in the underthrust Indian basement (for example Lash, 1988) combined with varying convergent velocities. This is also consistent with published modelling results that have suggested the equivalent elastic thickness of the lithosphere is lower beneath the east Ganga Plain than the west [Jordan and Watts, 2005]. This then raises the question of how, or whether, spatially variable subsidence can be expressed in the surface morphology of the Ganga Plain.

2.6.1 What are the time-scales of the controlling processes?

Various modelling studies have suggested that the relative impact of increased and decreased subsidence rates, sediment flux, water supply and gravel fraction on basin stratigraphy/response is strongly dependent on the timescale over which these variations occur (for example Paola *et al.*, 1992a; Heller and Paola, 1996; Duller *et al.*, 2010). To determine whether a forcing is slow or rapid, an equilibrium response time (T_{eq}) is calculated using the square of the basin length divided by the basin diffusivity [Paola *et al.*, 1992a]. For the Himalayan foreland basin, a T_{eq} of 2 Myr ($\pm$1 Myr) has been calculated [Heller and Paola, 1992]. Variations in parameters that occur over a timescale lower than T_{eq} are subsequently termed as rapid, and those higher than T_{eq} as slow. Along strike of the orogen, variations in the position of the gravel-sand transition on the Yamuna, Ganga, Sharda, Gandak and Kosi rivers are consistent with long term ($>$ 1 Myr) patterns of subsidence across the basin where lower subsidence rates in the west result in a more distal gravel-sand transition than regions experiencing higher rates of subsidence in the east Ganga Plain, where a greater proportion of

sediment is trapped in the proximal part of the basin due to a greater volume of accommodation being generated [Paola *et al.*, 1992b; Marr *et al.*, 2000].

2.6.2 What are the spatial characteristics of the controlling processes?

Previous works have also suggested that conditions imposed by local subsidence rates could modulate the gradient of large alluvial fan surfaces over millennial timescales [Allen *et al.*, 2013b]. Longitudinal profiles of the Gandak, Sharda, Ganga and Yamuna rivers reveal a distinct break in slope at the gravel-sand transition (Figure 2.6). The transport coefficients of sand and gravel differ by a factor of ∼10 [Marr *et al.*, 2000] which, in combination with bed slope, determine the total flux of sediment at a point on the fluvial surface:

$$q_s(x,t) = -v\frac{\delta z(x,t)}{\delta x} \tag{2.8}$$

where q_s is sediment flux, v is the transport coefficient and z is the surface elevation. The transport coefficients of gravel and sand (v) are reported as 0.01 and 0.1 km^2yr^{-1}, respectively. These transport coefficient values incorporate a number of independently known or quantifiable variables including water discharge, Shields stress, dimensionless sediment flux and sediment porosity [Marr *et al.*, 2000]. At the gravel-sand transition, an increase in transport coefficient associated with a change from a gravel-bed to sand-bed river may occur; however, the associated reduction in channel slope would also be expected to reduce sediment flux along the profile. Analogue modelling of gravel bed channels has also suggested that a reduction in both total sediment flux and grain size, as a result of upstream deposition, will reduce the required transport capacity of the channel downstream. The progressively finer and smaller sediment load could therefore remain in transport within a channel with a lower gradient [Paola *et al.*,

1992b]. This is consistent with our observations across the Ganga Plain, where a relatively distinct change in channel slope is associated with the gravel-sand transition (Figure 2.6).

Interestingly, the positions of the gravel-sand transitions on the Gandak and Kosi rivers are directly comparable to those observed in smaller foothill rivers (∼8 to 20 km downstream of the mountain front). The catchment area of these Piedmont rivers ranges from ∼25-350 km^2 [Dubille and Lavé, 2015] whilst the Gandak and Kosi catchment areas are an order of magnitude larger at ∼31,000 km^2 and ∼50,000 km^2, respectively (Table 3.3). The gravel-sand transition on the Gandak, which lies ∼100 km west of the foothill systems considered by Dubille and Lavé [2015], was noted at ∼20 km. The transition on the Kosi, which lies ∼100 km east of their study area, was noted at ∼13 km. This suggests that the distance that gravel progrades out from the mountain front is not strongly dependent on upstream catchment area, and therefore unlikely to be dependent on absolute sediment flux, given the dramatically different catchment areas of the foothill and mountain catchments. However, the abrupt change in slope associated with the gravel-sand transition is not a constant feature across these smaller foothill rivers. A less abrupt change in channel slope associated with the gravel-sand transition was observed in a number of smaller foothill-fed systems draining the Gandak-Kosi interfan area [Dubille and Lavé, 2015]. In this instance, the subdued break in slope was attributed to the relative high proportion of sand relative to gravel transported by the channel at the mountain outlet, where a steep channel gradient was still needed to transport the large proportion of sand downstream of the transition. Where coarse gravels or conglomerate made up less than ∼30% of the sediment load, no apparent break in slope was observed at the transition. Whether this same relationship scales up to the larger mountain fed systems has not been examined in detail. The most dominant cause of a rapid reduction in grain size associated with the gravel-sand transition in aggrading

Table 2.3: Catchment and grain size sample summary information

	Catchment area (km^2)	Grain size sample location (UTM)			D_{84} (phi units)		D_{50} (phi units)		Distance downstream of MFT (km)	Slope (m/m)
					Surface	Subsurface	Surface	Subsurface		
Yamuna	9,419	43R	746512	3353763	6.78	6.05	5.92	4.15	7.5	0.00212
		43R	734615	3337112	7.39	7.14	6.45	5.88	12.7	0.00240
		43R	738113	3340361	6.31	6.08	5.24	4.41	26.1	0.00180
		43R	743686	3350341	6.09	6.24	5.08	4.72	32.0	0.00123
		43R	730761	3334533	GST	GST	GST	GST	38.1	0.00066
Ganga	19,666	44R	237430	3327606	7.75	7.42	6.49	5.62	-4.3	0.00177
		44R	226118	3311830	7.46	6.94	6.78	5.67	8.7	0.00192
		44R	226950	3308723	7.22	6.83	6.60	4.85	11.7	0.00189
		44R	227127	3298543	6.26	6.41	5.24	5.19	22.1	0.00122
		44R	228600	3293808	GST	GST	GST	GST	28.2	0.00084
Sharda	13,182	44R	416513	3219623	8.26	7.96	6.39	7.03	2	0.00252
		44R	414750	3216389	-	6.12	-	4.63	6.2	0.00237
		44R	412283	3210500	7.61	7.27	6.59	5.39	13.6	0.00191
		44R	413532	3201761	6.35	6.77	5.72	5.57	23.7	0.00170
		44R	413564	3199562	6.65	5.86	5.78	4.79	26.2	0.00161
		44R	413059	3187971	6.17	4.55	5.55	4.48	39.5	0.00068
		44R	414630	3183209	GST	GST	GST	GST	44.5	0.00040
Gandak	31,460	44R	790722	3041214	6.35	6.37	5.58	5.21	0	0.00134
		44R	782608	3035567	6.43	5.97	5.39	4.61	11.5	0.00080
		44R	781464	3032900	5.97	5.81	5.17	4.22	14.8	0.00079
		44R	782154	3028042	GST	GST	GST	GST	19.8	0.00020
Kosi	50,079	45R	514824	2969129	8.16	7.29	6.41	5.65	0	0.00031
		45R	514304	2968166	7.68	7.19	6.80	5.72	1.2	0.00030
		45R	515151	2965578	6.41	6.94	5.40	4.85	4.2	0.00029
		45R	512280	2962778	7.08	6.80	5.99	5.19	8.8	0.00126
		45R	511857	2958589	GST	GST	GST	GST	12.9	0.00057

systems has been attributed to selective sorting [for example Paola *et al.*, 1992b; Ferguson *et al.*, 1996], where downstream fining by selective sorting is enhanced by bedload sedimentation [Rice, 1999; Dubille and Lavé, 2015]. Poorly sorted gravel mixtures and bimodal gravel inputs have been modelled to yield similar fining characteristics [Paola *et al.*, 1992b], suggesting that rapid fining by selective deposition at the gravel-sand transition is insensitive to input sediment grain size distributions. Our current understanding of sediment flux to the Ganga basin is based on a synthesis of published fluxes calculated from ^{10}Be concentrations measured in modern river sediments (Table 2.1). The variability within these data do not allow any robust conclusions to be drawn regarding spatial variations in the long-term sediment supply rate from the Himalayan catchments to the Ganga basin. A more thorough understanding in the observed variability in these ^{10}Be concentrations should be a target of future studies to better understand the role of sediment flux on these systems. Spatial variations in discharge from the Ganga catchment into the Plain could also contribute to the observed morphological signal. Whilst comparable discharge data are not available across these systems, the upstream catchment area of these systems yields an appropriate substitute, where numerous studies have shown a close correlation between these two variables (for example Knighton, 1998).

In general, where larger catchment areas are observed in the east, larger discharges would also be expected (Table 2.3) which is consistent with gauged measurements where available [Sinha *et al.*, 2005]. Annual precipitation estimates from the Tropical Rainfall Measuring Mission (TRMM) between 1998-2001 across the Himalaya have further suggested that precipitation is typically higher in catchments feeding into the east Ganga Plain [Anders *et al.*, 2006]. Interestingly, for a given sediment supply, increased rates of water supply have been modelled to correspond with advancing gravel fronts [Paola *et al.*, 1992a]. This doesnt appear to be a factor in the Ganga system where catchment area (and presumably

discharge) are greatest in the east Ganga Plain, and the gravel-sand transition is found in its most proximal position. Given that it appears that the position of the gravel-sand transition is independent of variations in input grain size distributions, upstream catchment area and sediment flux, it is suggested that longer term patterns of subsidence rate are a governing control on the grain size transition in the modern Ganga Plain.

Where gravels prograde farthest downstream in the rivers of the central and west Ganga Plain, channel gradients are found to be steeper close to the mountain front. In the east Ganga Plain, lower channel gradients are observed upstream of the gravel-sand transition, where the relative change in channel gradient across the gravel-sand transition is also less pronounced. Channel gradient measurements derived from SRTM DEM elevations (Figure 2.6) are not of sufficient spatial resolution or quality to compare with grain size measurements obtained as part of this study. However, given the lack of obvious pattern in grain size distributions measured at the mountain front (Figure 2.8) and relatively subtle changes in channel gradient at the gravel-sand transition identified in the east Ganga Plain compared to the west (Figure 2.6), it seems improbable that differences in grain size can account for the along strike variations in channel gradient and grain size fining rates.

Other possible interpretations of the variation in channel gradient are that profiles in the east experience higher subsidence rates at the mountain front, resulting in the gravel-sand transition being closer to the mountain front. Late Holocene sedimentation rates of 0.62-1.45 mm/yr [Sinha *et al.*, 1996] on the Ganga Plain are comparable or slightly lower than subsidence velocity estimates beneath the Kosi and Gandak Rivers of 1.6±0.6 and 1.4±0.4 mm/yr, respectively. Comparable information of sedimentation rates in the west Ganga Plain are not available. Alternatively, if there has been greater sediment flux in the west, then the channel may have experienced a greater degree of backfilling. Without evidence

for the latter, we suggest higher differential subsidence in the east Ganga Plain as the most probable mechanism. Relative differences in fining exponents of the gravel fraction downstream of the mountain front are consistent with along strike variations in subsidence, where gravels in the Kosi River have a fining exponent two to three times greater than systems in the west Ganga Plain (Figure 2.13). Whilst the Gandak River has a relatively high subsidence velocity estimate, this same pattern in fining exponent is not as apparent and has been attributed to the buffering role of the upstream Chitwan Dun. Based on these observations, we interpret that spatial variations in subsidence rates play a controlling role in along strike variations in the longitudinal profiles of these rivers and grain size fining rates. However, spatially variable subsidence rates alone do not explain the entrenchment of the western rivers.

2.6.3 Climate and signal preservation

Top down changes in sediment and water discharges must have also influenced these systems [Sinha *et al.*, 2005; Wobus *et al.*, 2010]. The seasonal nature of water and sediment delivery to the Ganga Plain is highly sensitive to variations in the strength of the Indian summer monsoon during which ∼80% of the annual flow is discharged. From marine isotope stage 3 into the Last Glacial Maximum (LGM), a combination of low insolation and strong glacial conditions are thought to have significantly weakened the Indian summer monsoon and regional precipitation [Goodbred Jr., 2003; Gibling *et al.*, 2005]. This is also reflected in much lower runoff values interpreted from proxy records of palaeosalinity and δ^{18}O in the Bay of Bengal during the LGM [Cullen, 1981; Duplessy, 1982]. Following the LGM, a variety of proxy records have suggested there was a widespread increase in precipitation, particularly after ∼12 ka [Cullen, 1981; Goodbred Jr., 2003; Srivastava *et al.*, 2003]. How fluvial systems react to these climate driven

variations in water and sediment discharges is more difficult to predict as both incision and aggradation can occur simultaneously within a catchment in response to a single perturbation [Tucker and Slingerland, 1997].

Numerous studies have examined the relationship between climatic transitions and phases of fluvial incision and aggradation (for example Tucker and Slingerland, 1997; Goodbred Jr., 2003; Gibling *et al.*, 2005; Srivastava *et al.*, 2003; Wobus *et al.*, 2010; Duller *et al.*, 2012; Densmore *et al.*, 2016). Modelling results from Marr *et al.* [2000] have suggested that a rapid increase (over timescales shorter than T_{eq}) in water flux and/or decrease in sediment flux can result in proximal erosion of gravel and advance of the gravel-sand transition. Rapid increases in sediment flux were also found to initiate an increase in proximal channel gradient and retreat of the gravel front [Marr *et al.*, 2000]. However, considerable variability in the geomorphic response generated by increased runoff intensity has also been modelled by Tucker and Slingerland [1997] using a physically based model of drainage basin evolution (GOLEM); significant variations in sediment flux were found to result from relatively modest variations in surface runoff, highlighting the difficulty in correlating a specific cause (climatic condition) to effect (geomorphic response). There are also complexities regarding how climatically driven waves of incision and aggradation are propagated downstream of the Himalaya into the Ganga Plain. The effects of stochastic forcing on sediment supply to channel networks has been considered in previous studies [Benda and Dunne, 1997a,b], where the intermittent storage and release of sediment within a catchment has been modelled to dramatically alter the sediment mass balance over thousand year time scales [Blöthe and Korup, 2013]. Using both modelling outputs and circumstantial field evidence, unsteady sediment supply was found to affect channel morphology through the generation of sediment waves and transient phases of aggradation [Benda and Dunne, 1997b]. If sediment transport through the catchment acts as a non-linear filter and buffers climatic signals [Jerolmack and

Paola, 2010; Blöthe and Korup, 2013], it raises the question of what magnitude and wavelength of climatic forcing is capable of being recorded in the sedimentary record of the Ganga Plain?

Thermo-luminescence dating of quartz sands and radiocarbon dating on shell and calcrete materials preserved in the upper 2-8 m on the Ganga-Yamuna interfluve yield ages between 6-21 ka (summarised in Srivastava *et al.*, 2003); these ages suggest that this was when the modern Ganga and Yamuna channels were last connected to the interfluve floodplain surface [Srivastava *et al.*, 2003; Gibling *et al.*, 2005]. Such a situation is consistent with climatic fluctuations associated with the end of the LGM and subsequent strengthening of the Indian summer monsoon at ∼11-7 ka [Goodbred Jr., 2003], which could have initiated widespread incision of channels into their respective mega-fans across the Ganga Plain. A corresponding increase in sediment delivery to the Bengal basin was also noted between ∼11-7 ka, which translates to a mean sediment load of more than double current load estimates derived from late Holocene deposits in the basin [Goodbred and Kuehl, 2000]. Estimates for sediment remobilisation during the early Holocene by incision across the Plain only account for ∼2-25% of the total volume of sediment deposited into the basin during this period, suggesting that sediment flux exported from the Himalaya must have been considerably elevated [Goodbred Jr., 2003]. Crucially, these observations in the Bengal basin imply that a wide scale climatic perturbation was rapidly propagated down the full length of the Ganga system. Whether this signal was locally amplified by reworking of vast deposits of stored sediment within the Himalaya (for example Blöthe and Korup, 2013) is unknown.

A downstream reduction in valley width and channel entrenchment identified on the Yamuna, Ganga and Karnali systems is consistent with a top down wave of incision, most likely initiated by a climate-induced increase in water or relative decrease in sediment discharges during the early Holocene [Tucker and

Slingerland, 1997; Goodbred and Kuehl, 2000; Goodbred Jr., 2003; Wobus *et al.*, 2010]. However, this signal is not apparent in the east Ganga Plain where channels show minimal signs of entrenchment. Whilst some aggradation is thought to have occurred during the late Holocene, these rates are not thought to have been sufficient to infill earlier valley incision [Goodbred Jr., 2003]. It therefore seems unlikely that the east Ganga Plain underwent any significant phase of incision, such as that experienced in the west Ganga Plain. This is consistent with well data drilled from the Kosi mega-fan [Singh *et al.*, 1993] that suggested that the Kosi River has maintained a relatively mobile braided channel throughout the Holocene, which migrated across much of the surface of the mega-fan depositing a gravelly sand to fine sand unit.

2.6.4 Subsidence vs. climate

The Kosi exhibits low channel and fan gradients, flows over the most rapidly subsiding portion of the basin and displays the highest sediment grain size fining rate. Where subsidence rates are higher, proximal vertical sedimentation rates would also be expected to be higher. This results in a smaller amount of sediment remaining in transport further downstream than for a comparable sediment flux in a system experiencing a slower rate of subsidence. The equilibrium gradient of the channel would therefore be expected to be lower where subsidence rates are higher and/or where a greater proportion of the total sediment load is trapped in the proximal basin, as a channel with a lower gradient should be able to convey the smaller sediment load [Robinson and Slingerland, 1998]. We hypothesise that patterns of incision and aggradation on this timescale reflect differences in the sensitivity of these systems to climatic forcing of sediment and water flux (Q_s and Q_w respectively), such as that experienced during the early Holocene in response to increased strength of the Indian summer monsoon between ∼11-7 ka at the end

of the LGM. The sensitivity of these systems to changes in Q_s and Q_w is dependent on the gradient of the equilibrium channel under the new Q_s and Q_w values relative to the subsidence controlled gradient of the wider fan surface, assuming that the channel was not originally entrenched. If the revised equilibrium channel gradient is lower than the original gradient of the alluvial fan, the channel will incise into the surface of the fan apex until a lower channel gradient is attained, producing an incised channel. For a constant climatic forcing of channel lowering along the strike of the Ganga Plain, incision will only occur where channel lowering rates outpace subsidence which will inherently be more difficult to achieve where subsidence rates are higher in the east Ganga Plain (Figure 2.14). Based on upstream catchment areas and satellite-derived precipitation data, it seems likely that systems in the east Ganga Plain experience higher discharges than those further west. Discharge may play a key role in shaping the wider fan morphology, but the position of the modern gravel-sand transition is not consistent with these spatial variations in precipitation or possible variations in sediment flux which could be related. Lower channel gradients in the east could reflect these higher water discharges [van den Berg, 1995; Knighton, 1998], but would fail to explain the triggering mechanism behind fan entrenchment in the west Ganga Plain. However, the proximal position of the gravel-sand transition and low channel gradients observed on the Kosi are consistent with the model results simulated under increased basin subsidence rates (over timescales greater than T_{eq}).

Whilst absolute sediment fluxes to the basins are uncertain, approximately 90% of the total flux is thought to bypass the basin [Lupker *et al.*, 2011] which would suggest that sediment availability does not limit these systems. Again, the proximal position of the gravel-sand transition relative to the mountain front further suggests that the majority of this bypassed sediment is likely to be transported in suspension. Spatial variations in the amount of coarse bedload exported into the Plain, and deposited upstream of the gravel-sand transition,

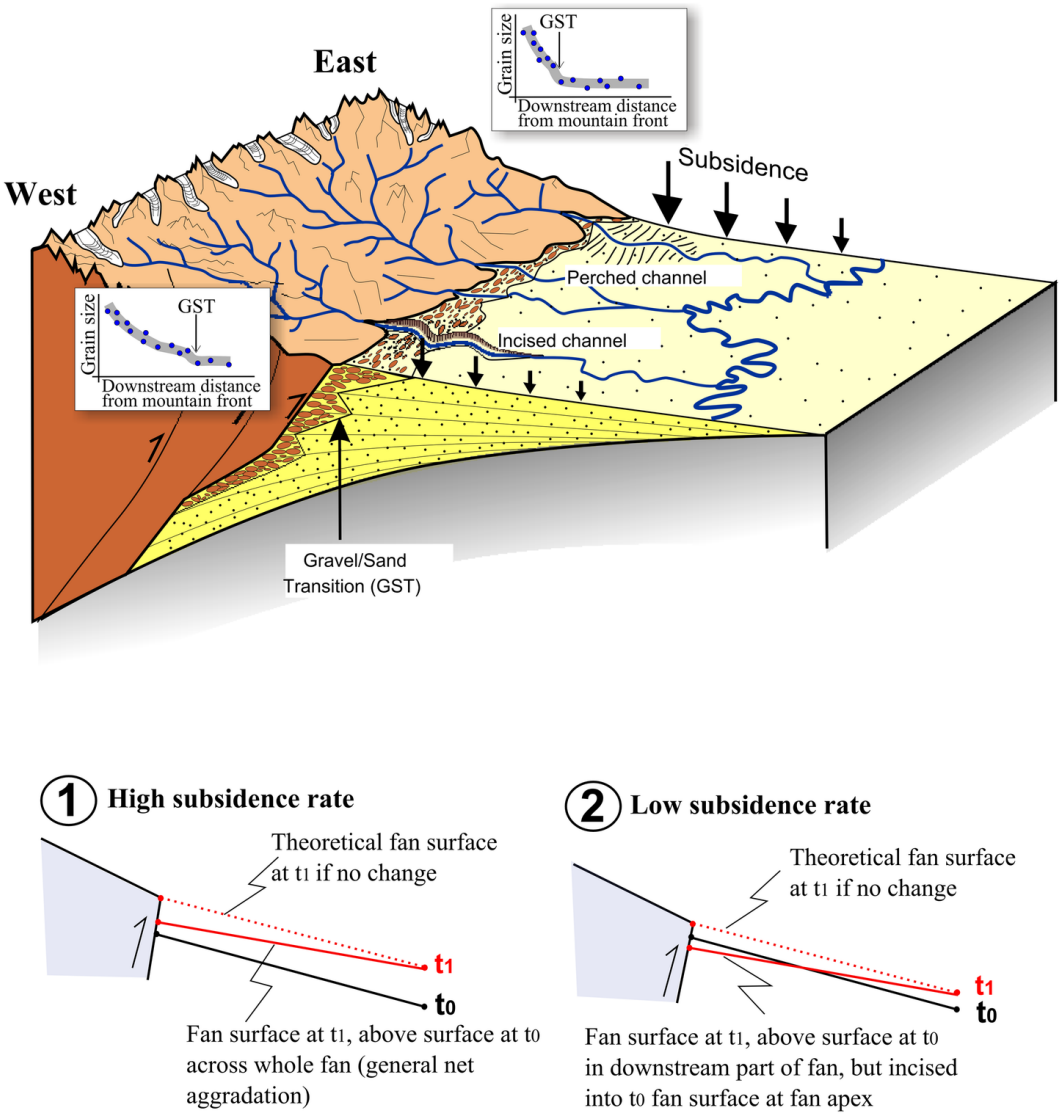

Figure 2.14: Cartoon illustrating the role of variable subsidence rate on surface morphology across the Ganga Plain, in response to climate-driven variations in water and sediment discharge. The relative lowering of the surface between time steps t_0 (black line) and t_1 (red dashed line) is equivalent to a fall in base level, where the gradient of the fan surface is similar between timesteps. The rate of base level fall is controlled by subsidence in these scenarios where it is assumed invariant between the two time steps. A change in external forcing (sediment flux, discharge) leads to an adjustment (reduction in this instance) of the fan slope between t_0 and t_1 (red solid line), which can be accommodated with net aggradation where subsidence rates are high (1) but requires vertical incision into the fan apex where subsidence rates are lower (2).

is unknown. Whilst beyond the scope of this study, this does appear to be a potential factor that could directly influence the morphology of these systems, as the entirety of this coarser sediment fraction is retained within the Plain. Further work is needed to better constrain the relative proportions of suspended load and bedload within the total sediment fluxes of these systems. The long term morphology of rivers in the east Ganga Plain appears to be primarily controlled by the relatively higher subsidence rates experienced in the eastern end of the basin. Furthermore, these systems appear to have been insensitive to wide scale changes in regional climate, such as that experienced at the end of the LGM, which initiated wide-spread incision in the west Ganga Plain.

2.7 Conclusions

A modified swath profile analysis has been applied to topographic data across much of the Himalayan foreland basin to characterise the broad nature of incision and aggradation over much of the Indo-Gangetic Plains. In general, we find that the degree of channel entrenchment increases from east to west across the Ganga Plain, and also decreases with distance downstream. First-order subsidence velocity estimates suggest a more rapidly subsiding basin in the east Ganga Plain with rates of up to 1.6±0.6 mm/yr. Further west, subsidence velocity estimates decrease to as little as 0.3±0.4 mm/yr. Grain size fining rates are also found to closely reflect these patterns of subsidence, with the highest fining rates observed in the east Ganga Plain and lowest in the west. Furthermore, data currently available does not support a strong west to east variation in sediment flux at the thousand year timescale. Assuming that 90% of sediment delivered into the foreland basin is bypassed downstream, it also seems more likely that the relative fraction of bedload delivered to the basin, which is trapped upstream of the gravel-sand transition, may have a more direct role on channel morphology than the

total sediment flux. We propose that higher subsidence rates are responsible for a deeper basin in the east with perched, low gradient river channels that are relatively insensitive to climatically driven changes in base-level. In contrast, the lower subsidence rates in the west are associated with a higher elevation basin topography, and entrenched river channels recording climatically induced lowering of river base-levels during the Holocene.

2.8 Chapter acknowledgements

We thank Ananta Gajurel, Jamie Stewart, Fred Bowyer, Konark Maheswari, Debojyoti Basuroy, Arkaprabha Sarkar, Bhairab Sitaula and Apex Adventure, and the Nepalese Department of Mines and Geology for their endless help, organisation and logistical support in the field. We are also grateful to the International Association of Sedimentologists, British Society for Geomorphology and the Edinburgh University Club of Toronto for their financial support of the fieldwork. We are grateful to reviewers Brian Dade and Paul Heller, and associate editor Sean Willett for valuable comments that helped modify the manuscript. Sadly, Paul Heller died unexpectedly before publication, and so this is likely to have been one of his last journal reviews. As a fervent advocate of integrating process sedimentology and basin analysis, and as someone with an ever-questioning mind, we would like to dedicate this contribution to his memory.

Chapter 3

Where does all the gravel go? Abrasion-set limits on Himalayan gravel flux

The work presented in this chapter was published as a Letter in Nature:

Dingle, E.H., Attal, M., and Sinclair, H.D. (2017) Abrasion-set limits on Himalayan gravel flux, *Nature*, 544(7651) p.471-474 doi: 10.1038/nature22039

The published format of this paper is presented in Appendix B. This research was conducted in collaboration with the named co-authors, who helped to collect field data, edit the manuscript and contributed to the abrasion modelling. E.H.D. and M.A. collected pebble lithology data and mapped positions of the gravelsand transition. E.H.D. calculated gravel fluxes and proportions. M.A. devised the pebble abrasion model, which E.H.D. ran and analysed the results from. E.H.D.,

M.A. and H.D.S. designed the study and all discussed the results to shape this manuscript. E.H.D. M.A. and H.D.S wrote the manuscript. Figures were produced by E.H.D.

3.1 Summary

Rivers sourced in the Himalaya carry some of the largest sediment loads on the planet [Milliman and Syvitski, 1992] , yet coarse gravel in these rivers vanishes within approximately 20-40 kilometres on entering the Ganga Plain. Understanding where the gravel goes is crucial to forecasting the response of rivers to large pulses of sediment triggered by earthquakes and storms. Rapid increase in gravel flux and subsequent channel bed aggradation following the 1999 Chi-Chi and 2008 Wenchuan earthquakes [Dadson *et al.*, 2003, 2004; Chen and Petley, 2005; Yanites *et al.*, 2010, 2011; Huang and Fan, 2013] reduced channel capacity and increased flood inundation [Chen and Petley, 2005]. Through an analysis of fan geometry, sediment grain size and lithology, we demonstrate that gravel flux from rivers draining the central Himalaya with contributing areas spanning three orders of magnitude is approximately constant. Our findings show that abrasion of gravel during fluvial transport can explain this observation; most of the gravel sourced from more than 100 km upstream is converted into sand by the time it reaches the Plain. These results indicate that earthquake-induced sediment pulses sourced from the Greater Himalaya, such as following the 2015 Gorkha earthquake [Kargel *et al.*, 2016], are unlikely to drive increased gravel aggradation at the mountain front. Instead, they should result in an elevated sand flux,

leading to distinct patterns of aggradation and flood risk in the densely populated, low-relief Ganga Plain.

3.2 Gravel flux from the Himalaya

Numerical models of foreland basin stratigraphy and modern river systems suggest that the location where river bed sediment texture changes from gravel to sand-dominated (the gravel-sand transition) is determined by: 1) basin subsidence rate; 2) total sediment flux; 3) gravel-size fraction, and 4) river discharge, over sub-millennial timescales [Paola *et al.*, 1992a; Parker and Cui, 1998; Robinson and Slingerland, 1998; Hoey and Bluck, 1999; Marr *et al.*, 2000]. However, few field data have previously been available to validate such models. The gravel-sand transition is marked by an abrupt decrease in grain size [Ferguson *et al.*, 1996; Ferguson, 2003; Marr *et al.*, 2000], believed to result from an exhaustion of gravel supply. The gravel-sand transition in large trans-Himalayan rivers feeding the Ganga Plain occurs at ∼12-20 km downstream of the mountain front in the east Ganga Plain, and slightly further at ∼28-45 km downstream in the west Ganga Plain (Figure 3.1); this transition is also associated with a marked decrease in channel gradient [Dingle *et al.*, 2016]. We find that the gravel-sand transition in rivers draining small foothill-fed catchments (<350 km^2) in the east Ganga Plain [Dubille and Lavé, 2015] is at a comparable distance downstream of the mountain front to the adjacent trans-Himalayan Gandak and Kosi rivers (>30,000 km^2) (Figure 3.1). While spatial variations in basin subsidence across the entire foreland basin may control the overall position of the gravel-sand transition [Paola *et al.*, 1992a; Dingle *et al.*, 2016], subsidence can be ruled out as a factor explaining this observation, as there is no evidence for a large variation in subsidence rate beneath the foothill-fed tributaries flowing in the interfan region between the Gandak and Kosi alluvial fans [Dingle *et al.*, 2016].

Given the substantial contrast in size between the trans-Himalayan Gandak and Kosi rivers and the smaller foothill-fed catchments, we would expect orders of magnitude differences in water and total sediment flux, which is at odds with the similarity in the positions of the gravel-sand transition. These fluxes are therefore also unlikely to play an important role in controlling the position of this transition. Gravel fining rates between the mountain front and the gravel-sand transition in the east Ganga Plain are also independent of the relatively rapid reduction in grain size observed across the gravel-sand transition [Dubille and Lavé, 2015; Dingle *et al.*, 2016]. This further indicates that neither abrasion downstream of the mountain front nor input grain size exert a dominant control on the distance to the transition in the Ganga Plain. Theory and experiments have implied that an increase in the fraction of gravel in the sediment supplied to the basin results in the downstream migration of the gravel front [Paola *et al.*, 1992a]. Having ruled out other likely controls, we further test whether the position of the gravel-sand transition across the east Ganga Plain reflects differences (or similarities) in gravel flux. We first compare the total mass flux of sediment exported into the Ganga Plain to the mass trapped upstream of the gravelsand transition. The volume of gravel between the mountain front and the mapped gravel-sand transitions [Dingle *et al.*, 2016] is calculated using the mean basin subsidence rate (which is believed to have been relatively constant over the last 10,000 years [Dingle *et al.*, 2016]), the distance to the gravel-sand transition, and the maximum width of the alluvial fan (see Methods). We assume that most gravel is trapped upstream of the gravel-sand transition, an assumption supported by the conspicuous lack of gravel downstream of the transition. The use of the basin subsidence rate assumes the degree of filling of the basin (defined by a depositional base level) during that interval is constant (see Extended Data Table 3.1). The gravel-to-total-load ratio was also calculated for each catchment. Total sediment flux data are only available for the trans-Himalayan rivers considered in this study [Lupker *et al.*, 2012], so to approximate total sediment flux from the smaller foothill catchments (Churre,

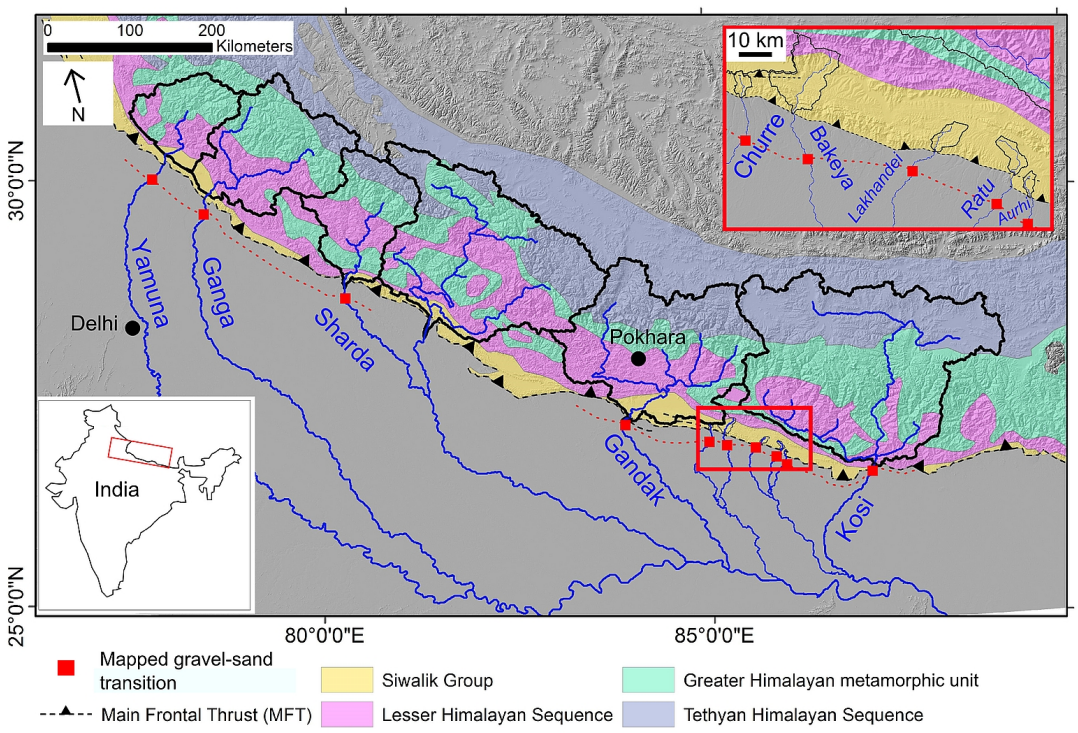

Figure 3.1: Study area and simplified geological map of the Ganga basin. The mapped gravel-sand transition is shown for both the major trans-Himalayan rivers [Dingle *et al.*, 2016] and smaller foothill-fed catchments [Dubille and Lavé, 2015] (see top right inset) considered in the east Ganga Plain. Major geological units [Yin, 2006] are all bound by major faults. The red dashed line links the position of mapped gravel-sand transitions between rivers in the Ganga Plain. Map adapted from Dingle *et al.* [2016], American Journal of Science.

Bakeya, Lakhandei, Ratu, and Aurhi), we have used ^{10}Be-derived catchment-averaged erosion rates from similar sized catchments further west in the Garhwal Himalaya [Scherler *et al.*, 2014] (see Methods).

We find that absolute gravel fluxes are lower across the foothill catchments, with values typically ranging between 0.05 megatonnes (Mt) of gravel per year and 0.72 Mt yr^{-1}, compared to values of 0.51-3.29 Mt yr^{-1} in the trans-Himalayan catchments, but the differences are much smaller than what would be expected from catchments with contributing areas spanning three orders of magnitude (Figure 3.2a). These absolute flux values should be treated as maxima, however, because we assume that the full surface of the fan is available to receive sediment (see Methods). Our gravel proportion (or gravel-to-total-load ratio) estimates for the large trans-Himalayan systems vary between 0.2% and 29%, with proportions generally lowest for the Gandak and Kosi rivers in the east Ganga Plain (Figure 3.2b). For average and maximum sediment flux scenarios (using average and maximum erosion rates), gravel proportions are systematically lower than estimates based on a similar abrasion model to predict gravel proportion for major Himalayan rivers at the mountain front [Attal and Lavé, 2006]. For the smaller foothill catchments, gravel proportions are notably higher, even under the maximum flux scenario with catchment-averaged erosion rates of 5 mm yr^{-1} (Figure 3.2b); for the gravel proportion to be lower than 50%, larger total sediment fluxes would be required, suggesting catchment-averaged erosion rates in excess of about 2.75 mm yr^{-1}.

3.3 Pebble lithology and abrasion

Identification of the provenance of gravel is facilitated by the fact that the Himalayan mountain range is divided into four major structural units that run broadly

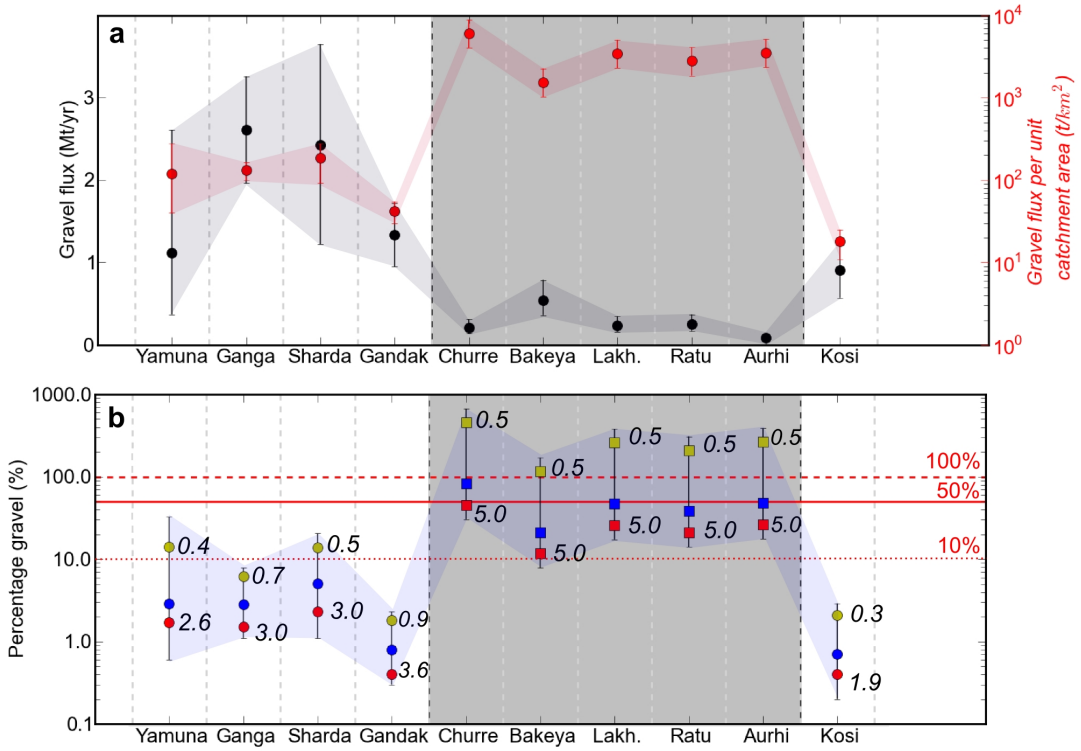

Figure 3.2: Gravel flux estimates. a, Estimates of absolute gravel flux (black) and of gravel flux per unit catchment area (red) for trans-Himalayan and foothill-fed (shaded in grey) rivers. b, Calculated percent gravel exported by trans-Himalayan rivers into the Ganga Plain (see Methods and Extended Data Tables 1-3). Foothill-fed catchments are shaded in grey. Red, blue and yellow data points correspond to maximum, average and minimum total sediment flux scenarios, respectively, with corresponding erosion rates (in units of mm yr^{-1}) indicated next to data points for maximum and minimum flux scenarios for reference. Error bars and red and black shading reflect differences in accommodation space available for sediment accumulation generated under maximum and minimum subsidence rates [Dingle *et al.*, 2016].

parallel from west to east and are composed of contrasting lithological units (Figure 3.1). These units are, from north to south: the Tethyan Himalayan Sequence, the Greater Himalayan metamorphic unit, the Lesser Himalayan Sequence and the Siwalik Group [Yin, 2006] (see Methods). The Main Frontal Thrust is the most southerly tectonic structure, situated between the Siwalik Group and the foreland basin, and absorbs approximately 80% of the approximately 21±1.5 mm yr^{-1} convergence between India and south Tibet [Lavé and Avouac, 2000]. During the low-flow season (October-May), a considerable portion of the channel bed of major rivers of the Ganga Basin is accessible, with extensive coarse gravel bars dominating the bed of the rivers as they cross the mountain front. To assess gravel provenance, pebble lithology was identified at a number of sites from about 30-50 km upstream of the mountain front down to the gravel-sand transition in each of the trans-Himalayan rivers (Fig. 1). Using a 25 m tape measure, pebble lithology was identified at 50 cm intervals along two transects at each site and categorized as outlined in Methods.

Clast characterization shows that gravel which could be identified as uniquely from the Tethyan Himalayan sedimentary lithologies was absent from all our sites (see Methods), despite this unit representing 10%-20% of the total catchment geology (Figure 3.3a and Extended Data Figure 1). Quartzites are considered separately because they are distributed within each of the contributing units but cannot be traced back to any specific one. Quartzites represent a small fraction of the rocks exposed in the catchments [Attal and Lavé, 2006], typically less than 10%, yet they constitute the majority of the pebbles sampled (about 40%-70%), consistent with observations along the Marsyandi River [Attal and Lavé, 2006]. Lesser Himalayan metamorphic lithologies comprised around 5%40% of sampled pebbles (Figure 3.3b). In general, where Lesser Himalayan lithologies covered a larger proportion of the total catchment area (such as for the Yamuna River), a higher proportion of Lesser Himalayan lithologies was found in the sampled

pebbles(Figure 3.3b). Greater Himalayan lithologies (igneous and medium to high-grade metamorphic) comprised a further 5%-40% of the sampled pebbles, with the greatest proportions found further east along the Gandak and Kosi rivers, where the Greater Himalayan source rocks extend further south. Sedimentary Siwalik lithologies made up a relatively small fraction (<10%) of the sampled pebbles. For our numerical model experiments, we used three pebble erodibility

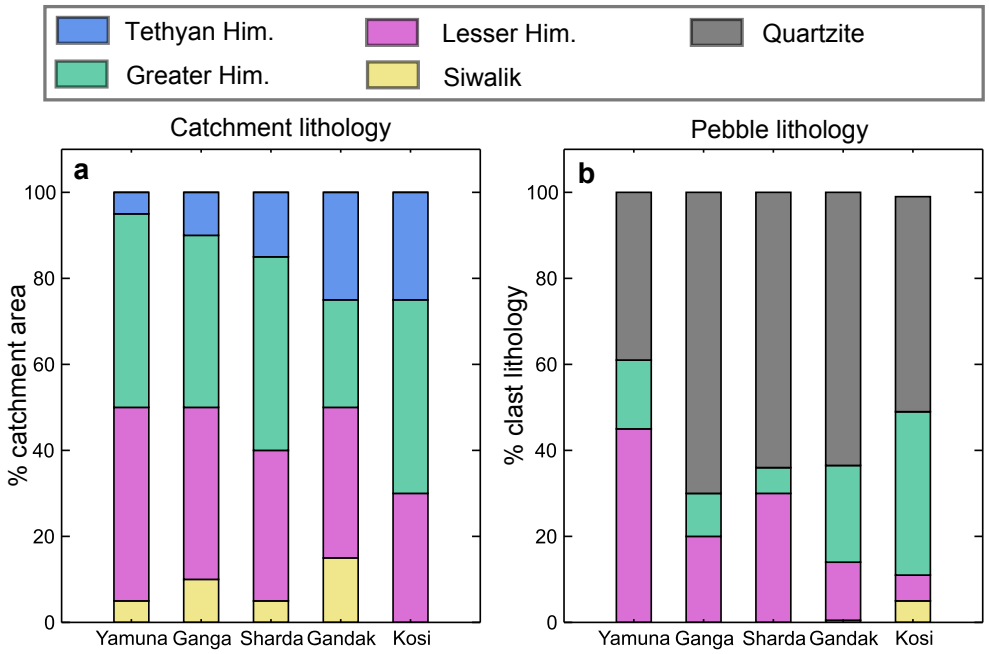

Figure 3.3: Catchment and pebble lithology. a, Proportion of area of major geological units in trans-Himalayan catchments upstream of the mountain front [Yin, 2006]. b, Average clast lithology composition recorded on exposed gravel bars between the mountain front and gravel-sand transition (see Extended Data Figure 3.5 for pebble lithology at each survey location). Quartzites are considered separately as they are distributed within each of the contributing units but cannot be traced back to any of these units they represent a small fraction of the rocks exposed in the catchments, typically less than 10% [Attal and Lavé, 2006]

coefficients typical of the Himalayan lithologies [Attal and Lavé, 2009] to assess the likelihood of gravel supplied from different parts of the catchments surviving as gravel after transportation to the mountain front. Using published percentage mass loss per travelled distance values [Attal and Lavé, 2009], we explored model

scenarios on the Kosi and Bakeya catchments to define how pebble erodibility influences the proportion of the catchment area contributing gravel to the Ganga Plain as a function of catchment size [Sklar *et al.*, 2006; Attal and Lavé, 2009] (see Methods). Modelling results show that for weak lithologies with high erodibility values (λ) such as schist and poorly cemented sandstones [Attal and Lavé, 2009], only locally sourced gravel is likely to survive at the mountain outlet (Figure 3.4). After a transport distance of about 20 km, most gravel with high erodibility (λ = 20% km^{-1}) is abraded and converted into sand and finer products [Attal and Lavé, 2009]; therefore, most of the easily erodible gravel supplied to the river at a distance greater than around 20 km upstream of the mountain front is unlikely to contribute to the gravel load, and is probably transported as washload or suspended load. Gravel with erodibility values of around 2% km^{-1}, representative of most Himalayan lithologies such as gneiss, granite, limestone and well cemented sandstone, can survive transport lengths of approximately 100-200 km. Clasts of these lithologies would probably constitute a greater proportion of gravel material at the outlet; this, however, is a conservative estimate, given that chemical weathering on hillslopes and during temporary storage may weaken pebbles [Heller *et al.*, 2001]. Under the lowest erodibility values (λ = 0.2% km^{-1}; for example, quartzite Attal and Lavé, 2009), a large proportion of the gravel supplied to the rivers is likely to survive to the mountain front (Figure 3.4).

3.4 Discussion and conclusions

Modelling of the abrasion of gravel as it is transported downstream suggests that beyond a critical fluvial transport length upstream of the mountain front, gravel delivered to the fluvial network reaches the Ganga Plain mainly as sand and finer sediment [Sklar *et al.*, 2006; Attal and Lavé, 2009; Lupker *et al.*, 2012](Figure 3.4). This is consistent with Sr-Nd isotopic mass balances of suspended sediment

in the Ganga Basin suggesting that 80%±10% of suspended sediment delivered to the Ganga Plain is of Greater Himalayan source, while only 20%±10% is sourced from the Lesser Himalaya [Galy and France-Lanord, 2001]. The critical fluvial transport length is dependent on pebble erodibility, which is a function of lithology, and was estimated to be in the order of $250/\lambda$ [Attal and Lavé, 2009]. For trans-Himalayan catchments, intermediate and low strength lithologies of the Lesser and Greater Himalaya sourced within around 100 km upstream of the mountain front will contribute a substantial fraction of the gravel exported and deposited upstream of the gravel-sand transition [Attal and Lavé, 2009]. Similar lithologies sourced further upstream will be abraded into sand before reaching the outlet, which is supported by the lack of pebbles distinctively sourced from the Tethyan Himalaya and relatively low proportions of Greater Himalayan pebbles in the Ganga Plain (Figure 3.3). Where Greater Himalayan rocks are exposed further south in these catchments, a larger proportion of Greater Himalayan pebbles reach the Ganga Plain as a result of shorter transport distances and generally lower percentage mass loss of Greater Himalaya lithologies (such as gneiss and granite) via abrasion, compared to the sedimentary and low-grade metamorphics from the other contributing units [Attal and Lavé, 2006, 2009].

More resistant quartzite lithologies, however, are sourced from all parts of the Himalaya [Attal and Lavé, 2006]. Even in catchments as large as the Kosi, more than 50% of quartzitic pebbles sourced from the catchment headwaters are likely to reach the mountain outlet as gravel, because the characteristic transport length for quartzite (>1,000 km; Attal and Lavé, 2009) is longer than the river network (Figure 3.4). We would therefore expect quartzite to dominate the lithologies of pebbles exported into the Ganga Plain, which is consistent with our observations (Figure 3.3b) and with previous modelling predicitions [Sklar *et al.*, 2006; Attal and Lavé, 2009]. The smaller foothill catchments are draining the Neogene Siwalik sediments (consisting of previously deposited Ganga Plain

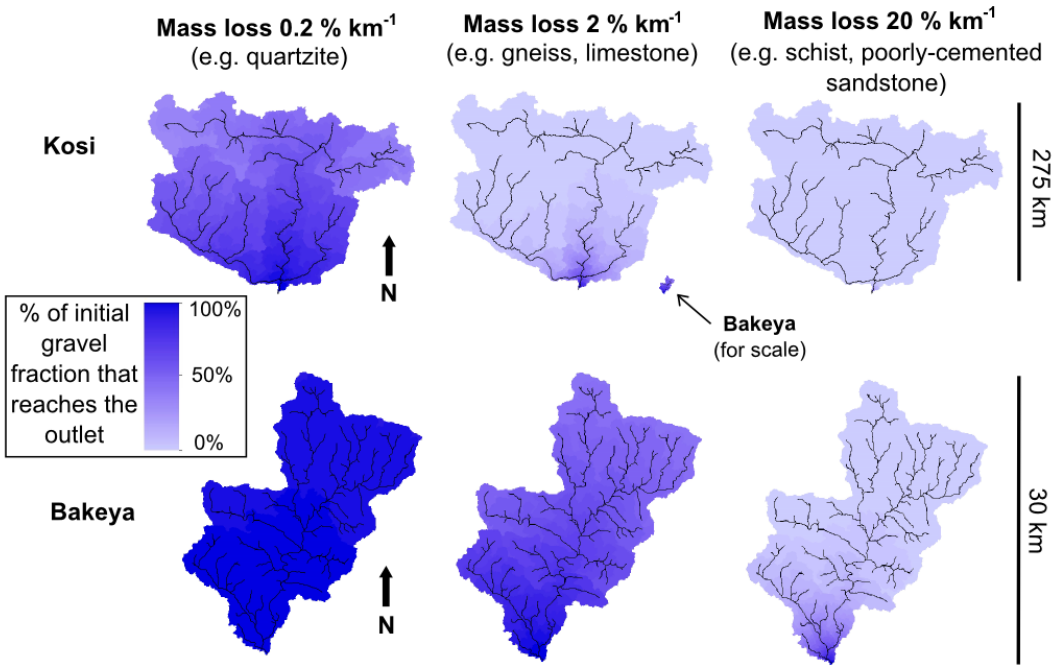

Figure 3.4: Abrasion scenarios for the Kosi (top panels; trans-Himalaya) and Bakeya (bottom panels; foothill-fed) rivers. Three pebble erodibility values are used, representative of Himalayan lithologies [Attal and Lavé, 2006, 2009]. Colour intensity indicates the percentage of gravel supplied to the river at this location that reaches the catchment outlet as gravel; the remaining percentage represents the mass loss by abrasion, assumed in this case to be sand and finer sediment. More than 50% of the gravel supplied at locations indicated by pixels in dark blue reaches the outlet as gravel; almost all of the gravel supplied at locations indicated by pixels in pale lilac is abraded into sand and finer products before reaching the outlet.

sediments), which are progressively incorporated back into the mountain range through frontal accretion of thrust units [Dubille and Lavé, 2015]. Therefore, the rivers are expected to recycle almost exclusively quartzitic gravel, which is confirmed by field observations. The low degree of cementation of the young Neogene sediment was also noted in the field, which probably explains the high catchment-averaged erosion rates. These observations explain why a very high proportion of the gravel delivered to the foothill channels survive into the Ganga Plain, and hence, why high gravel fluxes per unit catchment area are observed for these smaller systems (Figure 3.2a).

Our models and data demonstrate that increased sediment delivery to channels will result in an additional pulse of gravel reaching the Ganga Plain only if sediment delivery occurs within less than about 100 km upstream of the mountain front or is sourced in highly resistant lithologies (for example, quartzite). Increased gravel supply to rivers in the Siwalik Hills (proximal and quartzite-dominated), such as might be expected from landsliding following seismicity on the Main Frontal Thrust, will probably result in a pulse of gravel and aggradation in river channels of the proximal Ganga Plain. Conversely, widespread landsliding in the Greater Himalaya [Kargel *et al.*, 2016] initiated by the 2015 Gorkha earthquake (>200 km upstream of the mountain outlets) should result in elevated sand flux but is less likely to drive increased gravel flux to the Ganga Plain and thus leave a trace in the gravel stratigraphy of the foreland basin (see Extended Data Figure 3.7). Our results also suggest that over the length scale of trans-Himalayan rivers, abrasion facilitates the downstream translation and dispersion of earthquake-generated sediment [Cui *et al.*, 2003] through the transformation of gravel to more mobile sand. The 1950 Assam earthquake reportedly dislodged 47 billion cubic metres of landslide material [Keefer, 1999], resulting in long-term channel aggradation and a morphological change in tributaries of the Brahmaputra River[Sarma, 2005], although the relative effects of increased gravel

and sand delivery out of the mountain front were not explored. Rivers in the Ganga Plain are expected to respond differently to elevated sand or gravel input; our findings suggest that future research should aim to understand these responses better.

3.5 Methods

The volume of accommodation space available for gravel accumulation between the mountain front and mapped gravel-sand transition was calculated for each catchment. The volume generated each year was defined as the product of basin subsidence rate [Dingle *et al.*, 2016], distance to the gravel-sand transition, and maximum width of the alluvial fan upstream of the transition (derived from Google Earth imagery). The gravel-sand transition was mapped for each river by noting the point at which exposed deposits were nearly exclusively sand (>95%) [Dingle *et al.*, 2016]. The lateral extent of alluvial fans was determined by topographic barriers, or where fans from adjacent systems constrain lateral mobility [Leier *et al.*, 2005]. Where closely spaced, similar-sized channels exit the mountain front and it was difficult to constrain fan boundaries, the maximum width of each fan was set as the mid-point between the two channel outlets. This area represents the maximum extent over which the channel can deposit sediment upstream of the gravel-sand transition. We assume that deposition will occur over the total surface of this area over timescales of 10-1,000 years, based on documented avulsion pathways on the Kosi River which appear to inundate the surface of the Kosi mega-fan upstream of the gravel-sand transition over about 200 years [Chakraborty *et al.*, 2010], and for consistency with ^{10}Be-derived sediment fluxes that are averaged over 10^2-10^3 years [Lupker *et al.*, 2012]. Although the modern channel only occupies a portion of the fan surface, repetitive phases of channel infilling and avulsion over these timescales allow the channel to migrate

over the surface of the fan, making the entire fan surface available to receive sediment [Chakraborty *et al.*, 2010].

We also assume that the distance from the mountain front to the gravel-sand transition remains relatively constant over these timescales, which is supported by the presence of a channel slope break at the transition. A translation of this transition a few kilometres downstream or upstream would not hugely affect the gravel proportion estimates. This is demonstrated in Extended Data Figure 3.6, where gravel proportions have been recalculated on the basis of the gravel-sand transition being 5 km further upstream or downstream. The total available accommodation space upstream of the gravel-sand transition was converted to a total mass of sediment, assuming densities typical of quartzite (2.65 tonnes m^{-3}). The mass of coarse sediment trapped upstream of the gravel-sand transition was then converted to a proportion of the total sediment flux (see Extended Data Tables 1-3).

3.5.1 Foothill-fed catchment sediment fluxes

Where sediment flux data are not available for the foothill-fed catchments (Churre, Bakeya, Lakhandei, Ratu, and Aurhi), ^{10}Be-derived catchment-averaged erosion rates from similar-sized catchments further west in the Garhwal Himalaya [Scherler *et al.*, 2014] have been used to approximate total sediment fluxes. These sub-catchments form part of the Yamuna catchment, but are higher in elevation and catchment relief than the foothill-fed catchment considered in this study, with average elevations between 1,700 m and 4,000 m. With this in mind, we have calculated sediment fluxes for the foothill catchments using the maximum range of erosion rates reported from these data (0.5-5 mm yr^{-1}), and assuming an average rock density of 2.65 tonnes m^{-3}.

Bedload is commonly assumed to constitute about 10% of total river sediment loads in rivers originating from mountainous settings, although this proportion decreases to as low as 1% with increasing catchment areas above about 1,000 km^2 [Turowski *et al.*, 2010]. Our gravel flux estimates should represent a minimum bedload flux because they do not incorporate sediment finer than 2 mm, which may also be transported as bedload. Our gravel proportion estimates (and gravel flux per unit catchment area) appear much larger in small foothill-fed systems than in trans-Himalayan catchments. To generate total sediment fluxes large enough to allow gravel proportions in keeping within these empirical relationships [Turowski *et al.*, 2010], catchment-averaged erosion rates of 3-5 mm yr^{-1} are required in the foothill catchments. Either these catchments experience relatively high erosion rates (comparable to the fastest eroding catchments further west in the Garhwal Himalaya documented by Scherler *et al.*, 2014), or gravel makes up a larger proportion of the total sediment load (>50%) than might be expected based on an empirically derived catchment area scaling relationship [Turowski *et al.*, 2010]. Conversely, gravel proportions in the larger trans-Himalayan systems are low, representing as little as <1% of the total sediment load (Figure 3.2b). This could be a result of over-estimated ^{10}Be-derived erosion rates.

3.5.2 Influence of abrasion on spatial distribution of sources of gravel

We applied a simple abrasion model to produce (Figure 3.4). Using a 30 m Shuttle Radar Topography Mission Digital Elevation Model, we calculated the distance α between each contributing pixel and the catchment outlet and used Sternbergs law to calculate the proportion K of the gravel initially supplied by the pixel that

reaches the catchment outlet as gravel [Attal and Lavé, 2006, 2009]:

$$K = e^{-\lambda\alpha} \tag{3.1}$$

where α is the percentage of gravel (or pebble) mass loss per kilometre and $K = M/M_0$, where M_0 represents the mass of gravel initially supplied by the pixel and M the remaining mass of gravel after a transport distance α. We assume that all products of abrasion are sand and finer sediment [Attal and Lavé, 2009]. We made the calculation for three erodibility coefficients representative of Himalayan lithologies for both a trans-Himalayan catchment (Kosi River, maximum stream length about 600 km, drainage area about 50,000 km^2) and a foothill catchment (Bakeya River, maximum stream length about 50 km, drainage area about 350 km^2).

Maps were generated with constant erodibility coefficients across the whole catchments for illustrative purposes (Figure 3.4), using coefficients of 0.2%, 2% and 20% mass loss per kilometre, representative of the hardest, most common, and weakest lithologies exposed in the catchments, respectively [Attal and Lavé, 2006, 2009]. We note that spatial variations in erosion rates could affect the absolute gravel flux supplied from different parts of the catchment and therefore the relative proportions of a given lithology on gravel bars. For example, higher erosion rates are expected in areas supplying Greater Himalaya lithologies [Attal and Lavé, 2006; Lavé and Avouac, 2000], which should lead to a relatively higher abundance of gravel from these lithologies compared to a scenario with uniform erosion. However, this does not affect the maps shown in Figure 3.4 because they relate the fraction of gravel remaining after transport to the outlet to the fraction of gravel initially supplied by a given pixel, irrelevant of the absolute volume (or flux) supplied. Similarly, some lithologies may contribute a relatively greater amount of gravel than others [Attal and Lavé, 2006], but again this does not affect the maps shown in Figure 3.4.

3.5.3 Determination of pebble lithology in the field

The four major structural units running broadly parallel from west to east across the Himalayan orogen are, from north to south: the Tethyan Himalayan Sequence, the Greater Himalayan metamorphic unit, the Lesser Himalayan Sequence and the Siwalik Group [Gansser, 1964; Yin, 2006]. The Tethyan Sequence contains marine sedimentary to low-grade meta-sedimentary rocks. The Greater Himalayan metamorphic unit consists largely of medium to high-grade schist, paragneiss and orthogneiss [DeCelles *et al.*, 1998]. The Lesser Himalayan Sequence comprises lower-grade metasedimentary rocks including phyllite, quartzite, marble and dolostone [DeCelles *et al.*, 1998; Yin, 2006]. The Siwalik Group contains Neogene sandstones, conglomerates and shales, formed by the erosional products of the Lesser and Greater Himalaya [Kumar *et al.*, 2004].

Between six and eleven gravel bars located between up to approximately 100 km upstream of the mountain front and the gravel-sand transition were surveyed along each river. At each site, two 25 m long lines were positioned near the centre of the bar, parallel to the river, and the lithology of each pebble was recorded every 0.5 m [Attal and Lavé, 2006]. The percentage lithology numbers obtained from this survey are directly comparable to volumetric proportions, with surface and sub-surface samples typically yielding comparable results [Attal and Lavé, 2006]. In terms of lithological identification, quartzite is sourced from all across the Himalaya and, as such, it is not possible to distinguish the quartzite pebble source region from visual inspection. Therefore, quartzite pebbles were grouped into a separate lithology category. Low- to medium-grade metamorphic rocks were grouped as Lesser Himalayan, while medium- to high-grade metamorphic and igneous rocks were grouped as Greater Himalayan. No pebble that could definitively be related to the Tethyan Himalayan lithologies was found, though some quartzite pebbles are likely to be sourced from this unit. Similarly,

limestone, dolostone or even very low-grade metasedimentary clasts may derive from either Tethyan or Lesser Himalayan successions. Siwalik lithologies included Neogene non-metamorphosed sedimentary rocks such as sandstone, mudstones and conglomerates that were easily distinguishable in the field. Proportions of the different lithologies at each site are shown in Extended Data Figure 3.5. Only the sites downstream of the mountain front were used to produce the data in (Figure 3.3b).

3.6 Chapter Acknowledgements

We thank V. Singh, A. Gajurel, J. Stewart, F. Bowyer, K. Maheswari, D. Basuroy, A. Sarkar, B. Sitaula and Apex Adventure, and the Nepalese Department of Mines and Geology for their cooperation and logistical support in the field. C. Paola, E. Garzanti and an anonymous reviewer provided comments that helped to improve the manuscript. We are also grateful to the International Association of Sedimentologists, the British Society for Geomorphology and the Edinburgh University Club of Toronto for their financial support of the fieldwork. This study formed part of a Natural Environment Research Council (NERC)-funded PhD (NE/L501566/1).

3.7 Extended Data

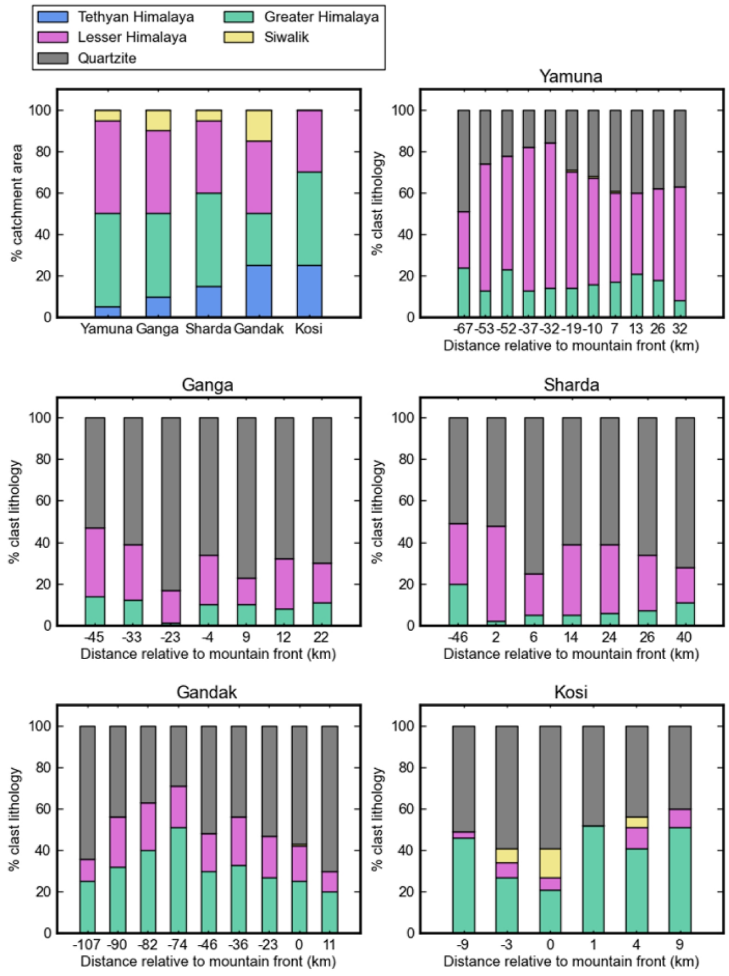

Figure 3.5: Details of pebble lithologies documented on exposed gravel bars along trans-Himalayan rivers upstream of the gravel-sand transition. Data in Figure 3.3b represent an average of the sites downstream of the mountain front for each river. Note that Siwalik lithologies were found on bars sampled along the Kosi River, despite no Siwalik units being mapped in the catchment geology [Yin, 2006]; this is probably due to the coarse nature of the Himalayan scale geological map [Yin, 2006], where small outcrops may have been omitted. Distances are relative to the mountain front, so negative distances are upstream of the mountain front.

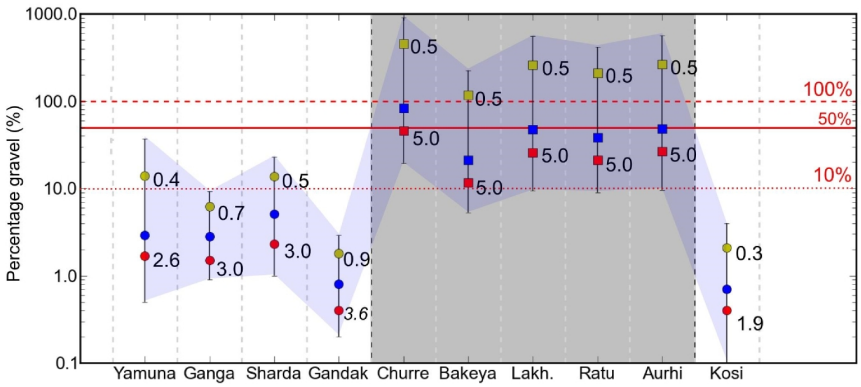

Figure 3.6: Sensitivity of gravel proportions to the position of the gravel-sand transition. Gravel proportions were calculated for instances where the gravel-sand transition was 5 km further downstream and upstream of the mapped position to test the effect on the results presented in 3.2b; these changes are reflected by the increased length of error bars associated with each river, but the overall patterns remain unchanged. As in 3.2b, gravel percentage values are estimated by dividing the flux of gravel calculated based on fan geometry and location of the gravel-sand transition by the total sediment flux from (1) catchment-averaged ^{10}Be derived erosion rates for trans-Himalayan catchments [Lupker *et al.*, 2012], and (2) a range of possible catchment0averaged erosion rates for the foothill-fed catchments [Scherler *et al.*, 2014]. Foothill-fed catchments are shaded in grey. Red, blue and yellow data points correspond to maximum, average and minimum total sediment flux scenarios, respectively, with corresponding erosion rates (in mm yr^{-1}) indicated next to data points for maximum and minimum flux scenarios for reference. Error bars reflect differences in accommodation space generated under maximum and minimum subsidence rates [Dingle *et al.*, 2016].

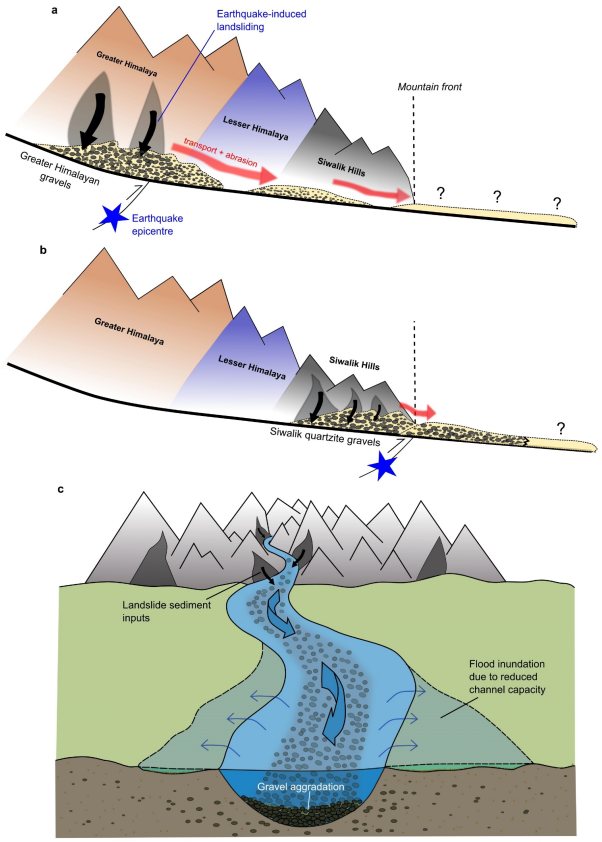

Figure 3.7: Schematic of gravel abrasion and sediment pulse delivery from the interior of the Himalayan mountains into the Ganga Plain. Schematic comparison of the evolution of coarse sediment pulses generated in the Greater Himalaya and Siwalik Hills, as a result of earthquake-induced landsliding. The magnitude and extent of the pulses as they travel downstream is unknown, as is the timescales over which the pulses migrate [Cui *et al.*, 2003]. a, As the sediment pulse is translated and dispersed downstream [Cui *et al.*, 2003], a combination of abrasion of weaker lithologies sourced in the Higher Himalaya and greater transport distances minimizes the gravel flux reaching the Ganga Plain, downstream of the mountain front. b, In contrast, stronger quartzite pebbles sourced from the Siwalik Hills undergo much less abrasion and, when combined with shorter transport distances, a larger gravel flux survives into the Ganga Plain when landsliding is focused closer to the mountain front. A large fraction of this gravel will likely remain trapped upstream of the gravel-sand transition, whereas more mobile sand and finer sediment (generated by the landslide inputs themselves and from the abrasion of coarser sediments) can be transported and deposited further downstream; where and when this finer sediment is deposited between the mountain front and the tip of the Bengal fan is less well understood. c, Where gravel flux downstream of the mountain front is enhanced, gravel aggradation could reduce channel capacity and enhance over-bank flooding. The extent of flooding is exacerbated by low-relief topography that characterizes sedimentary basins downstream of large mountain ranges.

Catchment	Catchment area (km^2)	Distance to transition (km)	Fan width (km)	Maximum subsidence rate (m/yr)	Average subsidence rate (m/yr)	Minimum subsidence rate (m/yr)
Yamuna	9,419	38	37	0.0007	0.0003	0.0001*
Ganga	19,666	28	44	0.0010	0.0008	0.0006
Sharda	13,182	45	51	0.0006	0.0004	0.0002
Gandak	31,460	20	18	0.0018	0.0014	0.0010
Churre	35	14	3.8	0.0022	0.0015†	0.0010
Bakeya	350	16	8.5	0.0022	0.0015†	0.0010
Lakhandei	70	11	5.5	0.0022	0.0015†	0.0010
Ratu	90	14	4.5	0.0022	0.0015†	0.0010
Aurhi	25	11	2	0.0022	0.0015†	0.0010
Kosi	50,079	13	16.5	0.0022	0.0016	0.0010

*where the subsidence rate beneath the Yamuna was 0.3±0.4 mm/yr [17], a minimum subsidence rate of 0.1 mm/yr was used given that the basin is actively subsiding.
†where the subsidence rates beneath the adjacent Gandak and Kosi rivers were given as 1.4 and 1.6 mm/yr [17], respectively, an average rate of 1.5 mm/yr was applied to the foothill-fed catchments which lie in in the interfan region of these two trans-Himalayan systems. The maximum and minimum rates reflect the maximum and minimum subsidence estimates of the Gandak and Kosi combined.

Table 3.1: Subsidence and fan geometries used to calculate gravel flux. Data used to calculate gravel fluxes for each catchment. Catchment areas are derived from a 90 m SRTM DEM, whilst distances to the gravel-sand transition are taken from Dingle *et al.* [2016] and Dubille and Lavé [2015]. Fan widths were determined as outlined in Methods. Maximum, average and minimum total (tectonic plus sediment-load induced) subsidence rates beneath the mountain front were taken from Dingle *et al.* [2016], based on depth to basement data derived from seismic surveys [Narula *et al.*, 2000], and horizontal shortening rates between the Ganga Plain and Himalaya. Given the short distances to the gravel-sand transition relative to the full width of the flexural profile that defines the basin, we do not expect a significant decrease in subsidence rate downstream over the lengths considered [Sinclair and Naylor, 2012] and as such have not incorporated it into our calculations.

Catchment	Minimum accommodation space (m^3/yr)	Average accommodation space (m^3/yr)	Maximum accommodation space (m^3/yr)	Minimum gravel flux (Mt/yr)	Average gravel flux (Mt/yr)	Maximum gravel flux (Mt/yr)
Yamuna	140,600	421,800	984,200	0.37	1.12	2.61
Ganga	739,200	985,600	1,232,000	1.96	2.61	3.26
Sharda	459,000	918,000	1,377,000	1.22	2.43	3.65
Gandak	360,000	504,000	648,000	0.95	1.34	1.72
Churre	53,200	79,800	117,040	0.14	0.21	0.31
Bakeya	136,000	204,000	299,200	0.36	0.54	0.79
Lakhandei	60,500	90,750	133,100	0.16	0.24	0.35
Ratu	63,000	94,500	138,600	0.17	0.25	0.37
Aurhi	22,000	33,000	48,400	0.06	0.09	0.13
Kosi	214,500	343,200	471,900	0.57	0.91	1.25

Table 3.2: Subsidence and fan geometries used to calculate gravel flux. The accommodation space created per year represents the product of the fan width, distance between mountain front and gravelsand transition, and the subsidence rate. These accommodation space values should be considered as a maximum, given that we assume that subsidence rate does not decrease with distance downstream of the mountain front, and that the entire surface of the fan is available to receive sediments (see Methods). Minimum, average and maximum gravel fluxes (in megatonnes per year) are calculated by multiplying the accommodation space generated by a density of 2.65 tonnes m^3, reflecting the quartzite and quartz sand (about 15%) nature of sediments trapped upstream of the gravelsand transition [Dingle *et al.*, 2016].

Catchment	Maximum sediment flux (Mt/yr) and erosion rate (mm/yr) in parenthesis	Average sediment flux (Mt/yr) and erosion rate (mm/yr) in parenthesis	Minimum sediment flux (Mt/yr) and erosion rate (mm/yr) in parenthesis	Maximum gravel proportion (%)	Average gravel proportion (%)	Minimum gravel proportion (%)
Yamuna	64 (2.6)	39 (1.6)	8 (0.4)	32.6	2.9	0.6
Ganga	176 (3.0)	93 (1.8)	42 (0.7)	7.8	2.8	1.1
Sharda*	107 (3.0)	47 (1.3)	18 (0.5)	20.5	5.1	1.1
Gandak	299 (3.6)	159 (1.9)	75 (0.9)	2.3	0.8	0.3
Churre	0.46 (5.0)	0.25 (2.75)	0.05 (0.5)	668.8	82.9	30.4
Bakeya	4.55 (5.0)	2.50 (2.75)	0.46 (0.5)	171.0	21.2	7.8
Lakhandei	0.91 (5.0)	0.50 (2.75)	0.09 (0.5)	380.3	47.1	17.3
Ratu	1.17 (5.0)	0.64 (2.75)	0.12 (0.5)	308.0	38.2	14.0
Aurhi	0.33 (5.0)	0.18 (2.75)	0.03 (0.5)	387.2	48.0	17.6
Kosi	242 (1.9)	130 (1.0)	43 (0.3)	2.9	0.7	0.2

*Erosion rate data were not available for the Sharda catchment; instead, the catchment-averaged erosion rates for the adjacent trans-Himalayan Karnali catchment[18] were used to generate sediment fluxes.

Table 3.3: Sediment fluxes and gravel ratios. Sediment fluxes, catchment-averaged erosion rates and gravel-to-total-sediment-load proportions. Gravel-to-total-sediment-load proportions (shown as percentage of gravel proportion) were calculated using the gravel fluxes shown in Extended Data Table 3.2 and the total sediment fluxes are taken from the literature [Lupker *et al.*, 2012; Dingle *et al.*, 2016]. The maximum gravel proportion here reflects the scenario with the lowest total sediment flux and the highest subsidence rate or maximum accommodation space. Conversely, the minimum gravel proportion represents the scenario with the highest sediment flux and the lowest subsidence rate or minimum accommodation space.

Chapter 4

Temporal variability in detrital ^{10}Be concentrations in large Himalayan catchments

The work presented in this chapter was submitted as an article to Earth Surface Dynamics in December 2017 for review:

Dingle, E.H., Sinclair, H.D., Attal, M., Rodés, A., and Singh, V. (in review) Temporal variability in detrital ^{10}Be concentrations in large Himalayan catchments, *Earth Surface Dynamics*

This research was conducted in collaboration with the named co-authors, who helped edit the final manuscript. E.H.D., H.S., M.A. and V.S. collected the samples used in the cosmogenic radionuclide analysis, which A.R. and E.H.D. prepared for analysis at SUERC. E.H.D. designed and carried out the numerical analysis. E.H.D. produced the figures and wrote the manuscript with discussions and contributions from H.D.S., M.A., and A.R.

Following the initial submission of this thesis, a revised version of this manuscript was resubmitted to Earth Surface Dynamics incorporating revisions. This revised version of the manuscript (text, figures and tables) is presented in Appendix C. Whilst the overall message of this chapter remains unchanged a number of revisions to the text and figures were made, the most significant of which are summarised below.

1. In order to address the difference between modelling work I have carried out in this thesis and previous works [Niemi *et al.*, 2005], I have added additional text outlining the following points. Unlike other studies, this analysis examines the effect of the largest events in a catchment rather than simulating how catchment-averaged concentrations vary in a landscape that has been allowed to evolve towards steady state conditions. Furthermore my analysis isn't fitted, or attempted to fit, to actual data such as carried out in Niemi *et al.* [2005]. Instead, I have tested how outlet concentrations vary in response to a large single event with variable characteristics. This allows a more detailed examination of whether there are certain conditions under which deeper landslides with lower CRN concentration sediment might have a greater impact. I also did not add a power-law distribution of landslide area/depths or have a landscape evolution style model, which would allow stochastic landslides to continually occur over the landscape until nuclide concentrations attain some kind of steady-state. Instead I have applied a background erosion rate (0.2-2 mm yr^{-1}) across the landscape (which I assume represents this steady state condition) and then add in an extreme event which generates numerous landslides to see what impact this has on outlet CRN concentrations.

2. I have also better justified the use of an average landslide depth. One could argue that the use of an average depth may be unrepresentative, given the power law distribution of landslide size/depth vs. frequency. But, at any one time it is

unlikely that a single concentration sample would integrate sediment from this full distribution of events. Instead, it seems more realistic that a catchment-averaged sample is likely to integrate a proportion of that distribution. As such, I have varied the average landslide depth to represent the variation in the position (or length) of that window along the power law distribution. I assume that the smaller and more frequent events inter-seismic, monsoon storm initiated landslides are captured in the background erosion rate. The event modelled is the equivalent of adding in events from the high magnitude tail end of a power law distribution that might record a seismic trigger.

3. I have also undertaken additional analysis of landscapes which are not at an initial steady state condition, where the surface CRN concentration is initially lower than the original set of model runs. In these additional scenarios, lower landslide surface CRN production rates of 10 atoms $g^{-1}yr^{-1}$ (rather than 35) were used, such that sediment generated by the landslides has a lower (depth-averaged) CRN concentration than the initial model runs. The results of this can be seen in Figure 9.

4. I have also included an additional plot (Figure 10) showing what happens to the catchment outlet concentration when different proportions of the landslide flux are delivered. I have explored what happens if 20, 10, 5 and 3% of the landslide generated sediment is mixed into the catchment average, respectively. What I find is that under faster background erosion rates, the magnitude of landsliding event can be lost in expected variability (i.e. all values are within 100% of the highest concentration) if only 5% of the landslide material makes it into the fluvial network. Under lower background erosion rates, to reduce all concentrations within ∼100% of the largest concentration, a maximum of ∼3% of the landslide material needs to be entrained. If greater quantities of landslide material get into the network, the catchment-averaged concentrations become much

lower (i.e. beyond what might be expected within natural variability) with deeper landsliding events. By incorporating this into these calculations, the relationship between volumetric and CRN-derived sediment fluxes is much more comparable which is consistent with findings from Niemi *et al.* [2005].

4.1 Abstract

Accurately quantifying sediment fluxes in large rivers draining tectonically active landscapes is complicated by the stochastic nature of sediment inputs. Cosmogenic ^{10}Be concentrations measured in modern river sands have been used to estimate 10^2-10^4 year sediment fluxes in these types of catchments, where upstream drainage areas are often in excess of 10,000 km^2. It is commonly assumed that within large catchments, the effects of stochastic sediment inputs are buffered such that ^{10}Be concentrations at the catchment outlet are relatively stable in time. We present eighteen new ^{10}Be concentrations of modern river and dated Holocene terrace and floodplain deposits from the Ganga River near to the Himalayan mountain front. We demonstrate that ^{10}Be concentrations measured in modern Ganga River sediments display a notable degree of variability, with concentrations ranging between ~9,000-19,000 atoms g^{-1}. We propose that this observed variability is driven by two factors. Firstly, by the nature of stochastic inputs of sediment (e.g. the dominant erosional process, surface production rates, depth of landsliding, degree of mixing) and, secondly, by the evacuation timescale of individual sediment deposits which buffer their impact on catchment-averaged concentrations. Despite intensification of the Indian Summer Monsoon and subsequent doubling of sediment delivery

to the Bay of Bengal at ∼11-7 ka, we also find that Holocene sediment ^{10}Be concentrations documented at the Ganga outlet have remained within the error of modern river concentrations. We demonstrate that in these systems, sediment flux cannot be simply approximated by converting detrital concentration into mean erosion rates and multiplying by catchment area as it is possible to generate considerably larger volumetric sediment fluxes whilst maintaining comparable average ^{10}Be concentrations.

4.2 Introduction

The quantity of sediment exported from large mountainous catchments is a fundamental control on downstream river morphology [Sinha and Friend, 1994; Dade and Friend, 1998; Church, 2006; Allen *et al.*, 2013b], the advance and retreat of coastlines [Syvitski *et al.*, 2005] and the growth of deltas [Orton and Reading, 1993; Goodbred and Kuehl, 1999; Galy *et al.*, 2007]. How sediment flux varies over thousand year times scales reflects changes in upstream landscape evolution which is set by climatic and tectonic conditions in active orogenic settings [Whipple and Tucker, 2002]. Quantification of sediment flux from large, tectonically active catchments is challenged by the nature of the river channels (e.g. size and access), the stochastic nature of sediment inputs [Benda and Dunne, 1997b; Kirchner *et al.*, 2001], and highly variable water discharge regimes (e.g. Collins and Walling, 2004; Singh *et al.*, 2005; Gitto *et al.*, 2017). Constraining sediment fluxes at intermediate timescales of 10^2-10^4 years has been significantly improved through the development of detrital ^{10}Be cosmogenic radionuclide (CRN) analysis (e.g. Brown *et al.*, 1995; Granger *et al.*, 1996; Niedermann, 2002; Kirchner *et al.*, 2001; Vance *et al.*, 2003; Von Blanckenburg, 2005). The concentration of ^{10}Be recorded in quartz-rich river sediments is assumed to reflect the rate of upstream landscape

lowering, assuming steady-state denudation averaged over the entire upstream catchment. Based on this approach, catchment-averaged denudation rates can be calculated, and converted into CRN-derived sediment fluxes which are typically averaged over hundred to thousand year timescales [Kirchner *et al.*, 2001; Lupker *et al.*, 2012] where these timescales are a function of the landscape erosion rate (i.e. the time taken to erode to a depth equivalent to the cosmic ray attenuation length in that landscape) [Lal, 1991].

Sediment production, delivery and transport out of large mountain catchments is heavily influenced by stochastic inputs such as hillslope mass wasting generated by earthquakes or intense storms, or glacial lake outburst floods [Benda and Dunne, 1997b; Hovius *et al.*, 2000]. In small catchments that are susceptible to such events, stochastic controls on sediment release may significantly perturb the ^{10}Be signal measured in sediment samples at the catchment outlet [Niemi *et al.*, 2005; Yanites *et al.*, 2009; West *et al.*, 2014]. In particular, deep-seated landslides excavate sediment from depths greater than the attenuation length of cosmic rays. This addition of ^{10}Be-poor landslide material dilutes ^{10}Be concentrations recorded in fluvial sediments sampled at the catchment outlet [Niemi *et al.*, 2005; West *et al.*, 2014] resulting in an over-estimation of the long-term erosion rate [Yanites *et al.*, 2009]. The timescales over which these stochastic inputs influence downstream ^{10}Be concentrations is related to the time taken to evacuate the sediment input from the impacted reach, and also depends on patterns of intermediate sediment storage and release (recycling) upstream of the sampling locality [Granger *et al.*, 1996; Yanites *et al.*, 2009; Blöthe and Korup, 2013; Scherler *et al.*, 2014; Schildgen *et al.*, 2016]. However, even in regions dominated by high rates of landslide occurrence, it is commonly assumed that given sufficiently large catchment areas and sufficient sediment mixing, the imprint of mass wasting processes on ^{10}Be concentrations measured at the outlet should be negligible [Niemi *et al.*, 2005; Yanites *et al.*, 2009].

The gross sediment flux from the Himalaya is the largest out of any mountain range on the planet and provides fertile soils for ∼10 % of the global population. The vast majority of this sediment flux is sequestered in the Indus and Ganga-Brahmaputra delta and submarine fans [Lupker *et al.*, 2011]. Sediment volumes in the Ganga-Brahmaputra delta imply that overall sediment flux from these two major Himalayan river systems has halved since the early Holocene, which has been linked to a reduction in monsoon rainfall since this time [Goodbred and Kuehl, 2000; Fleitmann *et al.*, 2007]. Our current understanding of how sediment flux from tributaries of the Ganga River into the Himalayan foreland basin varies is primarily from suspended sediment and detrital ^{10}Be concentration data collected over the last 20 years [Ghimire and Uprety, 1990; Jha *et al.*, 1993; Sinha and Friend, 1994; Vance *et al.*, 2003; Andermann *et al.*, 2012; Lupker *et al.*, 2012]. Suspended sediment data are generally based on a single daily measurement and are difficult to scale up spatially and temporally. Under these circumstances, ^{10}Be concentrations in modern river sands can be used to generate sediment flux estimates with the advantage of temporal and spatial averaging. However, substantial variations in ^{10}Be concentrations from repeat river sand samples at the catchment outlets of major Himalayan rivers have been documented [Vance *et al.*, 2003; Lupker *et al.*, 2012]. Concentrations measured on the Ganga River close to the mountain front (near Rishikesh) vary from 9.2±1.0 to 19.5±4.1 $\times 10^3$ atoms g^{-1} over a 13 year time period based on three samples [Vance *et al.*, 2003; Lupker *et al.*, 2012]; at the Kosi River near Chatara, measurements vary between 26.7±3.4 to 54.4±2.9 $\times 10^3$ atoms g^{-1} for three samples collected in August 2007 and November 2009, respectively [Lupker *et al.*, 2012]. Measurement errors on Ganga River samples record a 1σ of around 10-20 % of the measured concentration, whereas the measured variability from the repeat samples is >100 %. Similar observations were made along main stem samples on the Yamuna River, where discrepancies of up to ∼60 % between samples were observed [Scherler *et al.*, 2014, 2015]. This degree of variability could suggest that stochastic controls on sediment release may

influence the ^{10}Be signal, yet this is at odds with previous modelling and analysis of large catchments which has proposed that catchments of this size should be buffered against variations in detrital ^{10}Be concentrations induced by individual hillslope events [Niemi *et al.*, 2005].

Well preserved and dated river terraces [Srivastava *et al.*, 2003, 2008; Sinha *et al.*, 2010; Wasson *et al.*, 2013] associated with the Ganga River in the west Ganga Plain present a unique opportunity to test for variations in ^{10}Be concentrations in both ancient and modern fluvial sediments at the Himalayan mountain front. The half-life of ^{10}Be ($\sim$1.394 Myr) implies that any post-burial decay during the last 0.01 Myr is minimal and can be accounted for, making it the ideal technique for this approach. We analyse eighteen samples of river sands from near the outlet of the Ganga River as it crosses the mountain front. Samples are taken from modern river gravel bars, recent sand deposits of the 2013 Alaknanda floods [Dobhal *et al.*, 2013; Durga-Rao *et al.*, 2014; Devrani *et al.*, 2015], and dated terrace and floodplain deposits ranging in age from $\sim$200 to 23,500 years. Using these data, we evaluate the short-term variability in ^{10}Be concentrations and test for longer-term changes that are expected to reflect variations in the strength of the Indian Summer Monsoon [Sirocko *et al.*, 1993; Gupta *et al.*, 2005; Fleitmann *et al.*, 2007; Clift *et al.*, 2008; Dixit *et al.*, 2014]. Motivated by the results, we examine the impact of stochastic inputs of sediment from the upstream mountain catchment on ^{10}Be concentrations close to the mountain front (herein referred to as the Ganga outlet). We conclude by combining field observations, data and numerical analyses results to synthesise potential drivers of CRN concentration variability in large tectonically active catchments.

4.3 Study area and context

The Ganga River is a glacially-fed perennial river rising in the High Himalaya (Fig. 4.1). The Ganga has two major tributaries, the Bhagirathi and Alaknanda, which join near the village of Devprayag. Further downstream, the Ganga flows through the eastern end of the Dehra Dun, an intermontane valley in the Sub-Himalaya, prior to passing through the Mohand Anticline, exiting the mountains at Haridwar before reaching the Ganga Plain (Fig. 4.1). The Ganga catchment is characterised by a number of broad geomorphic process domains, which can be related to the distribution of tectonic structures, topographic relief and climatic influences which vary spatially across the catchment (Fig. 4.2). Upstream of

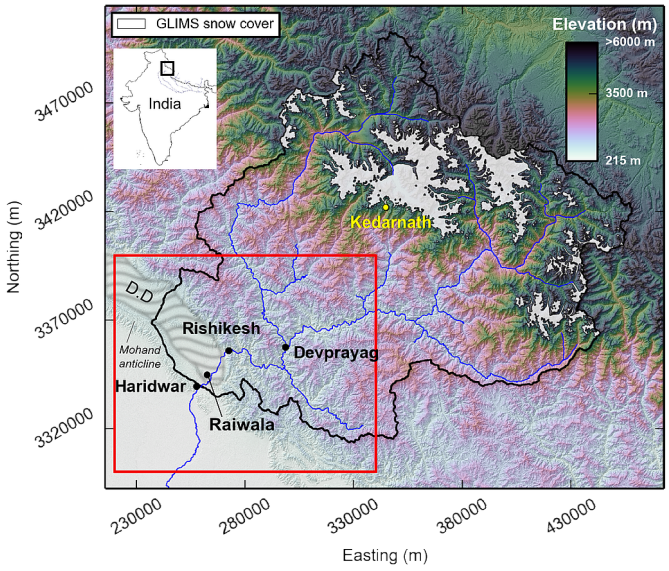

Figure 4.1: 30m Shuttle Radar Topography Mission (SRTM) Digital Elevation Model (DEM) of the Ganga catchment. Coordinates are projected in UTM Zone 44N. Glacier coverage as documented in the Global Land Ice Measurements from Space (GLIMS) database is also shown in white. The red box represents the spatial area shown in more detail in Fig. 4.3. D.D refers to the Dehra Dun region which is delineated by the grey striped area.

the mountain front, down cutting by the Ganga River has left behind a series of strath terraces cut into Lesser Himalayan or Siwalik rocks, and cut and fill

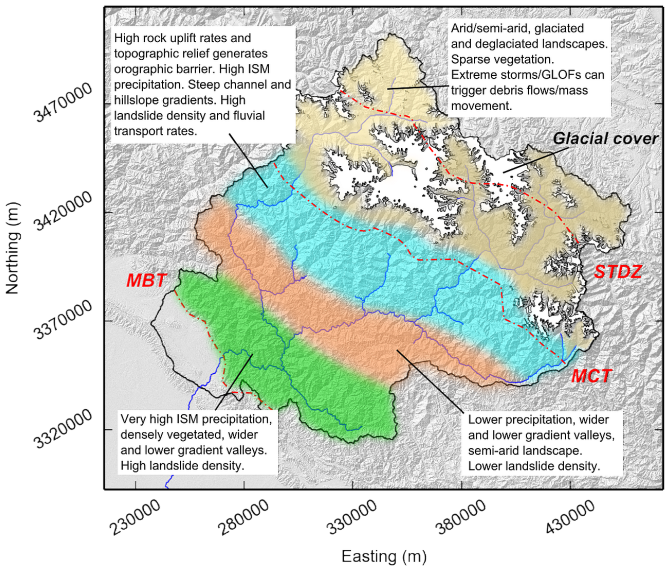

Figure 4.2: Broad distribution of geomorphic process domains across the Ganga catchment. The approximate positions of the Main Boundary Thrust (MBT), Main Central Thrust (MCT) and South Tibetan Detachment Zone (STDZ) are shown by red dashed lines following Ray and Srivastava [2010]. Relative landslide density was determined by manual mapping of >400 landslides across the Ganga catchment using GoogleEarth imagery, where landslides in glacially influenced parts of the catchment were excluded. ISM denotes the Indian Summer Monsoon.

terraces in Quaternary alluvial fan deposits [Sinha *et al.*, 2010]. A number of these terraces have been dated using optically stimulated luminescence (OSL) to reveal terrace ages of up to ∼14 ka (Sinha et al., 2010). During the transition from the Late Pleistocene to the Holocene, an intensification of the ISM is observed in a number of proxy records [Goodbred and Kuehl, 2000; Fleitmann *et al.*, 2003; Dixit *et al.*, 2014], which is believed to have driven a period of intense fluvial incision across much of the Himalaya [Sinha *et al.*, 2010; Dixit *et al.*, 2014]. Erosion of pre-Holocene sedimentary records during this period of intensified monsoon is proposed as one mechanism to explain the notable absence of older terraces [Pandey *et al.*, 2014]. Further changes in the intensity of the Indian Summer Monsoon during the Holocene have been inferred from marine sediments in the Bay of Bengal and Arabian Sea, and speleothems from Oman and China [Denniston *et al.*, 2000; Goodbred and Kuehl, 2000; Gupta *et al.*, 2005; Clift *et al.*, 2008; Dixit *et al.*, 2014]. Limited terrestrial records from the Indian subcontinent [Dixit *et al.*, 2014] suggest a period of intensified Indian Summer Monsoon during the early Holocene in response to changes in summer insolation forcing, which is consistent with terrace formation driven by enhanced fluvial incision during the early Holocene [Gupta *et al.*, 2005; Srivastava *et al.*, 2008; Sinha *et al.*, 2010; Ray and Srivastava, 2010]. Mean sediment flux to the lower Ganga Plains during the period 11-7 ka is estimated to have increased by over two fold [Goodbred and Kuehl, 2000; Sinha and Sarkar, 2009], which is in good agreement with stalagmite δ^{18}O profiles in Oman which indicate a rapid increase in Indian Summer Monsoon precipitation between ∼10.6 and 9.2 ka [Fleitmann *et al.*, 2007]. Arabian Sea records further indicate an earlier period of monsoon intensification at ∼13 ka, representing the major transition between the glacial and Holocene periods, although smaller magnitude changes in climate are observed even earlier [Sirocko *et al.*, 1993]. These phases of incision during the early Holocene are punctuated by minor depositional events that form sequences of fill terraces close to the mountain front. Slip on the underlying Himalayan

Frontal Thrust (HFT) produces vertical displacement rates of 4 to 6.9 mm yr^{-1} and may result in terrace abandonment [Sinha *et al.*, 2010]. During the mid-Holocene, stalagmite records in Oman and Yemen suggest that the ISM has been gradually weakening since ∼7.6 ka in response to a progressive decrease in summer insolation [Fleitmann *et al.*, 2007]. Evidence presented by Gupta *et al.* [2005] suggests that the ISM entered a more arid phase at ∼5 ka, although a number of abrupt events punctuate the mid to late Holocene record. For example, speleothem evidence from caves in central Nepal has suggested that between 2300-1500 yr BP there was a significant drop in monsoon precipitation [Denniston *et al.*, 2000; Fleitmann *et al.*, 2007]. In general however, the ISM appears to have been relatively stable over the last 1.5-2 ka.

A number of slack water and flood deposits in the Ganga valley record rapid sediment accumulation over the Ganga floodplain during high flow events in the late Holocene [Wasson *et al.*, 2013]. Seven of these flood units have been dated between ∼280 and 600 years old by OSL and calibrated with ^{14}C ages from preserved charcoal fragments [Wasson *et al.*, 2013]. These deposits are preserved in a slightly wider part of the bedrock gorge upstream of the mountain front, where flood waters would have backed up as the river enters the narrower gorge immediately downstream. Additional deposits were studied by Wasson *et al.* [2013] at Devprayag and Raiwala (Fig. 4.1) although they recorded small flood couplets as opposed to single flood event deposits. Stacked sand-silt couplets representing phases of persistent flooding were also identified between 2,500-1,200 and 320-209 yr BP at Devprayag and were attributed to changes in the spatial extent of the ISM based on geochemical evidence [Srivastava *et al.*, 2008].

During 2013, heavy rainfall between the 15^{th} and 17^{th} June was centred over the Alaknanda and Bhagirati catchments and generated significant flash flooding and numerous landslides, causing notable damage to the Kedarnath region in the Alaknanda catchment (Fig. 4.1). A moraine dammed lake (Chorabari) had

formed north west of the Kedarnath region in response to the elevated levels of snow-melt runoff in the preceding month, which is also understood to have burst on the morning of 17th June 2013, releasing water with a peak discharge estimated at 783 m^3 s^{-1} into the Alaknanda valley [Durga-Rao *et al.*, 2014]. Flash flooding is not an uncommon phenomenon in the Ganga basin; other large magnitude events were documented in 1894 and 1970 [Rana *et al.*, 2013]. Both of these flood events were attributed to the breaching of dams created by landslides on the tributaries of the Alaknanda River, following unusually high rainfall events. Sediment deposited following the 2013 floods upstream of Devprayag (Fig. 4.1) over-topped the 1970 flood sediment deposits (thought to be the largest flood during the last 600 years), suggesting that the 2013 flood water levels were the highest in the Alaknanada valley during at least the last 600 years [Rana *et al.*, 2013; Wasson *et al.*, 2013], and possibly since the Last Glacial Maximum [Devrani *et al.*, 2015]. The 2013 event also presents a rare opportunity to re-sample ^{10}Be concentrations following an extreme flood event in the modern Ganga River, to compare against pre-event concentrations as documented by Lupker *et al.* [2012].

4.4 Methods

Quartz-rich sand samples were taken from modern gravel bars (herein termed modern samples) and independently dated terrace and floodplain deposits (Fig. 4.3). ^{10}Be concentrations measured from floodplain samples are thought to accurately reflect upstream basin-averaged denudation rates if sediment residence time in the floodplain is sufficiently short to avoid additional ^{10}Be accumulation prior to burial [Gosse and Phillips, 2001; Lupker *et al.*, 2012]. In the instance of thick event beds (>2 m), sediment at the base of each bed is assumed to have been rapidly buried to a depth greater than the penetration range of cosmic rays, so will have remained shielded since burial and therefore should

have accumulated minimal post-depositional ^{10}Be. In order to reduce the impact of ^{10}Be accumulation after deposition of dated terraces, sediment samples were collected from the base of thick beds (> 1 m) that record individual flood events either as overbank fines, or as channel braid bars [Wasson *et al.*, 2013]. At least 2 kg of quartz-rich sand was sieved from the base of event beds. All samples were collected following horizontal digging for ∼1 m into steep cuts through the deposits to minimise post-burial CRN production. CRN concentrations from terrace and floodplain samples were corrected for post-depositional ^{10}Be accumulation by considering that the samples had been exposed to cosmic radiation since deposition at the same depth as they were sampled from. For the slower, long-term sedimentation rates of ∼2 mm yr^{-1} in the older early Holocene terraces, only samples from the base of very thick-bedded (>1-2 m) gravels were used to minimise post-depositional effects, where it is assumed that samples would have been largely shielded from further CRN production. Sample depths and post-depositional corrections are presented in Table 4.1. Sand was taken from the base of several metre thick sand deposits (RFLO and DV2013) abandoned following the summer 2013 Alaknanda flood event to evaluate the degree of mixing of sand during a single extreme event. Floodplain, terrace and modern river sand samples were first dried before sieving into a number of grain size fractions. The main grain size fraction of interest in this study is 250-500 μm. Samples with sufficient material in the 250-500 μm fraction were then passed through a horizontal Frantz to remove magnetic minerals. Samples were also supplemented with material from the 125-250 μm grain size fraction where there was insufficient material in the 250-500 μm fraction. Following this procedure, samples were put through repeated dissolutions in aqua regia and diluted HF and HNO_3 solutions to remove mineral phases other than quartz. Quartz samples were then etched with HF to remove between 30 and 50 % of their volume. The purity of the clean quartz cores were then tested by ICP-OES. All the Al concentrations in the quartz cores were below 300 ppm. Between 7 and 30 g of quartz cores were

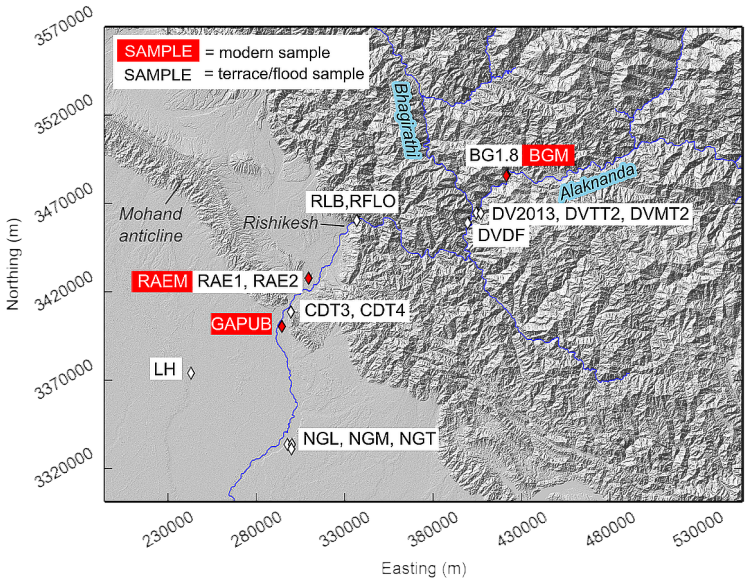

Figure 4.3: Modern (red) and terrace/floodplain/flood (white) sample locations and names in the lower Ganga catchment. See Table 4.1 for full description of samples.

dissolved in concentrated HF. Samples were spiked with c. 220 μg of a ^{9}Be carrier produced in the cosmogenic isotope analysis facility at the Scottish Universities Environmental Research Centre (SUERC) from phenakite crystals. The ^{10}Be carrier concentration is c. 9 $\times 10^{-16}$ ^{10}Be/^{9}Be. A procedural blank was prepared together with each group of samples. Be was isolated from the solutions following routine column chemistry [Darvill *et al.*, 2015]. ^{10}Be/^{9}Be ratios of the produced BeO targets were measured with the 5 MV Pelletron AMS at the SUERC [Xu *et al.*, 2010]. ^{10}Be data were calibrated against the National Institute of Standards and Technology standard reference material NIST SRM 4325. The activity of NIST SRM 4325 corresponds to a nominal ^{10}Be/^{9}Be ratio of 2.79 $\times 10^{-11}$ for a ^{10}Be half-life of 1.36 $\times 10^{6}$ years. The processed blank ratios ranged between 4 and 54 % of the sample ^{10}Be/^{9}Be ratios. The uncertainty of this correction is included in the stated standard uncertainties.

Catchment-averaged denudation rates were calculated for each sample using the CAIRN method [Mudd *et al.*, 2016], which estimates production and shielding

factors on a pixel-by-pixel basis, rather than a catchment-averaged shielding factor as in more commonly used CRN analysis packages such as CRONUS [Balco *et al.*, 2008]. Snow shielding (by year-round glacial cover rather than seasonal snow cover) was determined for the Ganga catchment using data downloaded from the Global Land Ice Measurements from Space (GLIMS) Glacier Database [Armstrong *et al.*, 2005]; production rates beneath these glaciers were assumed to be zero. The GLIMS data suggest that ∼14 % of the Ganga catchment is glaciated (Fig. 4.1), which is ∼12 % higher than estimates in Lupker *et al.* [2012] which were produced prior to the completion of the GLIMS database in this region. The proportion of catchment glacier cover is likely to have been notably higher during the early Holocene, and as such, production rates may have been lower when averaged over the full catchment. We therefore consider the production and erosion rates calculated for ancient deposits as maximum values.

4.4.1 Results

The ^{10}Be concentrations of the two modern samples near the mountain front (GAPUB and RAEM) are 17.70 and 13.56 $\times 10^3$ at g^{-1}, respectively. When combined with sample LUPK09 (with a concentration of 9.2 $\times 10^3$ at g^{-1}) from [Lupker *et al.*, 2012] which was similarly collected near the mountain front, an average concentration of 14.1 $\times 10^3$ at g^{-1} is estimated for modern samples. ^{10}Be concentrations of the majority of samples, both from ancient terraces and recent flood deposits, largely fall within the error of modern detrital samples (Fig. 4.4 and Table 4.1). Only three samples (BG1.8, DVDF and CDT4) display ^{10}Be concentrations considerably greater than the upper error bound (19.1 $\times 10^3$ at g^{-1}) of modern river samples; the average concentrations of these terrace samples are in excess of 20 $\times 10^3$ at g^{-1}. Only one sample, DVTT2, has an average concentration (6.66 $\times 10^3$ at g^{-1}) notably below the lower error bound of the

modern samples (8.20 $\times 10^3$ at g^{-1}). Samples taken from flood deposits associated with the 2013 Alaknanda flood (DV2013 and RFLO) reveal concentrations of 16.06 and 12.85 $\times 10^3$ at g^{-1}, respectively, which fall well within the error of modern river sediment samples. In a frequency-histogram of ^{10}Be concentration data

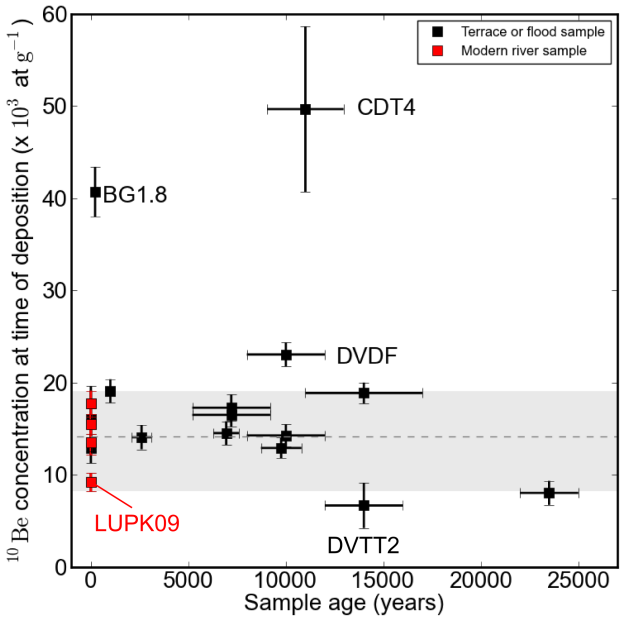

Figure 4.4: Measured modern river (red) and terrace or flood/floodplain (black) ^{10}Be concentrations relative to their depositional age. Horizontal error bars represent the published age error associated with the independently dated deposit, and vertical error bars represent error in ^{10}Be concentrations determined in this study. Sample LUPK09 from Lupker *et al.* [2012] is also included and labelled.

(Fig. 4.5a), the three samples with the highest concentrations (BG1.8, DVDF and CDT4) produce a positively skewed distribution. These samples represent a fine grained ~300 year flood deposit [Wasson *et al.*, 2013], ~10,000 year old terrace fill [Srivastava *et al.*, 2008] and ~11,000 year old terrace fill [Sinha *et al.*, 2010], respectively (See Appendix B for further sample details). With the removal of samples BG1.8 and CDT4 from the frequency-histogram, the ^{10}Be concentration data generate a near-normal distribution (Fig. 4.5a). Possible explanations for the high concentration measurement at BG1.8 may include insufficient shielding

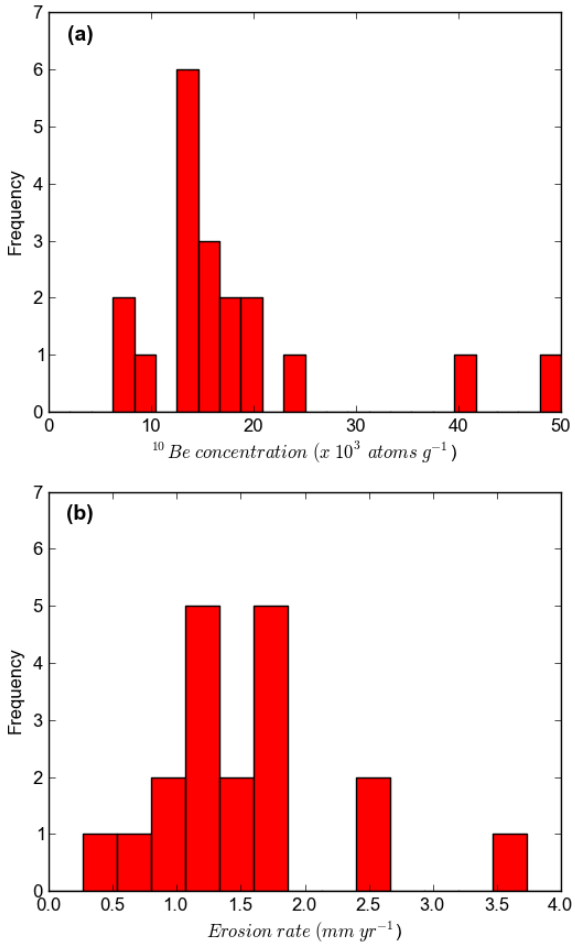

Figure 4.5: (a) Frequency histogram of mean ^{10}Be concentrations shown in Fig. 4.4. (b) Frequency histogram of mean erosion rates calculated using the CAIRN method.

since deposition, resulting in ^{10}Be enrichment of the deposit. Unlike other samples analysed here, the event bed associated with this sample was only ∼0.5 m thick so burial (and therefore complete shielding) was unlikely to be instantaneous. Whilst a number of additional samples were taken from this exposure to try and produce depth-concentration profiles, their grain size was too fine for CRN analysis. However, the maximum CRN enrichment at the site during burial is likely to only be ∼1650 atoms g^{-1} based on local CRN production rates and sample depth, which is less than the measurement uncertainty. With respect to the two terrace deposits (DVDF and CDT4), high concentrations could also have been produced if the samples were overwhelmed by locally derived, high concentration hillslope sediment which was not well mixed. Samples with the largest CRN concentration variability also seem to focus around 10-15 ka (Fig. 4.4), which may represent a period of post-glacial conditions where a combination of low CRN concentration material (generated by glacial erosion) and high CRN concentration sediment (due to lower precipitation rates and therefore slower erosion of non-glaciated landscapes) generated during the Last Glacial Maximum may have been mobilised as the ISM intensified during the early Holocene. Results from CAIRN modelling of all concentrations suggest that catchment-averaged denudation rates for each sample largely lie within the error of modern detrital samples (Fig. 4.5b). Based on the measured concentrations, these samples correspond to integration timescales of ∼500 years, representing the average time period when the erosion rate is considered to be constant, based on the time needed to erode one mean attenuation path length (approximately 60 cm/erosion rate) [Lal, 1991]. There does not appear to be a spatial trend between ^{10}Be concentration and upstream catchment area, even downstream of large tributary confluences (Fig. 4.6). The impact of high CRN concentration samples on the frequency-histogram of erosion rates calculated using CAIRN modelling is less apparent (Fig. 4.5b), but the distribution shows significant spread. Calculating sediment flux estimates from a single erosion rate at the upper end of the distribution could result in sediment

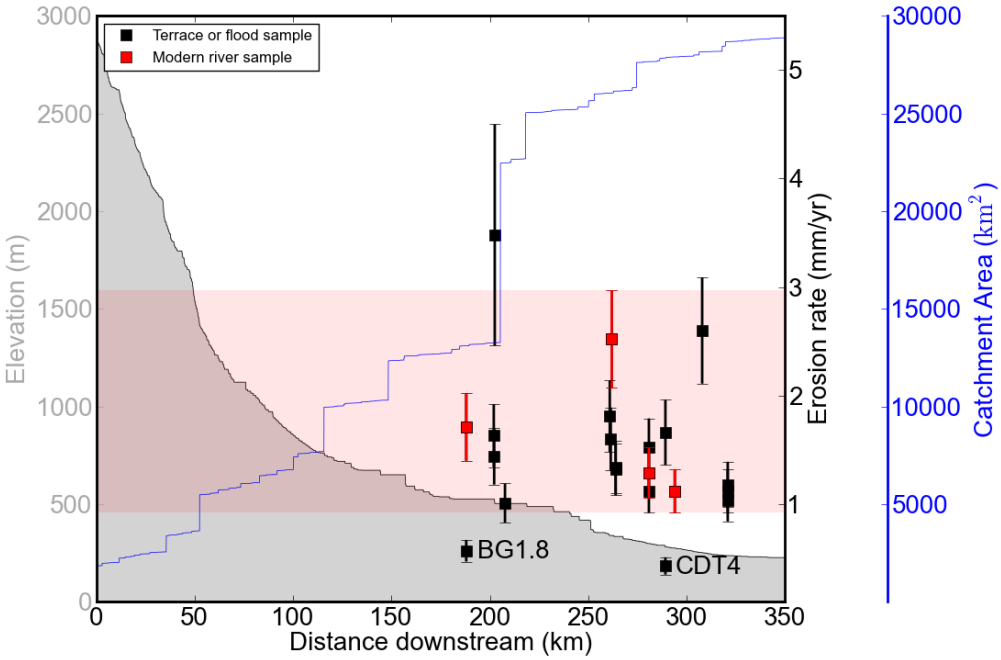

Figure 4.6: Modern river (red) and terrace or flood/floodplain (black) catchment-averaged erosion rates with respect to distance downstream, sample elevation (grey shaded region) and upstream catchment area (blue line). Vertical error bars represent error associated with the modelled erosion rate and propagated ^{10}Be concentration errors used to derive the erosion rate. The red shaded area represents erosion rates within the error of modern samples. Outliers BG1.8 and CDT4 are labelled.

flux estimate being up to seven times larger than one based on a sample at the lower end of the distribution.

Table 4.1: CRN sample details, ^{10}Be concentrations and modelled erosion rates. Full sample details are given in Extended Data.

Sample	Locality	Sampling date	Lat.	Lon.	Basin area (km^2)	Mean basin elevation (m)	Sample age (years)	Sample age reference	Sample elevation (m, from DEM)	Average shielding factor*	*Sample depth (cm)*	*Sample Be^{10} concentration* (x 10^3 at g^{-1})	*Be^{10} concentration at time of deposition* (x 10^3 at g^{-1})	CAIRN-derived erosion rate (mm yr^{-1})
BGM	Bagwan - modern	06-Oct-2014	30.2255	78.6823	10,920	3,825	Modern	n/a	498	0.868	0	13.57 ±1.40	13.56 ± 1.40	1.71 ± 0.31
BG1.8	Bagwan - terrace	06-Oct-2014	30.2253	78.6812	10,920	3,825	217 ± 76	Wasson et al. (2013) – OSL	504	0.868	500	40.70 ±2.69	40.69 ± 2.69	0.57 ± 0.10
DV2013	Devprayag – 2013 flood	05-Oct-2014	30.1499	78.6136	11,052	3,805	1	n/a	492	0.868	0	16.07 ±3.55	16.06 ± 3.55	1.44 ± 0.26
DVTT2	Devprayag - terrace	05-Oct-2014	30.1508	78.6107	11,052	3,805	14,000 ± 2,000	Srivastava et al. (2008) - OSL	530	0.868	600	7.09 ±2.45	6.66 ± 2.45	3.48 ± 1.02
DVMT2	Devprayag – terrace	05-Oct-2014	30.1508	78.6153	11,052	3,805	10,000 ± 2,000	Ray and Srivastava (2010) - OSL	517	0.868	650	14.69 ±1.22	14.27 ± 1.22	1.63 ± 0.29
DVDF	Devprayag - terrace	06-Oct-2014	30.1253	78.5905	18,716	3,870	10,000 ± 2,000	Ray and Srivastava (2010) - OSL	559	0.868	1,300	23.19 ±1.28	23.04 ± 1.28	1.01 ± 0.18
RLB	Rishikesh - terrace	03-Oct-2014	30.1305	78.3322	21,675	3,670	6,940 ± 650	Sinha et al. (2010) – OSL	393	0.868	300	15.61 ±1.27	14.52 ±1.28	1.60 ± 0.29
RFLO	Rishikesh – 2013 flood	03-Oct-2014	30.1328	78.3342	21,675	3,670	1	n/a	370	0.868	20	12.86 ±1.58	12.85 ±1.58	1.81 ± 0.33
RAE1	Raewalla - terrace	08-Oct-2014	30.0053	78.2195	23,030	3,580	2,600 ± 500	Wasson et al. (2013) – OSL	308	0.877	100	17.51 ±1.04	14.07 ± 1.31	1.52 ± 0.27
RAE2	Raewalla - terrace	08-Oct-2014	30.0053	78.2195	23,030	3,580	1,000 ± 200	Wasson et al. (2013) – OSL	308	0.877	80	20.76 ±1.09	19.08 ± 1.28	1.12 ± 0.20
RAEM	Raewalla - modern	08-Oct-2014	30.0054	78.2227	23,030	3,580	Modern	n/a	303	0.885	0	15.53 ±1.07	15.52 ± 1.07	1.29 ± 0.23
CDT3	Chandi Devi – terrace	03-Oct-2014	29.9431	78.1757	23,221	3,560	9,760 ± 1,040	Sinha et al. (2010) – OSL	309	0.877	320	14.19 ±1.11	12.91 ± 1.12	1.66 ± 0.30
CDT4	Chandi Devi – terrace	03-Oct-2014	29.9398	78.1788	23,221	3,560	11,080 ± 1,960	Sinha et al. (2010) – OSL	389	0.877	1,000	49.72 ±8.96	49.65 ± 8.96	0.43 ± 0.08
GAPUB	Haridwar - modern	11-Oct-2014	29.9067	78.1635	23,221	3,560	Modern	n/a	271	0.886	0	17.70 ±1.42	17.70 ± 1.42	1.12 ± 0.20
LH	Landhaura – terrace	07-Oct-2014	29.8105	77.946	23,941	3,510	23,500 ± 1,500	Verma (2016) – OSL	256	0.879	220	15.65 ±1.21	8.03 ± 1.31	2.60 ± 0.49
NGL	Nagal – terrace	07-Oct-2014	29.6698	78.1786	23,941	3,510	14,000 ± 3,000	Sinha et al. (2010) - OSL	249	0.889	1,260	19.07 ±1.13	18.86 ± 1.13	1.03 ± 0.19
NGM	Nagal – terrace	07-Oct-2014	29.6652	78.185	23,941	3,510	7,200 ± 2,000	Sinha et al. (2010) - OSL	258	0.889	850	16.67 ±1.28	16.49 ± 1.28	1.18 ± 0.21
NGT	Nagal - terrace	07-Oct-2014	29.6649	78.1859	23,941	3,510	7,200 ± 2,000	Sinha et al. (2010) - OSL	259	0.889	250	18.96 ±1.36	17.27 ± 1.44	1.12 ± 0.20
LUPK09**	Rishikesh - modern	11-Aug-2009	30.127	78.330	21,690	3,150	Modern	n/a	357	0.868	0	9.20 ± 1.0	n/a	2.52 ± 0.45

* Average shielding factor is the average of the combined shielding factors; topographic, snow and self-shielding values. These were calculated using a depth integrated approach (see Mudd *et al.*, 2016).

** Details for this sample (BR924) are from Table 1 in Lupker *et al.* (2012). We have recalculated the erosion rate using the CAIRN method (Mudd *et al.*, 2016).

4.5 Impact of stochastic inputs on CRN variability and sediment flux estimates

4.5.1 Impact of landslides on CRN variability

A range of processes are likely to drive temporal variability in CRN concentrations in sand sampled close to the outlet of large Himalayan catchments. The most obvious process is stochastic inputs generated by mass wasting of hillslopes, which generate large quantities of sediment with relatively low CRN concentrations. Frequency-histograms presented in Figure 4.5 suggest that such stochastic processes may form part of the natural background variability, as low concentration values tend not to skew the distributions. More samples would be needed to draw sa clearer picture on this. Below, we examine how different erosional processes may drive the observed variability in CRN concentrations measured close to the Ganga outlet. This is approached using a numerical analysis of catchment-averaged CRN concentrations derived under varying background erosion rates, landslide area, depth and surface CRN production rates. Given the complexity of this type of landscape (e.g. multiple geomorphic process domains, climatic variability), we do not attempt to mimic these processes and reproduce measured concentrations. Neither do we use this analysis to determine the relative contributions required from stochastic processes (e.g. area and depth of landsliding) to produce our observed concentrations. Instead, this numerical analysis is used to explore the sensitivity of outlet CRN concentrations to a range of parameters and scenarios that may drive variability.

The relative ^{10}Be contribution by landsliding can be approximated to first-order by calculating the volume of material generated by the event, and the average

concentration of that material. The concentration of landslide material is strongly controlled by the local surface CRN production rate and depth of the landslide. CRN production rates rapidly diminish in the upper few metres of the Earth's surface (Lal, 1991; Stone, 2000; Niedermann, 2002) following:

$$P(z) = P_0 e^{(\frac{-z\rho}{\Lambda})} \tag{4.1}$$

where z is the depth below the surface (cm), Λ is the attenuation length (g cm^{-2}), ρ is rock density (g cm^{-3}), and P_0 is the surface nuclide production rate (atoms g^{-1} yr^{-1}). At depths greater than ∼2 m the CRN production rate (by spallation reactions) is negligible, as is muon production, as atoms generated by muon interactions represents a small proportion ($< 2\%$) relative to those produced by spallation reactions in the upper 1-2 m of the Earth's surface (e.g. Niedermann, 2002). Here, we calculate the average concentration of landslide material by integrating the surface production rate within the upper 2 m; we find that the depth-averaged production rate of the upper 2 m (P_d) is ∼30 % of P_0. This was converted into a ^{10}Be concentration (C) in atoms g^{-1} using:

$$C = \frac{(P_d \Lambda)}{\rho(\epsilon + \Lambda\lambda/\rho)} \tag{4.2}$$

from Niedermann [2002], where we assume that the CRN decay constant (λ) is equal to 0 over the timescales we are concerned with ($<10^3$ years) relative to the half-life of ^{10}Be. We use ρ = 2.7 g cm^{-3} and Λ = 160 g cm^{-2}. We also assume a steady-state erosion-rate (ϵ) across the upstream catchment. For landslide depths of less than 2 m, the average concentration was calculated based on the production rate integral specific to that depth. For simplicity, we assume that the rest of the catchment is eroding uniformly at a background erosion rate, with a catchment average CRN production rate of 35 atoms g^{-1} yr^{-1} which is comparable to the catchment-averaged production rate calculated for the Ganga catchment in CAIRN. The concentrations calculated at the Ganga outlet also assume complete

sediment mixing. The CRN concentration at the catchment outlet ($\alpha_{event+uniform}$) is then calculated using:

$$\alpha_{event+uniform} = \frac{(\alpha_{uniform}\phi_{uniform}) + (\alpha_{event}\phi_{event})}{\phi_{uniform} + \phi_{event}} \tag{4.3}$$

where $\phi_{uniform}$ and $\alpha_{uniform}$ are the background sediment flux and ^{10}Be concentration, respectively. ϕ_{event} and α_{event} are the event or landslide generated sediment flux and ^{10}Be concentration, respectively. A series of sub-catchments were then selected to examine the influence of spatial variability in surface production rates across the Ganga basin, to provide a realistic range of values in the numerical analysis (Fig. 4.7). Average shielding factors (snow and topographic shielding) were first calculated for each of these sub-catchments using the CAIRN method [Mudd *et al.*, 2016], which were then used in the online CRONUS v2.3 calculator [Balco *et al.*, 2008] to calculate production rates, using a constant production rate model with a Lal/Stone scaling scheme for spallation (Fig. 4.7 and Table 4.2). The default landslide surface production rates were initially set to the same as the catchment-average production rate. The landslide surface production rates were then varied based on realistic production rates derived from sub-catchments across the Ganga catchment (Table 4.2). Earthquake-induced landsliding datasets from the 1999 Chi-Chi (Taiwan) and 2015 Gorkha (Himalaya) earthquakes [Lin and Tung, 2004; Martha *et al.*, 2017], state that the total landslide areas were ∼128 and 90 km^2, respectively. Areas of these sizes represent approximately 0.5 % of the Ganga catchment area. We therefore use the value of 0.5 % as an approximation of the proportion of the hypothetical catchment to have been impacted by landsliding. In the analysis, the average depth of the landslides was varied from 0.5 to 5 m, the average background erosion rate from 0.2 to 2.0 mm yr^{-1}, and the average landslide surface production rate from 10 to 60 atoms g^{-1} yr^{-1}. We use an average landslide depth where in reality, the depths of individual landslides occurring in response to an earthquake or intense storm are likely to fit

a power-law distribution [Hovius *et al.*, 1997]. However, at any point in time it is unlikely that the full power-law distribution of landslide depths is sampled or integrated into the catchment wide signal, due to the recurrence interval and amount of time taken to evacuate larger and deeper landslides. We also assume that the CRN concentration profile in the upper 2 m of the landscape is in steady-state before landsliding. This assumption is more important in slowly eroding landscapes, where it may take tens of thousands of years to reach secular equilibrium [Dunai, 2010]. This may result in over-estimated landslide CRN concentrations in our analysis, if the CRN concentration profile is not in equilibrium. However, by varying the landslide surface production rates in our analysis we can indirectly assess the importance of such an effect. We calculate 'volumetric sediment flux'

Table 4.2: Catchment area, average elevation and average ^{10}Be surface production rate for sub-catchments in the Ganga catchment

	Catchment Area (km^2)	Catchment-average elevation (m)	Production rate (atoms g^{-1} yr^{-1})
Sub-catchment 1	*1,955*	*1,606*	*11.08*
Sub-catchment 2	*4,635*	*4,716*	*56.02*
Sub-catchment 3	*1,801*	*5,033*	*70.51*
Sub-catchment 4	*1,449*	*2,642*	*24.28*
Sub-catchment 5	*169*	*4,483*	*49.13*
Sub-catchment 6	*181*	*1,868*	*12.82*
Sub-catchment 7	*253*	*1,404*	*9.57*
*Sub-catchment 8**	*39*	*4,806*	*49.61*
Ganga (whole)	*23,039*	*3,560*	*33.16*

**This sub-catchment represents the area upstream of the 2013 Alaknanda flooding*

by combining the flux derived from background erosion rates with the calculated

landslide flux, and compared these to sediment flux estimates derived from the ^{10}Be concentration at the catchment outlet (which we term the 'CRN-derived sediment flux'). For a catchment eroding at a uniform rate (ϵ in mm yr^{-1}), the CRN-derived sediment flux is the product of the erosion rate, catchment area (A in km^2) and average rock density (ρ in kg m^{-3}).

In this analysis, we assume that sediment storage between the region affected by landslides and the outlet is small relative to the total sediment flux of the catchment. Unlike the eastern and western Himalaya, the central Himalaya (which is largely drained by tributaries of the Ganga River) is comparatively void of large valley fills [Blöthe and Korup, 2013], which is likely to limit large volumes of sediment storage and sediment residence times. Recent modelling has also suggested that approximately 50 % of coarse material generated by post-seismic landsliding is evacuated within 5 to 25 years [Croissant *et al.*, 2017]. In our scenarios, we assume complete evacuation of material to the outlet within a year. The effect of reducing the amount of landslide derived sediment contributing to the outlet concentration are shown in the Supplementary Material for reference however. The default and range of values tested for each parameter in the analysis are shown in Table 4.3. Based on the above calculations, our results suggest that increasing the average landslide depth results in a marked decrease in outlet ^{10}Be concentration, most notably between depths of 0.5-3 m (Fig. 4.8a). This can be explained through the exponential decay in ^{10}Be production rates in the upper 2 m of the landslide [Lal, 1991; Stone, 2000; Niedermann, 2002]. This reduction in concentration is greatest under lower background erosion rates. Increasing background erosion rates from 0.2-2.0 mm yr^{-1} also reduces the effect of landsliding on outlet ^{10}Be concentrations (Fig.4.3b). Under lower background erosion rate, landslide material represents a greater proportion of the total sediment flux, so the system has less capacity to buffer the landslide input and the ^{10}Be concentration is more sensitive to deeper landslides. We also find that outlet

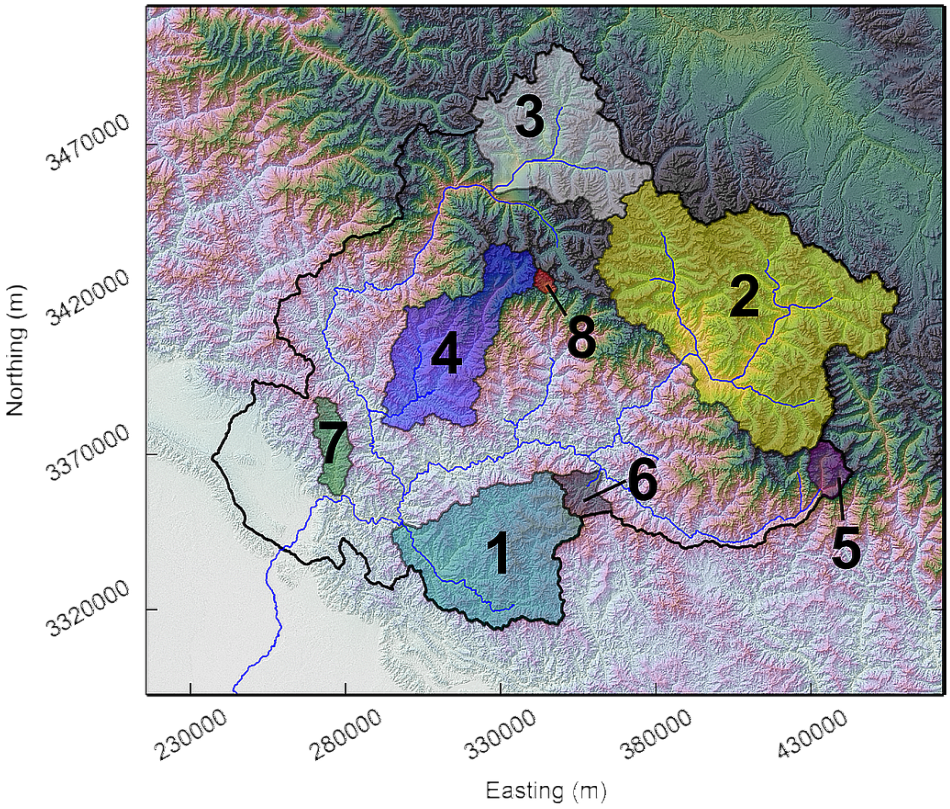

Figure 4.7: Location of sub-catchments used to determine the variability in production rate across the Ganga catchment (presented in Table 4.2).

Table 4.3: Default and range of parameter values used in numerical analysis.

Parameter	***Default value***	***Range of modelled values***
Landslide depth (m)	*2*	*0.5-5*
Catchment Area (km^2)	*23,000*	-
% of catchment impacted by landsliding	*0.5*	-
Catchment-averaged surface production rate (atoms g^{-1} yr^{-1})	*35*	-
Background erosion rate (mm yr^{-1})	*0.5*	*0.2-2.0*
Landslide surface production rate (atoms g^{-1} yr^{-1})	*35*	*10-60*

^{10}Be concentrations are sensitive to the average landslide surface production rate. Where the average surface production rate of the landsliding is increased (e.g. comparable to that expected in high altitude sub-catchments of the Ganga - see Table 4.2), predicted outlet ^{10}Be concentrations also increase relative to scenarios with otherwise identical parameter values (Fig. 4.8c). Interestingly, we also find that volumetric sediment flux estimates are consistently higher than CRN-derived fluxes (Fig. 4.8d). Increasing background erosion rates increases both CRN-derived and volumetric sediment flux estimates, but increasing average landslide depth or landslide CRN production rate can reduce CRN-derived sediment flux estimates to a much greater degree than volumetric flux estimates. Our analysis generates variability in CRN concentrations that is considerably larger than what we document in the Ganga catchment (Fig. 4.4), suggesting that buffering of stochastic inputs must occur [Croissant *et al.*, 2017]. The evacuation time of fine-grained sediment (sand and finer) is likely to be fast relative to the coarse fraction, as the fine-grained fraction is annually entrained and transported downstream during months impacted by the Indian Summer Monsoon. This is supported by grain size analysis [Dingle *et al.*, 2016] along a number of exposed gravel bars within the Ganga catchment, which demonstrate that the channel bed is comprised largely of grain sizes >1 mm, even beneath the surface armour layer. Typically, grain sizes <1 mm represent less than ∼15 % of the grain size distribution (Fig. 4.9) which is also observed across other catchments of the Ganga River. This suggests that there is relatively little in-channel storage (or mixing) of finer grained sediments relative to the large fluxes of these river systems, which on entering the Ganga Plain, are thought to be largely dominated (>90 %) by sand-sized (and finer) sediments [Dingle *et al.*, 2017]. However, the majority of landslide deposits are likely to be made of coarser material [Attal and Lavé, 2006; Attal *et al.*, 2015] which will take longer to be evacuated or abraded into smaller and more easily transportable grain sizes. Whilst landsliding may generate the quantities and ^{10}Be concentrations of sediment required to drive

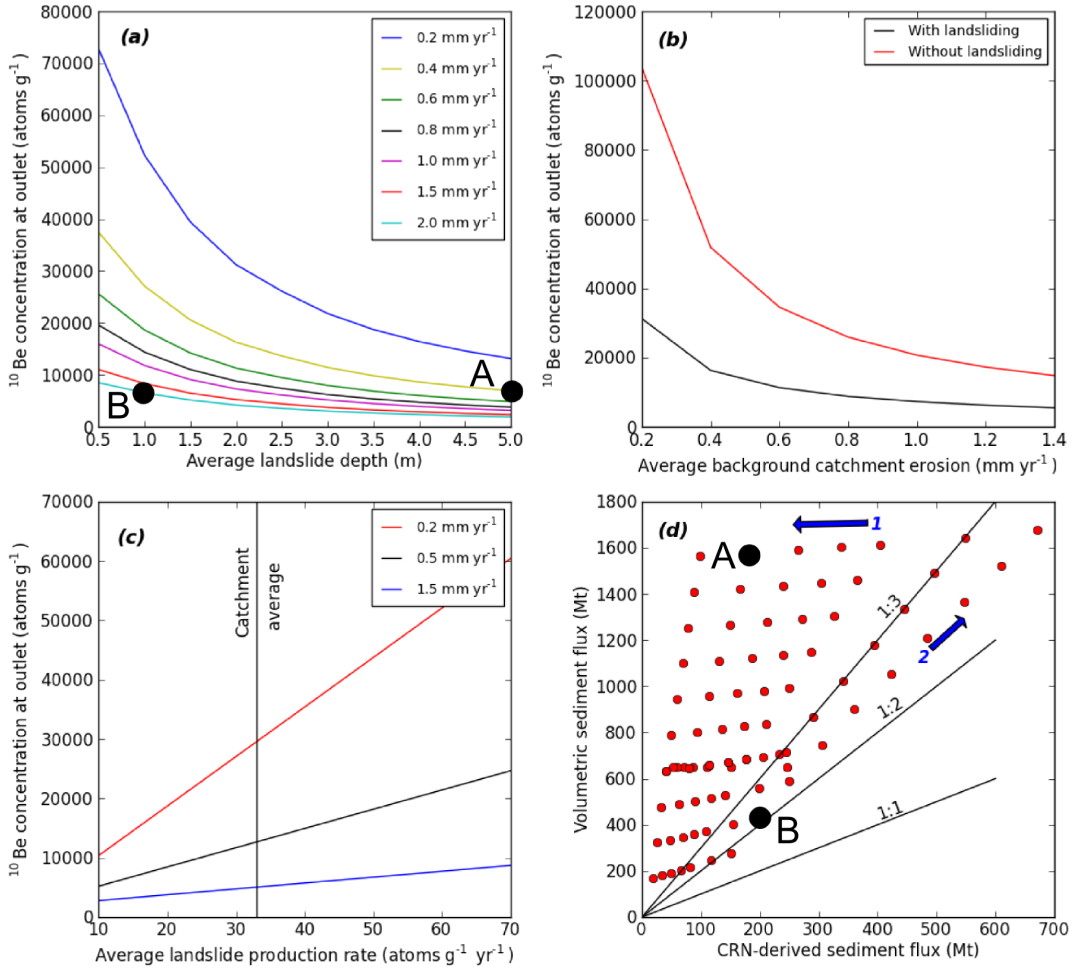

Figure 4.8: (a) Variations in ^{10}Be concentration predicted at the outlet in response to increasing landslide depth and as a function of background erosion rates (represented by coloured lines). (b) Outlet ^{10}Be concentration as a function of background erosion rate (where all other parameters are constant at default values - see Table 4.3), for a system undergoing no landsliding (red line - where erosion is driven purely by background erosion) and another with 2 m deep landsliding over 0.5 % of the catchment area (black line). (c) Outlet ^{10}Be concentration under varying average landslide ^{10}Be surface production rates (based on Table 4.2) and background erosion rates (coloured lines). The black vertical line represents the whole Ganga catchment-averaged production rate of ~33 atoms g^{-1} yr^{-1}. (d) Comparison of volumetric and CRN-derived sediment fluxes from analysis in Figures 4.8a-c. The blue arrow labelled 1 shows the effect of decreasing background erosion rate, and the blue arrow labelled 2 shows the effect of increasing landslide depth and/or landslide CRN production rate . The black dots in (a) and (d) represent scenarios A and B which are discussed in more detail later and in Fig. 4.10.

significant changes in concentration at the outlet, the evacuation timescales of these event sediments buffers their impact. Evacuation of event deposits over decadal to centennial timescales will reduce the ratio of background to event sediment fluxes [Croissant *et al.*, 2017], and likely limit the impact on ^{10}Be concentrations documented at the outlet.

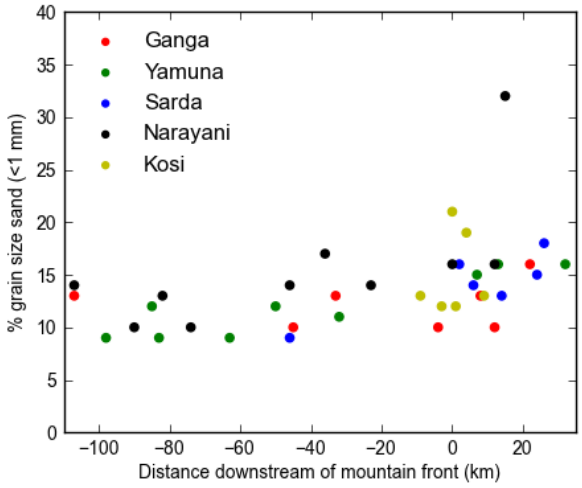

Figure 4.9: Volumetric sand (grain sizes <1 mm) proportions in sub-surface sediment samples along major tributaries of the Ganga River.

4.5.2 Other potential sources of variability in CRN concentration

Whilst landsliding with different depths and from different parts of the Ganga catchment is likely to represent a key component in CRN variability, a number of other factors may also contribute, which are discussed below. Firstly, spatially variable distributions of quartz-rich lithologies across the Ganga catchment may lead to over and under-estimation of denudation rates in specific lithological settings. However, potential variations in sediment quartz content have been assessed by Vance *et al.* [2003] in the Ganga catchment, who concluded that the

correction due to the dilution of quartz from sediments sourced from carbonate-rich series in the catchment is of a similar magnitude (maximum of ∼9 % change in erosion rate for sub-catchments in the High Himalaya) to the production rate estimates and analytical errors. Recent studies have also highlighted the effect of grain-size dependent ^{10}Be enrichment, where coarser gravel-sized fractions have been documented to yield higher apparent denudation rates than the medium sand-sized fraction which is typically sampled [Puchol *et al.*, 2014; Schildgen *et al.*, 2016; Lukens *et al.*, 2016] as a result of the process through which the different grain size fractions are generated (e.g. reworked hillslope material, landsliding), or differing sediment source elevations. Similarly, downstream lags in ^{10}Be denudation rate spikes have been observed along the Tsangpo-Brahmaputra River in the eastern Himalayan syntax [Lupker *et al.*, 2017], due to the distance which sediment generated in the rapidly uplifting Namche Barwa-Gyala Peri massif must travel before being abraded into the grain size fraction used for sampling. However, modern samples collected close to the Ganga outlet are not likely to be influenced by either process, as the majority of sediment has already been abraded into sand by this point [Dingle *et al.*, 2017]. Similarly, a number of the floodplain and terrace deposits sampled were entirely sand. Exceptions to this include terrace deposits CDT3, CDT4, DVDF, DVMT2, DVTT2 and RLB, where sand samples were taken from poorly consolidated fluvial deposits containing imbricated and well-rounded quartzite cobbles and pebbles. However, additional CRN samples were not run on individual clasts in these deposits to determine whether the coarser fraction yielded higher apparent denudation rates.

Glacial lake outburst floods (GLOFs) are not uncommon across the Himalaya (e.g. Cenderelli and Wohl, 2003; Kattelmann, 2003), and have the potential to generate and mobilise large quantities of sediment. Geomorphic analysis following the 1977 and 1985 GLOFs in the Mount Everest region [Cenderelli and Wohl, 2003] suggested that much of the sediment eroded from the upper 10-16 km of the GLOF

route was unconsolidated sediment (glacial till, colluvium, glacio-fluvial terraces). Erosion was typically found to be limited in valleys with resistant bedrock or consolidated side walls. Similarly, the availability of unconsolidated material is also thought to be a key limiting factor in the volume of debris flows triggered following GLOFs, which can limit the erosive potential of the flow [Breien *et al.*, 2008]. In the absence of existing studies which document ^{10}Be concentrations in proglacial lake sediments, we cannot infer how sediment released from the glacial lake may contribute to downstream variations in ^{10}Be concentration. Geomorphological evidence in reaches downstream of GLOFs suggests that much of the sediment eroded by the flood is largely unconsolidated (glacially-influenced) material from relatively shallow depths (<3 m; Cenderelli and Wohl, 2003) which is likely to have a complex exposure history. Given the relatively short length of the reach impacted downstream of the GLOF (relative to the full length of a system such as the Ganga), and the likely CRN enriched nature of surface deposits reworked by GLOFs, it seems unlikely that these types of events drive significant change in outlet ^{10}Be concentrations. This is supported by work in the Marsyandi River catchment in Nepal, which suggested that erosion in the upper glaciated catchment is almost an order of magnitude lower than fluvial incision rates in the upper Marsyandi River [Heimsath and McGlynn, 2008].

Extreme monsoonal storms, such as the one that generated the 2013 Alaknanda flooding, also have the potential to generate CRN variability if hillslope runoff mobilises large quantities of unconsolidated sediment on valley sides and initiates mass-wasting of hillslopes [Dobhal *et al.*, 2013; Devrani *et al.*, 2015]. Sample DV2013 was collected from a thick sand unit at the Ganga channel margins (∼18 m above the modern channel) near Devprayag, known locally to have been deposited following the 2013 Alaknanda flood. We find that the ^{10}Be concentration of this deposit (16.06 $\times 10^3$ at g^{-1}) also lies within the error of modern samples at the outlet. One interpretation is that the sediment generated

by this event was sufficiently well mixed: on reaching the Ganga outlet it had minimal impact on the outlet CRN concentration. Material mobilised by the Alaknanda flooding was largely unconsolidated, surficial hillslope material [Dobhal *et al.*, 2013]. As such, the ^{10}Be concentration of these sediments will reflect their local production rate ($\sim$50 atoms g^{-1} yr^{-1} - see Table 4.2) and background erosion rate. If erosion in the Alaknanda valley is driven primarily by large storm and flood events, unconsolidated surface sediments could have been accumulating ^{10}Be since as early as the LGM [Devrani *et al.*, 2015], with very low background erosion rates. As such, this type of erosive event may have generated sediment with a higher than expected CRN concentration (given the depth of material removed) as a result of this CRN-enriched surface layer.

Annual monsoonal storms may also contribute to the observed variability where storms tap into localised parts of the catchment. The hillslope sediments and reworked deposits these storms mobilise could vary in ^{10}Be concentration in the different geomorphic process domains, as they will have variable CRN production rates (which is a function of elevation), background erosion rates and deposit characteristics (e.g. deep-seated landslide). Background erosion rates in particular are likely to vary dramatically across the Ganga catchment as a result of spatially variable rock uplift, lithology, rainfall and vegetation cover [Vance *et al.*, 2003; Anders *et al.*, 2006; Bookhagen and Burbank, 2006]. Earthquake-induced landsliding, GLOFs and extreme storm events are all likely to generate large quantities of sediment with ^{10}Be concentrations that would be sufficient to drive significant change in the ^{10}Be concentration recorded at the Ganga outlet. However, the impact that these processes have is limited by the ability of the river to entrain and transport this sediment out of the catchment. The evacuation timescales of sediment generated by these processes will likely vary as a function of the frequency and magnitude of localised storm events which mobilise mass-flow deposits from hillslopes into rivers sediment.

If this sediment is sourced close to the sampling location, it is also unlikely to be fully homogenised. The distance required to fully mix localised hillslope or tributary inputs has been shown to be as much as several kilometres [Binnie *et al.*, 2006], which may induce variability in ^{10}Be concentrations recorded at the outlet. In terms of modern river samples, a number of small ephemeral streams drain directly in the main Ganga channel near the outlet. During the monsoon season when these channels are active, sediment of differing ^{10}Be concentrations will be transported to the main channel and may not be sufficiently mixed on reaching the outlet sampling locations. High concentration samples documented close to the Ganga outlet could therefore represent locally derived and poorly mixed sediments, which reflect the erosional processes specific to a small frontal region of the catchment.

4.5.3 Suitability of CRN as a proxy for sediment flux in large catchments

To understand the observed doubling in sediment delivery to the Bengal fan during the early Holocene, we explore whether it is possible to increase volumetric sediment flux whilst maintaining ^{10}Be concentrations within the natural degree of background variability. We use the same numerical analysis and run two scenarios. The first scenario represents a baseline condition; in the second scenario, we increase the background erosion rate, average landslide depth, landslide surface production rate and area of landsliding (Table 4.4). Landslide mapping following the 2015 Gorkha and Dolakha earthquakes suggests an area of ∼90 km^2 was affected, generating ∼0.62 km^3 of landslide material based on area-volume scaling [Martha *et al.*, 2017]. This corresponds to an average landslide depth of ∼6.8 m, indicating our assumed depths (of 2 m) are conservative. As discussed earlier however, it is unlikely that the full-distribution of landslide size or depth would be

sampled or integrated into the catchment-wide signal, and as such, a lower average depth might be more representative. We have varied parameters between the two scenarios based on what might be expected during periods of increased monsoon intensity: greater background erosion rate and landslide frequency. However, we have no constraint on the magnitude of change in these parameters and, as such, we use the numerical analysis in an informative sense to examine how increased storm-induced mass-wasting and background erosion rates might have impacted CRN concentrations in the Ganga catchment. We also assume that only 7 % and 10 % of the material generated by landsliding is transported to the outlet in scenarios 1 and 2, respectively, based on the 5-25 years timescales of evacuation suggested by Croissant *et al.* [2017]. A marginally higher proportion is used in the second scenario to represent the effect of elevated water discharge as a result of increased monsoonal precipitation.

Using the parameters shown in Table 4.4, we find that in both scenarios the ^{10}Be concentration at the outlet is within the magnitude of natural variability documented at the Ganga outlet. Sediment flux estimates generated from ^{10}Be concentrations (termed CRN-derived sediment flux) are within natural system variability as they only differ by ∼30 % between scenarios (Table 4.4). Interestingly under both sets of conditions, the volumetric sediment flux (calculated from the volume of material eroded under background erosion across the entire catchment and the imposed landslide dimensions) is higher than the CRN-derived sediment flux. Furthermore, the volumetric sediment flux generated in the second scenario is double the corresponding CRN-derived flux. This is consistent with results from the numerical analysis, where the volumetric sediment flux is typically at least two to three times greater than the CRN-derived flux (Fig. 4.8d). Our results suggest that, for ^{10}Be concentrations within a natural degree of system variability, the volumetric sediment flux could theoretically differ from that calculated directly from ^{10}Be concentrations (Fig. 4.8d and Table 4.3).

Table 4.4: Parameter values used to examine the difference in CRN-derived and volumetric sediment fluxes. More details are provided in Table S4 in Supplementary Material.

Parameters	*Scenario 1*	*Scenario 2*
Catchment area (km^2)	23,000	23,000
% of catchment impacted by landsliding	0.5	1.0
Background erosion rate (mm yr^{-1})	0.7	0.8
Average landslide depth (m)	2.0	2.5
Landslide surface production rate (atoms g^{-1} yr^{-1})	35	45
Outlet concentration (atoms g^{-1})	**19,477**	**12,545**
CRN-derived sediment flux (Mt)	**66**	**103**
Volumetric sediment flux (Mt)	**85**	**201**

Similar outlet CRN concentrations can be derived from landscapes dominated by different erosional processes within large catchments. For example, our analysis suggests that a 'fast eroding' landscape experiencing a background erosion rate of 2.0 mm yr^{-1} and 1 m deep landslides over 0.5 % of the catchment (e.g. a landscape dominated by shallow landsliding or debris flows) could produce comparable outlet CRN concentrations to a 'slow eroding' landscape experiencing 0.4 mm yr^{-1} background erosion and 5.0 m deep landslides over the same area (e.g. a landscape experiencing deep earthflows) (Fig. 4.10). The CRN-derived sediment fluxes between these two landscapes may be comparable, but the volumetric flux from the landscape with lower background erosion (and deeper landsliding) is considerably larger than from the landscape with higher background erosion (and shallower landsliding). Halving the area affected by landsliding in only the lower background erosion scenario (with deeper landsliding) still yields comparable CRN-derived fluxes (within 15 % of each other, rather than 6 %), but the volumetric flux is double that generated under higher background erosion rates (with shallower landsliding over a larger area) . These types 'slow eroding' landscapes which experience episodes of mass wasting are exemplified by arid

parts of the northwest Himalaya, which generally only experience high intensity rainstorms during abnormal monsoon years where the ISM can penetrate north of the orographic barrier formed by the Higher Himalaya [Bookhagen *et al.*, 2005] (Fig. 4.2). Similarly, slow moving earthflows in parts of the Eel River catchment in California which is characterised by long and low-gradient hillslopes mobilise huge quantities of sediment which contribute to the majority of the suspended sediment flux from the catchment [Mackey and Roering, 2011]. The two end-member models presented in Figure 4.10 suggest that under different geomorphic process domains, comparable mean CRN concentrations can be produced through very different CRN concentration populations. CRN-derived sediment fluxes are based on an average landscape lowering rate, and thus fail to incorporate the effects of spatially limited deeper inputs of sediment which are characterised by much lower CRN concentrations. Lower rates of background erosion means that sediment eroded off the surface is enriched in CRN (as sediment residence times in the upper 1-2 m of the Earth's surface are longer as a function of lower background erosion rates). This effectively averages out the influence of lower concentration input from deeper inputs, and results in near identical CRN concentrations at the mountain front to a system undergoing only a slightly faster (or more uniform) rate of background erosion. Thus, considerably different volumetric fluxes can be obtained for the same CRN concentration. This may explain the absence of a ^{10}Be concentration signature of Holocene climate change.

4.6 Conclusions

We present CRN analysis from a variety of modern and Holocene sedimentary deposits in a large trans-Himalayan catchment spanning more than 7000 m in relief, where sediment production is heavily influenced by stochastic inputs. We find a natural degree of variability in ^{10}Be concentrations documented in the

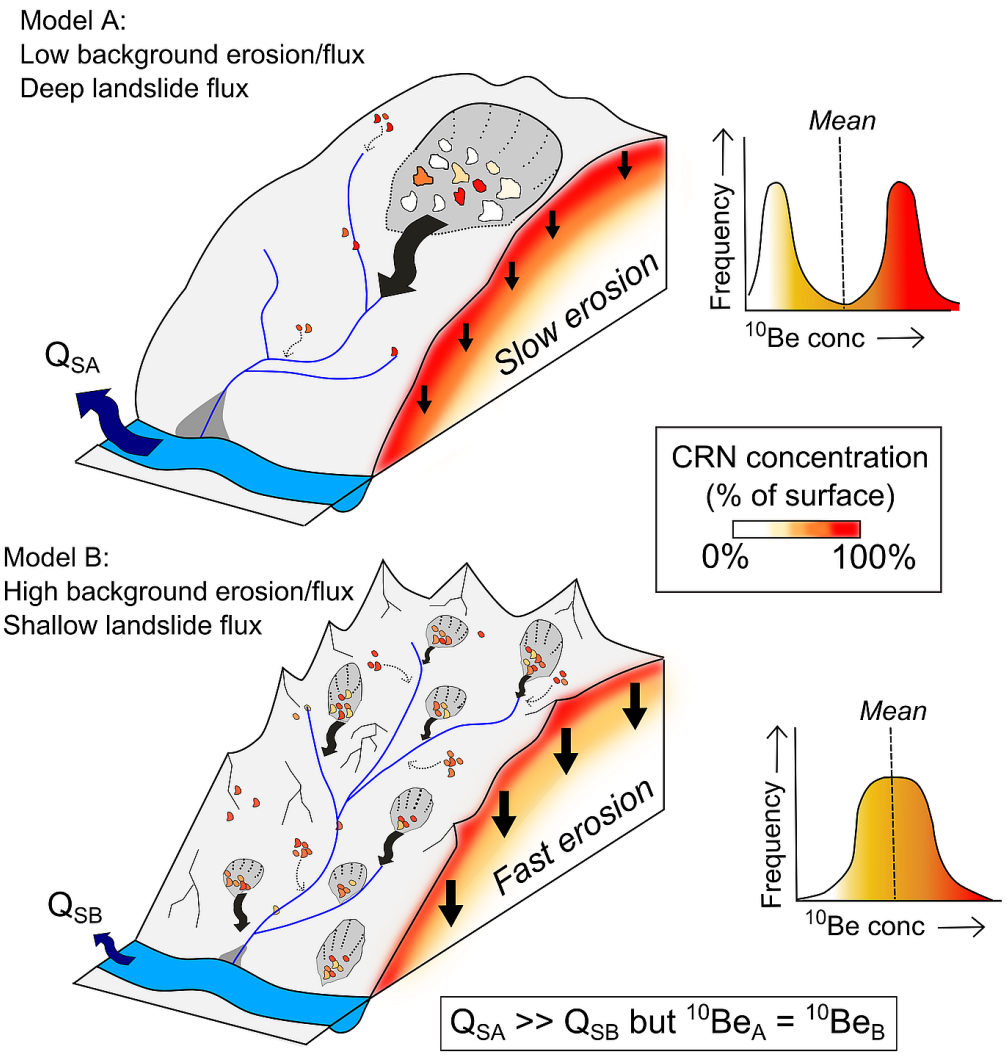

Figure 4.10: Schematic of how comparable mean CRN concentrations in river sand can be derived under two different erosion scenarios with different volumetric sediment fluxes. In these instances, slow background erosion rates and deep landsliding (Model A) result in comparable CRN concentrations to landscapes domianted by faster background erosion rates and shallow landsliding (Model B). If Model A is set with a background erosion rate of 0.4 mm yr^{-1} and 5 m deep landsliding over 0.5 % of the catchment, and Model B with 2 mm yr^{-1} background erosion rates and 1 m deep landsliding (over the same area), comparable CRN concentrations (see black dots marked on Fig. 4.8a) and CRN-derived sediment fluxes are generated, but volumetric sediment fluxes are over three times larger in Model A. This is due to the relative enrichment of ^{10}Be in the upper 2 m of the landscape with low background erosion rates, which when combined with low CRN concentration material from depth, results in two distinct CRN concentration populations. Where erosion is generally more homogeneous (Model B) and CRN concentrations are distributed more uniformly, comparable mean CRN concentrations are derived between the two models.

modern channel and Holocene flood deposits preserved near the catchment outlet. These concentrations appear insensitive to regional intensification of the Indian Summer Monsoon, thought to have occurred ∼11-7 ka. We demonstrate that it is possible to generate relatively constant ^{10}Be concentrations at large catchment outlets despite significant variability in volumetric sediment flux as a result of spatially variable background erosion rates and erosional processes such as earthquake-induced landsliding and storm events. We suggest that the observed variability is driven by 1) the nature of the stochastic inputs of sediment (e.g. the type of hillslope process, surface CRN production rates, degree of mixing), and 2) the evacuation timescales of these sediment deposits. Sediment deposits generated by processes such as earthquake-induced landsliding, GLOFs or storm events, are typically large in volume and low in ^{10}Be concentration, but the time taken to mobilise this sediment out of the catchment limits its impact on catchment-averaged concentrations. We suggest that in landscapes characterised by high topographic relief, spatially variable climate and multiple geomorphic process domains, the use of ^{10}Be concentrations to generate sediment flux estimates may not be truly representative, as comparable mean catchment CRN concentrations can be derived through dramatically different erosional processes. For a given CRN concentration, volumetric sediment flux estimates may vary considerably and under certain conditions, CRN concentrations may under-estimate actual erosion rates and hence sediment flux.

4.7 Chapter Acknowledgements

Elizabeth Dingle is funded under a NERC PhD Studentship (NE/L501566/1) and CRN analysis was undertaken at the SUERC CIAF (under grant application 9150.1014). We would like to thank the International Association of Sedimentologists, British Society of Geomorphology and the Edinburgh University Club of

Toronto for their financial support of the fieldwork, and Konark Maheswari for his assistance in the field. We are also grateful to Maarten Lupker, Shasta Marerro and Simon Mudd for discussions that have helped shape this manuscript.

4.8 Extended Data

The details and context of cosmogenic radionuclide samples used in this study are presented in Fig. 4.11 - Fig. 4.26. Locations can also be found in Fig. 4.3.

Figure 4.11: BGM - Sieved from upper layer of modern gravel bar. 82 mm long penknife in base of pit.

Figure 4.12: BG1.8 - Fine-grained sand deposit (∼7 m in thickness) corresponding to sequence of palaeoflood deposits from last ∼600 years. Sample taken 1.8 m from base of exposure which has been OSL dated at 225±72 years Wasson *et al.* [2013].

Figure 4.13: CDT3 - Sample from base of ∼3.2 m thick fill of poorly sorted fluvial pebble and cobble conglomerate, suggesting it was deposited during a single event. Approximately 26 m above the modern channel. OSL dated at 9,760 ±1,040 years [Ray and Srivastava, 2010]. 90 mm long penknife for scale.

Figure 4.14: CDT4 - Sample from poorly sorted fluvial pebble and cobble conglomerate terrace fill deposited during a single event. Sample ∼3 m below terrace surface and ∼80 m above modern channel. OSL dated at 11,080 ±1,960 years [Ray and Srivastava, 2010]. 90 mm long penknife for scale.

Figure 4.15: DVDF - Terrace deposit ∼95 m above modern channel. Sample taken from base of 4 m thick fluvial conglomerate layer. Capped by more angular phylite/schist deposit (erosional contact) suggesting input of locally derived landslide/debris flow material. Unit OSL dated at 10,000±2,000 years [Ray and Srivastava, 2010]. 90 mm long penknife for scale.

Figure 4.16: DVMT2 - Terrace deposit ∼77 m above modern channel. Poorly sorted and weakly consolidated fluvial pebble and cobble conglomerate. Sample taken from base of 6.5 m unit. Unit OSL dated at 10,000±2,000 years [Ray and Srivastava, 2010].

Figure 4.17: DVTT2 - Terrace deposit ∼112 m above modern channel. Fluvially derived coarse cobble and sand (poorly sorted) conglomerate interbedded within locally derived (Lesser Himalayan) phyllite deposits. 90 mm long penknife for scale.

Figure 4.18: RFLO - Sand flood deposit associated with 2013 Alaknanda flooding. ∼7 m above water level in October 2014.

Figure 4.19: RAEM - Sieved from upper layer of modern gravel bar.

Figure 4.20: RAE1/RAE2 - ∼0.8 m thick sand and silt deposit above cobble bed. Capped by ∼30-50 cm of soil. Samples taken from the lower-most and middle units identified in P1 in Wasson *et al.* [2013] which are dated at 2.6±0.6 ka and 1.0±0.2 ka, respectively.

Figure 4.21: NGM - Cross-bedded sand succession ∼17 m above modern channel. Sample taken from base of 1.5 m thick cross-bedded sand unit. Top of unit (S2) OSL dated at 7,200±2,000 years by Sinha *et al.* [2010].

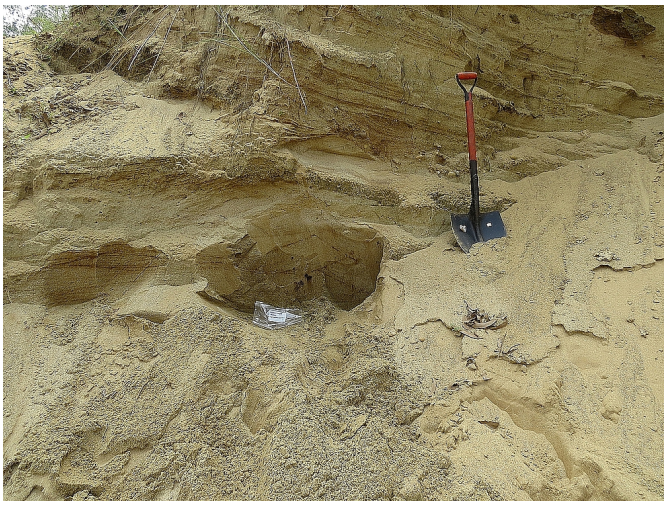

Figure 4.22: NGL - Cross-bedded medium-coarse sand unit ∼10 m above modern channel. Base of unit (S1) OSL dated at 14,000±3,000 years by Sinha *et al.* [2010].

Figure 4.23: NGT - 4 m high exposure of low angle cross-bedded sands, topped with finer silt and mud deposits. Corresponds to OSL sample from this part of unit dated at 7,200±2,000 years by Sinha *et al.* [2010].

Figure 4.24: LH - Cross-bedded sand exposure (4 m high). Sample taken 2.2 m from top of exposure. Corresponds to OSL sample from unit dated at 23,500±1,500 years by Verma [2016].

Figure 4.25: RLB - ∼42 m above modern channel on roadside cut. Poorly sorted, structureless fluvial conglomerate. Large, rounded boulders, cobbles and sands [Ray and Srivastava, 2010]. 90 mm long penknife for scale.

Figure 4.26: DV2013 - Laminated sand deposit ∼5 to 10 m thick formed in single event following the 2013 Alaknanda flooding.

4.9 Supplementary Material

Tables S1-S3 present the range of sediment flux and CRN concentrations derived when 100, 50 and 10% of landslide derived sediment is transported to the outlet. Scenarios A and B relate to erosion scenarios described in Figure 10.

Table S1. Assumes 100% delivery of landslide material

	Background flux (Mt yr^{-1})	*Landslide flux (Mt yr^{-1})*	*Background CRN concentration (atoms g^{-1})*	*Landslide CRN concentration (atoms g^{-1})*	*CRN-derived flux (Mt yr^{-1})*	*Volumetric flux (Mt yr^{-1})*
Scenario A	25	1,553	51,852	6,222	186	1,577
Scenario B	124	311	10,370	5,029	197	434

Table S2. Assumes 50% delivery of landslide material

	Background flux (Mt yr^{-1})	*Landslide flux (Mt yr^{-1})*	*Background CRN concentration (atoms g^{-1})*	*Landslide CRN concentration (atoms g^{-1})*	*CRN-derived flux (Mt yr^{-1})*	*Volumetric flux (Mt yr^{-1})*
Scenario A	25	1,553	51,852	6,222	169	801
Scenario B	124	311	10,370	5,029	174	279

Table S3. Assumes 10% delivery of landslide material

	Background flux (Mt yr^{-1})	*Landslide flux (Mt yr^{-1})*	*Background CRN concentration (atoms g^{-1})*	*Landslide CRN concentration (atoms g^{-1})*	*CRN-derived flux (Mt yr^{-1})*	*Volumetric flux (Mt yr^{-1})*
Scenario A	25	1,553	51,852	6,222	103	180
Scenario B	124	311	10,370	5,029	138	155

Table S4. Fluxes and concentrations relating to early Holocene monsoon intensification – more details in Table 4.

	Background flux (Mt yr^{-1})	*Landslide flux (Mt yr^{-1})*	*Background CRN concentration (atoms g^{-1})*	*Landslide CRN concentration (atoms g^{-1})*	*CRN-derived flux (Mt yr^{-1})*	*Volumetric flux (Mt yr^{-1})*
Pre-Holocene	43	621	29,630	8,515	68	87
Holocene	49	1,553	25,926	8,000	105	204

Chapter 5

Discussion

Understanding the geomorphological processes that shape the Earth's surface is fundamental to the relationship between society and the wider environment. Anthropogenic pressures on fluvial systems, such as the Ganga River, continue to increase in response to rapidly growing populations living on floodplains which raises important questions on how best to manage or live alongside these dynamic rivers. These types of decisions and strategies require an in-depth knowledge of processes that control large-scale river morphology, and is integral to understanding the sensitivity of river dynamics to external perturbations (e.g. projected climate change). While I have presented the previous three chapters as standalone papers, their key findings collectively contribute to answering a number of much broader and unsolved questions in geomorphology. The observations and conclusions drawn from this study present an important contribution towards the understanding of large-scale river morphology, and is not restricted to rivers draining the Himalayan foreland basin. A primary consideration of this thesis has been to approach the main research topics from a wider and more process-based approach, in order to drive advancement in our knowledge of general physical processes, as opposed to very site-specific controls and features. In particular,

this thesis has made progress towards answering the following questions:

1. Can long-term rates of basin subsidence influence the large-scale morphology of modern rivers?

2. Which processes control the grain size of sediment exported into foreland basins, and does this shape downstream river morphology?

3. How can we better quantify the sediment flux from large mountainous catchments into foreland basins?

In the rest of this chapter I will summarise the key findings from each of the previous three chapters in the context of these questions. The wider implications of my findings will also be discussed with particular reference to sediment transfer between active mountain ranges and depositional basins, and large-scale fluvial geomorphology. I will also discuss the uncertainties, limitations and issues raised by each of the thesis chapters. This will be followed by a broader section outlining possible avenues for future research.

5.1 Can long-term rates of basin subsidence influence the large-scale morphology of modern rivers?

In Chapter 2, I applied a new basin-scale approach to quantifying patterns of fluvial incision and aggradation across the Ganga Plain using a modified swath technique. This highlighted patterns of channel super-elevation and entrenchment across the extent of the entire Himalayan foreland basin. I explored potential controls on these observations through an analysis of basin subsidence rates and sediment grain size data. Subsidence rates were estimated across the Ganga Plain using basement profiles derived from seismic data, and previously published convergence velocity data. My analysis suggested that subsidence rates systematically increase from the west Ganga Plain (rates of 0.3±0.4 mm/yr) to the east Ganga Plain (rates of 1.6±0.6 mm/yr). These rates were also supported by Holocene sedimentation rate estimates in the east Ganga Plain [Sinha *et al.*, 1996; Lupker *et al.*, 2011], and new downstream sediment fining rates documented in gravel bars downstream of the Himalayan mountain front. Surface and subsurface sediment grain size distributions were collected along the Yamuna, Ganga, Sharda, Gandak and Kosi Rivers to determine downstream sediment fining rates. Sediment grain size fining rates have been used as a proxy for relative subsidence rates in a number of studies [Robinson and Slingerland, 1998; Duller *et al.*, 2010; Allen *et al.*, 2013b], and my results suggested higher sediment fining rates in the east Ganga Plain (and hence, also higher subsidence rates) which is in keeping with estimates made using basement profile and convergence velocity data.

The rate of basin subsidence governs the accommodation space generated in which to trap sediment exported out of the Himalayan mountains by river systems, which in turn may influence the development of topography and relief across

the surface of the basin. The amount of sediment trapped in the foreland basin represents a small fraction of the total load exported (∼10% based on estimates in Lupker *et al.* 2011), which suggests that sediment availability should not limit the amount trapped in the basin. Gravel-to-total sediment load estimates presented in Chapter 3 suggest that the vast majority of sediment exported out of the Himalayan mountains is in the sand (and finer) grain size fraction, and is therefore likely to be carried in suspension away from the mountain front, whilst the coarser fraction is retained or trapped in the proximal basin. The position of the gravel-sand transition in these river systems is also found to closely reflect the observed patterns of basin subsidence, where the transition is found much closer to the mountain front in the east Ganga Plain where subsidence rates are also highest. In Chapter 3 I demonstrate that the position of the gravel-sand transition is also independent of upstream catchment area, and is found at a comparable distance downstream of the mountain front in both small foothill-fed and large trans-Himalayan catchments in the east Ganga Plain. These observations suggest that the rate of basin subsidence may, in part at least, influence the position of the gravel-sand transition in these systems. It is also possible to argue that the position of the transition and also the observed contrast in channel morphology across the Ganga Plain is driven by spatial differences in water discharge. In general, the catchment area upstream of the mountain front is larger in systems in the east Ganga Plain. Combined with higher amounts of precipitation, which are visible in TRMM satellite data [Anders *et al.*, 2006], one might expect greater discharge in rivers draining into the east Ganga Plain. However, this is not consistent with modelled relationships between water discharge and position of the gravel-sand transition [Paola *et al.*, 1992a; Robinson and Slingerland, 1998] where higher discharges are thought to drive progradation (or downstream migration) of the gravel front or gravel-sand transition. Whilst a possible control on shaping wider alluvial fan morphology, these spatial variations in water discharge also fail to explain a triggering mechanism of fan entrenchment in the west Ganga Plain.

Absolute gravel flux estimates presented in Chapter 3 indicate that river systems further west (Yamuna, Ganga, Sharda) typically export larger amounts of gravel (and coarser sediments) than those in the east. This coarse sediment is subsequently trapped in the proximal basin, upstream of the gravel-sand transition. As rivers pass from the mountains and into the Ganga Plain, they dramatically lose their ability to transport this coarser material [Ferguson, 2003] as a result of the reduction in fluid shear stress associated with lower channel gradients in the Plain. One possible explanation for marginally steeper fan surfaces close to the mountain front in the west Ganga Plain may be due to higher gravel fluxes and lower vertical subsidence rates. If the vertical rate of gravel deposition exceeds the rate of subsidence, gravel deposition may prograde further downstream or result in steepening of the fan apex. Sand sized (and finer) particles are largely carried in suspension and are transported further downstream beyond the gravel-sand transition. In contrast, higher vertical subsidence rates and lower gravel fluxes in the east Ganga Plain may produce vertical (gravel) sedimentation rates in keeping with the rate of subsidence, yielding lower gradient fan surfaces.

In order to drive incision into alluvial fans downstream of the Himalayan mountain front, a reduction in equilibrium channel gradient must be imposed, as a result of base level lowering. Given the distance from the Bay of Bengal, it seems unlikely that base level changes driven by variations in sea level are likely to extend this far upstream. However, climatically driven reductions in base level triggering changes in water and sediment discharge exported out of the Himalayan mountains will likely initiate a top-down wave of incision or base level lowering [Wobus *et al.*, 2010]. This is consistent with our observations on patterns of incision across the Ganga Plain, where the degree of channel entrenchment reduces with distance away from the mountain front. For a constant climatic forcing of channel lowering along the strike of the Ganga Plain, incision will only occur where channel lowering rates outpace subsidence. This will inherently be easier

to achieve where subsidence rates are lower in the west Ganga Plain. In the east Ganga Plain, rates of subsidence are higher and the surface gradient of the Kosi and Gandak fans are exceptionally low, which will also limit the degree to which these systems can incise into their surfaces (in response to the same climatic forcing).

By integrating these observations, I proposed that higher subsidence rates in the east Ganga Plain were responsible for a deeper basin, with perched low-gradient rivers systems that are relatively insensitive to climatically driven changes in base-level. In contrast, lower basin subsidence rates in the west were associated with a shallower basin with entrenched river systems that are capable of recording climatically induced lowering of river base-level during the Holocene. The results of this thesis suggest that long-term rates of basin subsidence are capable of influencing the morphology of modern river systems, and in particular, their sensitivity to externally driven changes in base level. Furthermore, the observations made within this Chapter are consistent with predictions made in previous modelling works such as Paola *et al.* [1992a] and Robinson and Slingerland [1998] concerning the position of the gravel-sand transition (or gravel front) in relation to patterns of basin subsidence, and also further supports the use of sediment grain size as a potential proxy for patterns of basin subsidence rate [Duller *et al.*, 2010; Whittaker *et al.*, 2010, 2011] which I have shown is also applicable in modern river systems.

5.1.1 Limitations and further research

Whilst the data presented in Chapter 2 (grain size and subsidence estimates) suggest that there is a east-west variation in basin subsidence, this could be better supported or constrained to a higher degree of accuracy in a number of ways. Deriving subsidence rates using the depth-to-basement data is limited by

the resolution of the data, which was quite sparse in the proximal region of the foreland basin. These subsidence rate estimates could be supported further with additional sedimentation rate data derived from (dated) sediment cores taken in the proximal part of the basin, similar to those presented in Sinha *et al.* [1996]. Similarly, interferometric synthetic aperture radar (InSAR) data has been used to model land subsidence in various settings [Amelung *et al.*, 1999; Osmanoğlu *et al.*, 2011]. These data could be used across the foreland basin to help better constrain rates and patterns of subsidence as InSAR data can detect surface deformation down to millimetre precision. Furthermore, additional OSL samples from the west Ganga Plain would help constrain timing of the onset of channel entrenchment during the early Holocene. In particular, if samples were targeted with depth down the valley margin and also with distance away from the mountain front, a more complete model of how this wave of incision manifested could be developed.

5.2 Which processes control the grain size of sediment exported into foreland basins, and does this influence downstream river morphology?

Grain size distributions presented in Chapter 2 indicated that there is not a substantial difference in the grain size of sediment being exported into the Ganga Plain by major river systems. The presence of intermontane valleys (Duns) and barrages (water diversion structures) close to the mountain front may have an impact on the grain size measurements on the Yamuna and Gandak Rivers, where grain sizes were found to be typically slightly finer and grain size distributions were narrower. These observations suggest that variations in the grain size of

sediment being exported into the Ganga Plain is unlikely to directly influence the contrast in river morphologies in the east and west Ganga Plain. The position of the gravel-sand transition in these river systems was consistent with findings from various numerical and analytical modelling studies (e.g. Paola *et al.*, 1992a; Robinson and Slingerland, 1998; Marr *et al.*, 2000) where higher rates of basin subsidence yield gravel-sand transitions in more proximal positions (i.e. closer to the mountain front). This was explored in more detail in Chapter 3.

In Chapter 3, I demonstrated that gravel flux from rivers draining the east Ganga Plain is approximately constant, despite upstream contributing catchment areas spanning three orders of magnitude. Gravel flux estimates were made using fan geometry and basin subsidence rates, and were also compared to available sediment flux data to derive gravel-to-total sediment load ratios. My analysis suggested that absolute gravel fluxes out of these systems are surprisingly similar, ranging between ∼0.1 and 1.7 Mt/yr, which represents an average gravel-to-total load proportion of 0.2-2.9% for the trans-Himalayan Kosi and Gandak Rivers in the east Ganga Plain, and between 7.8-100% for a number of small foothill-fed river systems which drain the inter-fan area between the Kosi and Gandak. I explained the similarity in absolute gravel flux across these systems as a result of gravel abrasion during fluvial transport using a numerical model of pebble abrasion. I demonstrated that most of the gravel sourced more than 100 km upstream of the mountain front is abraded into sand by the time it reaches the Plain, as the characteristic transport distance of lithologies which dominate the Higher and Tethyan Himalaya (such as granite, schist, limestone and gneiss) is less than 100-150 km. Regardless of the grain size of sediment put into the fluvial system, if transported over distances greater than this, the input material will be abraded into sand. More resistant lithologies such as quartzite have characteristic transport distances in excess of 1000 km and, as such, are likely to be exported out of the Himalayan mountains in the grain size fraction larger than sand (e.g.

as gravels, pebbles or cobbles). This is because the maximum length of the fluvial network in the Kosi River (which is the largest catchment in the Ganga basin) is only ∼500-600 km.

This was also supported by pebble lithology transects of exposed gravel bars between the mountain front and gravel-sand transition, which showed that despite quartzitic lithologies only making up ∼10% of the mountainous catchment lithology [Attal and Lavé, 2006], quartzite dominated (>50%)the lithologies of gravel bar sediments. This suggested an over-representation of quartzitic lithologies surviving into the Plain, which I attributed to the selective abrasion of weaker lithologies during transport in the mountainous catchment. Small rivers in the Himalayan foothills largely drain the Neogene Siwalik sediments, composed of recycled fluvial sediments which are progressively incorporated back into the mountain range through the frontal accretion of thrust units along the mountain front. These Siwalik sediments are characterised by poorly cemented, well-rounded quartzitic gravels which (largely) survive transport to the mountain front due to their resistant lithology and the short transport distances associated with the foothill-fed catchments. I further considered the results from this chapter in the context of understanding the downstream response in rivers to large influxes of sediment generated by earthquakes and storms in the Higher Himalaya (e.g. the 2015 Gorkha earthquake).

5.2.1 Further questions

Whilst the development of the gravel-sand transition across the Himalayan foreland basin has not been directly addressed in this thesis, the data I have presented here provide a useful starting point for understanding the conditions which may be necessary for it's development. The differential abrasion of weaker lithologies likely generates bimodality of sediment grain sizes exported into the

Himalayan foreland basin, which is one of the conditions often associated with the development of gravel-sand transitions. The exact mechanism through which the gravel-sand transition develops (e.g. by selective deposition, abrasion, or suspended-sediment deposition) remains untested, but presents a worthwhile and obvious avenue for future research. In Chapter 2 I presented data which demonstrated that in general, sediment fining rates between the mountain front and gravel-sand transitions were quite low (0.02-0.06 km^{-1}). The reduction in grain size across the gravel-sand transition is considerably greater however, where the average D_{50} and D_{84} of the most downstream grain size samples along each river was ∼33 and ∼80 mm, respectively. Within a few kilometres downstream, the bed is composed nearly exclusively (> 95%) of sand. In Chapter 3 I demonstrated that the lithology of gravel exported into the Ganga Plain is largely quartzite, which explains the relatively low fining rates observed in the Plain. This aspect of my thesis is consistent with a number of previous publications in that it excludes abrasion as a potential driver for the development of the gravel-sand transition [Parker and Cui, 1998; Venditti and Church, 2014], where the rate of fining that would be required across the transition is an order of magnitude greater than what was observed between the mountain front and gravel-sand transition, and also in experimental pebble abrasion studies [Attal and Lavé, 2009].

Furthermore, there is little understanding of the contribution of recycled quartzite pebbles from the Siwalik hills relative to the modern gravel flux generated in the Lesser, Higher and Tethyan Himalaya. Fluvial incision rates inferred from Holocene and Pleistocene terraces by Lavé and Avouac [2001] suggest values in the order of 10-15 mm yr^{-1} across the Siwalik hills, whilst rates further north in the Lesser and Higher Himalaya do not exceed a ∼8 mm yr^{-1}. In river systems where there are larger outcrops of recycled Siwalik sediments there could be a significant component of recycled Siwalik pebbles in the modern gravel flux, as a result of these high incision rates and relatively low modern gravel fluxes exported into the

Plain. Future research is needed to better quantify and constrain the impact of these recycled sediment fluxes.

5.3 How can we better quantify the sediment flux from large catchments?

Our ability to accurately quantify the sediment flux of large river systems draining tectonically active catchments is constrained by the nature of the river channels (e.g. size and access), stochastic nature of sediment inputs [Benda and Dunne, 1997b; Kirchner *et al.*, 2001], and highly variable water discharge regimes (e.g. Collins and Walling, 2004; Singh *et al.*, 2005; Gitto *et al.*, 2017). These factors make it difficult to collect physical samples that give a representative estimate of sediment flux at large catchment outlets. Constraining sediment fluxes at intermediate timescales of 10^2-10^3 years has been developed by the use of detrital ^{10}Be CRN analysis over the past two decades (e.g. Brown *et al.*, 1995; Granger *et al.*, 1996; Kirchner *et al.*, 2001; Vance *et al.*, 2003; Von Blanckenburg, 2005). The concentration of ^{10}Be recorded in quartz-rich river sediments is assumed to reflect the rate of upstream landscape lowering, assuming steady-state denudation averaged over the entire upstream catchment. Using the concentration of cosmogenic ^{10}Be in modern river sands, catchment-averaged denudation rates can be calculated, and converted into CRN-derived sediment fluxes which are typically averaged over hundred to thousand year timescales [Kirchner *et al.*, 2001; Lupker *et al.*, 2012]. This is based on the premise that in river systems draining large catchments, the effects of stochastic inputs of sediment (which are typically characterised by low CRN concentrations) are buffered, and as such, should not drive significant variability in CRN concentrations documented at the catchment outlet over time. However, in Chapter 4 I presented new CRN

samples from modern river and ancient sediments preserved near the mountain front on the Ganga River (termed the outlet) which showed a degree of natural 'background' variability. This is at odds with many previous studies which have suggested that in catchments with upstream contributing areas in excess of $\sim$1000 km^2, the effects of stochastic inputs of relatively low CRN concentration sediment should be buffered such that the catchment outlet concentration should be relatively constant through time and representative of the long-term catchment erosion rate [Niemi *et al.*, 2005; Yanites *et al.*, 2009]. The variability in CRN concentration I have noted will produce uncertainties in modelled erosion rate and sediment flux estimates, if based on a single CRN sample. This suggested that an understanding of the degree of natural temporal variability in ^{10}Be concentrations is required, even in large catchments, to fully interpret CRN-derived erosion rates and sediment flux estimates.

I proposed that this observed variability is driven by two factors. Firstly, by the nature of stochastic inputs of sediment (e.g. the dominant erosional process, surface production rates, depth of landsliding, degree of mixing), and secondly, by the evacuation timescales of individual sediment deposits which buffers their impact on catchment-averaged concentrations. I further proposed that sediment flux cannot be simply approximated by converting detrital concentration into mean erosion rates and multiplying by catchment area in all landscapes. For a given CRN concentration, I suggested that it is possible to generate different volumetric sediment fluxes as a result of comparable average CRN concentrations being generated by different CRN concentration populations produced by variable geomorphic processes. Using CRN concentrations within this degree of natural variability, volumetric sediment fluxes may be two or three times larger than those derived from CRN concentrations and modelled erosion rates. In order to fully interpret CRN-derived erosion rate and sediment flux estimates, two factors need to be taken into account.

First, a sufficient number of CRN samples are required to determine the degree of background variability across sampling seasons, and to establish where statistical outliers occur. In this chapter, eighteen new CRN samples were presented. In general, the distribution of CRN concentrations was positively skewed by samples with very high CRN concentrations (which relates to sediment sourced under lower erosion rates). This suggested that stochastic inputs driven by processes that generate sediment with a relatively low CRN concentration may form part of the background variability in outlet CRN concentrations. However, this requires further testing and ideally more samples to form robust conclusions. Secondly, an understanding of the types of processes which generate stochastic inputs of sediment within the catchment are required, as these inputs can drive under-estimation of sediment fluxes if derived from CRN concentrations. Where catchments are large enough to generate spatial variability in climate, tectonic uplift or surface CRN production rate (as a result of high catchment relief), variability in CRN concentration is likely to be driven by intermittent mobilisation of sediment (e.g. by storms) stored within discrete parts of the catchment. These deposits are likely to be characterised by different erosional processes or geomorphic domains, which generates sediment with varying CRN concentrations. The input concentration, quantity, efficiency of removal and degree of mixing of sediment generated by these processes will control the degree to which it modifies the CRN concentration at the outlet.

5.3.1 Limitations and further considerations

Ideally more CRN samples would have been used to help thoroughly document and characterise variability in CRN concentration at the Ganga outlet. Whilst a number of additional samples were collected, there was insufficient material in the 250-500 μm fraction to analyse. In particular, more samples in the modern

system over a number of years and different flow conditions would have benefited this study, and helped further understand temporal variability in modern samples. CRN concentrations from different grain size fractions in the terrace deposits would may also have given more insight into the different erosional processes acting within the catchment. In order to better understand how stochastic inputs, sediment mixing and evacuation timescales drive differences in volumetric and CRN-derived sediment flux estimates, a more thorough understanding of the degree of temporal variability in volumetric sediment flux is required. Gravel-to-total sediment flux calculations I presented in Chapter 3 suggested that the majority of sediment (>85-90%) exported into the Plain is composed of sand (and finer) grain sizes. Suspended sediment concentration measurements could therefore help characterise the variability in sediment flux (where suspended flux is assumed to account for the majority of the sediment flux), although this may be more difficult to characterise under peak monsoonal conditions where 1) the majority of bedload (for a given annual flux) is mobilised, 2) grain sizes larger than sand may be transferred into suspension which is unlikely to be captured by traditional sampling instrumentation, and 3) temporal variability in sediment and water discharges (e.g. driven by a short-lived extreme event) may fail to be captured by a single daily reading if based on automatic gauging stations. Given that the majority of water and sediment discharges occur during the Indian Summer Monsoon, understanding variability during this period is the most critical for determining annual sediment fluxes.

5.4 Directions of future research

The key results and findings from this thesis have presented new opportunities and directions in which to focus or target future research within the scope of the wider implication of my research (discussed above), but also in a more applied

context. Below, I outline a series of questions and initial observations which I hope to expand on in future research. The direct relevance of this proposed research in terms of understanding river-related hazard across the Indo-Gangetic Plain is also discussed.

5.4.1 The significance of the gravel-sand transition on channel dynamics

Whilst migration of the gravel-sand transition is commonly thought to reflect environmental forcing, such as changes in basin subsidence rate or sediment supply [Paola *et al.*, 1992a; Robinson and Slingerland, 1998; Knighton, 1999], much less is known about how the position of the gravel-sand transition drives changes in channel dynamics across the wider landscape. Initial results from recent (unpublished) work I have been involved in recently on the Karnali River in west Nepal identifies distinct patterns of channel migration that are defined by the position of the gravel-sand transition (Fig. 5.1). This small project was funded through the NERC Global Challenges Research Fund, and I was able to interrupt my PhD to work as a Research Associate on it. Upstream of the gravel-sand transition, channel migration is dominated by channel avulsion which is found to occur over 10^2-10^3 year timescales based on new Optically Stimulated Luminescence (OSL) dating of palaeo-channels (Fig. 5.2), the ages of which are presented in Table 5.1. These palaeo-channels are distinct and well-defined, suggesting that they have not undergone significant lateral erosion or meander migration. More subtle internal reorganisation (such as braid bar migration and switching) occurs upstream of the gravel-sand transition over annual timescales which is consistent with anastomosing river morphologies [Makaske, 2001]. Downstream of the transition, channel margins become considerably more mobile, and vegetated braid bars and islands present upstream of the transition are replaced with large mobile

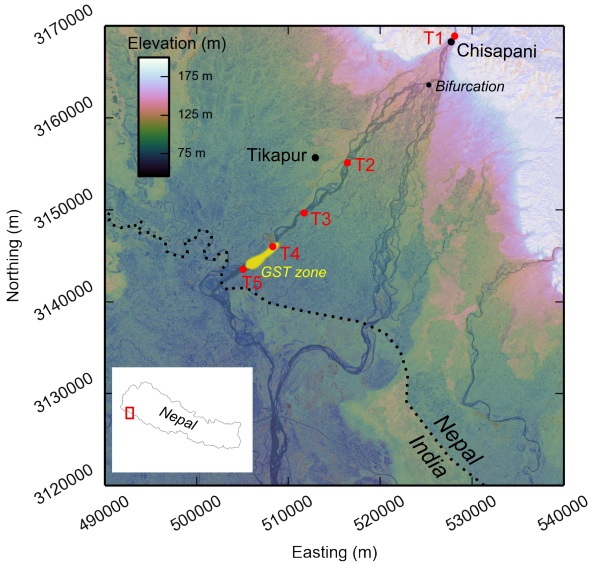

Figure 5.1: Position of the gravel-sand transition (GST) shown in yellow on the Karnali River in west Nepal. Red labels T1-T5 relate to suspended sediment sampling locations.

sand bars and bedforms, which are reworked during peak monsoonal discharges (between May and September). Channel migration is dominated by high rates of lateral bank erosion and meander migration, as opposed to channel avulsion (Fig. 5.3). Analysis of optical satellite imagery over the last 40 years documents individual meanders migrating at rates of hundreds to thousands of metres a year (Fig. 5.3). In the Karnali River, the position of the gravel-sand transition appears to mark an important threshold between different styles of channel migration. This transition also represents an important and previously unrecognised spatial change in river-related hazard. Upstream of the gravel-sand transition, the channel bed is well armoured and the margins are relatively stable. The dominant mechanism of flooding is therefore likely to be via over-bank flow, and channel avulsion. This latter mechanism is rarely incorporated into flood risk modelling, perhaps due to uncertainties regarding the necessary conditions required to trigger channel avulsion or the complexities of the mechanisms involved [Slingerland and Smith, 2004; Ashworth *et al.*, 2004; Ganti *et al.*, 2014]. Unlike over-bank flooding where the flow discharge exceeds the channel bankfull capacity, channel avulsion

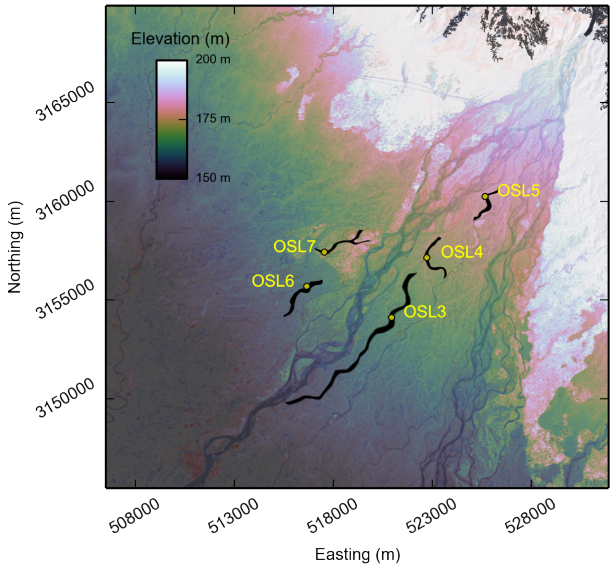

Figure 5.2: Optically Stimulated Luminescence (OSL) sample locations (OSL3-7) in palaeo-channels identified from satellite imagery upstream of the gravel-sand transition on the Karnali River. For OSL ages see Table 5.1.

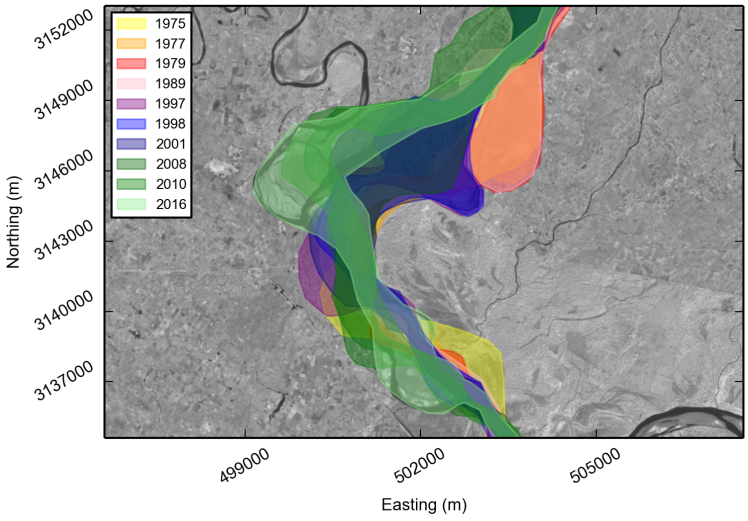

Figure 5.3: Position of channel boundaries identified from LandSat and Sentinel-2 optical satellite imagery between 1975 and 2016 downstream of the gravel-sand transition on the Karnali River.

Table 5.1: OSL ages for abandoned palaeo-channels identified upstream of the gravel-sand transition and shown in Fig. 5.2.

Sample ID	OSL age (years)
OSL3	850±310
OSL4	490±150
OSL5	2,560±1,220
OSL6	1,470±410
OSL7	4,090±540

can re-route flows into parts of the floodplain that were considerable distances away from the main channel. This type of avulsion-driven flooding occurred on the Kosi River in 2008 [Sinha, 2009; Sinha *et al.*, 2014b] resulting in the displacement of more than a million people. Downstream of the gravel-sand transition, river-related hazards are likely driven by a combination of over-bank flooding, but also by lateral channel and meander migration. This will have a direct impact on people living and working on land adjacent to the main channel, where based on field observations under moderate flow conditions, it is suspected that rates of bank retreat could be in the order of tens to hundreds of metres per day under peak discharge conditions. By understanding the mechanisms through which river-related hazards develop, flood management and land use planning can be better tailored to reflect the dominant processes and mechanisms. To understand the relationship between the gravel-sand transition, channel dynamics and river-related hazards, more research is needed into understanding:

1) Through which mechanism is sediment transferred from suspension (in the water column) to the channel bed, and does this process enhance rates of bed aggradation and make channels more susceptible to channel avulsion?

2) How does channel geometry and morphology change across the gravel-sand transition and enhance rates of channel lateral mobility? Are there metrics we can use to predict where the highest rates of lateral migration are likely to occur?

3) What processes drive the development of the gravel-sand transition, and how do these processes respond to extreme sediment generating events within the mountain catchment?

Suspended sediment sampling carried out along the Karnali River in August 2017 also suggests that downstream of the gravel-sand transition, there is a significant contribution of recycled floodplain sediment being worked back into the modern channel. This is inferred from unpublished point suspended sediment samples taken at different depths through the water column at five points (T1-T5) marked on Figure 5.1. Immediately downstream of the gravel-sand transition, there is a dramatic increase in near bed suspended sediment concentration and grain sizes. By converting these point samples at sites T1-T5 into average cross-sectional sediment concentrations and combining with discharge measurements taken at each site, it is possible to calculate an 'instantaneous' sediment flux at each site. Initial values suggest a doubling of suspended sediment flux between sites T1 and T5 in Figure 5.1, which indicates a significant component of floodplain sediments are being re-incorporated into the modern channel. This needs to be explored in more detail to understand the implications this may have on both sediment and geochemical budgets further downstream of the Himalaya.

Chapter 6

Conclusions

The main conclusions from this thesis are:

1. *Long-term rates of basin subsidence modulate the response of large-scale river morphology to climatically-driven changes in base level.* Spatial patterns of long-term (millenial) basin subsidence rate likely modulated how rivers draining the Ganga Plain responded to a climatically driven reduction in base level following the Last Glacial Maximum. In the west Ganga Plain, lower rates of basin subsidence are likely to have contributed to the development of a top-down wave of incision, resulting in entrenched or degrading river systems. This wave of incision was unlikely to have been recorded in the east Ganga Plain as a result of higher basin subsidence rates, which promotes the development of low-gradient and perched river systems which are relatively insensitive to changes in base level.

2. *The differential abrasion of non-quartzitic lithologies places an upper limit on the amount of gravel exported from the Himalayan mountains.* Whilst no correlation between grain size distribution and river morphology was observed in major rivers across the Ganga Plain, the amount of gravel exported into the Ganga Plain

was found to be small relative to the total sediment flux. The amount of gravel exported in the Ganga Plain is independent of upstream catchment area, sediment flux and water discharge and is instead related to the differential abrasion of non-quartzitic lithologies during fluvial transport. Despite quartzitic lithologies only making up ∼10% of the mountainous catchment, gravels sourced from these regions make up the majority of gravel preserved downstream of the Himalayan mountain front. Gravels present in the modern foreland basin were likely generated within ∼150 km of the mountain front.

3. *The use of cosmogenic radionuclide concentrations as a proxy for sediment flux may not be appropriate in large Himalayan catchments.* Considerable temporal variability is observed in cosmogenic radionuclide (CRN) concentrations near the outlet of the Ganga River, despite previous studies having suggested that with increasing catchment area the effects of stochastic inputs of sediment should buffer variability in CRN concentrations. At least ∼20 samples are required in order to characterise this degree of variability. In large catchments with high topographic relief characterised by spatially variable climate, tectonics, lithology and vegetation, different erosional processes may contribute to the observed CRN variability and also drive differences in volumetric and CRN-derived sediment flux estimates.

4. *More research is needed into understanding the development of the gravel-sand transition and its influence on channel dynamics.* The exact mechanism through which gravel-sand transitions develop still remains debated despite several decades of experimental, field, numerical and analytical modelling research. The position of the gravel-sand transition may be a powerful measure of how wider landscapes are responding to changing climate and increased anthropogenic pressures, which modify water and sediment discharges in rivers. Initial result from the Karnali

River in Nepal also suggest that the gravel-sand transition is more than an indicator of change, as defines a boundary between different channel morphologies and dynamics. Future research should be focused on developing an understanding of the relationship between the gravel-sand transition, channel dynamics, floodplain sediment recycling and river-related hazards.

References

Allen, G.H., Barnes, J.B., Pavelsky, T.M. and Kirby, E. (2013a). Lithologic and tectonic controls on bedrock channel form at the northwest Himalayan front. *Journal of Geophysical Research: Earth Surface*, **118**, 1806–1825.

Allen, P.A. and Allen, J.R. (2013). *Basin analysis: Principles and application to petroleum play assessment*. John Wiley & Sons.

Allen, P.A., Armitage, J.J., Carter, A., Duller, R.A., Michael, N.A., Sinclair, H.D., Whitchurch, A.L. and Whittaker, A.C. (2013b). The Qs problem: Sediment volumetric balance of proximal foreland basin systems. *Sedimentology*, **60**, 102–130.

Amans, O., Beiping, W. and Ziggah, Y. (2013). Assessing vertical accuracy of SRTM Ver 4.1 and ASTER GDEM Ver 2 using differential GPS measurements - case study in Ondo State Nigeria. *International Journal of Scientific & Engineering Research*, **4**, 523 – 531.

Amelung, F., Galloway, D.L., Bell, J.W., Zebker, H.A. and Laczniak, R.J. (1999). Sensing the ups and downs of Las Vegas: InSAR reveals structural control of land subsidence and aquifer-system deformation. *Geology*, **27**, 483–486.

Andermann, C., Crave, A., Gloaguen, R., Davy, P. and Bonnet, S. (2012). Connecting source and transport: Suspended sediments in the Nepal Himalayas. *Earth and Planetary Science Letters*, **351352**, 158–170.

Anders, A., Roe, G., Hallet, B., Montgomery, D., Finnegan, N. and Putkonen, J. (2006). Spatial patterns of precipitation and topography in the Himalaya. *Geological Society of America*.

Armstrong, R., Raup, B., Khalsa, S., Barry, R., Kargel, J., Helm, C. and Kieffer, H. (2005). GLIMS glacier database. *National Snow and Ice Data Center, Boulder, Colorado, USA*.

Ashworth, P.J., Best, J.L. and Jones, M. (2004). Relationship between sediment supply and avulsion frequency in braided rivers. *Geology*, **32**, 21–24.

Attal, M. and Lavé, J. (2006). Changes of bedload characteristics along the Marsyandi River (central Nepal): Implications for understanding hillslope sediment supply, sediment load evolution along fluvial networks, and denudation in active orogenic belts. vol. 398, 143–171, Geological Society of America.

Attal, M. and Lavé, J. (2009). Pebble abrasion during fluvial transport: Experimental results and implications for the evolution of the sediment load along rivers. *Journal of Geophysical Research: Earth Surface*, **114**, F04023.

Attal, M., Mudd, S.M., Hurst, M.D., Weinman, B., Yoo, K. and Naylor, M. (2015). Impact of change in erosion rate and landscape steepness on hillslope and fluvial sediments grain size in the Feather River basin (Sierra Nevada, California). *Earth Surface Dynamics*, **3**, 201–222.

Bagnold, R.A. (1966). *An approach to the sediment transport problem from general physics*. US government printing office.

Balco, G., Stone, J.O., Lifton, N.A. and Dunai, T.J. (2008). A complete and easily accessible means of calculating surface exposure ages or erosion rates from 10 Be and 26 Al measurements. *Quaternary geochronology*, **3**, 174–195.

Benda, L. and Dunne, T. (1997a). Stochastic forcing of sediment routing and storage in channel networks. *Water Resources Research*, **33**, 2865–2880.

Benda, L. and Dunne, T. (1997b). Stochastic forcing of sediment supply to channel networks from landsliding and debris flow. *Water Resources Research*, **33**, 2849–2863.

Binnie, S.A., Phillips, W.M., Summerfield, M.A. and Fifield, L.K. (2006). Sediment mixing and basin-wide cosmogenic nuclide analysis in rapidly eroding mountainous environments. *Quaternary Geochronology*, **1**, 4–14.

Blöthe, J.H. and Korup, O. (2013). Millennial lag times in the Himalayan sediment routing system. *Earth and Planetary Science Letters*, **382**, 38–46.

Bookhagen, B. and Burbank, D.W. (2006). Topography, relief, and TRMM-derived rainfall variations along the Himalaya. *Geophysical Research Letters*, **33**, L08405.

Bookhagen, B., Thiede, R.C. and Strecker, M.R. (2005). Abnormal monsoon years and their control on erosion and sediment flux in the high, arid northwest Himalaya. *Earth and Planetary Science Letters*, **231**, 131–146.

Breien, H., De Blasio, F.V., Elverhøi, A. and Høeg, K. (2008). Erosion and morphology of a debris flow caused by a glacial lake outburst flood, western Norway. *Landslides*, **5**, 271–280.

Bridge, J.S. and Leeder, M.R. (1979). A simulation model of alluvial stratigraphy. *Sedimentology*, **26**, 617–644.

Brown, E.T., Stallard, R.F., Larsen, M.C., Raisbeck, G.M. and Yiou, F. (1995). Denudation rates determined from the accumulation of in situ-produced 10Be in the Luquillo Experimental Forest, Puerto Rico. *Earth and Planetary Science Letters*, **129**, 193–202.

Brozovic, N. and Burbank, D.W. (2000). Dynamic fluvial systems and gravel progradation in the Himalayan foreland. *Geological Society of America Bulletin*, **112**, 394–412.

Bryant, M., Falk, P. and Paola, C. (1995). Experimental study of avulsion frequency and rate of deposition. *Geology*, **23**, 365–368.

Burbank, D., Beck, R. and Mulder, T. (1996). The Himalayan foreland basin. In *The Tectonic Evolution of Asia*, 149–188, Cambridge University Press, ed. by a. yin and m. harrison edn.

Burbank, D.W. (1992). Causes of recent Himalayan uplift deduced from deposited patterns in the Ganges basin. *Nature*, **357**, 680–683.

Burbank, D.W. and Beck, R.A. (1991). Models of aggradation versus progradation in the Himalayan foreland. *Geologische Rundschau*, **80**, 623–638.

Cenderelli, D.A. and Wohl, E.E. (2003). Flow hydraulics and geomorphic effects of glacial-lake outburst floods in the Mount Everest region, Nepal. *Earth Surface Processes and Landforms*, **28**, 385–407.

Chakraborty, T. and Ghosh, P. (2010). The geomorphology and sedimentology of the Tista megafan, Darjeeling Himalaya: Implications for megafan building processes. *Geomorphology*, **115**, 252–266.

Chakraborty, T., Kar, R., Ghosh, P. and Basu, S. (2010). Kosi megafan: Historical records, geomorphology and the recent avulsion of the Kosi River. *Quaternary International*, **227**, 143–160.

Chen, H. and Petley, D.N. (2005). The impact of landslides and debris flows triggered by Typhoon Mindulle in Taiwan. *Quarterly Journal of Engineering Geology and Hydrogeology*, **38**, 301–304.

Church, M. (2006). Bed material transport and the morphology of alluvial river channels. *Annual Review of Earth and Planetary Sciences*, **34**, 325–354.

Church, M., McLean, D. and Wolcott, J. (1987). River bed gravels: sampling and analysis. In *Sediment Transport in Gravel-Bed Rivers*, p43–88, John Wiley and Sons New York.

Clift, P.D., Giosan, L., Blusztajn, J., Campbell, I.H., Allen, C., Pringle, M., Tabrez, A.R., Danish, M., Rabbani, M., Alizai, A. *et al.* (2008). Holocene erosion of the Lesser Himalaya triggered by intensified summer monsoon. *Geology*, **36**, 79–82.

Collins, A.L. and Walling, D.E. (2004). Documenting catchment suspended sediment sources: problems, approaches and prospects. *Progress in Physical Geography*, **28**, 159–196.

Croissant, T., Lague, D., Steer, P. and Davy, P. (2017). Rapid post-seismic landslide evacuation boosted by dynamic river width. *Nature Geoscience*, **10**, ngeo3005.

Cui, Y. and Parker, G. (1998). The arrested gravel front: stable gravel-sand transitions in rivers Part 2: General numerical solution. *Journal of Hydraulic Research*, **36**, 159–182.

Cui, Y., Parker, G., Lisle, T.E., Gott, J., Hansler-Ball, M.E., Pizzuto, J.E., Allmendinger, N.E. and Reed, J.M. (2003). Sediment pulses in mountain rivers: 1. Experiments. *Water Resources Research*, **39**, 1239.

Cullen, J.L. (1981). Microfossil evidence for changing salinity patterns in the bay of Bengal over the last 20 000 years. *Palaeogeography, Palaeoclimatology, Palaeoecology*, **35**, 315–356.

Dade, W. and Friend, P. (1998). Grain-size, sediment-transport regime, and channel slope in alluvial rivers. *The Journal of Geology*, **106**, 661–676.

Dade, W.B. (2000). Grain size, sediment transport and alluvial channel pattern. *Geomorphology*, **35**, 119–126.

Dadson, S.J., Hovius, N., Chen, H., Dade, W.B., Hsieh, M.L., Willett, S.D., Hu, J.C., Horng, M.J., Chen, M.C., Stark, C.P., Lague, D. and Lin, J.C. (2003). Links between erosion, runoff variability and seismicity in the Taiwan orogen. *Nature*, **426**, 648–651.

Dadson, S.J., Hovius, N., Chen, H., Dade, W.B., Lin, J.C., Hsu, M.L., Lin, C.W., Horng, M.J., Chen, T.C., Milliman, J. and Stark, C.P. (2004). Earthquake-triggered increase in sediment delivery from an active mountain belt. *Geology*, **32**, 733–736.

Darvill, C.M., Bentley, M.J., Stokes, C.R., Hein, A.S. and Rodés, Á. (2015). Extensive MIS 3 glaciation in southernmost Patagonia revealed by cosmogenic nuclide dating of outwash sediments. *Earth and Planetary Science Letters*, **429**, 157–169.

DeCelles, P.G. and Giles, K.A. (1996). Foreland basin systems. *Basin Research*, **8**, 105–123.

DeCelles, P.G., Gehrels, G.E., Quade, J., Ojha, T.P., Kapp, P.A. and Upreti, B.N. (1998). Neogene foreland basin deposits, erosional unroofing, and the kinematic history of the Himalayan fold-thrust belt, western Nepal. *Geological Society of America Bulletin*, **110**, 2–21.

Denniston, R.F., Gonzlez, L.A., Asmerom, Y., Sharma, R.H. and Reagan, M.K. (2000). Speleothem evidence for changes in Indian summer monsoon precipitation over the last 2300 years. *Quaternary Research*, **53**, 196–202.

Densmore, A.L., Sinha, R., Sinha, S., Tandon, S.K. and Jain, V. (2016). Sediment storage and release from Himalayan piggyback basins and implications for downstream river morphology and evolution. *Basin Research*.

Devrani, R., Singh, V., Mudd, S. and Sinclair, H. (2015). Prediction of flash flood hazard impact from Himalayan river profiles. *Geophysical Research Letters*, **42**, 5888–5894.

Dietrich, W.E., Kirchner, J.W., Ikeda, H. and Iseya, F. (1989). Sediment supply and the development of the coarse surface layer in gravel-bedded rivers. *Nature*, **340**, 215–217.

Dingle, E.H., Sinclair, H.D., Attal, M., Milodowski, D.T. and Singh, V. (2016). Subsidence control on river morphology and grain size in the Ganga Plain. *American Journal of Science*, **316**, 778–812.

Dingle, E.H., Attal, M. and Sinclair, H.D. (2017). Abrasion-set limits on Himalayan gravel flux. *Nature*, **544**, 471–474.

Dixit, Y., Hodell, D.A., Sinha, R. and Petrie, C.A. (2014). Abrupt weakening of the Indian summer monsoon at 8.2 kyrB.P. *Earth and Planetary Science Letters*, **391**, 16–23.

Dobhal, D., Gupta, A.K., Mehta, M. and Khandelwal, D. (2013). Kedarnath disaster: facts and plausible causes. *Current Science*, **105**, 171–174.

Dubille, M. and Lavé, J. (2015). Rapid grain size coarsening at sandstone/conglomerate transition: similar expression in Himalayan modern rivers and Pliocene molasse deposits. *Basin Research*, **27**, 26–42.

Duller, R.A., Whittaker, A.C., Fedele, J.J., Whitchurch, A.L., Springett, J., Smithells, R., Fordyce, S. and Allen, P.A. (2010). From grain size to tectonics. *Journal of Geophysical Research: Earth Surface*, **115**, F03022.

Duller, R.A., Whittaker, A.C., Swinehart, J.B., Armitage, J.J., Sinclair, H.D., Bair, A. and Allen, P.A. (2012). Abrupt landscape change post6 Ma on the central Great Plains, USA. *Geology*, **40**, 871–874.

Dunai, T.J. (2010). *Cosmogenic nuclides: Principles, concepts and applications in the Earth surface sciences*. Cambridge University Press.

Duplessy, J.C. (1982). Glacial to interglacial contrasts in the northern Indian Ocean. *Nature*, **295**, 494–498.

Durga-Rao, K., Venkateshwar-Rao, V., Dadhwal, V. and Diwakar, P. (2014). Kedarnath flash floods: a hydrological and hydraulic simulation study. *Current Science*, **106**, 598–603.

Edmonds, D.A., Hoyal, D.C., Sheets, B.A. and Slingerland, R.L. (2009). Predicting delta avulsions: Implications for coastal wetland restoration. *Geology*, **37**, 759–762.

Fedele, J.J. and Paola, C. (2007). Similarity solutions for fluvial sediment fining by selective deposition. *Journal of Geophysical Research: Earth Surface*, **112**, F02038.

Feldl, N. and Bilham, R. (2006). Great Himalayan earthquakes and the Tibetan plateau. *Nature*, **444**, 165–170.

Ferguson, R., Hoey, T., Wathen, S. and Werritty, A. (1996). Field evidence for rapid downstream fining of river gravels through selective transport. *Geology*, **24**, 179–182.

Ferguson, R.I. (2003). Emergence of abrupt gravel to sand transitions along rivers through sorting processes. *Geology*, **31**, 159–162.

Fleitmann, D., Burns, S.J., Mudelsee, M., Neff, U., Kramers, J., Mangini, A. and Matter, A. (2003). Holocene forcing of the Indian monsoon recorded in a stalagmite from southern Oman. *Science*, **300**, 1737–1739.

Fleitmann, D., Burns, S.J., Mangini, A., Mudelsee, M., Kramers, J., Villa, I., Neff, U., Al-Subbary, A.A., Buettner, A., Hippler, D. and Matter, A. (2007). Holocene ITCZ and Indian monsoon dynamics recorded in stalagmites from Oman and Yemen (Socotra). *Quaternary Science Reviews*, **26**, 170–188.

Flemings, P.B. and Jordan, T.E. (1989). A synthetic stratigraphic model of foreland basin development. *Journal of Geophysical Research: Solid Earth*, **94**, 3851–3866.

Friend, P.F. and Sinha, R. (1993). Braiding and meandering parameters. *Geological Society, London, Special Publications*, **75**, 105–111.

Gabet, E.J., Burbank, D.W., Pratt-Sitaula, B., Putkonen, J. and Bookhagen, B. (2008). Modern erosion rates in the High Himalayas of Nepal. *Earth and Planetary Science Letters*, **267**, 482–494.

Galy, A. and France-Lanord, C. (2001). Higher erosion rates in the Himalaya: Geochemical constraints on riverine fluxes. *Geology*, **29**, 23–26.

Galy, V., France-Lanord, C., Beyssac, O., Faure, P., Kudrass, H. and Palhol, F. (2007). Efficient organic carbon burial in the Bengal fan sustained by the Himalayan erosional system. *Nature*, **450**, 407–410.

Gansser, A. (1964). *Geology of the Himalayas*. Wiley Interscience.

Ganti, V., Chu, Z., Lamb, M.P., Nittrouer, J.A. and Parker, G. (2014). Testing morphodynamic controls on the location and frequency of river avulsions on fans versus deltas: Huanghe (Yellow River), China. *Geophysical Research Letters*, **41**, 2014GL061918.

Geddes, A. (1960). The alluvial morphology of the Indo-Gangetic Plain: Its mapping and geographical significance. *Transactions and Papers (Institute of British Geographers)*, 253–276.

Ghimire, G.P.S. and Uprety, B.K. (1990). Causes and effects of siltation on the environment of Nepal. *Environmentalist*, **10**, 55–65.

Gibling, M.R., Tandon, S.K., Sinha, R. and Jain, M. (2005). Discontinuity-bounded alluvial sequences of the southern Gangetic Plains, India: Aggradation and degradation in response to monsoonal strength. *Journal of Sedimentary Research*, **75**, 369–385.

Gitto, A., Venditti, J., Kostaschuk, R. and Church, M. (2017). Representative point-integrated suspended sediment sampling in rivers. *Water Resources Research*, **53**, 2956–2971.

Godard, V., Bourls, D.L., Spinabella, F., Burbank, D.W., Bookhagen, B., Fisher, G.B., Moulin, A. and Lanni, L. (2014). Dominance of tectonics over climate in Himalayan denudation. *Geology*, G35342.1.

Goodbred, S.L. and Kuehl, S.A. (1999). Holocene and modern sediment budgets for the Ganges-Brahmaputra river system: Evidence for highstand dispersal to flood-plain, shelf, and deep-sea depocenters. *Geology*, **27**, 559–562.

Goodbred, S.L. and Kuehl, S.A. (2000). Enormous Ganges-Brahmaputra sediment discharge during strengthened early Holocene monsoon. *Geology*, **28**, 1083–1086.

Goodbred Jr., S.L. (2003). Response of the Ganges dispersal system to climate change: a source-to-sink view since the last interstade. *Sedimentary Geology*, **162**, 83–104.

Gosse, J.C. and Phillips, F.M. (2001). Terrestrial in situ cosmogenic nuclides: theory and application. *Quaternary Science Reviews*, **20**, 1475–1560.

Granger, D.E., Kirchner, J.W. and Finkel, R. (1996). Spatially averaged long-term erosion rates measured from in situ-produced cosmogenic nuclides in alluvial sediment. *The Journal of Geology*, **104**, 249–257.

Gupta, A.K., Das, M. and Anderson, D.M. (2005). Solar influence on the Indian summer monsoon during the Holocene. *Geophysical Research Letters*, **32**, L17703.

Hajek, E.A. and Edmonds, D.A. (2014). Is river avulsion style controlled by floodplain morphodynamics? *Geology*, G35045.1.

Heimsath, A.M. and McGlynn, R. (2008). Quantifying periglacial erosion in the Nepal high Himalaya. *Geomorphology*, **97**, 5–23.

Heller, P.L. and Paola, C. (1992). The large-scale dynamics of grain-size variation in alluvial basins, 2: Application to syntectonic conglomerate. *Basin Research*, **4**, 91–102.

Heller, P.L. and Paola, C. (1996). Downstream changes in alluvial architecture: An exploration of controls on channel-stacking patterns. *Journal of Sedimentary Research*, **66**.

Heller, P.L., Beland, P.E., Humphrey, N.F., Konrad, S.K., Lynds, R.M., McMillan, M.E., Valentine, K.E., Widman, Y.A. and Furbish, D.J. (2001). Paradox of downstream fining and weathering-rind formation in the lower Hoh River, Olympic Peninsula, Washington. *Geology*, **29**, 971–974.

Hergarten, S., Robl, J. and Stwe, K. (2014). Extracting topographic swath profiles across curved geomorphic features. *Earth Surface Dynamics*, **2**, 97–104.

Hobley, D.E.J., Sinclair, H.D. and Cowie, P.A. (2010). Processes, rates, and time scales of fluvial response in an ancient postglacial landscape of the northwest Indian Himalaya. *Geological Society of America Bulletin*, **122**, 1569–1584.

Hoey, T.B. and Bluck, B.J. (1999). Identifying the controls over downstream fining of river gravels. *Journal of Sedimentary Research*, **69**.

Horowitz, A.J., Rinella, F.A., Lamothe, P., Miller, T.L., Edwards, T.K., Roche, R.L. and Rickert, D.A. (1990). Variations in suspended sediment and associated trace element concentrations in selected riverine cross sections. *Environmental science & technology*, **24**, 1313–1320.

Hoth, S., Hoffmann-Rothe, A. and Kukowski, N. (2007). Frontal accretion: An internal clock for bivergent wedge deformation and surface uplift. *Journal of Geophysical Research: Solid Earth*, **112**.

Hovius, N., Stark, C.P. and Allen, P.A. (1997). Sediment flux from a mountain belt derived by landslide mapping. *Geology*, **25**, 231–234.

Hovius, N., Stark, C.P., Hao-Tsu, C. and Jiun-Chuan, L. (2000). Supply and removal of sediment in a landslide-dominated mountain belt: Central Range, Taiwan. *The Journal of Geology*, **108**, 73–89.

Huang, R. and Fan, X. (2013). The landslide story. *Nature Geoscience*, **6**, 325–326.

Immerzeel, W.W., Beek, L.P.H.v. and Bierkens, M.F.P. (2010). Climate change will affect the Asian water towers. *Science*, **328**, 1382–1385.

Jackson, J., McKenzie, D.a.N., Priestley, K. and Emmerson, B. (2008). New views on the structure and rheology of the lithosphere. *Journal of the Geological Society*, **165**, 453–465.

Jain, V. and Sinha, R. (2003). River systems in the Gangetic plains and their comparison with the Siwaliks: A review. *Current Science*, **84(08)**.

Jerolmack, D.J. and Brzinski, T.A. (2010). Equivalence of abrupt grain-size transitions in alluvial rivers and eolian sand seas: A hypothesis. *Geology*, **38**, 719–722.

Jerolmack, D.J. and Mohrig, D. (2007). Conditions for branching in depositional rivers. *Geology*, **35**, 463–466.

Jerolmack, D.J. and Paola, C. (2007). Complexity in a cellular model of river avulsion. *Geomorphology*, **91**, 259–270.

Jerolmack, D.J. and Paola, C. (2010). Shredding of environmental signals by sediment transport. *Geophysical Research Letters*, **37**, n/a–n/a.

Jha, P.K., Vaithiyanathan, P. and Subramanian, V. (1993). Mineralogical characteristics of the sediments of a Himalayan river: Yamuna River- a tributary of the Ganges. *Environmental Geology*, **22**, 13–20.

Jones, L. and Schumm, S. (1999). Causes of avulsion: an overview. In *Fluvial Sedimentology VI: Special Publication Number 28 of the International Association of Sedimentologists*, vol. 28, 171–178, Blackwell Science, edited by n.d. smith and j.rogers edn.

Jordan, T.A. and Watts, A.B. (2005). Gravity anomalies, flexure and the elastic thickness structure of the India-Eurasia collisional system. *Earth and Planetary Science Letters*, **236**, 732–750.

Jordan, T.E. (1981). Thrust loads and foreland basin evolution, Cretaceous, western United States. *AAPG bulletin*, **65**, 2506–2520.

Kargel, J.S., Leonard, G.J., Shugar, D.H., Haritashya, U.K., Bevington, A., Fielding, E.J., Fujita, K., Geertsema, M., Miles, E.S., Steiner, J., Anderson,

E., Bajracharya, S., Bawden, G.W., Breashears, D.F., Byers, A., Collins, B., Dhital, M.R., Donnellan, A., Evans, T.L., Geai, M.L., Glasscoe, M.T., Green, D., Gurung, D.R., Heijenk, R., Hilborn, A., Hudnut, K., Huyck, C., Immerzeel, W.W., Liming, J., Jibson, R., Kb, A., Khanal, N.R., Kirschbaum, D., Kraaijenbrink, P.D.A., Lamsal, D., Shiyin, L., Mingyang, L., McKinney, D., Nahirnick, N.K., Zhuotong, N., Ojha, S., Olsenholler, J., Painter, T.H., Pleasants, M., Pratima, K.C., Yuan, Q.I., Raup, B.H., Regmi, D., Rounce, D.R., Sakai, A., Donghui, S., Shea, J.M., Shrestha, A.B., Shukla, A., Stumm, D., Kooij, M.v.d., Voss, K., Xin, W., Weihs, B., Wolfe, D., Lizong, W., Xiaojun, Y., Yoder, M.R. and Young, N. (2016). Geomorphic and geologic controls of geohazards induced by Nepals 2015 Gorkha earthquake. *Science*, **351**, aac8353.

Kattelmann, R. (2003). Glacial lake outburst floods in the Nepal Himalaya: a manageable hazard? *Natural Hazards*, **28**, 145–154.

Keefer, D.K. (1999). Earthquake-induced landslides and their effects on alluvial fans. *Journal of Sedimentary Research*, **69**.

Kellerhals, R. and Bray, D.I. (1971). Sampling procedures for coarse fluvial sediments. *Journal of Hydraulic Engineering*, **97**, 1165–1180.

Kimura, K. (1999). Diachronous evolution of sub-Himalayan piggyback basins, Nepal. *Island Arc*, **8**, 99–113.

Kirchner, J.W., Finkel, R.C., Riebe, C.S., Granger, D.E., Clayton, J.L., King, J.G. and Megahan, W.F. (2001). Mountain erosion over 10 yr, 10 ky, and 10 Myr time scales. *Geology*, **29**, 591–594.

Knighton, A.D. (1999). The gravel-sand transition in a disturbed catchment. *Geomorphology*, **27**, 325–341.

Knighton, D. (1998). *Fluvial Forms and Processes: A New Perspective*. Routledge.

Kumar, R., Sangode, S.J. and Ghosh, S.K. (2004). A multistorey sandstone complex in the Himalayan Foreland Basin, NW Himalaya, India. *Journal of Asian Earth Sciences*, **23**, 407–426.

Labbe, J.M., Hadley, K.S., Schipper, A.M., Leuven, R.S. and Gardiner, C.P. (2011). Influence of bank materials, bed sediment, and riparian vegetation on channel form along a gravel-to-sand transition reach of the Upper Tualatin River, Oregon, USA. *Geomorphology*, **125**, 374–382.

Lal, D. (1991). Cosmic ray labeling of erosion surfaces: in situ nuclide production rates and erosion models. *Earth and Planetary Science Letters*, **104**, 424–439.

Lamb, M.P. and Venditti, J.G. (2016). The grain size gap and abrupt gravel-sand transitions in rivers due to suspension fallout. *Geophysical Research Letters*, **43**, 3777–3785.

Lash, G.G. (1988). Along-strike variations in foreland basin evolution: possible evidence for continental collision along an irregular margin. *Basin Research*, **1**, 71–83.

Lavé, J. and Avouac, J.P. (2000). Active folding of fluvial terraces across the Siwaliks Hills, Himalayas of central Nepal. *Journal of Geophysical Research: Solid Earth*, **105**, 5735–5770.

Lavé, J. and Avouac, J.P. (2001). Fluvial incision and tectonic uplift across the Himalayas of central Nepal. *Journal of Geophysical Research: Solid Earth*, **106**, 26561–26591.

Leeder, M.R., Harris, T. and Kirkby, M.J. (1998). Sediment supply and climate change: implications for basin stratigraphy. *Basin Research*, **10**, 7–18.

Leier, A.L., DeCelles, P.G. and Pelletier, J.D. (2005). Mountains, monsoons, and megafans. *Geology*, **33**, 289–292.

Leopold, L. (1992). Sediment size that determines channel morphology. *Dynamics of gravel-bed rivers*, 297–311.

Lin, M.L. and Tung, C.C. (2004). A GIS-based potential analysis of the landslides induced by the Chi-Chi earthquake. *Engineering Geology*, **71**, 63–77.

Lukens, C.E., Riebe, C.S., Sklar, L.S. and Shuster, D.L. (2016). Grain size bias in cosmogenic nuclide studies of stream sediment in steep terrain. *Journal of Geophysical Research: Earth Surface*, **121**, 978–999.

Lupker, M., France-Lanord, C., Lavé, J., Bouchez, J., Galy, V., Métivier, F., Gaillardet, J., Lartiges, B. and Mugnier, J.L. (2011). A Rouse-based method to integrate the chemical composition of river sediments: Application to the Ganga basin. *Journal of Geophysical Research: Earth Surface*, **116**, F04012.

Lupker, M., Blard, P.H., Lavé, J., France-Lanord, C., Léanni, L., Puchol, N., Charreau, J. and Bourlès, D. (2012). 10Be-derived Himalayan denudation rates and sediment budgets in the Ganga basin. *Earth and Planetary Science Letters*, **333334**, 146–156.

Lupker, M., Lavé, J., France-Lanord, C., Christl, M., Bourlès, D., Carcaillet, J., Maden, C., Wieler, R., Rahman, M., Bezbaruah, D. *et al.* (2017). 10 Be systematics in the Tsangpo-Brahmaputra catchment: the cosmogenic nuclide legacy of the eastern Himalayan syntaxis. *Earth Surface Dynamics*, **5**, 429–449.

Lyon-Caen, H. and Molnar, P. (1983). Constraints on the structure of the Himalaya from an analysis of gravity anomalies and a flexural model of the lithosphere. *Journal of Geophysical Research: Solid Earth*, **88**, 8171–8191.

Lyon-Caen, H. and Molnar, P. (1985). Gravity anomalies, flexure of the Indian Plate, and the structure, support and evolution of the Himalaya and Ganga Basin. *Tectonics*, **4**, 513–538.

Mackey, B.H. and Roering, J.J. (2011). Sediment yield, spatial characteristics, and the long-term evolution of active earthflows determined from airborne LiDAR and historical aerial photographs, Eel River, California. *Geological Society of America Bulletin*, **123**, 1560–1576.

Makaske, B. (2001). Anastomosing rivers: a review of their classification, origin and sedimentary products. *Earth-Science Reviews*, **53**, 149–196.

Marr, J.G., Swenson, J.B., Paola, C. and Voller, V.R. (2000). A two-diffusion model of fluvial stratigraphy in closed depositional basins. *Basin Research*, **12**, 381–398.

Martha, T.R., Roy, P., Mazumdar, R., Govindharaj, K.B. and Kumar, K.V. (2017). Spatial characteristics of landslides triggered by the 2015 Mw 7.8 (Gorkha) and Mw 7.3 (Dolakha) earthquakes in Nepal. *Landslides*, **14**, 697–704.

Meade, R.H. and Stevens, H.H. (1990). Strategies and equipment for sampling suspended sediment and associated toxic chemicals in large riverswith emphasis on the Mississippi River. *Science of the Total Environment*, **97**, 125–135.

Milliman, J.D. and Syvitski, J.P.M. (1992). Geomorphic/tectonic control of sediment discharge to the ocean: The importance of small mountainous rivers. *The Journal of Geology*, **100**, 525–544.

Montgomery, D.R. and Buffington, J.M. (1997). Channel-reach morphology in mountain drainage basins. *Geological Society of America Bulletin*, **109**, 596–611.

Mudd, S.M., Hurst, M.D., Grieve, S.W. and Marrero, S.M. (2016). The CAIRN method: automated, reproducible calculation of catchment-averaged denudation rates from cosmogenic nuclide concentrations. *Earth Surface Dynamics*, **4**, 655.

Mugnier, J.L. and Huyghe, P. (2006). Ganges basin geometry records a pre-15 Ma isostatic rebound of Himalaya. *Geology*, **34**, 445–448.

Mugnier, J.L., Leturmy, P., Mascle, G., Huyghe, P., Chalaron, E., Vidal, G., Husson, L. and Delcaillau, B. (1999). The Siwaliks of western Nepal: I. Geometry and kinematics. *Journal of Asian Earth Sciences*, **17**, 629–642.

Narula, P., Acharyya, S. and Banerjee, J. (2000). Seismotectonic Atlas of India and its Environs: Calcutta, The Geological Survey of India.

Naylor, M. and Sinclair, H.D. (2007). Punctuated thrust deformation in the context of doubly vergent thrust wedges: Implications for the localization of uplift and exhumation. *Geology*, **35**, 559–562.

Niedermann, S. (2002). Cosmic-ray-produced noble gases in terrestrial rocks: dating tools for surface processes. *Reviews in Mineralogy and Geochemistry*, **47**, 731–784.

Niemi, N.A., Oskin, M., Burbank, D.W., Heimsath, A.M. and Gabet, E.J. (2005). Effects of bedrock landslides on cosmogenically determined erosion rates. *Earth and Planetary Science Letters*, **237**, 480–498.

Niño, Y., Lopez, F. and Garcia, M. (2003). Threshold for particle entrainment into suspension. *Sedimentology*, **50**, 247–263.

Orton, G. and Reading, H. (1993). Variability of deltaic processes in terms of sediment supply, with particular emphasis on grain size. *Sedimentology*, **40**, 475–512.

Osmanoğlu, B., Dixon, T.H., Wdowinski, S., Cabral-Cano, E. and Jiang, Y. (2011). Mexico City subsidence observed with persistent scatterer InSAR. *International Journal of Applied Earth Observation and Geoinformation*, **13**, 1–12.

Pandey, A.K., Pandey, P., Singh, G.D. and Juyal, N. (2014). Climate footprints in the Late Quaternary-Holocene landforms of Dun Valley, NW Himalaya, India. *Current Science*, **106**, 245–253.

Paola, C. and Seal, R. (1995). Grain size patchiness as a cause of selective deposition and downstream fining. *Water Resources Research*, **31**, 1395–1407.

Paola, C., Heller, P.L. and Angevine, C.L. (1992a). The large-scale dynamics of grain-size variation in alluvial basins, 1: Theory. *Basin Research*, **4**, 73–90.

Paola, C., Parker, G., Seal, R., Sinha, S.K., Southard, J.B. and Wilcock, P.R. (1992b). Downstream fining by selective deposition in a laboratory flume. *Science*, **258**, 1757–1760.

Parker, G. (1990). Surface-based bedload transport relation for gravel rivers. *Journal of Hydraulic Research*, **28**, 417–436.

Parker, G. (1991). Selective sorting and abrasion of river gravel. i: Theory. *Journal of Hydraulic Engineering*, **117**, 131–147.

Parker, G. and Cui, Y. (1998). The arrested gravel front: Stable gravel-sand transitions in rivers part 1: Simplified analytical solution. *Journal of Hydraulic Research*, **36**, 75–100.

Parker, G. and Toro-Escobar, C.M. (2002). Equal mobility of gravel in streams: The remains of the day. *Water Resources Research*, **38**, 1264.

Pratt-Sitaula, B., Garde, M., Burbank, D.W., Oskin, M., Heimsath, A. and Gabet, E. (2007). Bedload-to-suspended load ratio and rapid bedrock incision from Himalayan landslide-dam lake record. *Quaternary Research*, **68**, 111–120.

Puchol, N., Lavé, J., Lupker, M., Blard, P.H., Gallo, F., France-Lanord, C., Team, A. *et al.* (2014). Grain-size dependent concentration of cosmogenic 10 Be and erosion dynamics in a landslide-dominated Himalayan watershed. *Geomorphology*, **224**, 55–68.

Rana, N., Singh, S., Sundriyal, Y. and Juyal, N. (2013). Recent and past floods in the Alaknanda valley: causes and consequences. *Current Science*, **105**, 1209–1212.

Ray, Y. and Srivastava, P. (2010). Widespread aggradation in the mountainous catchment of the AlaknandaGanga River System: timescales and implications to Hinterlandforeland relationships. *Quaternary Science Reviews*, **29**, 2238–2260.

Rice, S. (1999). The nature and controls on downstream fining within sedimentary links. *Journal of Sedimentary Research*, **69**.

Rice, S.P. and Church, M. (2001). Longitudinal profiles in simple alluvial systems. *Water Resources Research*, **37**, 417–426.

Robinson, R.A.J. and Slingerland, R.L. (1998). Origin of fluvial grain-size trends in a foreland basin: The Pocono Formation on the Central Appalachian basin. *Journal of Sedimentary Research*, **68**.

Sambrook Smith, G.H. and Ferguson, R.I. (1995). The gravel-sand transition along river channels. *Journal of Sedimentary Research*, **65**.

Sarma, J. (2005). Fluvial process and morphology of the Brahmaputra River in Assam, India. *Geomorphology*, **70**, 226–256.

Scherler, D., Bookhagen, B. and Strecker, M.R. (2014). Tectonic control on 10Be-derived erosion rates in the Garhwal Himalaya, India. *Journal of Geophysical Research: Earth Surface*, **119**, 2013JF002955.

Scherler, D., Bookhagen, B., Wulf, H., Preusser, F. and Strecker, M.R. (2015). Increased late Pleistocene erosion rates during fluvial aggradation in the Garhwal Himalaya, northern India. *Earth and Planetary Science Letters*, **428**, 255–266.

Schildgen, T.F., Robinson, R.A., Savi, S., Phillips, W.M., Spencer, J.Q., Bookhagen, B., Scherler, D., Tofelde, S., Alonso, R.N., Kubik, P.W. *et al.* (2016). Landscape response to late Pleistocene climate change in NW Argentina: Sediment flux modulated by basin geometry and connectivity. *Journal of Geophysical Research: Earth Surface*, **121**, 392–414.

Seal, R., Paola, C., Parker, G., Southard, J.B. and Wilcock, P.R. (1997). Experiments on downstream fining of gravel: I. Narrow-channel runs. *Journal of Hydraulic Engineering*, **123**, 874–884.

Shah, B.A. (2007). Role of Quaternary stratigraphy on arsenic-contaminated groundwater from parts of Middle Ganga Plain, UPBihar, India. *Environmental Geology*, **53**, 1553–1561.

Shields, A. (1936). Anwendung der aehnlichkeitsmechanik und der turbulenzforschung auf die geschiebebewegung. *PhD Thesis Technical University Berlin*.

Shukla, U.K., Singh, I.B., Sharma, M. and Sharma, S. (2001). A model of alluvial megafan sedimentation: Ganga Megafan. *Sedimentary Geology*, **144**, 243–262.

Shukla, U.K., Srivastava, P. and Singh, I.B. (2012). Migration of the Ganga River and development of cliffs in the Varanasi region, India during the late Quaternary: Role of active tectonics. *Geomorphology*, **171172**, 101–113.

Sinclair, H.D. and Naylor, M. (2012). Foreland basin subsidence driven by topographic growth versus plate subduction. *Geological Society of America Bulletin*, **124**, 368–379.

Singer, M.B. (2008). Downstream patterns of bed material grain size in a large, lowland alluvial river subject to low sediment supply. *Water Resources Research*, **44**.

Singh, H., Parkash, B. and Gohain, K. (1993). Facies analysis of the Kosi megafan deposits. *Sedimentary Geology*, **85**, 87–113.

Singh, I.B. (1996). Geological evolution of Ganga Plain - an overview. *Journal of The Palaeontological Society of India*, **41**, 99–137.

Singh, P., Haritashya, U.K., Ramasastri, K. and Kumar, N. (2005). Diurnal variations in discharge and suspended sediment concentration, including runoff-delaying characteristics, of the Gangotri glacier in the Garhwal Himalayas. *Hydrological Processes*, **19**, 1445–1457.

Sinha, R. (2005). Why do Gangetic rivers aggrade or degrade? *Current Science*, **89**, pp836–840.

Sinha, R. (2009). The great avulsion of Kosi on 18 August 2008. *Current Science*, **97**, 429–433, wOS:000268947600031.

Sinha, R. and Friend, P.F. (1994). River systems and their sediment flux, Indo-Gangetic plains, Northern Bihar, India. *Sedimentology*, **41**, 825–845.

Sinha, R. and Sarkar, S. (2009). Climate-induced variability in the Late PleistoceneHolocene fluvial and fluvio-deltaic successions in the Ganga plains, India: A synthesis. *Geomorphology*, **113**, 173–188.

Sinha, R., Friend, P.F. and Switsur, V.R. (1996). Radiocarbon dating and sedimentation rates in the Holocene alluvial sediments of the northern Bihar plains, India. *Geological Magazine*, **133**, 85–90.

Sinha, R., Jain, V., Babu, G.P. and Ghosh, S. (2005). Geomorphic characterization and diversity of the fluvial systems of the Gangetic Plains. *Geomorphology*, **70**, 207–225.

Sinha, R., Gaurav, K., Chandra, S. and Tandon, S.K. (2013). Exploring the channel connectivity structure of the August 2008 avulsion belt of the Kosi River, India: Application to flood risk assessment. *Geology*, **41**, 1099–1102.

Sinha, R., Ahmad, J., Gaurav, K. and Morin, G. (2014a). Shallow subsurface stratigraphy and alluvial architecture of the Kosi and Gandak megafans in the Himalayan foreland basin, India. *Sedimentary Geology*, **301**, 133–149.

Sinha, R., Sripriyanka, K., Jain, V. and Mukul, M. (2014b). Avulsion threshold and planform dynamics of the Kosi River in north Bihar (India) and Nepal: A GIS framework. *Geomorphology*.

Sinha, S., Suresh, N., Kumar, R., Dutta, S. and Arora, B.R. (2010). Sedimentologic and geomorphic studies on the Quaternary alluvial fan and terrace deposits along the Ganga exit. *Quaternary International*, **227**, 87–103.

Sirocko, F., Sarnthein, M., Erlenkeuser, H., Lange, H., Arnold, M. and Duplessy, J.C. (1993). Century-scale events in monsoonal climate over the past 24,000 years. *Nature*, **364**, 322–324.

Sklar, L.S., Dietrich, W.E., Foufoula-Georgiou, E., Lashermes, B. and Bellugi, D. (2006). Do gravel bed river size distributions record channel network structure? *Water Resources Research*, **42**, W06D18.

Slingerland, R. and Smith, N.D. (2004). River avulsions and their deposits. *Annual Review of Earth and Planetary Sciences*, **32**, 257–285.

Smith, G.H.S. and Ferguson, R.I. (1996). The gravel-sand transition: flume study of channel response to reduced slope. *Geomorphology*, **16**, 147–159.

Srivastava, P., Singh, I.B., Sharma, M. and Singhvi, A.K. (2003). Luminescence chronometry and Late Quaternary geomorphic history of the Ganga Plain, India. *Palaeogeography, Palaeoclimatology, Palaeoecology*, **197**, 15–41.

Srivastava, P., Tripathi, J.K., Islam, R. and Jaiswal, M.K. (2008). Fashion and phases of late Pleistocene aggradation and incision in the Alaknanda River Valley, western Himalaya, India. *Quaternary Research*, **70**, 68–80.

Sternberg, H. (1875). Untersuchungen aber lungen-und querprofil geschiebefahrender flasse. *Zeitschrift far Bauwesen*, **25**, p483–506.

Stevens, V.L. and Avouac, J.P. (2015). Interseismic coupling on the main Himalayan thrust. *Geophysical Research Letters*, 2015GL064845.

Stone, J.O. (2000). Air pressure and cosmogenic isotope production. *Journal of Geophysical Research: Solid Earth*, **105**, 23753–23759.

Syvitski, J.P. and Brakenridge, G.R. (2013). Causation and avoidance of catastrophic flooding along the Indus River, Pakistan. *GSA Today*, **23**, 4–10.

Syvitski, J.P., Vörösmarty, C.J., Kettner, A.J. and Green, P. (2005). Impact of humans on the flux of terrestrial sediment to the global coastal ocean. *Science*, **308**, 376–380.

Tandon, S., Gibling, M., Sinha, R., Singh, V., Ghazanfari, P., Dasgupta, A., Jain, M. and Jain, V. (2006). Alluvial valleys of the Gangetic Plains, India: causes and timing of incision. *Incised Valleys in Time and Space, SEPM Special Publication*, **85**, 15–35.

Telbisz, T., Kovács, G., Székely, B. and Szabó, J. (2013). Topographic swath profile analysis: a generalization and sensitivity evaluation of a digital terrain analysis tool. *Zeitschrift für Geomorphologie*, **57**, 485–513.

Thiede, R.C. and Ehlers, T.A. (2013). Large spatial and temporal variations in Himalayan denudation. *Earth and Planetary Science Letters*, **371372**, 278–293.

Tucker, G.E. and Slingerland, R. (1997). Drainage basin responses to climate change. *Water Resources Research*, **33**.

Turowski, J.M., Rickenmann, D. and Dadson, S.J. (2010). The partitioning of the total sediment load of a river into suspended load and bedload: a review of empirical data. *Sedimentology*, **57**, 1126–1146.

van den Berg, J.H. (1995). Prediction of alluvial channel pattern of perennial rivers. *Geomorphology*, **12**, 259–279.

Vance, D., Bickle, M., Ivy-Ochs, S. and Kubik, P.W. (2003). Erosion and exhumation in the Himalaya from cosmogenic isotope inventories of river sediments. *Earth and Planetary Science Letters*, **206**, 273–288.

Venditti, J.G. and Church, M. (2014). Morphology and controls on the position of a gravel-sand transition: Fraser River, British Columbia. *Journal of Geophysical Research: Earth Surface*, **119**, 1959–1976.

Venditti, J.G., Domarad, N., Church, M. and Rennie, C.D. (2015). The gravel-sand transition: Sediment dynamics in a diffuse extension. *Journal of Geophysical Research: Earth Surface*, **120**, 943–963.

Verma, N. (2016). *Geomorphic and morphometric investigation of the Ganga River*. Ph.D. thesis, Department of Geology, University of Delhi.

Von Blanckenburg, F. (2005). The control mechanisms of erosion and weathering at basin scale from cosmogenic nuclides in river sediment. *Earth and Planetary Science Letters*, **237**, 462–479.

Wasson, R.J., Sundriyal, Y.P., Chaudhary, S., Jaiswal, M.K., Morthekai, P., Sati, S.P. and Juyal, N. (2013). A 1000-year history of large floods in the Upper Ganga catchment, central Himalaya, India. *Quaternary Science Reviews*, **77**, 156–166.

Wathen, S.J., Ferguson, R.I., Hoey, T.B. and Werritty, A. (1995). Unequal mobility of gravel and sand in weakly bimodal river sediments. *Water Resources Research*, **31**, 2087–2096.

Wells, N.A. and Dorr, J.A. (1987). Shifting of the Kosi River, northern India. *Geology*, **15**, 204–207.

Wesnousky, S.G., Kumar, S., Mohindra, R. and Thakur, V.C. (1999). Uplift and convergence along the Himalayan Frontal Thrust of India. *Tectonics*, **18**, 967–976.

West, A.J., Hetzel, R., Li, G., Jin, Z., Zhang, F., Hilton, R.G. and Densmore, A.L. (2014). Dilution of 10be in detrital quartz by earthquake-induced landslides: Implications for determining denudation rates and potential to provide insights into landslide sediment dynamics. *Earth and Planetary Science Letters*, **396**, 143–153.

Whipple, K.X. and Tucker, G.E. (2002). Implications of sediment-flux-dependent river incision models for landscape evolution. *Journal of Geophysical Research: Solid Earth*, **107**, ETG 3–1.

Whittaker, A.C., Attal, M. and Allen, P.A. (2010). Characterising the origin, nature and fate of sediment exported from catchments perturbed by active tectonics. *Basin Research*, **22**, 809–828.

Whittaker, A.C., Duller, R.A., Springett, J., Smithells, R.A., Whitchurch, A.L. and Allen, P.A. (2011). Decoding downstream trends in stratigraphic grain size as a function of tectonic subsidence and sediment supply. *Geological Society of America Bulletin*, **123**, 1363–1382.

Wobus, C., Whipple, K.X., Kirby, E., Snyder, N., Johnson, J., Spyropolou, K., Crosby, B. and Sheehan, D. (2006). Tectonics from topography: Procedures, promise, and pitfalls. *Geological Society of America Special Papers*, **398**, 55–74.

Wobus, C.W., Tucker, G.E. and Anderson, R.S. (2010). Does climate change create distinctive patterns of landscape incision? *Journal of Geophysical Research: Earth Surface*, **115**, F04008.

Xu, S., Dougans, A.B., Freeman, S.P., Schnabel, C. and Wilcken, K.M. (2010). Improved 10 Be and 26 Al-AMS with a 5MV spectrometer. *Nuclear Instruments and Methods in Physics Research Section B: Beam Interactions with Materials and Atoms*, **268**, 736–738.

Yanites, B.J., Tucker, G.E. and Anderson, R.S. (2009). Numerical and analytical models of cosmogenic radionuclide dynamics in landslide-dominated drainage basins. *Journal of Geophysical Research: Earth Surface*, **114**.

Yanites, B.J., Tucker, G.E., Mueller, K.J. and Chen, Y.G. (2010). How rivers react to large earthquakes: Evidence from central Taiwan. *Geology*, **38**, 639–642.

Yanites, B.J., Tucker, G.E., Hsu, H.L., Chen, C.c., Chen, Y.G. and Mueller, K.J. (2011). The influence of sediment cover variability on long-term river incision rates: An example from the Peikang River, central Taiwan. *Journal of Geophysical Research: Earth Surface*, **116**, F03016.

Yatsu, E. (1955). On the longitudinal profile of the graded river. *Eos, Transactions American Geophysical Union*, **36**, 655–663.

Yin, A. (2006). Cenozoic tectonic evolution of the Himalayan orogen as constrained by along-strike variation of structural geometry, exhumation history, and foreland sedimentation. *Earth-Science Reviews*, **76**, 1–131.

Appendix A

Appendix A

[American Journal of Science, Vol. 316, October, 2016, P. 778–812, DOI 10.2475/08.2016.03]

SUBSIDENCE CONTROL ON RIVER MORPHOLOGY AND GRAIN SIZE IN THE GANGA PLAIN

ELIZABETH H. DINGLE*,†, HUGH D. SINCLAIR*, MIKAËL ATTAL*,
DAVID T. MILODOWSKI**, and VIMAL SINGH***

ABSTRACT. The Ganga Plain represents a large proportion of the current foreland basin to the Himalaya. The Himalayan-sourced waters irrigate the Plain via major river networks that support approximately 10 percent of the global population. However, some of these rivers are also the source of devastating floods. The tendency for some of these rivers to flood is directly linked to their large scale morphology. In general, the rivers that drain the east Ganga Plain have channels that are perched at a higher elevation relative to their floodplain, leading to more frequent channel avulsion and flooding. In contrast, those further west have channels that are incised into the floodplain and are historically less prone to flooding. Understanding the controls on these contrasting river forms is fundamental to determining the sensitivity of these systems to projected climate change and the growing water resource demands across the Plain. Here, we present a new basin scale approach to quantifying floodplain and channel topography that identifies areas where channels are super-elevated or entrenched relative to their adjacent floodplain. We explore the probable controls on these observations through an analysis of basin subsidence rates, sediment grain size data and sediment supply from the main river systems that traverse the Plain (Yamuna, Ganga, Karnali, Gandak and Kosi rivers). Subsidence rates are approximated by combining basement profiles derived from seismic data with known convergence velocities; results suggest a more slowly subsiding basin in the west than the east. Grain size fining rates are also used as a proxy for relative subsidence rates along the strike of the basin; the results also indicate higher fining rates (and hence subsidence rates for given sediment supply) in the east. By integrating these observations, we propose that higher subsidence rates are responsible for a deeper basin in the east with perched, low gradient river systems that are relatively insensitive to climatically driven changes in base-level. In contrast, the lower subsidence rates in the west are associated with a higher elevation basin topography, and entrenched river systems recording climatically induced lowering of river base-levels during the Holocene.

Keywords: Subsidence, grain size, Ganga Plain, river morphology, topographic analysis

INTRODUCTION

Many of the rivers of the Ganga Plain are prone to abrupt switching of channel courses (avulsion) causing devastating floods over some of the most densely populated regions on the globe. The Kosi River that drains central Nepal and discharges onto the Ganga Plain of Bihar State has a well-documented history of frequent channel avulsion and flooding (Wells and Dorr, 1987). During 2008, a single channel avulsion event resulted in a temporary eastward shift of the Kosi River by tens of kilometers where the channel breached its eastern levee resulting in extensive flooding (Sinha and others, 2005, 2013, 2014a; Chakraborty and others, 2010). Similarly, levee failures and channel avulsion resulted in catastrophic flooding of the Indus Plain of Pakistan in 2010 and the displacement of at least 10 million people (Syvitski and Brakenridge, 2013). The

* School of GeoSciences, University of Edinburgh, Drummond Street, Edinburgh, EH10 5EQ, United Kingdom
** School of GeoSciences, University of Edinburgh, Crew Building, Edinburgh, EH9 3JN, United Kingdom
*** Department of Geology, University of Delhi, Delhi 110007, India
† Corresponding author: elizabeth.dingle@ed.ac.uk

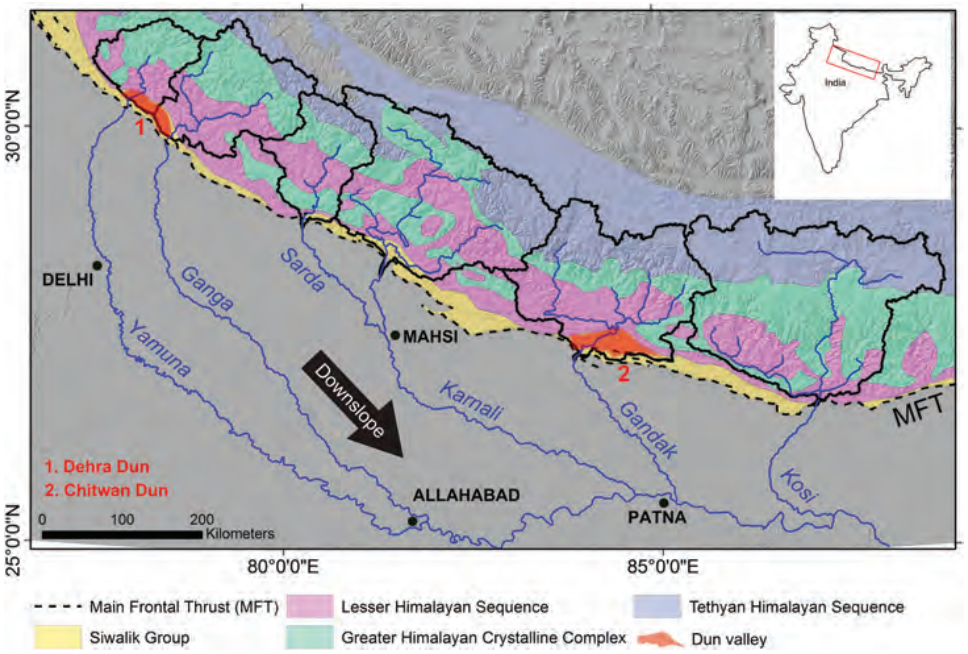

Fig. 1. Study catchments, location of major Dun valleys and geology (from Yin, 2006) in the Ganga basin on a 90 m Shuttle Radar Topography Mission (SRTM) derived Digital Elevation Model (DEM).

nature and frequency of channel avulsion is also a first-order control on alluvial stratigraphy, defining the geometric distributions of channel and floodplain deposits (Bridge and Leeder, 1979; Slingerland and Smith, 2004). In the Ganga Plain, the distribution of Quaternary channel sands and floodplain muds determines groundwater pathways and associated arsenic pollution (Shah, 2007). Given the significance of floodwaters and groundwater pathways in the Ganga Plain, documenting and understanding variations in the morphology of river channel and floodplain systems represents a research priority, particularly in light of changes in monsoon intensity, glacial meltwater discharge and the water demands of a growing population (Fleitmann and others, 2007; Immerzeel and others, 2010).

Systematic variations in the large-scale morphology of the river systems are recognized across the extent of the Ganga foreland basin (fig. 1) (Sinha and others, 2005). Rivers of the east Ganga Plain are characterized by shallow aggrading channels that frequently avulse and flood, whilst those in the west are characterized by degrading systems with incised channels and extensive areas of badland topography. In the east Ganga Plain, numerous channel avulsions and random switching of the loci of fan lobe aggradation has resulted in a net westward migration of >113 km of the Kosi River over the surface of its mega-fan during the last two centuries (Wells and Dorr, 1987; Chakraborty and others, 2010). Palaeochannels are well preserved across much of the surface of the Kosi and Gandak fans (Sinha and others, 2014b), reflecting the dynamic and mobile nature of these systems. In the west Ganga Plain, the Ganga River is described as a braided channel within a narrow incised valley with exposed cliffs extending 15 to 30 m above the modern channel in parts (Shukla and others, 2001; Gibling and others, 2005; Shukla and others, 2012). Numerous phases of incision and aggradation are documented within both the Yamuna and Ganga valleys where distinct geomorphic surfaces and facies associations are preserved in exposed valley walls (Shukla and others, 2001, 2012; Gibling and others, 2005; Tandon and others, 2006).

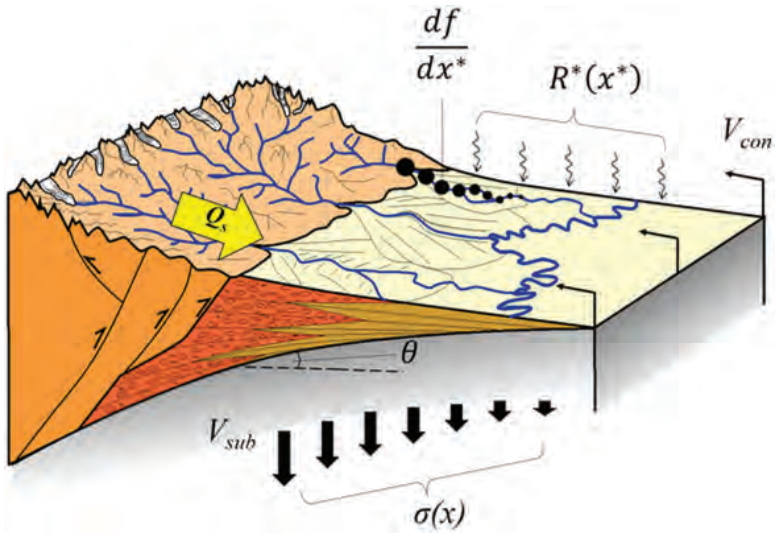

Fig. 2. Major controls on large scale channel morphology across the Ganga Plain. These controls include sediment flux, q_s, to the basin; the distribution of tectonic subsidence, $\sigma(x)$, across the basin; the spatial distribution of sediment deposition down-system, $R^*(x^*)$; sediment grain size fining rate, df/dx^*; and basin subsidence velocity, V_{sub}, which is a product of the horizontal convergence velocity across the Himalaya, V_{con}, and dip of the basement beneath the mountain front, θ.

In order to understand the controls on the variations in river morphology along the Ganga Plain, we need to consider a range of possible scenarios. As rivers exit mountain ranges, they commonly evolve into broad alluvial systems where river morphology (channel pattern, geometry, gradient) is typically determined by water and sediment discharges, sediment grain sizes, basin subsidence rates and vegetative patterns (fig. 2) (van den Berg, 1995; Dade and Friend, 1998; Dade, 2000; Marr and others, 2000; Duller and others, 2010; Allen P.A. and others, 2013). In addition, first-order predictions from various studies (for example Paola and others, 1992a; Robinson and Slingerland, 1998; Duller and others, 2010; Allen P.A. and others, 2013) are that downstream grain size trends are also controlled by sediment supply and subsidence rate, with increased sediment supply reducing fining rates, and increased basin subsidence increasing fining rates as a result of enhanced rates of deposition or aggradation promoting selective deposition in the proximal region of the basin. Grain size fining trends impact the location of the gravel-sand transition (Dubille and Lavé, 2015), and variations in river morphology (Dade and Friend, 1998).

This paper initially quantifies the basin-wide variability in incision and aggradation of the river systems across the Ganga Plain from digital topography using a swath based technique to map relative elevation of channels above or below their floodplains. The implications are that the lateral variations in incision versus aggradation should be recorded in the underlying basin stratigraphy, and that the relative contributions of sediment derived from the western and eastern Himalaya to the Ganges-Brahmaputra Delta are likely to be affected by the relative efficiency of sediment transport and bypass across the Ganga Plain. In addition to quantifying the relief along the valleys of the rivers, we also generate new basin-wide data on subsidence rates and grain size fining rates from the proximal foreland basin near to the mountain front. We finally discuss and analyze these data in context of the observed patterns in incision and aggradation of the river systems across the Ganga Plain.

A challenge when determining longer-term (millennial) controls on fluvial morphologies is to differentiate signals driven by shorter-term stochastic variations in

climate or tectonic activity in the upstream catchment (Benda and Dunne, 1997a; Tucker and Slingerland, 1997; Leeder and others, 1998). Forward models have simulated the effects of varying parameters such as sediment flux and basin subsidence over different timescales relative to the equilibrium time period of the basin, defined as the period required for streams within the basin to attain a steady-state profile (Paola and others, 1992a; Heller and Paola, 1996; Robinson and Slingerland, 1998; Marr and others, 2000). In a system as large as the Ganga Plain, potential short-term ($<10^4$ years) controls on sediment flux and grain size could be linked to climatic changes in precipitation patterns, glacial discharge and extreme storm events or earthquakes. In contrast, subsidence rates, which are controlled by topographic loading and the flexural response and subduction velocity of the underlying lithosphere (Sinclair and Naylor, 2012) are unlikely to vary at these timescales. Below, we discuss current knowledge and data available on the potential controlling parameters on the large-scale morphology of rivers across the Ganga Plain: sediment flux, basin subsidence and sediment grain size of rivers across the Ganga Plain.

Current Constraints on Sediment Flux, Basin Subsidence and Sediment Grain Size across the Ganga Plain

Our current understanding of sediment flux into the Ganga foreland basin is based principally on suspended sediment data from gauging station networks, but the spatial coverage of these data is restricted (Blöthe and Korup, 2013). Advances in detrital cosmogenic radionuclide (CRN) analysis have allowed ^{10}Be concentrations to be measured in modern river sediments, allowing approximation of average denudation rates from the source catchments over timescales of thousands of years (Vance and others, 2003; Lupker and others, 2012; Godard and others, 2014). The published CRN data give an indication of how sediment flux delivered to the foreland basin varies spatially between the major river systems that drain the Himalaya. The mean erosion rates of ~1 mm/yr derived from these data can be used to infer the timescales over which the rates are averaged, <1000 years in this case based on the reduction in CRN production rates with depth. Sediment fluxes calculated from ^{10}Be concentrations measured from the modern river sediment reveal marginally lower fluxes at the western end of the Ganga basin (fig. 3, table 1). However, estimates vary by up to a factor of three between sampling years of a single river, highlighting the difficulty in accurately quantifying sediment flux to the foreland basin using this approach (Lupker and others, 2012). Until we have a better understanding of the controls on the variability in ^{10}Be concentrations, it remains difficult to quantify spatial variations in millennial-scale sediment supply rate from Himalayan catchments. Similarly, longer term erosion rates estimated from bedrock mineral cooling ages of the Greater Himalaya Sequence along the strike of the range do not suggest a significant west to east variation in erosion rates, although rates further east are marginally (~0.5 mm/yr) higher (Thiede and Ehlers, 2013). Denudation rates over the past 4 Myr vary between ~1 to 2.5 mm/yr across the Greater Himalayan Sequence within the Ganga basin, but there are large uncertainties with these data (Thiede and Ehlers, 2013). Furthermore, erosion rates in the Greater Himalaya are thought to be relatively high in comparison to the Lesser Himalaya (Lavé and Avouac, 2001), and as such, denudation rates derived from thermochronology studies in this region do not represent catchment averaged rates. The timescales over which these denudation rates have been averaged may also be too large to reflect spatial patterns in modern or sub-millennial sediment fluxes to the Ganga Plain, and should not be interpreted as comparable rates to those derived from ^{10}Be concentrations.

Basin subsidence histories across the Indo-Gangetic Plain requires multiple, well documented wells with good stratigraphic resolution (Allen P.A. and Allen J.R., 2013), but these types of data are not available for this region (Burbank and others, 1996).

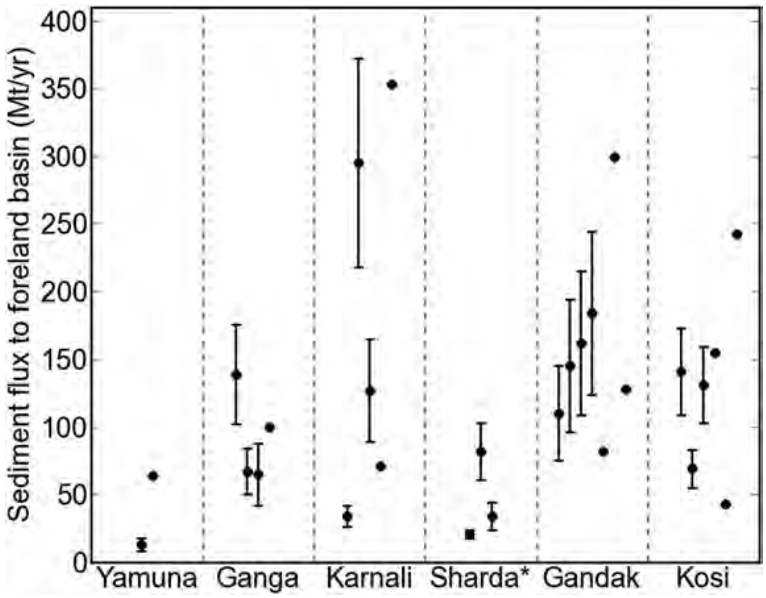

Fig. 3. Sediment flux estimates derived from cosmogenic ^{10}Be concentrations (and errors) and suspended sediment concentrations. (*) Where no data were available for the Sharda catchment, catchment-averaged erosion rates derived from the adjacent Karnali catchment (from Lupker and others, 2012) were used to calculate sediment flux estimates.

Therefore, for this study, we calculate the tectonic forcing of subsidence using the depth to the crystalline basement that underlies the Siwalik succession derived from the Seismotectonic Atlas of India, prepared by the Geological Survey of India (Narula and others, 2000), integrated with the local subduction velocities (Sinclair and Naylor, 2012).

Grain size data from the principal Himalayan rivers are not available, and are therefore a key component of the new data presented in this study. We note that detailed downstream grain size fining trends have been analyzed from smaller Himalayan rivers (Dubille and Lavé, 2015) that drain the foothills termed 'Piedmont Rivers' (Sinha and Friend, 1994). The grain size data show a clear transition from gravel to sand in the rivers at approximately 8 to 20 km from the mountain front. Given the order of magnitude increase in catchment size and likely sediment supply from the larger rivers that drain the high mountains of the Himalaya, it is reasonable to predict an increase in distance from the mountain front to the gravel-sand transition for the main rivers presented here.

REGIONAL CONTEXT

The Himalayan foreland basin formed as a result of the ongoing collision between the Indian and Eurasian plates, where crustal thickening generates high topography that is supported by the flexural rigidity of the underlying lithosphere (Lyon-Caen and Molnar, 1985; Flemings and Jordan, 1989; Burbank and Beck, 1991; Burbank, 1992; Brozovic and Burbank, 2000). Along the strike of the mountain range, variations in lithospheric rigidity and basement faulting are believed to have modulated both basin width and large-scale patterns of subsidence (Burbank and others, 1996). The Himalayan orogen is split into four major structural units that run broadly parallel from west to east (fig. 1). These units are from south to north: the Neogene Siwalik Group, the Proterozoic Lesser Himalayan Sequence, the Proterozoic-Ordovician Greater Himala-

TABLE 1

Sediment flux estimates summarized from Blöthe and Korup (2013)

River name	Sediment flux (Mt yr^{-1}) at mountain front	Source
Yamuna	13±5	Lupker and others, 2012*
	64	Jha and others, 1993***
Ganga	139±37	Lupker and others, 2012*
	67±17	Vance and others, 2003*
	65±23	Vance and others, 2003*
	100	Wasson, 2003***
Karnali	34±8	Lupker and others, 2012*
	295±77	Lupker and others, 2012*
	127±38	Lupker and others, 2012*
	71	Ghimire and Uprety, 1990***
	353	Andermann and others, 2012**
Gandak	110±35	Lupker and others, 2012*
	145±49	Lupker and others, 2012*
	162±53	Lupker and others, 2012*
	184±60	Lupker and others, 2012*
	82	Sinha and Friend, 1994***
	299	Andermann and others, 2012**
	128	Ghimire and Uprety, 1990***
Kosi	141±32	Lupker and others, 2012*
	69±14	Lupker and others, 2012*
	131±28	Lupker and others, 2012*
	155	Ghimire and Uprety, 1990***
	43	Sinha and Friend, 1994***
	242	Andermann and others, 2012**

* Sediment flux derived from ^{10}Be concentration in sand.
** Based on a mean daily suspended sediment flux (1973-2006).
*** Suspended sediment concentration.

yan Crystalline Complex and the Proterozoic to Eocene Tethyan Himalayan Sequence (Yin, 2006). These lithological units are bound by major faults, the most active of which is the Main Frontal Thrust (MFT). The MFT is the most southerly structure, situated between the Siwalik Group and the foreland basin, and absorbs approximately 80 percent of the ~21±1.5 mm/yr convergence) between India and south Tibet in central Nepal (Lavé and Avouac, 2000).

Sediment generated by the erosion of the Himalayan mountain range accumulates in the foreland basin. The thickness of the basin fill reduces progressively with distance from the mountain front, consistent with asymmetric subsidence caused by thrusting of the overlying orogen (Burbank and Beck, 1991; Burbank, 1992; Yin, 2006). The basin fill is dominated by the Neogene Siwalik Group and the pre-Miocene Rawalpindi Group (Burbank and others, 1996). The Siwalik Group comprises thick molasse deposits formed by the erosional products of the Lesser and Higher Himalaya (for example Kumar and others, 2004). Thin-skinned tectonics associated with the MFT have incorporated these poorly consolidated molasse deposits in the hanging wall

of frontal structures, forming the Siwalik Hills which represent the youngest and southernmost topography of the Himalaya (Mugnier and others, 1999). The foredeep basin (*sensu* DeCelles and Giles, 1996) lies immediately south of the Siwalik Hills, forming the Indo-Gangetic Plain. Immediately inboard of the thrust front are several wedge-top basins, locally termed 'Duns' that act to buffer the sediment delivery to the foredeep (Densmore and others, 2016). In comparison to the confined bedrock channel both upstream and downstream of the Dun, the laterally unconfined and lower gradient surface of these Dun valleys has promoted sediment deposition during periods of heightened sediment export from the mountains, producing a thick alluvial valley fill. Dun valleys of direct relevance to this study are the Chitwan and Dehra Dun valleys where the Gandak, Ganga and Yamuna rivers flow through prior to passing the MFT and exiting onto the Plain (fig. 1).

The Ganga Plain (and henceforth Plain) forms the central third of the Indo-Gangetic Plain and covers an area of 250,000 km^2, whilst the drainage area of the entire Ganga basin is in excess of 1,060,000 km^2 (Singh, 1996). The hydrology of rivers draining the basin is dominated by the Indian Summer Monsoon (ISM), when over 85 percent of the annual rainfall falls between June and September (Sinha and Friend, 1994; Tandon and others, 2006), producing broad peaked annual hydrographs. Along strike gradients in precipitation have been identified using passive microwave data (Bookhagen and others, 2005; Anders and others, 2006) where catchments in the east typically experience more Indian summer monsoon precipitation than those in the west. A strong north-south precipitation gradient has also been identified as a result of orographic enhancement of precipitation, where the heaviest rainfall is induced by the first significant topography encountered by southerly air masses originating from the Bay of Bengal (Bookhagen and others, 2005; Bookhagen and Burbank, 2006; Anders and others, 2006). Apatite fission track ages from across the entire Himalaya do not reveal any systematic change in exhumation rates along the strike of the range (Thiede and Ehlers, 2013).

Sediment carried into the foreland basin that is not immediately deposited, typically sand and finer material, can continue downstream via the Ganga, Brahmaputra and Indus rivers ultimately reaching the sea where it accumulates in the Bengal and Indus fans. This fraction represents up to ~90 percent of the total sediment load exported from the Himalaya (Lupker and others, 2011). Sediment trapped within the foreland basin is deposited across vast alluvial fans that are separated by broad interfan or interfluve areas that are drained by foothill or Plain fed rivers (Jain and Sinha, 2003; Sinha and others, 2005). These interfan parts of the basin are filled primarily with sediments eroded from the frontal Siwalik range, and sediments derived and reworked locally from the Plain (Sinha and others, 2005).

The rivers feeding the Plain can be divided into mountain, foothill and Plain fed (Sinha and Friend, 1994). Mountain-fed rivers originate from large source areas within the Himalayan orogen, typically with a glacial source. Foothill or 'Piedmont' rivers have relatively small catchment areas of 20 to 2500 km^2 (Dubille and Lavé, 2015) and drain the interfluve region between alluvial fans created by sediment deposition of the much larger mountain fed rivers. Plain fed rivers repetitively rework sediment deposited by the mountain and foothill fed rivers (Sinha and others, 2005). Grain size measurements in central Nepal across a number of interfan or foothill fed channels have documented a rapid gravel-sand transition occurring ~8 to 20 km downstream of the mountain front (Dubille and Lavé, 2015). This same rapid transition is consistent with vertical grain size measurements taken from the Siwalik molasse exposed in the frontal Himalayan folds (Dubille and Lavé, 2015). Grain size fining rates have not been documented for the mountain fed rivers.

METHODOLOGY

Topographic Analysis

Effective mapping of channel elevations relative to their adjacent alluvial fan surface reveals spatial variations in both aggradation and incision of active fluvial systems. Existing approaches to identify regions where channels are perched above their adjacent floodplain, or 'super-elevated' (Bryant and others, 1995), are typically limited to linear elevation transects across target alluvial fans using digital elevation models (DEMs) (for example Sinha and others, 2005; Chakraborty and Ghosh, 2010; Chakraborty and others, 2010). A number of limitations arise from this approach: (i) the approach is limited in its spatial resolution as each transect only records elevation across a small portion of the fan, which may not necessarily be coincident with areas of highest avulsion risk; (ii) the orientation of the transects does not directly reflect the geometry of either the channel or fan system; (iii) differentiating data noise from geomorphic features such as channel levees that are often comparable in amplitude (Chakraborty and others, 2010), requiring significant degrees of smoothing to pick out first order features of the alluvial fan system (Chakraborty and Ghosh, 2010). Sinha and others (2014a) addressed the first of these issues by taking a series of profiles following parallel linear transects at 2 km spacing down the Kosi fan, permitting an assessment of changes in channel super-elevation along the length of the alluvial fan; however, the spatial resolution is still limited to the transects themselves, and suffers from the same problems relating to transect orientation and noise outlined above. Noise reduction could potentially be achieved using swath profiles which provide a means of increasing the signal-noise ratio, and should highlight characteristics of the along-profile topography (Telbisz and others, 2013; Hergarten and others, 2014). More recent generalized swath profile methods permit the use of arbitrary, non-linear baselines, such as river courses, enabling the unbiased characterization of river valley morphology, but averaging along the length of a stream reach, reducing resolution (Hergarten and others, 2014).

We present a new, spatially distributed method to map patterns of fluvial incision and aggradation across alluvial fan systems that addresses the above issues. The premise of this method is that when a channel is elevated relative to its floodplain or adjacent fan surface, the adjacent surface will lie below the elevation of the channel; when incised, the adjacent surface will have a higher elevation relative to the channel. Therefore, by mapping every location within the DEM to the closest point in the channel, it is possible to assess the relative elevation of the channel compared to the rest of the fan.

In order to produce maps of channel super-elevation, we use a swath-based method, similar to that developed by Hergarten and others (2014) to construct generalized swath profiles using curvi-linear baselines.

The first step in our procedure is to extract the trunk channel on the alluvial fan from the DEM. For this work, river networks were extracted from a 90 m resolution Shuttle Radar Topography Mission (SRTM) DEM using ESRI ArcMap v10.1, using a steepest-descent flow routing algorithm. Channel elevations along these river networks represent the elevation of the water surface in 2000, the time of the SRTM data capture. The root mean squared error (RMSE) of these data in mountainous regions is ± 7.75 m, while in less mountainous regions, the RMSE of the SRTM is ± 14.48 m (Amans and others, 2013). Given that the flow stage will be highly variable through the year, there may be a small impact on these results, although this is likely to be within the RMSE error of the DEM. As such, the use of these data should provisionally be limited to the interpretation of very large scale patterns or where relief exceeds the RMSE of the data ($\sim \pm 10$–15 m).

These trunk channels are subsequently used as a baseline along which we generate an 80 km wide swath. This swath determines the region in which we map the relative super-elevation of the trunk channel, and in other applications can be modified for other river systems as required. Within this neighbourhood, we iterate through every pixel, p_i, and map it to the nearest point in the trunk channel baseline, following Hergarten and others (2014); DEM pixels for which the closest point on the baseline is at either of the termini are excluded. The elevation difference between the fan surface and the nearest point on the trunk channel is then calculated, with the resultant swath revealing spatial variations in the elevation of the fan surface relative to the closest point in the active channel (fig. 4). Negative values indicate areas of the fan that are lower in elevation to the closest point in the trunk channel (the channel is perched above the neighboring fan surface); these areas are shaded red on the swath in figure 4. Conversely, where the trunk channel is entrenched, elevations on the neighboring fan surface are greater than the closest point in the trunk channel; the more entrenched portions of the swath are colored in blue on figure 4. Areas of the swath that are at a similar elevation to the channel are shaded in yellow, and areas more than 100 m above the channel are in purple, which typically represents mountainous topography.

Channel lengths extending from the Himalayan mountain front (defined as the most southerly area of notable relief) to the Ganga trunk stream were extracted for each river. Longitudinal profiles of each river were also extracted from the DEM from which slope values averaged over a 10 km moving window were then calculated. Normalized channel steepness (k_{sn}) was also calculated at the fan apex using a reference concavity of 0.5, to allow comparison of channel gradients independently of upstream catchment area (Wobus and others, 2006; Allen G.H. and others, 2013). Similar profiles were constructed from the surface of the adjacent floodplains, or valley tops where channels were entrenched in the west Ganga Plain. These profiles followed transects that were broadly parallel to the channel.

Basin Subsidence

The distribution of sediment deposition, or the spatial apportioning of sediment sorting, at a given distance (x) can be expressed as:

$$R(x) = \frac{r}{q_s} \tag{1}$$

where r is the rate of sediment deposition, and q_s is sediment flux (Paola and Seal, 1995). R can be made non-dimensional such that:

$$R^*(x^*) = C_0 \frac{r(x)}{q_s(x)} L \tag{2}$$

where R^* is the non-dimensional function that describes the distribution of deposition, C_0 is the volumetric sediment concentration on the bed, r is the rate of sediment deposition, q_s is the sediment flux, and L is the length of the depositional stream (Paola and Seal, 1995). Assuming that the rate of sediment deposition is controlled by the rate of tectonic subsidence, defined as $\sigma(x)$, $R^*(x^*)$ can also be expressed as:

$$R^*(x^*) = (1 - \lambda_p) L \frac{\sigma(x)}{q_s(x)} \tag{3}$$

where L is the length of the depositional stream, $q_s\,(x)$ is the rate of decay in sediment flux downstream ($L\ t^{-1}$), λ_p is the sediment porosity and x^* is the normalized longitudinal location along a deposition system of length L (Duller and others, 2010).

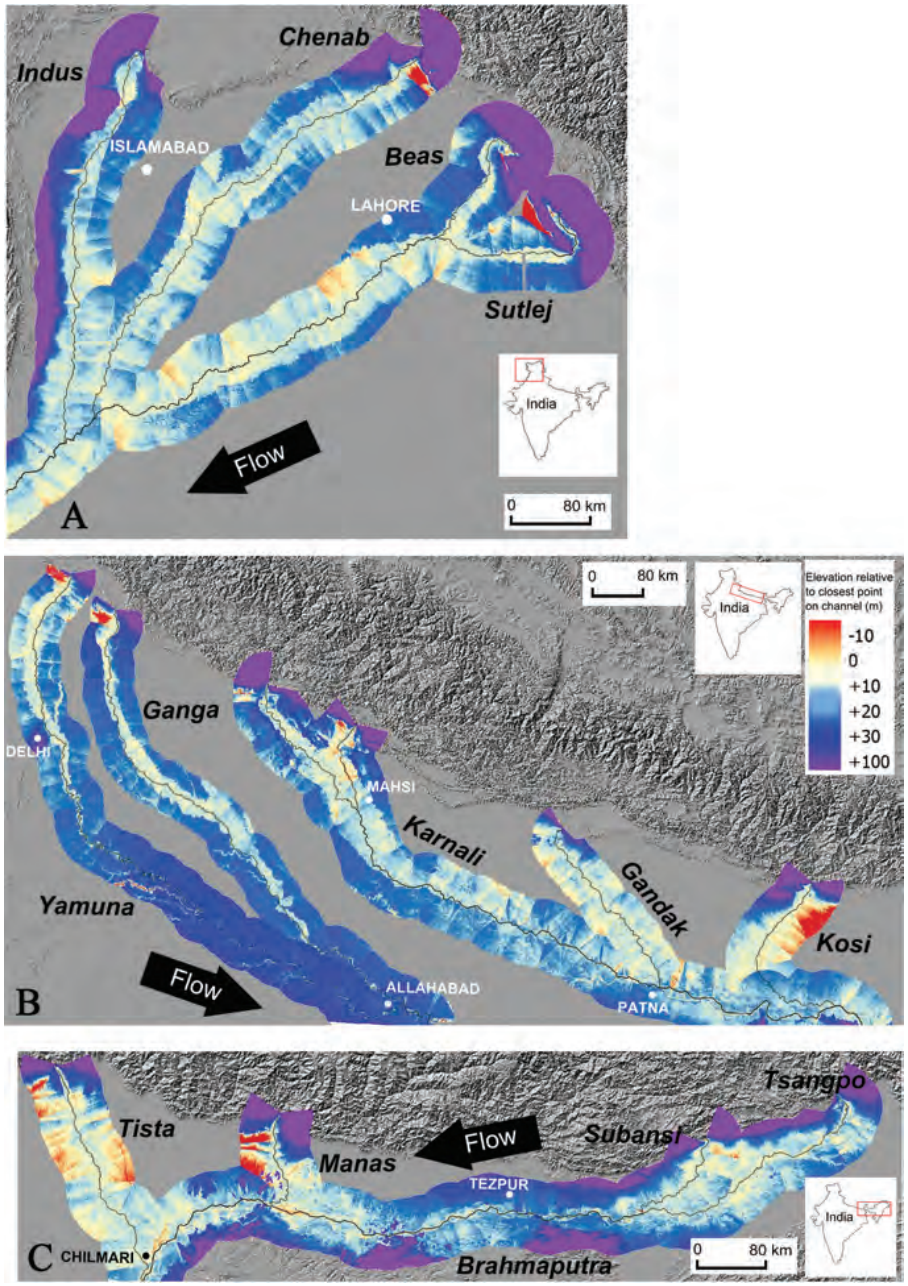

Fig. 4. Valley topography from swath profile analysis for the three major river basins across the Himalayan foreland basin from west to east; (A) Indus (B) Ganga and (C) Brahmaputra.

If R^* determines how sediment sorting is apportioned spatially, most sorting will occur at the upstream end of the system where the greatest proportion of sediment is deposited (Duller and others, 2010). The rate of down-system grain size fining can also be described by the fractional Exner sediment mass balance (Paola and Seal, 1995), also incorporating tectonic subsidence through the R^* function:

$$\frac{df}{dx^*} = f\left[R^*\left(1 - \frac{1}{J}\right)\right] - \frac{1}{J}\frac{dJ}{dx^*} \tag{4}$$

where f is the fraction of a given sediment size in the deposit and $J = p/f$, where p is the fraction of a given sediment size in the transporting system (Duller and others, 2010). This predicts a correlation between subsidence rates, sediment grain size fining rate and hence river morphology.

The methodology for calculating the tectonic forcing of subsidence of the surface near the mountain front uses new maps of the depth to crystalline basement derived from seismic data combined with known shortening rates (Stevens and Avouac, 2015). The approach doesn't use the depth to basement, but instead utilizes the gradient of the basement nearest to the mountain front (Sinclair and Naylor, 2012). By reconstructing the gradient of the basement of the subducting slab (θ) and combining it with known convergence velocities (V_{con}) between the Ganga Plain and the Himalaya (Stevens and Avouac, 2015), we can derive the vertical velocity which determines the modern subsidence velocity at the surface (V_{sub}) at point x using:

$$V_{sub}(x) = V_{con}\ tan\ \theta(x) \tag{5}$$

This tectonic forcing of surface lowering (subsidence) at the mountain front remains steady as long as the following remain constant: 1) the mean distribution and magnitude of topography; 2) the density structure of the mountain range; 3) the convergence velocity between the subducting lithosphere and the distributed load of the range, and 4) the gradient of the subducting lithosphere. Within these parameters, the most likely to vary at a high spatial and temporal scale is the distribution of topography, as thrust units are accreted at the front of the range. Analogue and numerical experiments from thrust wedges indicate that fluctuations in frontal accretion versus internal thickening of the wedge can result in punctuated topographic growth at a timescale characterized by the length of accreted thrust sheets divided by the convergence velocity (Hoth and others, 2007; Naylor and Sinclair, 2007). For the Himalayas, typical spacing of thrust units are approximately 12 km, which when divided by a mean convergence velocity of 18 km/Myr yields a timescale of probable topographic variations of 0.66 Myr.

Additionally, the rate of stratigraphic onlap of the Siwalik Group onto the basement of the foredeep is 19±5 km/Myr which is comparable to the convergence velocity, suggesting these parameters have been in steady state for the recent history of the thrust wedge and foreland basin system (Lyon-Caen and Molnar, 1985; Mugnier and Huyghe, 2006). Based on these arguments, we do not envisage the tectonic forcing of subsidence to have varied significantly for at least the last 100,000 years.

For this study, the time interval of interest is the period over which the present morphology of the river systems of the Ganga Plains is defined; this interval may be approximated by the topographic relief of the fluvial system divided by the sediment accumulation rates. In this case, the local relief of the incised and super-elevated channel systems is up to 30 m. Holocene sedimentation rates for the proximal basin are of the order of 1 mm/yr (Sinha and others, 1996). Based on these rates, we propose that the time interval of interest in determining the basin's surface morphology is approximately 30,000 years. Consequently, we see no reason to consider that subsidence rates have varied at any given location in the basin during the development of the present-fluvial morphology across the Ganga Plain.

The long-term ($>10^6$ yr) and recent convergent velocity between the subducting plate and the Himalayan topography can be approximated from the stratigraphy of the foreland basin, and modern GPS data respectively. As outlined above, stratigraphic sequences observed in deep well and seismic data imply convergence rates of between

~10 to 20 mm/yr over the past 15 to 20 Ma from these data (Lyon-Caen and Molnar, 1985). Contemporary GPS data (Feldl and Bilham, 2006; Stevens and Avouac, 2015) have demonstrated along strike differences in modern India-Tibet convergence rates. Rates in the eastern Himalayan arc are typically 18 to 20 mm/yr compared to 12 to 15 mm/yr in the west. The tectonic displacement of fluvial terrace surfaces in central Nepal (Lavé and Avouac, 2000) and northwest India (Wesnousky and others, 1999) further support a systematic east to west decrease in convergence rates with estimates of 21.5±1.5 mm/yr and 11.9±3.1 mm/yr, respectively.

Models calibrated against gravity data have also indicated that the flexural rigidity of the Ganga Basin varies along strike of the basin (Lyon-Caen and Molnar, 1985; Jordan and Watts, 2005). Jordan and Watts (2005) demonstrated that the central Himalayan foreland basin, which relates to the west Ganga Plain, has a higher effective elastic thickness (~70 km) compared to regions in the east and west (~30–50 km).

The gradient of the basement beneath the proximal foreland basin (θ) is measured using the depth to basement plots of the Ganga basin derived from depth converted reflection seismic data (fig. 5A). The dip of the basement beneath the mountain front has been calculated using the average gradient of the first 30 km of each profile basin-ward of the mountain front, thus reflecting a control on basin subsidence velocities of the proximal basin. Six cross-sections of the foreland basin have been generated from these plots and second order polynomial equations and curves have been fitted through the data to extend the cross section to a point beneath the mountain front to account for increasing rates of subsidence close to the mountain front (Sinclair and Naylor, 2012). A range of V_{sub} values have been calculated along the course of each river using variable V_{con} values to assess the impact on V_{sub} estimates. The variable convergence rate estimates used are based on Stevens and Avouac (2015) with values of 13.3±1.7 mm/yr for the Yamuna and Ganga, 18.5±1.8 mm/yr for the Sharda and Karnali and 20.2±1.1 mm/yr for the Kosi and Gandak. Previously mentioned convergence rate estimates from Wesnousky and others (1999) and Lavé and Avouac (2000) have also been included in this analysis.

Grain Size

Extensive coarse gravel bars dominate the bed of the major rivers of the Ganga Plain as they exit the mountain front. During the low-flow season (October-May), a considerable portion of the channel bed is accessible. If it is assumed that equal mobility conditions (Parker and Toro-Escobar, 2002) are attained during monsoon flows, allowing full reworking of gravel bar material, then the gravel deposits visible during this period should represent bedload transported and deposited during the preceding monsoon (Attal and Lavé, 2006). Equal mobility implies that the grain size distribution of the annual transported yield is finer than that of the gravel in the armored surface exposed at low flow, and similar to that beneath the armored layer in the subsurface (Parker and Toro-Escobar, 2002). Grain size measurements were taken from ~30 to 50 km upstream of the mountain front down to the gravel-sand transition of each of the Kosi, Gandak, Sharda, Ganga and Yamuna rivers. Ideally, measurements would have been carried out at regular intervals but sampling was restricted by access and in-channel structures. Where large engineered dams (barrages) have been constructed to divert water into channels for irrigation were present, samples were taken at least 1 to 2 km upstream or downstream of the structure to minimise localized hydrodynamic and trapping effects, this being the distance over which the influence of the barrage appeared to dissipate.

Grain size measurements were taken of both the surface and subsurface material using photographic and volumetric analysis, respectively, to account for the effects of surface coarsening (Dietrich and others, 1989; Parker, 1990). Samples were restricted to parts of the bar which appeared recently reworked with imbricated and sub-rounded

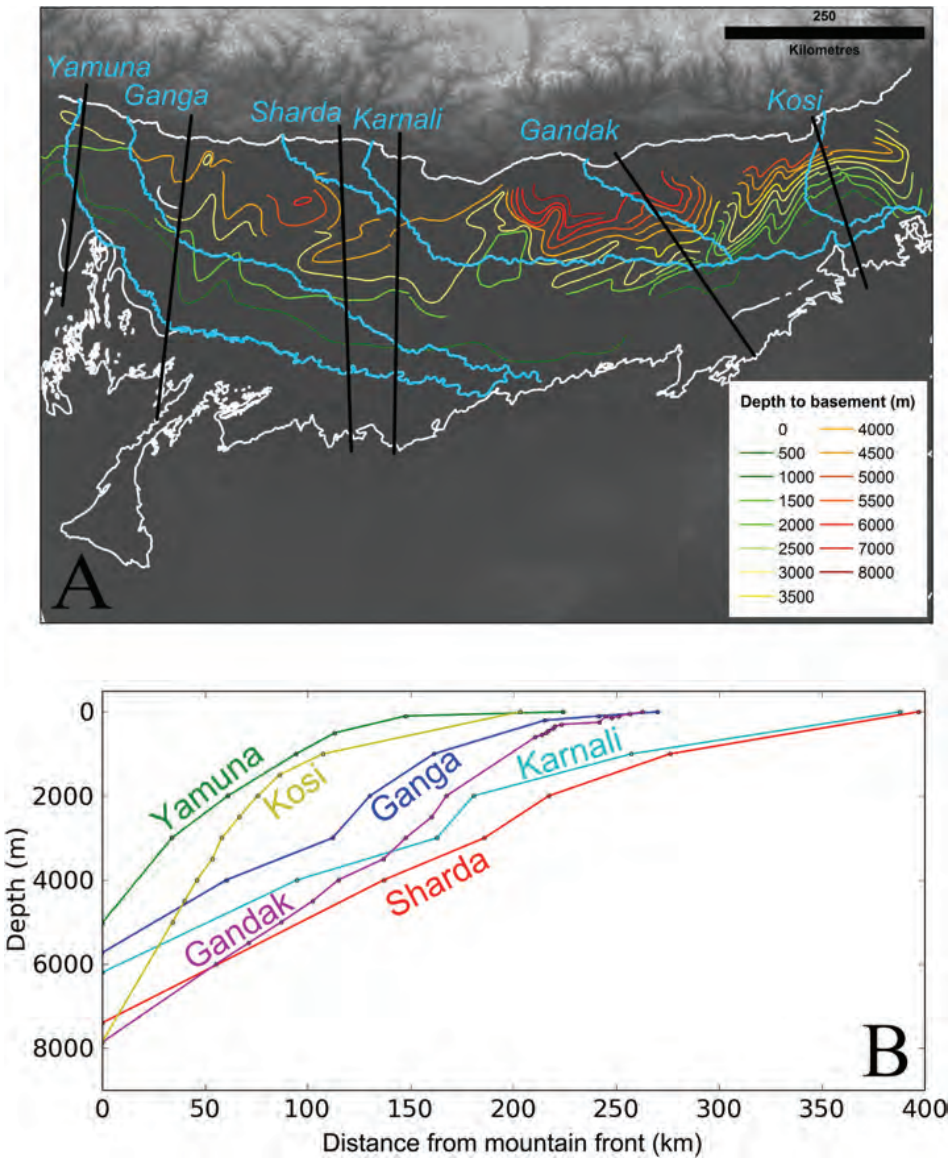

Fig. 5. (A) Depth to basement contours across the Ganga basin showing positions of basin cross sections (black line) for each river and (B) basin profiles constructed using depth to basement contours in proximity of the Yamuna, Ganga, Sharda, Karnali, Gandak and Kosi rivers. Data sources: 90 m SRTM DEM and Geological Survey of India.

to rounded gravel (clearly fluvial in origin). Gravel size variations were observed down the length of the gravel bars so sites were chosen in the centre of the coarsest fraction for consistency. At each site, 5 to 10 photos were taken of the channel bed to use for photo counting. Particle sizes were measured from each photo by overlaying a regular numeric square grid with 100 nodes, and measuring the intermediate *b*-axis of each pebble beneath the nodes (Attal and Lavé, 2006; Whittaker and others, 2011). Due to the coarse nature of much of the gravel bars, larger pebbles were often covered by multiple grid intersections. Consistent with the sampling method of Attal and others

(2015), pebbles covering n grid intersections were counted n times. This premise is based on Kellerhals and Bray's analysis (1971) using a voidless cube model, although it is noted that this method results in over estimation of D_{84} values (Attal and others, 2015). Results from each photo at a given site were combined to create a single grain size distribution at each sampling location.

Volumetric subsurface measurements were taken using techniques documented by a number of studies (Attal and Lavé, 2006; Whittaker and others, 2010; Dubille and Lavé, 2015). Surface material was first removed from the site location (to a depth equal to the size of the largest pebble) and 100 to 300 kg of material was excavated and sieved through a series of 1, 2 and 4 cm square mesh sieves. Pebbles larger than 8 cm were individually weighed, and the weight of each fraction was recorded. For pebbles with *b*-axis greater than 8 cm, a representative diameter was calculated by assuming that the pebble was roughly spherical and had a density of 2650 kg m^{-3} (Whittaker and others, 2010). A well-mixed representative sample of ~1 kg of the fraction < 1 cm was sieved using a 1 mm sieve, from which a ratio was calculated and applied to the whole <1 cm fraction.

The presence of boulders on some gravel bars meant that the recommendation that the largest clast represents < 5 percent of the sample mass was not always fulfilled (Church and others, 1987). For both surface and subsurface measurements, the effects of excessively large pebbles on D_{84} and D_{50} measurements was assessed using the same method outlined in Attal and others (2015). This process involves the removal of the largest clast from the distribution and recalculating the D_{84} and D_{50} values. This process was then repeated but with the addition of a large clast, similar in mass to the largest clast recorded within that sample. The recalculated D_{84} and D_{50} values with the removal or addition of the largest clast are plotted as upper and lower error bars on subsurface volumetric samples. Due to the large number of measurements obtained for each surface sample, following the same procedure on surface grain size distributions produced minimal variation (< 5%) in D_{84} and D_{50} values. Instead, a more conservative approach was taken, as outlined in Whittaker and others (2011), where an error margin of ±15 percent was applied to account for subjective bias when measuring the intermediate axis of each pebble beneath the grid node. This margin of 15 percent was estimated by Whittaker and others (2011) based on the differences in grain size distribution from repeat sampling of the same photo.

The position of the gravel-sand transition was also mapped for each river, by noting the point at which exposed deposits were near exclusively sand (> 95%). In some instances, small patches of gravels were present but represented a very small proportion (~1–5 %) of the bed fraction based on visual observations.

Downstream fining rates of the gravel fraction along each river were calculated using Sternberg's exponential function of the form:

$$D_x = D_0 e^{-\alpha x} \tag{6}$$

where D_0 is the predicted input or initial characteristic grain size in the system (such as D_{84}), α is the downstream fining exponent and x is the distance downstream (Sternberg, 1875). Linear functions have also been fitted to account for alternative fining patterns observed in the literature (Rice, 1999; Whittaker and others, 2011):

$$D_x = D_0 - \beta x \tag{7}$$

where β is the dimensionless fining rate (grain size reduction/km). The two key processes that are commonly seen to control downstream fining rates in fluvial systems are (1) the selective transport and deposition of particles and (2) abrasion of particles where larger particles are broken down by mechanical processes (Paola and others, 1992b, 1992a; Ferguson and others, 1996; Rice and Church, 2001; Attal and Lavé, 2006;

Fedele and Paola, 2007; Duller and others, 2010). The effect of pebble abrasion is considered negligible in this instance, as the lithology of gravel bars in all rivers was dominantly quartzite, suggesting that grain size fining by abrasion is likely to be similar across all systems. Any differences in grain size fining will likely reflect spatial variations in the grain size distribution of sediment delivered to the Plain from the Himalaya, sediment flux, the spatial distribution of basin subsidence, and local hydraulic and topographic effects (Paola and others, 1992a; Robinson and Slingerland, 1998; Fedele and Paola, 2007; Duller and others, 2010; Whittaker and others, 2011).

RESULTS

Topographic Analysis

Along the strike of the mountain front, results of the swath profile analysis are consistent with previous findings (Gibling and others, 2005; Sinha, 2005; Sinha and others, 2005) where the degree of channel entrenchment was found to increase from east to west (fig. 4). In the far west of the Ganga Plain, both the Yamuna and Ganga rivers are clearly entrenched within well-defined broad valleys that are incised into the surface of their respective alluvial fans. These incised valleys narrow with distance downstream of the mountain front from ~20 km to < 1 km at a point immediately upstream of the Ganga and Yamuna confluence at Allahabad (fig. 4B). Close to the mountain front, the valley sides are ~30 m high and reduce to 10 to 20 m by ~80 km downstream. Lateral incision into valley walls by large meander loops are clearly preserved in the lower half of the Ganga River. The Sharda and Karnali rivers converge at Mahsi, ~100 km downstream of the mountain front, to form the Karnali system which is also known as the Ghaghara River in India (fig. 4B). Both tributaries of the Karnali River flow down a well-defined incised valley up to 40 km in width. Downstream of the Sharda and Karnali confluence, the river course turns more sharply to the east and the incised valley loses definition as the degree of entrenchment into the fan surface is reduced. Much of the surrounding floodplain is of a comparable elevation (within 10 m) to the active channel here. Further east, the Gandak and Kosi rivers show minimal signs of entrenchment on the surface of their respective alluvial fans. Much of the surrounding floodplain is of a similar or lower elevation, most notably on the Kosi River (Chakraborty and others, 2010; Sinha and others, 2013; Sinha and others, 2014a).

The Kosi channel currently occupies the western margin of its alluvial fan where the channel bed is marginally elevated with respect to the surface of the central area of the fan. This pattern is most apparent in the upper ~80 km of the fan where much of the floodplain on the east bank is relatively lower in elevation, in some cases by up to nearly 10 m, than the active channel (fig. 4A). Whilst still within the RMSE of the DEM, this observation appears consistent with independent observations. In 2008 the Kosi River breached its eastern embankment at Kusaha, Nepal (Sinha and others, 2009; Chakraborty and others, 2010). Much of the avulsion belt occupied the depressed area identified as lower in elevation in the SRTM data that were captured several years earlier in 2000. For the remaining length of the fan, the Kosi channel sits at a very similar elevation to that of the fan surface.

This west to east gradient also extends beyond the Ganga Basin into the wider Indo Gangetic Plain. East of the Ganga Plain, tributaries of the Brahmaputra River appear similar in nature to the Gandak and Kosi rivers where channels are either at a similar elevation or marginally super-elevated relative to their surrounding floodplain (fig. 4C). Further west, rivers in the Indus basin show similar characteristics to those in the west Ganga Plain where active channels are laterally constrained in broad incised valleys (fig. 4A). Unlike the Ganga Plain however, these valleys widen with distance downstream and the degree of entrenchment appears lower at 10 to 20 m. This is

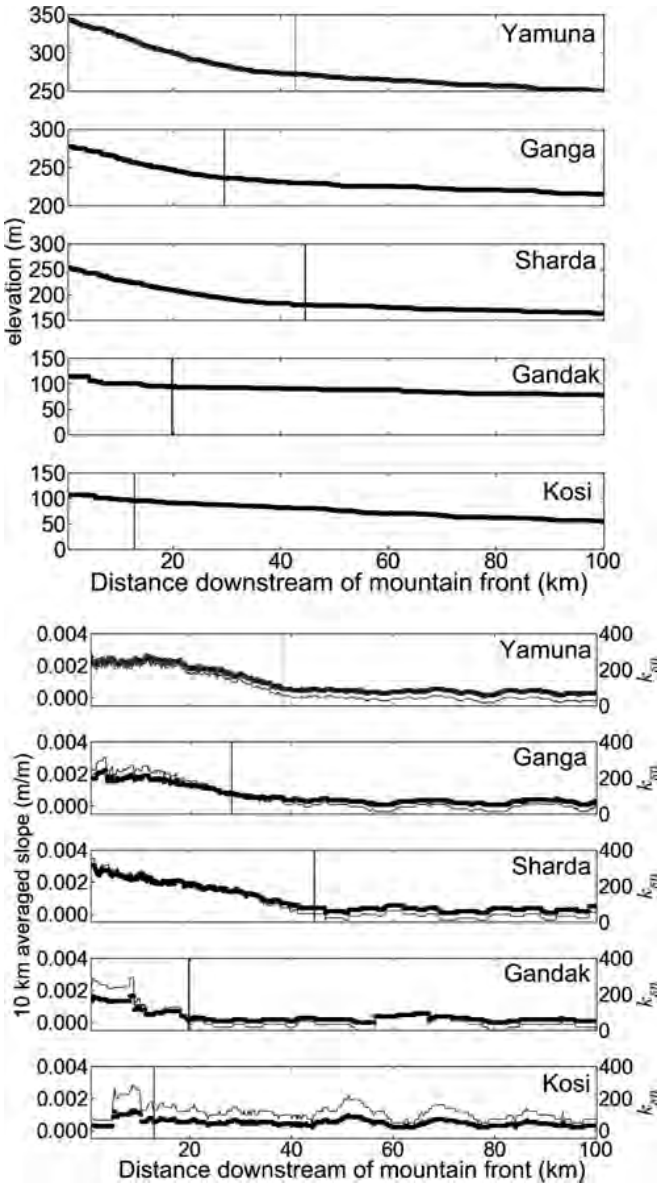

Fig. 6. Longitudinal profiles, 10 km averaged slope and normalized channel steepness (k_{sn}) values for major tributaries of the Ganga basin. k_{sn} values are shown by the thinner black line on the slope plots. Vertical lines represent the position of the mapped gravel-sand transition.

interpreted as a contrast in dominant controls on channel morphology between the Indus and Ganga basins.

Longitudinal river profiles and 10 km averaged slope values extracted from SRTM data show that the Yamuna, Sharda and Karnali rivers exhibit elevated slope values relative to rivers further east within the first 40 km downstream of the mountain front (fig. 6). The Ganga however appears to exit the mountain front with a marginally lower gradient than the other west and central Ganga Plain rivers. In the east Ganga Plain the Gandak and Kosi rivers are lower in gradient, with maximum values of ~0.0015 m/m

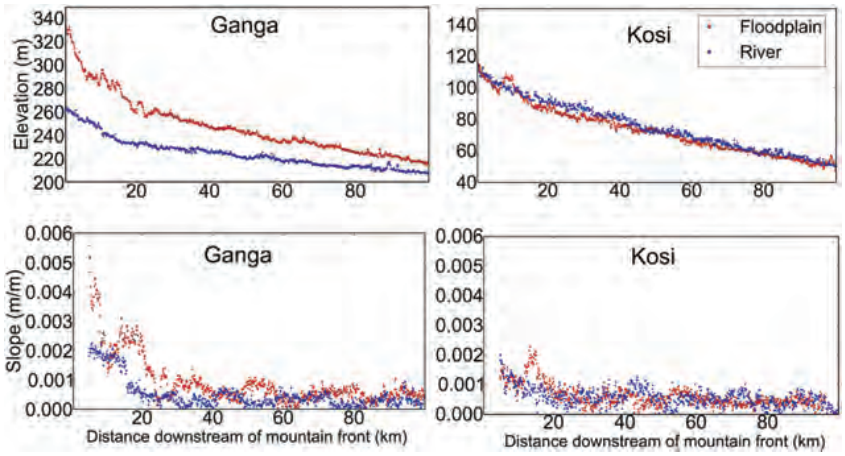

Fig. 7. Absolute elevation and 10 km averaged slope values of the modern Ganga and Kosi channels and their adjacent fan surfaces at the fan apex. Fan surface profiles followed transects that were broadly parallel to the channel, either from the top of the valley side where channels were entrenched or within ~5 km of the modern channel.

in the first 10 km, rapidly decreasing to ~0.0005 m/m by 20 km downstream of the mountain front. The Kosi maintains a more consistent and initially lower gradient down the length of its fan, attaining a maximum value of ~0.001 m/m. By 40 km downstream, all of the channel gradients converge at ~0.0005 m/m and fluctuate between 0 to 0.001 m/m for the remainder of the profile (fig. 5B). By normalizing channel gradient for upstream catchment area (k_{sn}), similar patterns are displayed where systems in the west and central Ganga Plain are typically steeper at the fan apex, with k_{sn} values of 200 to 300 (fig. 6). Whilst both 10 km averaged slope and k_{sn} values appear to be influenced by some noise along the first 10 km of the Gandak and Kosi profiles, k_{sn} values in the east Ganga Plain appear slightly lower (150–250). With the exception of noise in the Gandak profile, there were no evident knickpoints that were larger in magnitude than the RMSE (~15 m) of the data.

Comparing the average gradient of the Ganga and Kosi channels to their adjacent fan surfaces, we see that the Ganga fan surface is steeper than the active channel (fig. 7). This is more pronounced at the fan apex where the degree of channel entrenchment is also greatest. In contrast, the surface gradient of the Kosi fan is comparable to the gradient of the active channel, and an absence of significant channel entrenchment is also clearly highlighted.

Basin Subsidence

The depth to basement plots (fig. 5B) demonstrate an along strike variation in the geometry of the Ganga basin, as has also been recognized previously by Singh (1996). In the east Ganga Plain, the basin is deeper (5000–6000 m) and relatively narrow at ~200 km. The basement has a steep or even convex, distal edge. Further west, the basin widens beneath the Sharda and Karnali rivers. Generally, the basin is shallower here but there are isolated basement lows such as on the Sharda section where the basin reaches 6000 m near to the mountain front. In the far west, the basin is notably shallower at 3000 to 4000 m and again narrows to ~200 km wide. These variations in depth to basement at the mountain front broadly correlate with the variations in flexural rigidity of the downgoing lithosphere (Jordan and Watts, 2005), with lower rigidities correlating with greater basin depth at the mountain front.

Results indicate that the highest average subsidence velocities (V_{sub}) at the mountain front are located in the east of the region near the Kosi fan, with rates of 1.6±0.6 mm/yr. Further west average subsidence rates decrease to 1.4±0.4 mm/yr beneath the Gandak, 0.4±0.2 mm/yr beneath the Karnali, 0.8±0.2 mm/yr beneath the Ganga, and 0.3±0.4 mm/yr beneath the Yamuna. V_{sub} estimates are generally comparable across all but the Kosi and Gandak systems, which are notably higher. When these calculated subsidence estimates are compared to documented short term sedimentation rates across the Ganga Plain, values are comparable. An average sedimentation rate of ~0.08 (±0.19) mm/yr for the entire Ganga floodplain has been calculated from chemical mass balance equations (Lupker and others, 2011). Sedimentation rates would be expected to increase exponentially from the cratonic to orogenic margin of the basin however (Flemings and Jordan, 1989), which is consistent with sedimentation rates documented closer to the mountain front. Sedimentation rates of 0.62 to 1.45 mm/yr have been calculated from radiocarbon dating of organic material in northern Bihar upstream of the axial Ganga channel between the Kosi and Gandak rivers, averaged over a time period of 700 to 2500 yr (Sinha and others, 1996). The comparison of calculated long term subsidence rates of 1.6±0.6 mm/yr beneath the Kosi fan with the short term sedimentation rates of 0.62 to 1.45 mm/yr suggest the system is broadly in balance, with subsidence slightly outpacing sediment accumulation in this part of the basin.

Grain Size

Grain size distributions from sites closest to the mountain front have been compared across each of the sampled channels and are found to be comparable between systems (fig. 8). Subsurface grain sizes documented close to the mountain front on the Yamuna are generally finer than other sites, where a D_{84} value of 66 mm was recorded compared to values ranging between 146 to 248 mm for the Kosi, Sharda and Ganga. This is attributed to the upstream barrage near Faizabad (~3 km upstream). Compared to similar barrages located close to the mountain front on the Ganga, Sharda and Gandak rivers, a much larger proportion of flow is diverted into extensive canal networks at the Yamuna barrage, resulting in severely reduced flows downstream in the natural channel. During low flow conditions, parts of the Yamuna channel are entirely dry. It seems reasonable to interpret that a greater proportion of coarser material is trapped upstream or very close to the barrage, where there is insufficient discharge to rework or mobilise the coarsest fraction. The D_{84} of the subsurface Gandak sample was also found to be relatively fine (83 mm) compared to the Kosi, Sharda and Ganga samples, which is likely a function of the upstream Chitwan Dun. The coarse fraction of the sediment load is likely to be deposited at the upstream edge of the Dun, where bedrock channels emerge onto the low gradient alluvial surface of the Dun. This is consistent with grain size measurements taken within the Dun which show an overall fining and narrowing of the grain size distributions (fig. 9), where the main source of sediment into the channel is restricted to seasonal inputs by ephemeral channels draining the surface of piedmont alluvial fans comprised of Upper Siwalik Group conglomerates (Kimura, 1999; Densmore and others, 2016). Hillslope processes are largely absent in these piedmont catchments where the primary source of sediment is from recycled Siwalik deposits, resulting in a much narrower input grain size distribution into the main Gandak channel. Subsurface D_{84} and D_{50} values measured on the Gandak within the Chitwan Dun vary by ~50 mm, compared to values of 100 to 200 mm upstream of the Dun (fig. 9).

In general, there is a strong correlation between subsurface and surface grain size measurements in terms of relative change between values down each profile. Whilst there is a clear surface coarsening visible, local changes in subsurface grain size are also reflected in surface grain size measurements, adding confidence to this sampling

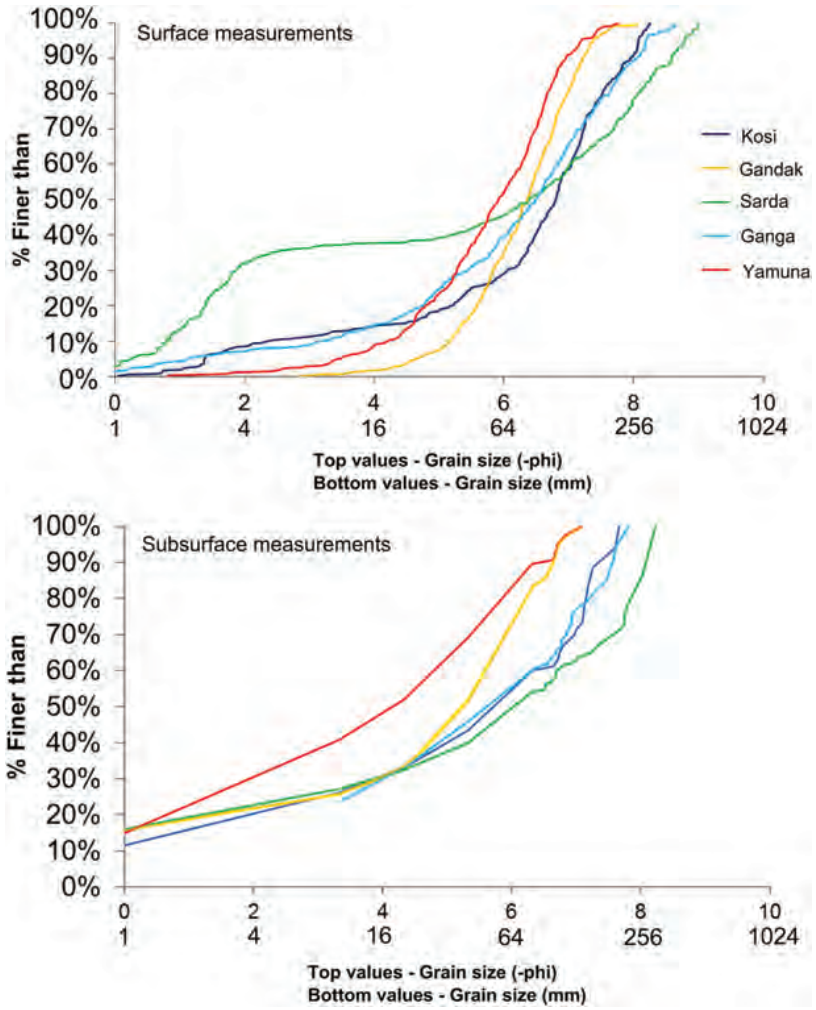

Fig. 8. Surface and subsurface grain size distributions of gravel bar sediment at the mountain outlet of each river.

approach. This trend is more apparent in the coarser (D_{84}) fraction of the sediment load (fig. 10). The position of the gravel-sand transition and downstream fining rates in each channel shows a considerable west to east variation (fig. 11), irrespective of the grain size distribution of the supplied sediment (fig. 8). The mapped position of the gravel-sand transition relative to the mountain front on each river suggests that gravel progrades further into the basin for rivers in the central and west Ganga Plain (fig. 11). For the Gandak and Kosi rivers in the east Ganga Plain, the gravel-sand transition was documented within 20 km downstream of the mountain front. The gravel-sand transition observed at the Yamuna, Ganga and Sharda rivers was notably further downstream at ~38, 28 and 45 km respectively. The gravel-sand transition was also not found to be an abrupt transition; in most instances a zone of ~2 to 5 km was noted where the bed was predominantly sand but large patches (up to 25% of the total bed fraction) of gravels were present, although these patches reduced in extent downstream. The position of the gravel-sand transition relative to long channel profiles (fig. 6) is

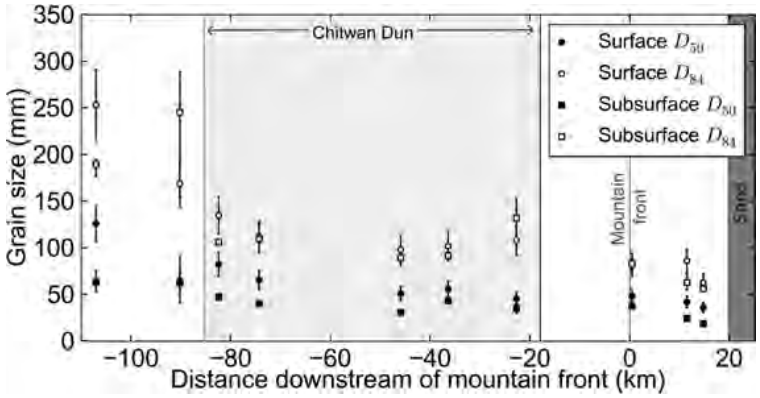

Fig. 9. D_{84} and D_{50} values along the Gandak River. A notable fining and overall narrowing of the grain size distribution is visible as the channel enters the Chitwan Dun, resulting in a much narrower grain size distribution being transported into the Ganga Plain.

coincident with a break in channel slope, where a steeper channel gradient exists upstream of the transition. This break in slope is less apparent in the east Ganga Plain on the Gandak and Kosi profiles, which may be explained by the noise in the DEM from which the long channel profiles were extracted. It seems more probable that any change in gradient associated with the gravel-sand transition is not as pronounced in the east Ganga Plain due to the gradients of these channels being lower overall. Upstream of the gravel-sand transition on the Sharda, Ganga and Yamuna, channel gradient and the absolute elevation of channels exiting the mountain front are also greater than for the Gandak and Kosi (fig. 12).

Fining rates were generally comparable across the Yamuna, Ganga and Sharda rivers (table 2 and fig. 13). For each site, r^2 values determined using each model were also near identical suggesting that the rate of exponential decay is very low (table 2). Using the linear decay model, fining rates of 1.31 to 4.75 mm/km were observed for D_{84} values across the Yamuna, Ganga, Sharda and Gandak channels whilst a rate of 10.5 mm/km was obtained for the Kosi (fig. 11). This same increase in fining rate is also apparent in the D_{50} fraction, where rates increase from 0.83 to 1.24 mm/km across systems in the west and central Plain, to 3.21 mm/km along the Kosi. Comparable spatial differences in fining exponents (α) obtained from the exponential model were

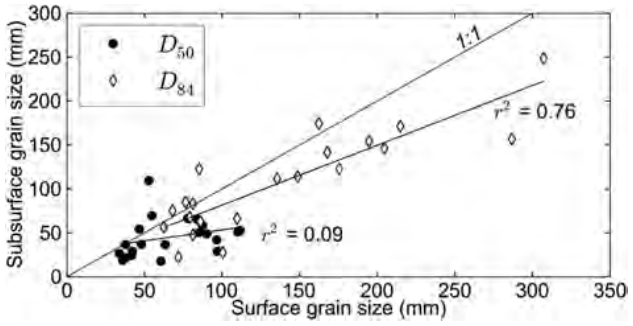

Fig. 10. Comparison of surface and subsurface measurements for the D_{84} (diamonds) and D_{50} (circles) values at each site across the Ganga Plain. There is a much stronger correlation between surface and subsurface values in the D_{84} values than D_{50}.

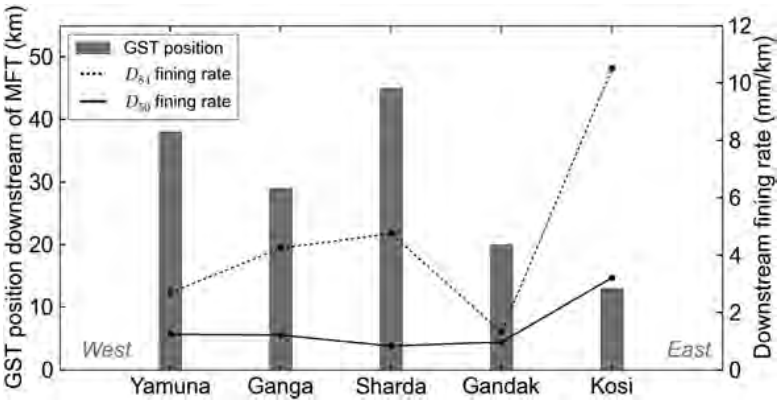

Fig. 11. Downstream distance from the mountain front (MFT) to the gravel-sand transition (GST) and linear model fining rates on averaged surface and subsurface D_{84} (dashed line) and D_{50} (solid line) grain sizes.

also found and are presented in figure 12. The relatively low fining exponent on the D_{84} fraction of the Gandak is likely to reflect upstream deposition of the coarsest fraction of the sediment load within the Chitwan Dun. As previously discussed, the grain size distribution exiting the Dun is much narrower (that is the D_{84} and D_{50} values are quite similar) on the Gandak relative to other systems (fig. 9). The D_{84} and D_{50} values are also lower than comparable sites at the mountain front in other systems.

DISCUSSION

Topographic analysis of the west Ganga Plain has highlighted the degree of channel entrenchment in the surface of the Yamuna and Ganga fans, compared to the relatively subdued surfaces of the Gandak and Kosi fans further east. Subsidence velocity estimates and downstream grain size fining rates have been found to be highest in the east Ganga Plain, where fan gradients are typically less steep and the gravel-sand transition is found closer to the mountain front. In the west Ganga Plain, the basement depth of the basin is notably lower than the east Ganga Plain, which when combined with known convergence velocities, suggests that the west Ganga Plain is subsiding less rapidly. Assuming basement gradient and convergence velocity yield a reasonable proxy for recent subsidence rates, then clear along strike variations in subsidence rate exist across the Ganga basin. These variations arise from differences in the elastic thickness of the underlying lithosphere (Lyon-Caen and Molnar, 1983, 1985; Jordan and Watts, 2005; Jackson and others, 2008) and/or local inherited morphological variations in the underthrust Indian basement (for example Lash, 1988) combined with varying convergent velocities. This is also consistent with published modeling results that have suggested the equivalent elastic thickness of the lithosphere is lower beneath the east Ganga Plain than the west (Jordan and Watts, 2005). This then raises the question of how, or whether, spatially variable subsidence can be expressed in the surface morphology of the Ganga Plain.

What Are the Timescales of the Controlling Processes?

Various modeling studies have suggested that the relative impact of increased and decreased subsidence rates, sediment flux, water supply and gravel fraction on basin stratigraphy/response is strongly dependent on the timescale over which these variations occur (for example Paola and others, 1992a; Heller and Paola, 1996; Duller and

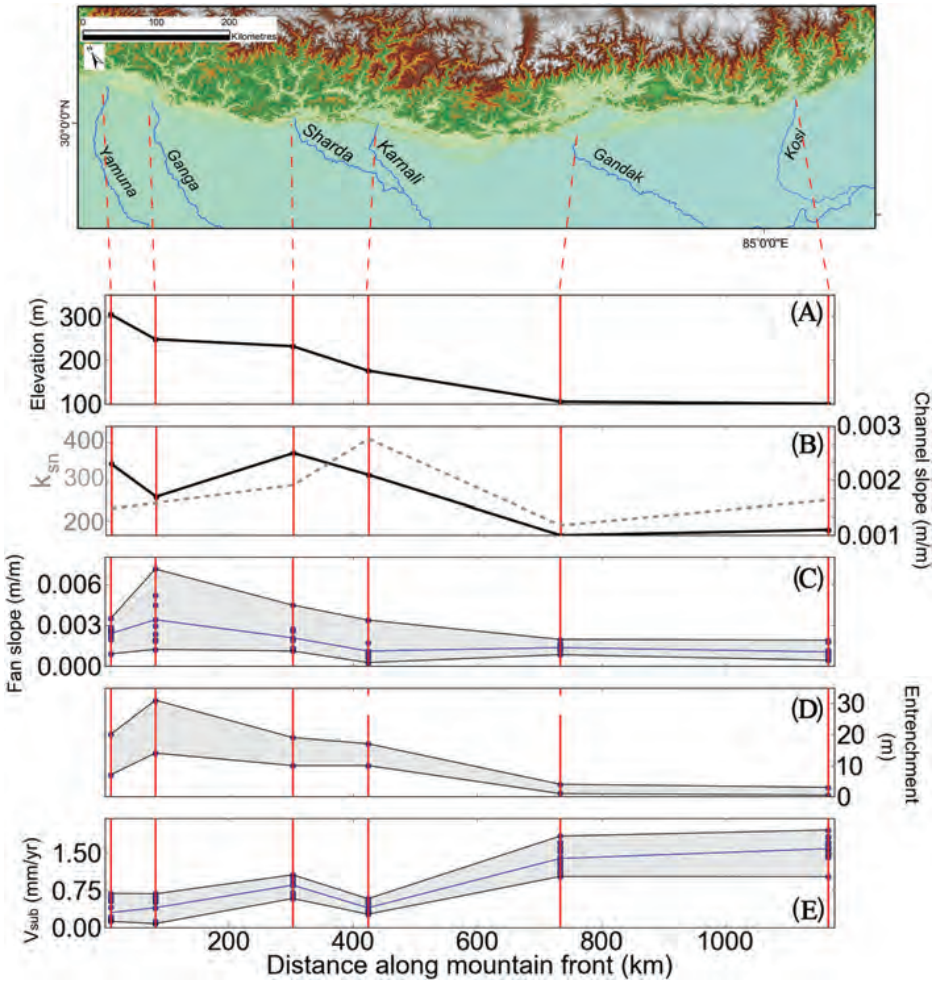

Fig. 12. Lateral variations in (A) outlet elevation, (B) 10 km average channel gradient and normalized channel steepness (k_{sn}) at fan apex and (C) proximal fan apex slopes, (D) channel entrenchment at the fan apex and (E) calculated subsidence velocity (V_{sub}) beneath the proximal foreland basin across the Ganga Plain.

others, 2010). To determine whether a forcing is slow or rapid, an equilibrium response time (T_{eq}) is calculated using the square of the basin length divided by the basin diffusivity (Paola and others, 1992a). For the Himalayan foreland basin, a T_{eq} of 2 Myr (±1 Myr) has been calculated (Heller and Paola, 1992). Variations in parameters that occur over a timescale lower than T_{eq} are subsequently termed as rapid, and those higher than T_{eq} as slow. Along strike of the orogen, variations in the position of the gravel-sand transition on the Yamuna, Ganga, Sharda, Gandak and Kosi rivers are consistent with long term (>1 Myr) patterns of subsidence across the basin where lower subsidence rates in the west result in a more distal gravel-sand transition than regions experiencing higher rates of subsidence in the east Ganga Plain, where a greater proportion of sediment is trapped in the proximal part of the basin due to a greater volume of accommodation being generated (Paola and others, 1992; Marr and others, 2000).

Table 2

D_{50} and D_{84} grain size fining rate data using both exponential and linear equations

River	Exponential fit				Linear fit			
	$D_{84}\ \alpha$ (km^{-1})	r^2	$D_{50}\ \alpha$ (km^{-1})	r^2	$D_{84}\ \beta$ (mm/km)	r^2	$D_{50}\ \beta$ (mm/km)	r^2
Yamuna	0.024	0.53	0.025	0.31	2.69	0.54	1.24	0.40
Ganga	0.032	0.81	0.022	0.20	4.24	0.80	1.21	0.15
Sharda	0.033	0.59	0.016	0.19	4.75	0.57	0.83	0.22
Gandak	0.019	0.52	0.031	0.36	1.31	0.50	0.97	0.38
Kosi	0.062	0.37	0.052	0.18	10.5	0.36	3.21	0.18

What Are the Spatial Characteristics of the Controlling Processes?

Previous works have also suggested that conditions imposed by local subsidence rates could modulate the gradient of large alluvial fan surfaces over millennial timescales (Allen P.A. and others, 2013). Longitudinal profiles of the Gandak, Sharda, Ganga and Yamuna rivers reveal a distinct break in slope at the gravel-sand transition (fig. 6). The transport coefficients of sand and gravel differ by a factor of ~10 (Marr and others, 2000) which, in combination with bed slope, determine the total flux of sediment at a point on the fluvial surface:

$$q_s(x,t) = -v\frac{\delta z(x,t)}{\delta x} \tag{8}$$

where q_s is sediment flux, v is the transport coefficient and z is the surface elevation. The transport coefficients of gravel and sand (v) are reported as 0.01 and 0.1 $km^2\,yr^{-1}$, respectively. These transport coefficient values incorporate a number of independently known or quantifiable variables including water discharge, Shields stress, dimensionless sediment flux and sediment porosity (Marr and others, 2000). At the gravel-sand transition, an increase in transport coefficient associated with a change from a gravel-bed to sand-bed river may occur; however, the associated reduction in channel slope would also be expected to reduce sediment flux along the profile. Analogue modeling of gravel bed channels has also suggested that a reduction in both total sediment flux and grain size, as a result of upstream deposition, will reduce the required transport capacity of the channel downstream. The progressively finer and smaller sediment load could therefore remain in transport within a channel with a lower gradient (Paola and others, 1992b). This is consistent with our observations across the Ganga Plain, where a relatively distinct change in channel slope is associated with the gravel-sand transition (fig. 5B). Interestingly, the positions of the gravel-sand transitions on the Gandak and Kosi rivers are directly comparable to those observed in smaller foothill or 'Piedmont' rivers (~8 – 20 km downstream of the mountain front). The catchment area of these Piedmont rivers ranges from ~25 to 350 km^2 (Dubille and Lavé, 2015) whilst the Gandak and Kosi catchment areas are an order of magnitude larger at ~31,000 km^2 and ~50,000 km^2, respectively (table 3). The gravel-sand transition on the Gandak, which lies ~100 km west of the foothill systems considered by Dubille and Lavé (2015), was noted at ~20 km. The transition on the Kosi, which lies ~100 km east of their study area, was noted at ~13 km. This suggests that the distance that gravel progrades out from the mountain front is not strongly dependent on upstream catchment area, and therefore unlikely to be dependent on absolute sediment flux, given the dramatically different catchment areas of the foothill and mountain catchments. However, the abrupt change in slope associated with the

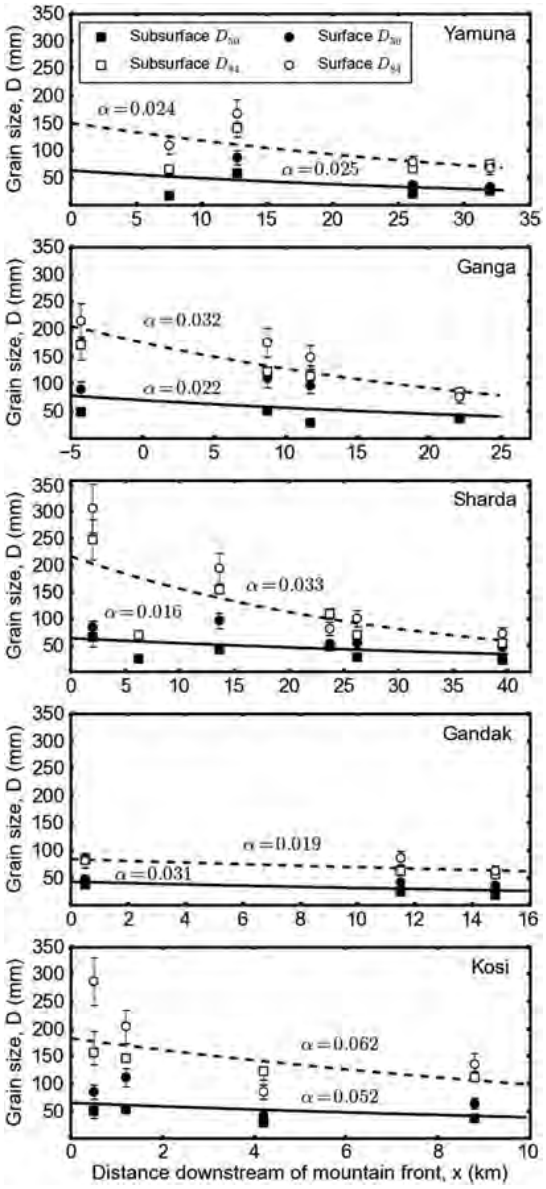

Fig. 13. Evolution of sediment grain size on gravel bars. Downstream fining exponents (α) for surface and subsurface averaged D_{84} and D_{50} values downstream of the mountain front for the Yamuna, Ganga, Sharda, Gandak and Kosi rivers. Error bars were calculated for surface samples by applying a ±15% error margin to account for subjective bias. Error margins on subsurface samples reflect the effects of the addition and removal of large clasts from the sample on D_{84} and D_{50} measurements. It should be noted that the scale of the horizontal axis is changing between plots.

gravel-sand transition is not a constant feature across these smaller Piedmont rivers. A less abrupt change in channel slope associated with the gravel-sand transition was observed in a number of smaller foothill-fed systems draining the Gandak-Kosi interfan area (Dubille and Lavé, 2015). In this instance, the subdued break in slope was attributed to the relative high proportion of sand relative to gravel transported by the

Table 3

Catchment and grain size sample summary information

	Catchment area (km^2)	Grain size sample location (UTM)			D_{84} (phi units)		D_{50} (phi units)		Distance downstream of MFT (km)	Slope (m/m)
					Surface	Subsurface	Surface	Subsurface		
Yamuna	9,419	43R	746512	3353763	6.78	6.05	5.92	4.15	7.5	0.00212
		43R	734615	3337112	7.39	7.14	6.45	5.88	12.7	0.00240
		43R	738113	3340361	6.31	6.08	5.24	4.41	26.1	0.00180
		43R	743686	3350341	6.09	6.24	5.08	4.72	32.0	0.00123
		43R	730761	3334533	GST	GST	GST	GST	38.1	0.00066
Ganga	19,666	44R	237430	3327606	7.75	7.42	6.49	5.62	-4.3	0.00177
		44R	226118	3311830	7.46	6.94	6.78	5.67	8.7	0.00192
		44R	226950	3308723	7.22	6.83	6.60	4.85	11.7	0.00189
		44R	227127	3298543	6.26	6.41	5.24	5.19	22.1	0.00122
		44R	228600	3293808	GST	GST	GST	GST	28.2	0.00084
Sharda	13,182	44R	416513	3219623	8.26	7.96	6.39	7.03	2	0.00252
		44R	414750	3216389	-	6.12	-	4.63	6.2	0.00237
		44R	412283	3210500	7.61	7.27	6.59	5.39	13.6	0.00191
		44R	413532	3201761	6.35	6.77	5.72	5.57	23.7	0.00170
		44R	413564	3199562	6.65	5.86	5.78	4.79	26.2	0.00161
		44R	413059	3187971	6.17	4.55	5.55	4.48	39.5	0.00068
		44R	414630	3183209	GST	GST	GST	GST	44.5	0.00040
Gandak	31,460	44R	790722	3041214	6.35	6.37	6.37	5.21	0	0.00134
		44R	782608	3035567	6.43	5.97	5.97	4.61	11.5	0.00080
		44R	781464	3032900	5.97	5.81	5.81	4.22	14.8	0.00079
		44R	782154	3028042	GST	GST	GST	GST	19.8	0.00020
Kosi	50,079	45R	514824	2969129	8.16	7.29	6.41	5.65	0	0.00031
		45R	514304	2968166	7.68	7.19	6.80	5.72	1.2	0.00030
		45R	515151	2965578	6.41	6.94	5.40	4.85	4.2	0.00029
		45R	512280	2962778	7.08	6.80	5.99	5.19	8.8	0.00126
		45R	511857	2958589	GST	GST	GST	GST	12.9	0.00057

channel at the mountain outlet, where a steep channel gradient was still needed to transport the large proportion of sand downstream of the transition. Where coarse gravels or conglomerate made up less than ~30 percent of the sediment load, no apparent break in slope was observed at the transition. Whether this same relationship scales up to the larger mountain fed systems has not been examined in detail.

The most dominant cause of a rapid reduction in grain size associated with the gravel-sand transition in aggrading systems has been attributed to selective sorting (for example Paola and others, 1992b; Ferguson and others, 1996), where downstream fining by selective sorting is enhanced by bedload sedimentation (Rice, 1999; Dubille and Lavé, 2015). Poorly sorted gravel mixtures and bimodal gravel inputs have been modeled to yield similar fining characteristics (Paola and others, 1992b), suggesting that rapid fining by selective deposition at the gravel-sand transition is insensitive to input sediment grain size distributions. Our current understanding of sediment flux to the Ganga basin is based on a synthesis of published fluxes calculated from ^{10}Be concentrations measured in modern river sediments (table 1). The variability within these data do not allow any robust conclusions to be drawn regarding spatial variations in the long-term sediment supply rate from the Himalayan catchments to the Ganga basin. A more thorough understanding in the observed variability in these ^{10}Be concentrations should be a target of future studies to better understand the role of sediment flux on these systems. Spatial variations in discharge from the Ganga catchment into the Plain could also contribute to the observed morphological signal. Whilst comparable discharge data are not available across these systems, the upstream catchment area of these systems yields an appropriate substitute, where numerous studies have shown a close correlation between these two variables (for example Knighton, 1998). In general, where larger catchment areas are observed in the east, larger discharges would also be expected (table 3) which is consistent with gauged measurements where available (Sinha and others, 2005). Annual precipitation estimates from the Tropical Rainfall Measuring Mission (TRMM) between 1998–2001 across the Himalaya have further suggested that precipitation is typically higher in catchments feeding into the east Ganga Plain (Anders and others, 2006). Interestingly, for a given sediment supply, increased rates of water supply have been modelled to correspond with advancing gravel fronts (Paola and others, 1992a). This doesn't appear to be a factor in the Ganga system where catchment area (and presumably discharge) are greatest in the east Ganga Plain, and the gravel-sand transition is found in its most proximal position. Given that it appears that the position of the gravel-sand transition is independent of variations in input grain size distributions, upstream catchment area and sediment flux, it is suggested that longer term patterns of subsidence rate are a governing control on the grain size transition in the modern Ganga Plain.

Where gravels prograde farthest downstream in the rivers of the central and west Ganga Plain, channel gradients are found to be steeper close to the mountain front. In the east Ganga Plain, lower channel gradients are observed upstream of the gravel-sand transition, where the relative change in channel gradient across the gravel-sand transition is also less pronounced. Channel gradient measurements derived from SRTM DEM elevations (fig. 6) are not of sufficient spatial resolution or quality to compare with grain size measurements obtained as part of this study. However, given the lack of obvious pattern in grain size distributions measured at the mountain front (fig. 8) and relatively subtle changes in channel gradient at the gravel-sand transition identified in the east Ganga Plain compared to the west (fig. 6), it seems improbable that differences in grain size can account for the along strike variations in channel gradient and grain size fining rates. Other possible interpretations of the variation in channel gradient are that profiles in the east experience higher subsidence rates at the

mountain front, resulting in the gravel-sand transition being closer to the mountain front. Late Holocene sedimentation rates of 0.62 to 1.45 mm/yr (Sinha and others, 1996) on the Ganga Plain are comparable or slightly lower than subsidence velocity estimates beneath the Kosi and Gandak Rivers of 1.6 ± 0.6 and 1.4 ± 0.4 mm/yr, respectively. Comparable information of sedimentation rates in the west Ganga Plain are not available. Alternatively, if there has been greater sediment flux in the west, then the channel may have experienced a greater degree of backfilling. Without evidence for the latter, we suggest higher differential subsidence in the east Ganga Plain as the most probable mechanism. Relative differences in fining exponents of the gravel fraction downstream of the mountain front are consistent with along strike variations in subsidence, where gravels in the Kosi River have a fining exponent two to three times greater than systems in the west Ganga Plain (fig. 13). Whilst the Gandak River has a relatively high subsidence velocity estimate, this same pattern in fining exponent is not as apparent and has been attributed to the buffering role of the upstream Chitwan Dun. Based on these observations, we interpret that spatial variations in subsidence rates play a controlling role in along strike variations in the longitudinal profiles of these rivers and grain size fining rates. However, spatially variable subsidence rates alone do not explain the entrenchment of the western rivers.

Climate and Signal Preservation

Top down changes in sediment and water discharges must have also influenced these systems (Sinha and others, 2005; Wobus and others, 2010). The seasonal nature of water and sediment delivery to the Ganga Plain is highly sensitive to variations in the strength of the Indian summer monsoon during which ~80 percent of the annual flow is discharged. From marine isotope stage 3 into the Last Glacial Maximum (LGM), a combination of low insolation and strong glacial conditions are thought to have significantly weakened the Indian summer monsoon and regional precipitation (Goodbred Jr., 2003; Gibling and others, 2005). This is also reflected in much lower runoff values interpreted from proxy records of palaeosalinity and $\delta^{18}O$ in the Bay of Bengal during the LGM (Cullen, 1981; Duplessy, 1982). Following the LGM, a variety of proxy records have suggested there was a widespread increase in precipitation, particularly after ~12 ka (Cullen, 1981; Goodbred Jr., 2003; Srivastava and others, 2003). How fluvial systems react to these climate driven variations in water and sediment discharges is more difficult to predict as both incision and aggradation can occur simultaneously within a catchment in response to a single perturbation (Tucker and Slingerland, 1997).

Numerous studies have examined the relationship between climatic transitions and phases of fluvial incision and aggradation (for example Tucker and Slingerland, 1997; Goodbred Jr., 2003; Gibling and others, 2005; Srivastava and others, 2008; Wobus and others, 2010; Duller and others, 2012; Densmore and others, 2016). Modeling results from Marr and others (2000) have suggested that a rapid increase (over timescales shorter than T_{eq}) in water flux and/or decrease in sediment flux can result in proximal erosion of gravel and advance of the gravel-sand transition. Rapid increases in sediment flux were also found to initiate an increase in proximal channel gradient and retreat of the gravel front (Marr and others, 2000). However, considerable variability in the geomorphic response generated by increased runoff intensity has also been modeled by Tucker and Slingerland (1997) using a physically based model of drainage basin evolution (GOLEM); significant variations in sediment flux were found to result from relatively modest variations in surface runoff, highlighting the difficulty in correlating a specific cause (climatic condition) to effect (geomorphic response). There are also complexities regarding how climatically driven waves of incision and aggradation are propagated downstream of the Himalaya into the Ganga Plain. The effects of stochastic forcing on sediment supply to channel networks has been

considered in previous studies (Benda and Dunne, 1997a, 1997b), where the intermittent storage and release of sediment within a catchment has been modeled to dramatically alter the sediment mass balance over thousand year time scales (Blöthe and Korup, 2013). Using both modeling outputs and circumstantial field evidence, unsteady sediment supply was found to affect channel morphology through the generation of sediment waves and transient phases of aggradation (Benda and Dunne, 1997b). If sediment transport through the catchment acts as a non-linear filter and buffers climatic signals (Jerolmack and Paola, 2010; Blöthe and Korup, 2013), it raises the question of what magnitude and wavelength of climatic forcing is capable of being recorded in the sedimentary record of the Ganga Plain?

Thermo-luminescence dating of quartz sands and radiocarbon dating on shell and calcrete materials preserved in the upper 2 to 8 m on the Ganga-Yamuna interfluve yield ages between 6 to 21 ka (summarized in Srivastava and others, 2003); these ages suggest that this was when the modern Ganga and Yamuna channels were last connected to the interfluve floodplain surface (Srivastava and others, 2003; Gibling and others, 2005). Such a situation is consistent with climatic fluctuations associated with the end of the LGM and subsequent strengthening of the Indian summer monsoon at ~11 to 7 ka (Goodbred Jr., 2003), which could have initiated widespread incision of channels into their respective mega-fans across the Ganga Plain. A corresponding increase in sediment delivery to the Bengal basin was also noted between ~11 to 7 ka, which translates to a mean sediment load of more than double current load estimates derived from late Holocene deposits in the basin (Goodbred and Kuehl, 2000). Estimates for sediment remobilisation during the early Holocene by incision across the Plain only account for ~2 to 25 percent of the total volume of sediment deposited into the basin during this period, suggesting that sediment flux exported from the Himalaya must have been considerably elevated (Goodbred Jr., 2003). Crucially, these observations in the Bengal basin imply that a wide scale climatic perturbation was rapidly propagated down the full length of the Ganga system. Whether this signal was locally amplified by reworking of vast deposits of stored sediment within the Himalaya (for example Blöthe and Korup, 2013) is unknown.

A downstream reduction in valley width and channel entrenchment identified on the Yamuna, Ganga and Karnali systems is consistent with a top down wave of incision, most likely initiated by a climate-induced increase in water or relative decrease in sediment discharges during the early Holocene (Tucker and Slingerland, 1997; Goodbred and Kuehl, 2000; Goodbred Jr., 2003; Wobus and others, 2010). However, this signal is not apparent in the east Ganga Plain where channels show minimal signs of entrenchment. Whilst some aggradation is thought to have occurred during the late Holocene, these rates are not thought to have been sufficient to infill earlier valley incision (Goodbred Jr., 2003). It therefore seems unlikely that the east Ganga Plain underwent any significant phase of incision, such as that experienced in the west Ganga Plain. This is consistent with well data drilled from the Kosi mega-fan (Singh and others, 1993) that suggested that the Kosi River has maintained a relatively mobile braided channel throughout the Holocene, which migrated across much of the surface of the mega-fan depositing a gravelly sand to fine sand unit.

Subsidence vs. Climate

The Kosi exhibits low channel and fan gradients, flows over the most rapidly subsiding portion of the basin and displays the highest sediment grain size fining rate. Where subsidence rates are higher, proximal vertical sedimentation rates would also be expected to be higher. This results in a smaller amount of sediment remaining in transport further downstream than for a comparable sediment flux in a system experiencing a slower rate of subsidence. The equilibrium gradient of the channel would therefore be expected to be lower where subsidence rates are higher and/or

where a greater proportion of the total sediment load is trapped in the proximal basin, as a channel with a lower gradient should be able to convey the smaller sediment load (Robinson and Slingerland, 1998). We hypothesize that patterns of incision and aggradation on this timescale reflect differences in the sensitivity of these systems to climatic forcing of sediment and water flux (Q_s and Q_w respectively), such as that experienced during the early Holocene in response to increased strength of the Indian summer monsoon between ~11 to 7 ka at the end of the LGM. The sensitivity of these systems to changes in Q_s and Q_w is dependent on the gradient of the equilibrium channel under the new Q_s and Q_w values relative to the subsidence controlled gradient of the wider fan surface, assuming that the channel was not originally entrenched. If the revised equilibrium channel gradient is lower than the original gradient of the alluvial fan, the channel will incise into the surface of the fan apex until a lower channel gradient is attained, producing an incised channel. For a constant climatic forcing of channel lowering along the strike of the Ganga Plain, incision will only occur where channel lowering rates outpace subsidence which will inherently be more difficult to achieve where subsidence rates are higher in the east Ganga Plain (fig. 14).

Based on upstream catchment areas and satellite-derived precipitation data, it seems likely that systems in the east Ganga Plain experience higher discharges than those further west. Discharge may play a key role in shaping the wider fan morphology, but the position of the modern gravel-sand transition is not consistent with these spatial variations in precipitation or possible variations in sediment flux, which could be related. Lower channel gradients in the east could reflect these higher water discharges (van den Berg, 1995; Knighton, 1998), but would fail to explain the triggering mechanism behind fan entrenchment in the west Ganga Plain. However, the proximal position of the gravel-sand transition and low channel gradients observed on the Kosi are consistent with the model results simulated under increased basin subsidence rates (over timescales greater than T_{eq}).

Whilst absolute sediment fluxes to the basins are uncertain, approximately 90 percent of the total flux is thought to bypass the basin (Lupker and others, 2011) which would suggest that sediment availability does not limit these systems. Again, the proximal position of the gravel-sand transition relative to the mountain front further suggests that the majority of this bypassed sediment is likely to be transported in suspension. Spatial variations in the amount of coarse bedload exported into the Plain, and deposited upstream of the gravel-sand transition, is unknown. Whilst beyond the scope of this study, this does appear to be a potential factor that could directly influence the morphology of these systems, as the entirety of this coarser sediment fraction is retained within the Plain. Further work is needed to better constrain the relative proportions of suspended load and bedload within the total sediment fluxes of these systems. The long term morphology of rivers in the east Ganga Plain appears to be primarily controlled by the relatively higher subsidence rates experienced in the eastern end of the basin. Furthermore, these systems appear to have been insensitive to wide scale changes in regional climate, such as that experienced at the end of the LGM, which initiated wide-spread incision in the west Ganga Plain.

CONCLUSIONS

A modified swath profile analysis has been applied to topographic data across much of the Himalayan foreland basin to characterize the broad nature of incision and aggradation over much of the Indo-Gangetic Plains. In general, we find that the degree of channel entrenchment increases from east to west across the Ganga Plain, and also decreases with distance downstream. First-order subsidence velocity estimates suggest a more rapidly subsiding basin in the east Ganga Plain with rates of up to 1.6 ± 0.6 mm/yr. Further west, subsidence velocity estimates decrease to as little as 0.3 ± 0.4

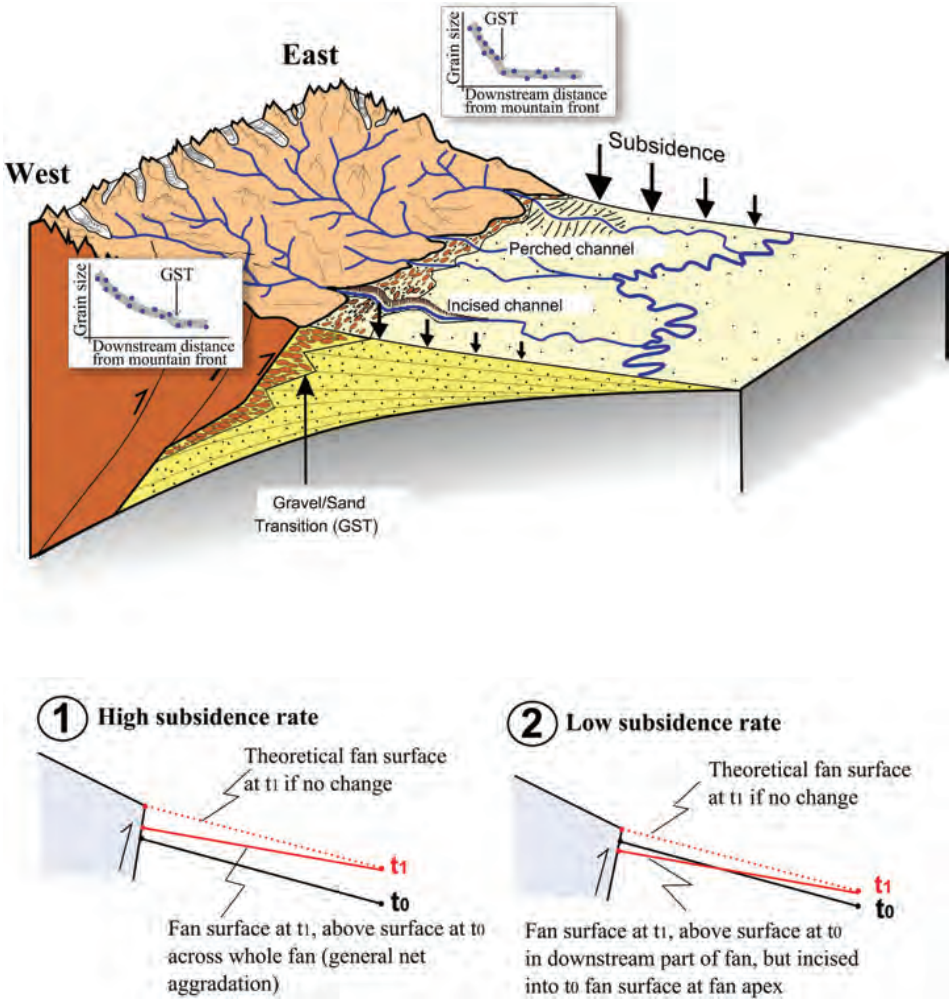

Fig. 14. Cartoon illustrating the role of variable subsidence rate on surface morphology across the Ganga Plain, in response to climate-driven variations in water and sediment discharge. The relative lowering of the surface between time steps t_0 (black line) and t_1 (red dashed line) is equivalent to a fall in base level, where the gradient of the fan surface is similar between surfaces. The rate of base level fall is controlled by subsidence in these scenarios where it is assumed invariant between the two time steps. A change in external forcing (sediment flux, discharge) leads to an adjustment (reduction in this instance) of the fan slope between t_0 and t_1 (red solid line), which can be accommodated with net aggradation where subsidence rates are high (1) but requires vertical incision into the fan apex where subsidence rates are lower (2).

mm/yr. Grain size fining rates are also found to closely reflect these patterns of subsidence, with the highest fining rates observed in the east Ganga Plain and lowest in the west. Furthermore, data currently available does not support a strong west to east variation in sediment flux at the thousand year timescale. Assuming that ~90 percent of sediment delivered into the foreland basin is bypassed downstream, it also seems more likely that the relative fraction of bedload delivered to the basin, which is trapped upstream of the gravel-sand transition, may have a more direct role on channel morphology than the total sediment flux. We propose that higher subsidence rates are responsible for a deeper basin in the east with perched, low gradient river channels that are relatively insensitive to climatically driven changes in base-level. In contrast,

the lower subsidence rates in the west are associated with a higher elevation basin topography, and entrenched river channels recording climatically induced lowering of river base-levels during the Holocene.

ACKNOWLEDGMENTS

We thank Ananta Gajurel, Jamie Stewart, Fred Bowyer, Konark Maheswari, Debojyoti Basuroy, Arkaprabha Sarkar, Bhairab Sitaula and Apex Adventure, and the Nepalese Department of Mines and Geology for their endless help, organisation and logistical support in the field. We are also grateful to the International Association of Sedimentologists, British Society for Geomorphology and the Edinburgh University Club of Toronto for their financial support of the fieldwork. Much of the motivation for this study originated from discussions with Prof. S. J. Tandon and Prof. R. Sinha while at a Royal Society/DST funded conference in Dehra Dun, India. This study formed part of a Natural Environment Research Council (NERC) funded Ph. D. (NE/L501566/1). We are grateful to reviewers Brian Dade and Paul Heller, and Associate Editor Sean Willett for valuable comments that helped modify the manuscript. Sadly, Paul Heller died unexpectedly before publication, and so this is likely to have been one of his last journal reviews. As a fervent advocate of integrating process sedimentology and basin analysis, and as someone with an ever-questioning mind, we would like to dedicate this contribution to his memory.

REFERENCES

Allen, G. H., Barnes, J. B., Pavelsky, T. M., and Kirby, E., 2013, Lithologic and tectonic controls on bedrock channel form at the northwest Himalayan front: Journal of Geophysical Research Earth Surface, v. 118, n. 3, p. 1806–1825, http://dx.doi.org/10.1002/jgrf.20113

Allen, P. A., and Allen, J. R., 2013, Basin Analysis: Principles and Application to Petroleum Play Assessment: West Sussex, England, John Wiley & Sons, 642 p.

Allen, P. A., Armitage, J. J., Carter, A., Duller, R. A., Michael, N. A., Sinclair, H. D., Whitchurch, A. L., and Whittaker, A. C., 2013, The Qs problem: Sediment volumetric balance of proximal foreland basin systems: Sedimentology, v. 60, n. 1, p. 102–130, http://dx.doi.org/10.1111/sed.12015

Amans, O., Beiping, W., and Ziggah, Y., 2013, Assessing vertical accuracy of SRTM Ver 4.1 and ASTER GDEM Ver 2 using differential GPS measurements- case study in Ondo State Nigeria: International Journal of Scientific & Engineering Research, v. 4, n. 12, p. 523–531.

Andermann, C., Crave, A., Gloaguen, R., Davy, P., and Bonnet, S., 2012, Connecting source and transport: Suspended sediments in the Nepal Himalayas: Earth and Planetary Science Letters, v. 351–352, p.158–170, http://dx.doi.org/10.1016/j.epsl.2012.06.059

Anders, A. M., Roe, G. H., Hallet, B., Montgomery, D. R., Finnegan, N. J., and Putkonen, J., 2006, Spatial patterns of precipitation and topography in the Himalaya: Geological Society of America Special Paper, v. 398, p. 39–53, http://dx.doi.org/10.1130/2006.2398(03)

Attal, M., and Lavé, J., 2006, Changes of bedload characteristics along the Marsyandi River (central Nepal): Implications for understanding hillslope sediment supply, sediment load evolution along fluvial networks, and denudation in active orogenic belts, *in* Tectonics, Climate and Landscape Evolution: Geological Society of America Special Paper, v. 398, p. 143–171, http://dx.doi.org/10.1130/2006.2398(09)

Attal, M., Mudd, S. M., Hurst, M. D., Weinman, B., Yoo, K., and Naylor, M., 2015, Impact of change in erosion rate and landscape steepness on hillslope and fluvial sediments grain size in the Feather River basin (Sierra Nevada, California): Earth Surface Dynamics, v. 3, p. 201–222, http://dx.doi.org/10.5194/esurf-3-201-2015

Benda, L., and Dunne, T., 1997a, Stochastic forcing of sediment supply to channel networks from landsliding and debris flow: Water Resources Research, v. 33, n. 12, p. 2849–2863, http://dx.doi.org/10.1029/97WR02388

——— 1997b, Stochastic forcing of sediment routing and storage in channel networks: Water Resources Research, v. 33, n. 12, p. 2865–2880, http://dx.doi.org/10.1029/97WR02387

Blöthe, J. H., and Korup, O., 2013, Millennial lag times in the Himalayan sediment routing system: Earth and Planetary Science Letters, v. 382, p. 38–46, http://dx.doi.org/10.1016/j.epsl.2013.08.044

Bookhagen, B., and Burbank, D. W., 2006, Topography, relief, and TRMM-derived rainfall variations along the Himalaya: Geophysical Research Letters, v. 33, n. 8, L08405, http://dx.doi.org/10.1029/2006GL026037

Bookhagen, B., Thiede, R. C., and Strecker, M. R., 2005, Abnormal monsoon years and their control on erosion and sediment flux in the high, arid northwest Himalaya: Earth and Planetary Science Letters, v. 231, p. 131–146, http://dx.doi.org/10.1016/j.epsl.2004.11.014

Bridge, J. S., and Leeder, M. R., 1979, A simulation model of alluvial stratigraphy: Sedimentology, v. 26, n. 5, p. 617–644, http://dx.doi.org/10.1111/j.1365-3091.1979.tb00935.x
Brozovic, N., and Burbank, D. W., 2000, Dynamic fluvial systems and gravel progradation in the Himalayan foreland: Geological Society of America Bulletin, v. 112, n. 3, p. 394–412, http://dx.doi.org/10.1130/0016-7606(2000)112<394:DFSAGP>2.0.CO;2
Bryant, M., Falk, P., and Paola, C., 1995, Experimental study of avulsion frequency and rate of deposition: Geology, v. 23, n. 4, p. 365–368, http://dx.doi.org/10.1130/0091-7613(1995)023<0365:ESOAFA>2.3.CO;2
Burbank, D. W., 1992, Causes of recent Himalayan uplift deduced from deposited patterns in the Ganges basin: Nature, v. 357, p. 680–683, http://dx.doi.org/10.1038/357680a0
Burbank, D. W., and Beck, R. A., 1991, Models of aggradation versus progradation in the Himalayan Foreland: Geologische Rundschau, v. 80, n. 3, p. 623–638, http://dx.doi.org/10.1007/BF01803690
Burbank, D. W., Beck, R. A., and Mulder, T., 1996, The Himalayan foreland basin, *in* Yin, A., and Harrison, editors, The Tectonic Evolution of Asia: Cambridge, England, Cambridge University Press, p. 149–188.
Chakraborty, T., and Ghosh, P., 2010, The geomorphology and sedimentology of the Tista megafan, Darjeeling Himalaya: Implications for megafan building processes: Geomorphology, v. 115, n. 3–4, p. 252–266, http://dx.doi.org/10.1016/j.geomorph.2009.06.035
Chakraborty, T., Kar, R., Ghosh, P., and Basu, S., 2010, Kosi megafan: Historical records, geomorphology and the recent avulsion of the Kosi River: Quaternary International, v. 227, n. 2, p. 143–160, http://dx.doi.org/10.1016/j.quaint.2009.12.002
Church, M. A., McLean, D. G., and Wolcott, J. F., 1987, River bed gravels: Sampling and analysis, *in* Thorne, C. R., Bathurst, J. C., and Hey, R. D., editors, Sediment Transport in Gravel-Bed Rivers: New York, John Wiley and Sons New York, p. 43–88.
Cullen, J. L., 1981, Microfossil evidence for changing salinity patterns in the Bay of Bengal over the last 20 000 years: Palaeogeography, Palaeoclimatology, Palaeoecology, v. 35, p. 315–356, http://dx.doi.org/10.1016/0031-0182(81)90101-2
Dade, W. B., 2000, Grain size, sediment transport and alluvial channel pattern: Geomorphology, v. 35, n. 1–2, p. 119–126, http://dx.doi.org/10.1016/S0169-555X(00)00030-1
Dade, W. B., and Friend, P. F., 1998, Grain–Size, Sediment–Transport Regime, and Channel Slope in Alluvial Rivers: The Journal of Geology, v. 106, p. 661–676, http://dx.doi.org/10.1086/516052
DeCelles, P. G., and Giles, K. A., 1996, Foreland basin systems: Basin Research, v. 8, n. 2, p. 105–123, http://dx.doi.org/10.1046/j.1365-2117.1996.01491.x
Densmore, A. L., Sinha, R., Sinha, S., Tandon, S. K., and Jain, V., 2016, Sediment storage and release from Himalayan piggyback basins and implications for downstream river morphology and evolution: Basin Research, v. 28, n. 4, p. 1–16, http://dx.doi.org/10.1111/bre.12116
Dietrich, W. E., Kirchner, J. W., Ikeda, H., and Iseya, F., 1989, Sediment supply and the development of the coarse surface layer in gravel-bedded rivers: Nature, v. 340, p. 215–217, http://dx.doi.org/10.1038/340215a0
Dubille, M., and Lavé, J., 2015, Rapid grain size coarsening at sandstone / conglomerate transition: Similar expression in Himalayan modern rivers and Pliocene molasse deposits: Basin Research, v. 27, n. 1, p. 26–42, http://dx.doi.org/10.1111/bre.12071
Duller, R. A., Whittaker, A. C., Fedele, J. J., Whitchurch, A. L., Springett, J., Smithells, R., Fordyce, S., and Allen, P. A., 2010, From grain size to tectonics: Journal of Geophysical Research Earth Surface, v. 115, F03022, http://dx.doi.org/10.1029/2009JF001495
Duller, R. A., Whittaker, A. C., Swinehart, J. B., Armitage, J. J., Sinclair, H. D., Bair, A., and Allen, P. A., 2012, Abrupt landscape change post–6 Ma on the central Great Plains, USA: Geology, v. 40, n. 10, p. 871–874, http://dx.doi.org/10.1130/G32919.1
Duplessy, J. C., 1982, Glacial to interglacial contrasts in the northern Indian Ocean: Nature, v. 295, p. 494–498, http://dx.doi.org/10.1038/295494a0
Fedele, J. J., and Paola, C., 2007, Similarity solutions for fluvial sediment fining by selective deposition: Journal of Geophysical Research Earth Surface, v. 112, n. F2, http://dx.doi.org/10.1029/2005JF000409
Feldl, N., and Bilham, R., 2006, Great Himalayan earthquakes and the Tibetan plateau: Nature, v. 444, p. 165–170, http://dx.doi.org/10.1038/nature05199
Ferguson, R., Hoey, T., Wathen, S., and Werritty, A., 1996, Field evidence for rapid downstream fining of river gravels through selective transport: Geology, v. 24, n. 2, p. 179–182, http://dx.doi.org/10.1130/0091-7613(1996)024<0179:FEFRDF>2.3.CO;2
Fleitmann, D., Burns, S. J., Mangini, A., Mudelsee, M., Kramers, J., Villa, I., Neff, U., Al-Subbary, A. A., Buettner, A., Hippler, D., and Matter, A., 2007, Holocene ITCZ and Indian monsoon dynamics recorded in stalagmites from Oman and Yemen (Socotra): Quaternary Science Reviews, v. 26, n. 1–2, p. 170–188, http://dx.doi.org/10.1016/j.quascirev.2006.04.012
Flemings, P. B., and Jordan, T. E., 1989, A synthetic stratigraphic model of foreland basin development: Journal of Geophysical Research Solid Earth, v. 94, n. B4, p. 3851–3866, http://dx.doi.org/10.1029/JB094iB04p03851
Ghimire, G. P. S., and Uprety, B. K., 1990, Causes and effects of siltation on the environment of Nepal: Environmentalist, v. 10, n. 1, p. 55–65, http://dx.doi.org/10.1007/BF02239558
Gibling, M. R., Tandon, S. K., Sinha, R., and Jain, M., 2005, Discontinuity-Bounded Alluvial Sequences of the Southern Gangetic Plains, India: Aggradation and Degradation in Response to Monsoonal Strength: Journal of Sedimentary Research, v. 75, n. 3, p. 369–385, http://dx.doi.org/10.2110/jsr.2005.029
Godard, V., Bourlès, D. L., Spinabella, F., Burbank, D. W., Bookhagen, B., Fisher, G. B., Moulin, A., and Léanni, L., 2014, Dominance of tectonics over climate in Himalayan denudation: Geology, v. 42, n. 3, p. 243–246, G35342.1, http://dx.doi.org/10.1130/G35342.1
Goodbred, S. L., Jr., 2003, Response of the Ganges dispersal system to climate change: A source-to-sink view

since the last interstade: Sedimentary Geology, v. 162, n. 1–2, p. 83–104, http://dx.doi.org/10.1016/S0037-0738(03)00217-3

Goodbred, S. L., Jr., and Kuehl, S. A., 2000, Enormous Ganges-Brahmaputra sediment discharge during strengthened early Holocene monsoon: Geology, v. 28, n. 12, p. 1083–1086, http://dx.doi.org/10.1130/0091-7613(2000)28<1083:EGSDDS>2.0.CO;2

Heller, P. L., and Paola, C., 1992, The large-scale dynamics of grain-size variation in alluvial basins, 2: Application to syntectonic conglomerate: Basin Research, v. 4, n. 2, p. 91–102, http://dx.doi.org/10.1111/j.1365-2117.1992.tb00146.x

——— 1996, Downstream Changes In Alluvial Architecture: An Exploration of Controls on Channel-stacking Patterns: Journal of Sedimentary Research, v. 66, n. 2, p. 297–306, http://dx.doi.org/10.1306/D4268333-2B26-11D7-8648000102C1865D

Hergarten, S., Robl, J., and Stüwe, K., 2014, Extracting topographic swath profiles across curved geomorphic features: Earth Surface Dynamics, v. 2, p. 97–104, http://dx.doi.org/10.5194/esurf-2-97-2014

Hoth, S., Hoffmann-Rothe, A., and Kukowski, N., 2007, Frontal accretion: An internal clock for bivergent wedge deformation and surface uplift: Journal of Geophysical Research Solid Earth, v. 112, n. B6, http://dx.doi.org/10.1029/2006JB004357

Immerzeel, W. W., van Beek, L. P. H., and Bierkens, M. F. P., 2010, Climate Change Will Affect the Asian Water Towers: Science, v. 328, n. 5984, p. 1382–1385, http://dx.doi.org/10.1126/science.1183188

Jackson, J., McKenzie, D., Priestley, K., and Emmerson, B., 2008, New views on the structure and rheology of the lithosphere: Journal of the Geological Society, v. 165, n. 2, p. 453–465, http://dx.doi.org/10.1144/0016-76492007-109

Jain, V., and Sinha, R., 2003, River systems in the Gangetic plains and their comparison with the Siwaliks: A review: Current Science, v. 84, n. 8, p. 1025–1033.

Jerolmack, D. J., and Paola, C., 2010, Shredding of environmental signals by sediment transport: Geophysical Research Letters, v. 37, n. 19, L19401, http://dx.doi.org/10.1029/2010GL044638

Jha, P. K., Vaithiyanathan, P., and Subramanian, V., 1993, Mineralogical characteristics of the sediments of a Himalayan river: Yamuna River– a tributary of the Ganges: Environmental Geology, v. 22, n. 1, p. 13–20, http://dx.doi.org/10.1007/BF00775279

Jordan, T. A., and Watts, A. B., 2005, Gravity anomalies, flexure and the elastic thickness structure of the India–Eurasia collisional system: Earth and Planetary Science Letters, v. 236, n. 3–4, p. 732–750, http://dx.doi.org/10.1016/j.epsl.2005.05.036

Kellerhals, R., and Bray, D. I., 1971, Sampling procedures for coarse fluvial sediments: Journal of Hydraulic Engineering, v. 97, p. 1165–1180.

Kimura, K., 1999, Diachronous evolution of sub-Himalayan piggyback basins, Nepal: Island Arc, v. 8, n. 1, p. 99–113, http://dx.doi.org/10.1046/j.1440-1738.1999.00224.x

Knighton, D., 1998, Fluvial Forms and Processes: A New Perspective, London, Routledge, 383 p.

Kumar, R., Sangode, S. J., and Ghosh, S. K., 2004, A multistorey sandstone complex in the Himalayan Foreland Basin, NW Himalaya, India: Journal of Asian Earth Sciences, v. 23, n. 3, p. 407–426, http://dx.doi.org/10.1016/S1367-9120(03)00176-7

Lash, G. G., 1988, Along-strike variations in foreland basin evolution: Possible evidence for continental collision along an irregular margin: Basin Research, v. 1, n. 2, p. 71–83, http://dx.doi.org/10.1111/j.1365-2117.1988.tb00006.x

Lavé, J., and Avouac, J. P., 2000, Active folding of fluvial terraces across the Siwalik Hills, Himalayas of central Nepal: Journal of Geophysical Research Solid Earth, v. 105, n. B3, p. 5735–5770, http://dx.doi.org/10.1029/1999JB900292

——— 2001, Fluvial incision and tectonic uplift across the Himalayas of central Nepal: Journal of Geophysical Research Solid Earth, v. 106, n. B11, p. 26561–26591, http://dx.doi.org/10.1029/2001JB000359

Leeder, M. R., Harris, T., and Kirkby, M. J., 1998, Sediment supply and climate change: Implications for basin stratigraphy: Basin Research, v. 10, n. 1, p. 7–18, http://dx.doi.org/10.1046/j.1365-2117.1998.00054.x

Lupker, M., France-Lanord, C., Lavé, J., Bouchez, J., Galy, V., Métivier, F., Gaillardet, J., Lartiges, B., and Mugnier, J.-L., 2011, A Rouse-based method to integrate the chemical composition of river sediments: Application to the Ganga basin. Journal of Geophysical Research Earth Surface, v. 116, n. F4, http://dx.doi.org/10.1029/2010JF001947

Lupker, M., Blard, P.-H., Lavé, J., France-Lanord, C., Léanni, L., Puchol, N., Charreau, J., and Bourlès, D., 2012, ^{10}Be-derived Himalayan denudation rates and sediment budgets in the Ganga basin: Earth and Planetary Science Letters, v. 333–334, p. 146–156, http://dx.doi.org/10.1016/j.epsl.2012.04.020

Lyon-Caen, H., and Molnar, P., 1983, Constraints on the structure of the Himalaya from an analysis of gravity anomalies and a flexural model of the lithosphere: Journal of Geophysical Research Solid Earth, v. 88, n. B10, p. 8171–8191, http://dx.doi.org/10.1029/JB088iB10p08171

——— 1985, Gravity anomalies, flexure of the Indian Plate, and the structure, support and evolution of the Himalaya and Ganga Basin: Tectonics, v. 4, n. 6, p. 513–538, http://dx.doi.org/10.1029/TC004i006p00513

Marr, J. G., Swenson, J. B., Paola, C., and Voller, V. R., 2000, A two-diffusion model of fluvial stratigraphy in closed depositional basins: Basin Research, v. 12, n. 3–4, p. 381–398, http://dx.doi.org/10.1046/j.1365-2117.2000.00134.x

Mugnier, J.-L., and Huyghe, P., 2006, Ganges basin geometry records a pre-15 Ma isostatic rebound of Himalaya: Geology, v. 34, n. 6, p. 445–448, http://dx.doi.org/10.1130/G22089.1

Mugnier, J. L., Leturmy, P., Mascle, G., Huyghe, P., Chalaron, E., Vidal, G., Husson, L., and Delcaillau, B., 1999, The Siwaliks of western Nepal: I. Geometry and kinematics: Journal of Asian Earth Sciences, v. 17, n. 5–6, p. 629–642, http://dx.doi.org/10.1016/S1367-9120(99)00038-3

Narula, P. L., Acharyya, S. K., and Banerjee, J., 2000, Seismotectonic Atlas of India and its Environs: Calcutta, India, The Geological Survey of India.
Naylor, M., and Sinclair, H. D., 2007, Punctuated thrust deformation in the context of doubly vergent thrust wedges: Implications for the localization of uplift and exhumation: Geology, v. 35, n. 6, p. 559–562, http://dx.doi.org/10.1130/G23448A.1
Paola, C., and Seal, R., 1995, Grain Size Patchiness as a Cause of Selective Deposition and Downstream Fining: Water Resources Research, v. 31, n. 5, p. 1395–1407, http://dx.doi.org/10.1029/94WR02975
Paola, C., Heller, P. L., and Angevine, C. L., 1992a, The large-scale dynamics of grain-size variation in alluvial basins, 1: Theory: Basin Research, v. 4, n. 2, p. 73–90, http://dx.doi.org/10.1111/j.1365-2117.1992.tb00145.x
Paola, C., Parker, G., Seal, R., Sinha, S. K., Southard, J. B., and Wilcock, P. R., 1992b, Downstream Fining by Selective Deposition in a Laboratory Flume: Science, v. 258, n. 5089, p. 1757–1760, http://dx.doi.org/10.1126/science.258.5089.1757
Parker, G., 1990, Surface-based bedload transport relation for gravel rivers: Journal of Hydraulic Research, v. 28, n. 4, p. 417–436, http://dx.doi.org/10.1080/00221689009499058
Parker, G., and Toro-Escobar, C. M., 2002, Equal mobility of gravel in streams: The remains of the day: Water Resources Research, v. 38, n. 11, p. 46-1–46-8, http://dx.doi.org/10.1029/2001WR000669
Rice, S., 1999, The Nature and Controls on Downstream Fining Within Sedimentary Links: Journal of Sedimentary Research, v. 69, n. 1, p. 32–39, http://dx.doi.org/10.2110/jsr.69.32
Rice, S. P., and Church, M., 2001, Longitudinal profiles in simple alluvial systems: Water Resources Research, v. 37, n. 2, p. 417–426, http://dx.doi.org/10.1029/2000WR900266
Robinson, R. A. J., and Slingerland, R. L., 1998, Origin of Fluvial Grain-Size Trends in a Foreland Basin: The Pocono Formation on the Central Appalachian Basin: Journal of Sedimentary Research, v. 68, n. 3, p. 473–486, http://dx.doi.org/10.2110/jsr.68.473
Shah, B. A., 2007, Role of Quaternary stratigraphy on arsenic-contaminated groundwater from parts of Middle Ganga Plain, UP–Bihar, India: Environmental Geology, v. 53, n. 7, p. 1553–1561, http://dx.doi.org/10.1007/s00254-007-0766-y
Shukla, U. K., Singh, I. B., Sharma, M., and Sharma, S., 2001, A model of alluvial megafan sedimentation: Ganga Megafan: Sedimentary Geology, v. 44, n. 3–4, p. 243–262. http://dx.doi.org/10.1016/S0037-0738(01)00060-4
Shukla, U. K., Srivastava, P., and Singh, I. B., 2012, Migration of the Ganga River and development of cliffs in the Varanasi region, India during the late Quaternary: Role of active tectonics: Geomorphology, v. 171–172, p. 101–113, http://dx.doi.org/10.1016/j.geomorph.2012.05.009
Sinclair, H. D., and Naylor, M., 2012, Foreland basin subsidence driven by topographic growth versus plate subduction: Geological Society of America Bulletin, v. 124, n. 3, p. 368–379, http://dx.doi.org/10.1130/b30383.1
Singh, H., Parkash, B., and Gohain, K., 1993, Facies analysis of the Kosi megafan deposits: Sedimentary Geology, v. 85, n. 1–4, p. 87–113, http://dx.doi.org/10.1016/0037-0738(93)90077-I
Singh, I. B., 1996, Geological evolution of Ganga Plain - an overview: Journal of the Palaeontological Society of India, v. 41, p. 99–137.
Sinha, R., 2005, Why do Gangetic rivers aggrade or degrade?: Current Science, v. 89, n. 5, p. 836–840.
Sinha, R., and Friend, P. F., 1994, River systems and their sediment flux, Indo-Gangetic plains, Northern Bihar, India: Sedimentology, v. 41, n. 4, p. 825–845, http://dx.doi.org/10.1111/j.1365-3091.1994.tb01426.x
Sinha, R., Friend, P. F., and Switsur, V. R., 1996, Radiocarbon dating and sedimentation rates in the Holocene alluvial sediments of the northern Bihar plains, India: Geological Magazine London, v. 133, n. 1, p. 85–90, http://dx.doi.org/10.1017/S0016756800007263
Sinha, R., Jain, V., Babu, G. P., and Ghosh, S., 2005, Geomorphic characterization and diversity of the fluvial systems of the Gangetic Plains: Geomorphology, v. 70, n. 3–4, p. 207–225, http://dx.doi.org/10.1016/j.geomorph.2005.02.006
Sinha, R., Kettanah, Y., Gibling, M. R., Tandon, S. K., Jain, M., Bhattacharjee, P. S., Dasgupta, A. S., and Ghazanfari, P., 2009, Craton-derived alluvium as a major sediment source in the Himalayan Foreland Basin of India: Geological Society of America Bulletin, v. 121, n. 1112, p. 1596–1610, http://dx.doi.org/10.1130/B26431.1
Sinha, R., Gaurav, K., Chandra, S., and Tandon, S. K., 2013, Exploring the channel connectivity structure of the August 2008 avulsion belt of the Kosi River, India: Application to flood risk assessment: Geology, v. 41, n. 10, p. 1099–1102, http://dx.doi.org/10.1130/G34539.1
Sinha, R., Sripriyanka, K., Jain, V., and Mukul, M., 2014a, Avulsion threshold and planform dynamics of the Kosi River in north Bihar (India) and Nepal: A GIS framework: Geomorphology, v. 216, p. 157–170, http://dx.doi.org/10.1016/j.geomorph.2014.03.035
Sinha, R., Ahmad, J., Gaurav, K., and Morin, G., 2014b, Shallow subsurface stratigraphy and alluvial architecture of the Kosi and Gandak megafans in the Himalayan foreland basin, India: Sedimentary Geology, v. 301, p. 133–149, http://dx.doi.org/10.1016/j.sedgeo.2013.06.008
Slingerland, R., and Smith, N. D., 2004, River Avulsions and Their Deposits: Annual Review of Earth and Planetary Sciences, v. 32, p. 257–285, http://dx.doi.org/10.1146/annurev.earth.32.101802.120201
Srivastava, P., Singh, I. B., Sharma, M., and Singhvi, A. K., 2003, Luminescence chronometry and Late Quaternary geomorphic history of the Ganga Plain, India, *in* Gupta, A. K., Anderson, D. M., and Malmgren, B. A., editors, Indian Ocean Monsoons: Land and Sea Record: Palaeogeography, Palaeoclimatology, Palaeoecology, v. 197, n. 1–2, p. 15–41, http://dx.doi.org/10.1016/S0031-0182(03)00384-5
Srivastava, P., Tripathi, J. K., Islam, R., and Jaiswal, M. K., 2008, Fashion and phases of late Pleistocene aggradation and incision in the Alaknanda River Valley, western Himalaya, India: Quaternary Research, v. 70, n. 1, p. 68–80, http://dx.doi.org/10.1016/j.yqres.2008.03.009

Sternberg, H., 1875, Untersuchungen über längen-und querprofil geschiebeführender flüsse: Zeitschrift für Bauwesen, v. 25, p. 483–506.
Stevens, V. L., and Avouac, J. P., 2015, Interseismic coupling on the main Himalayan thrust: Geophysical Research Letters, v. 42, n. 14, p. 5828–5837, http://dx.doi.org/10.1002/2015GL064845
Syvitski, J. P. M., and Brakenridge, G. R., 2013, Causation and avoidance of catastrophic flooding along the Indus River, Pakistan: GSA Today, v. 23, p. 4–10, http://dx.doi.org/10.1130/GSATG165A.1
Tandon, S. K., Gibling, M. R., Sinha, R., Singh, V., Ghazanfari, P., Dasgupta, A., Jain, M., and Jain, V., 2006, Alluvial Valleys of the Ganga Plains, India: Timing and Causes of Incision, *in* Dalrymple, R. W., Leckie, D. A., and Tilliman, R. W., editors, Incised Valleys in Time and Space: SEPM Special Publication, v. 85, p. 15–35, http://dx.doi.org/10.2110/pec.06.85.0015
Telbisz, T., Kovács, G., Székely, B., and Szabó, J., 2013, Topographic swath profile analysis: A generalization and sensitivity evaluation of a digital terrain analysis tool: Zeitschrift für Geomorphologie, v. 57, n. 4, p. 485–513, http://dx.doi.org/10.1127/0372-8854/2013/0110
Thiede, R. C., and Ehlers, T. A., 2013, Large spatial and temporal variations in Himalayan denudation: Earth and Planetary Science Letters, v. 371–372, p. 278–293, http://dx.doi.org/10.1016/j.epsl.2013.03.004
Tucker, G. E., and Slingerland, R., 1997, Drainage basin responses to climate change: Water Resources Research, v. 33, n. 8, p. 2031–2047, http://dx.doi.org/10.1029/97WR00409
van den Berg, J. H., 1995, Prediction of alluvial channel pattern of perennial rivers: Geomorphology, v. 12, n. 4, p. 259–279, http://dx.doi.org/10.1016/0169-555X(95)00014-V
Vance, D., Bickle, M., Ivy-Ochs, S., and Kubik, P. W., 2003, Erosion and exhumation in the Himalaya from cosmogenic isotope inventories of river sediments: Earth and Planetary Science Letters, v. 206, n. 3–4, p. 273–288, http://dx.doi.org/10.1016/S0012-821X(02)01102-0
Wasson, R. J., 2003, A sediment budget for the Ganga-Brahmaputra catchment: Current Science, v. 84, n. 8, p. 1041–1047.
Wells, N. A., and Dorr, J. A., 1987, Shifting of the Kosi River, northern India: Geology, v. 15, n. 3, p. 204–207, http://dx.doi.org/10.1130/0091-7613(1987)15<204:SOTKRN>2.0.CO;2
Wesnousky, S. G., Kumar, S., Mohindra, R., and Thakur, V. C., 1999, Uplift and convergence along the Himalayan Frontal Thrust of India: Tectonics, v. 18, n. 6, p. 967–976, http://dx.doi.org/10.1029/1999TC900026
Whittaker, A. C., Attal, M., and Allen, P. A., 2010, Characterising the origin, nature and fate of sediment exported from catchments perturbed by active tectonics: Basin Research, v. 22, n. 6, p. 809–828, http://dx.doi.org/10.1111/j.1365-2117.2009.00447.x
Whittaker, A. C., Duller, R. A., Springett, J., Smithells, R. A., Whitchurch, A. L., and Allen, P. A., 2011, Decoding downstream trends in stratigraphic grain size as a function of tectonic subsidence and sediment supply: Geological Society of America Bulletin, v. 123, p. 1363–1382, http://dx.doi.org/10.1130/B30351.1
Wobus, C., Whipple, K. X., Kirby, E., Snyder, N., Johnson, J., Spyropolou, K., Crosby, B., and Sheehan, D., 2006, Tectonics from topography: Procedures, promise, and pitfalls: Geological Society of America Special Papers, v. 398, p. 55–74, http://dx.doi.org/10.1130/2006.2398(04)
Wobus, C. W., Tucker, G. E., and Anderson, R. S., 2010, Does climate change create distinctive patterns of landscape incision?: Journal of Geophysical Research Earth Surface, v. 115, n. F4, , http://dx.doi.org/10.1029/2009JF001562
Yin, A., 2006, Cenozoic tectonic evolution of the Himalayan orogen as constrained by along-strike variation of structural geometry, exhumation history, and foreland sedimentation: Earth-Science Reviews, v. 76, n. 1–2, p. 1–131, http://dx.doi.org/10.1016/j.earscirev.2005.05.004

Appendix B

Appendix B

LETTER

doi:10.1038/nature22039

Abrasion–set limits on Himalayan gravel flux

Elizabeth H. Dingle[1], Mikaël Attal[1] & Hugh D. Sinclair[1]

Rivers sourced in the Himalayan mountain range carry some of the largest sediment loads on the planet[1], yet coarse gravel in these rivers vanishes within approximately 10–40 kilometres on entering the Ganga Plain (the part of the North Indian River Plain containing the Ganges River). Understanding the fate of gravel is important for forecasting the response of rivers to large influxes of sediment triggered by earthquakes or storms. Rapid increase in gravel flux and subsequent channel bed aggradation (that is, sediment deposition by a river) following the 1999 Chi-Chi and 2008 Wenchuan earthquakes[2–7] reduced channel capacity and increased flood inundation[3]. Here we present an analysis of fan geometry, sediment grain size and lithology in the Ganga Basin. We find that the gravel fluxes from rivers draining the central Himalayan mountains, with upstream catchment areas ranging from about 350 to 50,000 square kilometres, are comparable. Our results show that abrasion of gravel during fluvial transport can explain this observation; most of the gravel sourced more than 100 kilometres upstream is converted into sand by the time it reaches the Ganga Plain. These findings indicate that earthquake-induced sediment pulses sourced from the Greater Himalayas, such as that following the 2015 Gorkha earthquake[8], are unlikely to drive increased gravel aggradation at the mountain front. Instead, we suggest that the sediment influx should result in an elevated sand flux, leading to distinct patterns of aggradation and flood risk in the densely populated, low-relief Ganga Plain.

Numerical models of foreland basin stratigraphy and modern river systems suggest that the location where river-bed sediment texture changes from gravel- to sand-dominated (the gravel–sand transition) is determined by: (1) basin subsidence rate; (2) total sediment flux; (3) gravel-size fraction; and (4) river discharge, over sub-millennial timescales[9–13]. However, few field data have previously been available to validate such models. The gravel–sand transition is marked by an abrupt decrease in grain size[14–16], believed to result from an exhaustion of gravel supply. The gravel–sand transition in large trans-Himalayan rivers feeding the Ganga Plain occurs about 12–20 km downstream of the mountain front in the east Ganga Plain, and slightly further (about 28–45 km) downstream in the west Ganga Plain (Fig. 1); this transition is also associated with a marked decrease in channel gradient[17]. We find that the gravel–sand transition in rivers draining small foothill-fed catchments ($<350\,km^2$) in the east Ganga Plain[16] is at a comparable distance downstream of the mountain front to that in the adjacent trans-Himalayan Gandak and Kosi rivers ($>30{,}000\,km^2$) (Fig. 1). While spatial variations in basin subsidence across the entire foreland basin may control the overall position of the gravel–sand transition[9,17], subsidence can be ruled out as a factor explaining this observation, because there is no evidence for a large variation in subsidence rate beneath the foothill-fed tributaries flowing in the interfan region between the Gandak and Kosi alluvial fans[17]. Given the substantial contrast in size between the trans-Himalayan Gandak and Kosi rivers and the smaller foothill-fed catchments, we would expect orders-of-magnitude differences in water and total sediment flux, which is at odds with the similarity in the positions of the gravel–sand transition. These fluxes are therefore also unlikely to have an important role in controlling the position of this transition. Gravel fining rates between the mountain front and the gravel–sand transition in the east Ganga Plain are also independent of the relatively rapid reduction in grain size observed across the gravel–sand transition[16,17]. This further indicates that neither abrasion downstream of the mountain front nor input grain size exert a dominant control on the distance to the transition in the Ganga Plain. Theory and experiments have implied that an increase in the fraction of gravel in the sediment supplied to the basin results in the downstream migration of the gravel front[9]. Having ruled out other likely controls, we further test whether the position of the gravel–sand transition across the east Ganga Plain reflects differences (or similarities) in gravel flux.

We first compare the total mass flux of sediment exported into the Ganga Plain to the mass trapped upstream of the gravel–sand transition. The volume of gravel between the mountain front and the mapped gravel–sand transitions[17] is calculated using the mean basin subsidence rate (which is believed to have been relatively constant over the past 10,000 years[17]), the distance to the gravel–sand transition, and the maximum width of the alluvial fan (see Methods). We assume that most gravel is trapped upstream of the gravel–sand transition, an assumption supported by the conspicuous lack of gravel downstream of the transition. The use of the basin subsidence rate assumes the degree of filling of the basin (defined by a depositional base level) during that interval is constant (see Extended Data Table 1). The gravel-to-total-load ratio was also calculated for each catchment. Total sediment flux data are only available for the trans-Himalayan rivers considered in this study[18], so to approximate total sediment flux from the smaller foothill catchments (Churre, Bakeya, Lakhandei, Ratu and Aurhi), we have used ^{10}Be-derived catchment-averaged erosion rates from similar sized catchments further west in the Garhwal Himalaya[19] (see Methods).

We find that absolute gravel fluxes are lower across the foothill catchments, with values typically ranging between 0.05 megatonnes (Mt) of gravel per year and 0.72 Mt yr^{-1}, compared to values of 0.51–3.29 Mt yr^{-1} in the trans-Himalayan catchments, but the differences are much smaller than what would be expected from catchments with contributing areas spanning three orders of magnitude (Fig. 2a). These absolute flux values should be treated as maxima, however, because we assume that that the full surface of the fan is available to receive sediment (see Methods). Our gravel proportion (or gravel-to-total-load ratio) estimates for the large trans-Himalayan systems vary between 0.2% and 29%, with proportions generally lowest for the Gandak and Kosi rivers in the east Ganga Plain (Fig. 2b). For average and maximum sediment flux scenarios (using average and maximum erosion rates), gravel proportions are systematically lower than estimates based on a similar abrasion model to predict gravel proportion for major Himalayan rivers at the mountain front[20]. For the smaller foothill catchments, gravel proportions are notably higher, even under the maximum flux scenario with catchment-averaged erosion rates of 5 mm yr^{-1} (Fig. 2b); for the gravel proportion to be lower than 50%, larger total sediment fluxes would be required, suggesting catchment-averaged erosion rates in excess of about 2.75 mm yr^{-1}.

Identification of the provenance of gravel is facilitated by the fact that the Himalayan mountain range is divided into four major structural units that run broadly parallel from west to east and are composed of

[1]School of GeoSciences, University of Edinburgh, Drummond Street, Edinburgh EH8 9XP, UK.

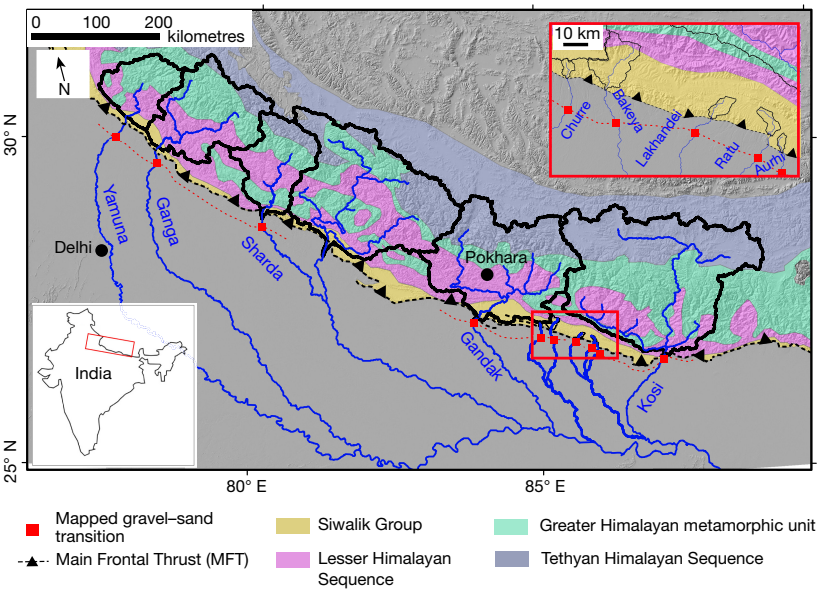

Figure 1 | Study area and simplified geological map of the Ganga basin. The mapped gravel–sand transition is shown for both the major trans-Himalayan rivers[17] and smaller foothill-fed catchments[16] (see top right inset) considered in the east Ganga Plain. Major geological units[21] are all bound by major faults. The red dashed line links the position of mapped gravel–sand transitions between rivers in the Ganga Plain. Map adapted from ref. 17, American Journal of Science.

contrasting lithological units (Fig. 1). These units are, from north to south: the Tethyan Himalayan Sequence, the Greater Himalayan metamorphic unit, the Lesser Himalayan Sequence and the Siwalik Group[21] (see Methods). The Main Frontal Thrust is the most southerly tectonic structure, situated between the Siwalik Group and the foreland basin, and absorbs approximately 80% of the approximately 21 ± 1.5 mm yr^{-1} convergence between India and south Tibet[22]. During the low-flow season (October–May), a considerable portion of the channel bed of major rivers of the Ganga Basin is accessible, with extensive coarse gravel bars dominating the bed of the rivers as they cross the mountain front. To assess gravel provenance, pebble lithology was identified at a number of sites from about 30–50 km upstream of the mountain front down to the gravel–sand transition in each of the trans-Himalayan rivers (Fig. 1). Using a 25-m tape measure, pebble lithology was identified at 50-cm intervals along two transects at each site and categorized as outlined in Methods.

Clast characterization shows that gravel which could be identified as uniquely from the Tethyan Himalayan sedimentary lithologies was absent from all our sites (see Methods), despite this unit representing 10%–20% of the total catchment geology (Fig. 3a and Extended Data Fig. 1). Quartzites are considered separately because they are distributed within each of the contributing units but cannot be traced back to any specific one. Quartzites represent a small fraction of the rocks exposed in the catchments[20], typically less than 10%, yet they constitute the majority of the pebbles sampled (about 40%–70%), consistent with observations along the Marsyandi River[20]. Lesser Himalayan metamorphic lithologies comprised around 5%–40% of sampled pebbles (Fig. 3b). In general, where Lesser Himalayan lithologies covered a larger proportion of the total catchment area (such as for the Yamuna River), a higher proportion of Lesser Himalayan lithologies was found in the sampled pebbles (Fig. 3b). Greater Himalayan lithologies (igneous and medium- to high-grade metamorphic) comprised a further 5%–40% of

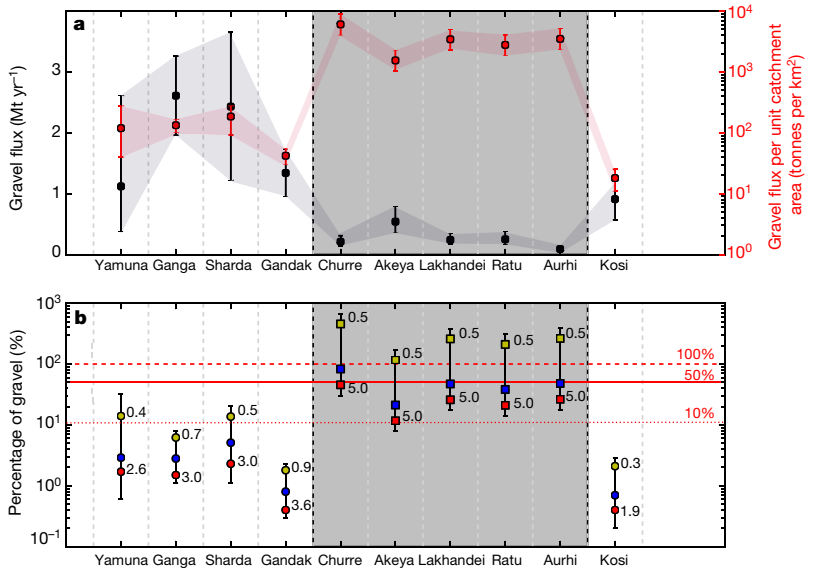

Figure 2 | Gravel flux estimates. a, Estimates of absolute gravel flux (black) and of gravel flux per unit catchment area (red) for trans-Himalayan and foothill-fed (shaded in grey) rivers. **b**, Calculated per cent gravel exported by trans-Himalayan rivers into the Ganga Plain (see Methods and Extended Data Tables 1–3). Foothill-fed catchments are shaded in grey. Red, blue and yellow data points correspond to maximum, average and minimum total sediment flux scenarios, respectively, with corresponding erosion rates (in units of mm yr^{-1}) indicated next to data points for maximum and minimum flux scenarios for reference. Error bars and red and black shading reflect differences in accommodation space available for sediment accumulation generated under maximum and minimum subsidence rates[17].

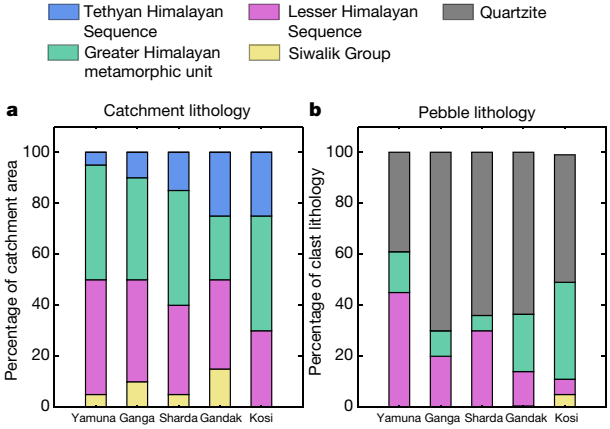

Figure 3 | Catchment and pebble lithology. a, Proportion of area of major geological units in trans-Himalayan catchments upstream of the mountain front[21]. **b**, Average clast lithology composition recorded on exposed gravel bars between the mountain front and the gravel–sand transition (see Extended Data Fig. 1 for pebble lithology at each survey location). Quartzites are considered separately as they are distributed within each of the contributing units but cannot be traced back to any of these units; they represent a small fraction of the rocks exposed in the catchments, typically less than 10% (ref. 20).

the sampled pebbles, with the greatest proportions found further east along the Gandak and Kosi rivers, where the Greater Himalayan source rocks extend further south. Sedimentary Siwalik lithologies made up a relatively small fraction (<10%) of the sampled pebbles.

For our numerical model experiments, we used three pebble erodibility coefficients typical of the Himalayan lithologies[23] to assess the likelihood of gravel supplied from different parts of the catchments surviving as gravel after transportation to the mountain front. Using published percentage mass loss per travelled distance values[23], we explored model scenarios on the Kosi and Bakeya catchments to define how pebble erodibility influences the proportion of the catchment area contributing gravel to the Ganga Plain as a function of catchment size[23,24] (see Methods).

Modelling results show that for weak lithologies with high erodibility values (λ) such as schist and poorly cemented sandstones[23], only locally sourced gravel is likely to survive at the mountain outlet (Fig. 4). After a transport distance of about 20 km, most gravel with high erodibility ($\lambda = 20\%\ km^{-1}$) is abraded and converted into sand and finer products[23]; therefore, most of the easily erodible gravel supplied to the river at a distance greater than around 20 km upstream of the mountain front is unlikely to contribute to the gravel load, and is probably transported as washload or suspended load. Gravel with erodibility values of around $2\%\ km^{-1}$, representative of most Himalayan lithologies such as gneiss, granite, limestone and well cemented sandstone, can survive transport lengths of approximately 100–200 km. Clasts of these lithologies would probably constitute a greater proportion of gravel material at the outlet; this, however, is a conservative estimate, given that chemical weathering on hillslopes and during temporary storage may weaken pebbles[25]. Under the lowest erodibility values ($\lambda = 0.2\%\ km^{-1}$; for example, quartzite[23]), a large proportion of the gravel supplied to the rivers is likely to survive to the mountain front (Fig. 4).

Modelling of the abrasion of gravel as it is transported downstream suggests that beyond a critical fluvial transport length upstream of the mountain front, gravel delivered to the fluvial network reaches the Ganga Plain mainly as sand and finer sediment[18,23,24] (Fig. 4). This is consistent with Sr–Nd isotopic mass balances of suspended sediment in the Ganga Basin suggesting that 80% ± 10% of suspended sediment delivered to the Ganga Plain is of Greater Himalayan source, while only 20% ± 10% is sourced from the Lesser Himalaya[26]. The critical fluvial transport length is dependent on pebble erodibility, which is a function of lithology, and was estimated to be about $250/\lambda$ (ref. 23). For trans-Himalayan catchments, intermediate- and low-strength lithologies of the Lesser and Greater Himalayas sourced within around 100 km upstream of the mountain front will contribute a substantial fraction of the gravel exported and deposited upstream of the gravel–sand transition[23]. Similar lithologies sourced further upstream will be abraded into sand before reaching the outlet, which is supported by the lack of pebbles distinctively sourced from the Tethyan Himalaya and relatively low proportions of Greater Himalayan pebbles in the Ganga Plain (Fig. 3). Where Greater Himalayan rocks are exposed further south in these catchments, a larger proportion of Greater Himalayan pebbles reach the Ganga Plain as a result of shorter transport distances and generally lower percentage mass loss of Greater Himalaya lithologies (such as gneiss and granite) via abrasion, compared to the sedimentary and low-grade metamorphics from the other contributing units[20,23].

More resistant quartzite lithologies, however, are sourced from all parts of the Himalaya[20]. Even in catchments as large as the Kosi, more than 50% of quartzitic pebbles sourced from the catchment headwaters are likely to reach the mountain outlet as gravel, because the characteristic transport length for quartzite (>1,000 km; ref. 23) is longer than the river network (Fig. 4). We would therefore expect quartzite to dominate the lithologies of pebbles exported into the Ganga Plain, which is consistent with our observations (Fig. 3b) and with previous modelling

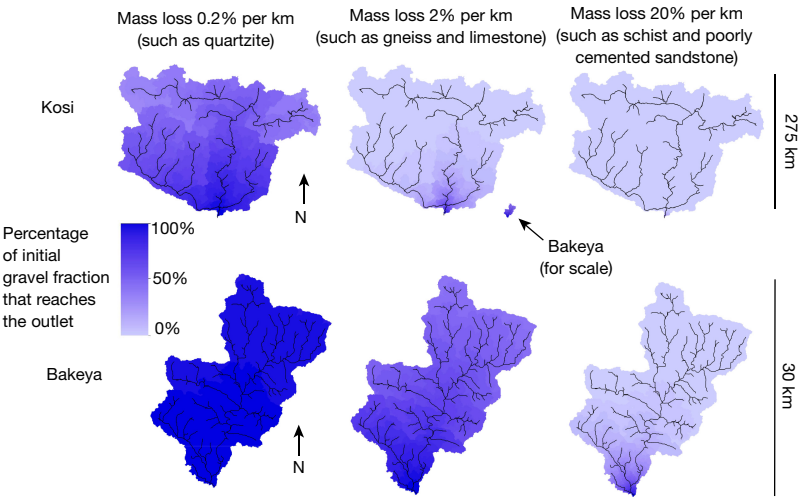

Figure 4 | Abrasion scenarios for the Kosi (top panels; trans-Himalayan) and Bakeya (bottom panels; foothill-fed) rivers. Three pebble erodibility values are used, representative of Himalayan lithologies[20,23]. Colour intensity indicates the percentage of gravel supplied to the river at this location that reaches the catchment outlet as gravel; the remaining percentage represents the mass loss by abrasion, assumed in this case to be sand and finer sediment. More than 50% of the gravel supplied at locations indicated by pixels in dark blue reaches the outlet as gravel; almost all of the gravel supplied at locations indicated by pixels in pale lilac is turned into sand and finer products before reaching the outlet.

predicitions[23,24]. The smaller foothill catchments are draining the Neogene Siwalik sediments (consisting of previously deposited Ganga Plain sediments), which are progressively incorporated back into the mountain range through frontal accretion of thrust units[16]. Therefore, the rivers are expected to recycle almost exclusively quartzitic gravel, which is confirmed by field observations. The low degree of cementation of the young Neogene sediment was also noted in the field, which probably explains the high catchment-averaged erosion rates. These observations explain why a very high proportion of the gravel delivered to the foothill channels survive into the Ganga Plain, and hence, why high gravel fluxes per unit catchment area are observed for these smaller systems (Fig. 2a).

Our models and data demonstrate that increased sediment delivery to channels will result in an additional pulse of gravel reaching the Ganga Plain only if sediment delivery occurs within less than about 100 km upstream of the mountain front or is sourced in highly resistant lithologies (for example, quartzite). Increased gravel supply to rivers in the Siwalik Hills (proximal and quartzite-dominated), such as might be expected from landsliding following seismicity on the Main Frontal Thrust, will probably result in a pulse of gravel and aggradation in river channels of the proximal Ganga Plain. Conversely, widespread landsliding in the Greater Himalaya[8] initiated by the 2015 Gorkha earthquake (>200 km upstream of the mountain outlets) should result in elevated sand flux but is less likely to drive increased gravel flux to the Ganga Plain and thus leave a trace in the gravel stratigraphy of the foreland basin (see Extended Data Fig. 3). Our results also suggest that over the length scale of trans-Himalayan rivers, abrasion facilitates the downstream translation and dispersion of earthquake-generated sediment[27] through the transformation of gravel to more mobile sand. The 1950 Assam earthquake reportedly dislodged 47 billion cubic metres of landslide material[28], resulting in long-term channel aggradation and a morphological change in tributaries of the Brahmaputra River[29], although the relative effects of increased gravel and sand delivery out of the mountain front were not explored. Rivers in the Ganga Plain are expected to respond differently to elevated sand or gravel input; our findings suggest that future research should aim to understand these responses better.

Online Content Methods, along with any additional Extended Data display items and Source Data, are available in the online version of the paper; references unique to these sections appear only in the online paper.

Received 16 September 2016; accepted 31 January 2017.

1. Milliman, J. D. & Syvitski, J. P. M. Geomorphic/tectonic control of sediment discharge to the ocean: the importance of small mountainous rivers. *J. Geol.* **100,** 525–544 (1992).
2. Dadson, S. J. *et al.* Earthquake-triggered increase in sediment delivery from an active mountain belt. *Geology* **32,** 733–736 (2004).
3. Chen, H. & Petley, D. N. The impact of landslides and debris flows triggered by Typhoon Mindulle in Taiwan. *Q. J. Eng. Geol. Hydrogeol.* **38,** 301–304 (2005).
4. Yanites, B. J., Tucker, G. E., Mueller, K. J. & Chen, Y.-G. How rivers react to large earthquakes: evidence from central Taiwan. *Geology* **38,** 639–642 (2010).
5. Dadson, S. J. *et al.* Links between erosion, runoff variability and seismicity in the Taiwan orogen. *Nature* **426,** 648–651 (2003).
6. Huang, R. & Fan, X. The landslide story. *Nat. Geosci.* **6,** 325–326 (2013).
7. Yanites, B. J. *et al.* The influence of sediment cover variability on long-term river incision rates: an example from the Peikang River, central Taiwan. *J. Geophys. Res.* **116,** F03016 (2011).
8. Kargel, J. S. *et al.* Geomorphic and geologic controls of geohazards induced by Nepal's 2015 Gorkha earthquake. *Science* **351,** aac8353 (2016).
9. Paola, C., Heller, P. L. & Angevine, C. L. The large-scale dynamics of grain-size variation in alluvial basins, 1: theory. *Basin Res.* **4,** 73–90 (1992).
10. Parker, G. & Cui, Y. The arrested gravel front: stable gravel-sand transitions in rivers. Part 1: Simplified analytical solution. *J. Hydraul. Res.* **36,** 75–100 (1998).
11. Robinson, R. A. J. & Slingerland, R. L. Origin of fluvial grain-size trends in a foreland basin: the Pocono Formation on the Central Appalachian Basin. *J. Sediment. Res.* **68,** 473 (1998).
12. Hoey, T. B. & Bluck, B. J. Identifying the controls over downstream fining of river gravels. *J. Sediment. Res.* **69,** 40 (1999).
13. Marr, J. G., Swenson, J. B., Paola, C. & Voller, V. R. A two-diffusion model of fluvial stratigraphy in closed depositional basins. *Basin Res.* **12,** 381–398 (2000).
14. Ferguson, R., Hoey, T., Wathen, S. & Werritty, A. Field evidence for rapid downstream fining of river gravels through selective transport. *Geology* **24,** 179–182 (1996).
15. Ferguson, R. I. Emergence of abrupt gravel to sand transitions along rivers through sorting processes. *Geology* **31,** 159–162 (2003).
16. Dubille, M. & Lavé, J. Rapid grain size coarsening at sandstone/conglomerate transition: similar expression in Himalayan modern rivers and Pliocene molasse deposits. *Basin Res.* **27,** 26–42 (2015).
17. Dingle, E. H., Sinclair, H. D., Attal, M., Milodowski, D. T. & Singh, V. Subsidence control on river morphology and grain size in the Ganga Plain. *Am. J. Sci.* **316,** 778–812 (2016).
18. Lupker, M. *et al.* ^{10}Be-derived Himalayan denudation rates and sediment budgets in the Ganga basin. *Earth Planet. Sci. Lett.* **333–334,** 146–156 (2012).
19. Scherler, D., Bookhagen, B. & Strecker, M. R. Tectonic control on ^{10}Be-derived erosion rates in the Garhwal Himalaya, India. *J. Geophys. Res. Earth Surf.* **119,** 2013JF002955 (2014).
20. Attal, M. & Lavé, J. in *Tectonics, Climate and Landscape Evolution* 143–171 (Geological Society of America Special Paper 398, GSA, 2006).
21. Yin, A. Cenozoic tectonic evolution of the Himalayan orogen as constrained by along-strike variation of structural geometry, exhumation history, and foreland sedimentation. *Earth Sci. Rev.* **76,** 1–131 (2006).
22. Lavé, J. & Avouac, J. P. Active folding of fluvial terraces across the Siwaliks Hills, Himalayas of central Nepal. *J. Geophys. Res. Solid Earth* **105,** 5735–5770 (2000).
23. Attal, M. & Lavé, J. Pebble abrasion during fluvial transport: Experimental results and implications for the evolution of the sediment load along rivers. *J. Geophys. Res.* **114,** F04023 (2009).
24. Sklar, L. S., Dietrich, W. E., Foufoula-Georgiou, E., Lashermes, B. & Bellugi, D. Do gravel bed river size distributions record channel network structure? *Wat. Resour. Res.* **42,** W06D18 (2006).
25. Heller, P. L. *et al.* Paradox of downstream fining and weathering-rind formation in the lower Hoh River, Olympic Peninsula, Washington. *Geology* **29,** 971–974 (2001).
26. Galy, A. & France-Lanord, C. Higher erosion rates in the Himalaya: geochemical constraints on riverine fluxes. *Geology* **29,** 23–26 (2001).
27. Cui, Y. *et al.* Sediment pulses in mountain rivers: 1. Experiments. *Wat. Resour. Res.* **39,** 1239 (2003).
28. Keefer, D. K. Earthquake-induced landslides and their effects on alluvial fans. *J. Sediment. Res.* **69,** 84 (1999).
29. Sarma, J. N. Fluvial process and morphology of the Brahmaputra River in Assam, India. *Geomorphology* **70,** 226–256 (2005).

Acknowledgements We thank V. Singh, A. Gajurel, J. Stewart, F. Bowyer, K. Maheswari, D. Basuroy, A. Sarkar, B. Sitaula and Apex Adventure, and the Nepalese Department of Mines and Geology for their cooperation and logistical support in the field. C. Paola and E. Garzanti provided comments that helped to improve the manuscript. We are also grateful to the International Association of Sedimentologists, the British Society for Geomorphology and the Edinburgh University Club of Toronto for their financial support of the fieldwork. This study formed part of a Natural Environment Research Council (NERC)-funded PhD (NE/L501566/1).

Author Contributions E.H.D. and M.A. collected pebble lithology data and mapped positions of the gravel–sand transition. E.H.D. calculated gravel fluxes and proportions. M.A. devised the pebble abrasion model, which E.H.D. ran and analysed the results from. E.H.D., M.A. and H.D.S. designed the study and all discussed the results to shape this manuscript. E.H.D., M.A. and H.D.S wrote the manuscript. Figures were produced by E.H.D.

Author Information Reprints and permissions information is available at www.nature.com/reprints. The authors declare no competing financial interests. Readers are welcome to comment on the online version of the paper. Publisher's note: Springer Nature remains neutral with regard to jurisdictional claims in published maps and institutional affiliations. Correspondence and requests for materials should be addressed to E.H.D. (elizabeth.dingle@ed.ac.uk).

Reviewer Information *Nature* thanks E. Garzanti, C. Paola and the other anonymous reviewer(s) for their contribution to the peer review of this work.

METHODS

Gravel flux estimates. The volume of accommodation space available for gravel accumulation between the mountain front and the mapped gravel–sand transition was calculated for each catchment. The volume generated each year was defined as the product of basin subsidence rate[17], distance to the gravel–sand transition, and maximum width of the alluvial fan upstream of the transition (derived from Google Earth imagery). The gravel–sand transition was mapped for each river by noting the point at which exposed deposits were nearly exclusively sand (>95%)[17].

The lateral extent of alluvial fans was determined by topographic barriers, or where fans from adjacent systems constrain lateral mobility[30]. Where closely spaced, similar-sized channels exit the mountain front and it was difficult to constrain fan boundaries, the maximum width of each fan was set as the mid-point between the two channel outlets. This area represents the maximum extent over which the channel can deposit sediment upstream of the gravel–sand transition. We assume that deposition will occur over the total surface of this area over timescales of 10–1,000 years, based on documented avulsion pathways on the Kosi River which appear to inundate the surface of the Kosi mega-fan upstream of the gravel–sand transition over about 200 years[31], and for consistency with ^{10}Be-derived sediment fluxes that are averaged over 10^2–10^3 years[18]. Although the modern channel only occupies a portion of the fan surface, repetitive phases of channel infilling and avulsion over these timescales allow the channel to migrate over the surface of the fan, making the entire fan surface available to receive sediment[31]. We also assume that the distance from the mountain front to the gravel–sand transition remains relatively constant over these timescales, which is supported by the presence of a channel slope break at the transition. A translation of this transition a few kilometres downstream or upstream would not very much affect the gravel proportion estimates. This is demonstrated in Extended Data Fig. 2, where gravel proportions have been recalculated on the basis of the gravel–sand transition being 5 km further upstream or downstream. The total available accommodation space upstream of the gravel–sand transition was converted to a total mass of sediment, assuming densities typical of quartzite (2.65 tonnes m^{-3}). The mass of coarse sediment trapped upstream of the gravel–sand transition was then converted to a proportion of the total sediment flux (see Extended Data Tables 1–3).

Foothill-fed catchment sediment fluxes. Where sediment flux data are not available for the foothill-fed catchments (Churre, Bakeya, Lakhandei, Ratu and Aurhi), ^{10}Be-derived catchment-averaged erosion rates from similar-sized catchments further west in the Garhwal Himalaya[19] were used to approximate total sediment fluxes. These sub-catchments form part of the Yamuna catchment, but are higher in elevation and catchment relief than the foothill-fed catchment considered in this study, with average elevations between 1,700 m and 4,000 m. With this in mind, we have calculated sediment fluxes for the foothill catchments using the maximum range of erosion rates reported from these data (0.5–5 mm yr^{-1}), and assuming an average rock density of 2.65 tonnes m^{-3}.

Bedload is commonly assumed to constitute about 10% of total river sediment loads in rivers originating from mountainous settings, although this proportion decreases to as low as 1% with increasing catchment areas above about 1,000 km^2 (ref. 32). Our gravel flux estimates should represent a minimum bedload flux because they do not incorporate sediment finer than 2 mm, which may also be transported as bedload. Our gravel proportion estimates (and gravel flux per unit catchment area) appear much larger in small foothill-fed systems than in trans-Himalayan catchments. To generate total sediment fluxes large enough to allow gravel proportions in keeping within these empirical relationships[32], catchment-averaged erosion rates of 3–5 mm yr^{-1} are required in the foothill catchments. Either these catchments experience relatively high erosion rates (comparable to the fastest eroding catchments further west in the Garhwal Himalaya[19]), or gravel makes up a larger proportion of the total sediment load (>50%) than might be expected based on an empirically derived catchment area scaling relationship[32]. Conversely, gravel proportions in the larger trans-Himalayan systems are low, representing as little as ≤1% of the total sediment load (Fig. 2b). This could be a result of over-estimated ^{10}Be-derived erosion rates.

Influence of abrasion on spatial distribution of sources of gravel. We applied a simple abrasion model to produce Fig. 4. Using a 30-m Shuttle Radar Topography Mission Digital Elevation Model, we calculated the distance α between each contributing pixel and the catchment outlet and used Sternberg's law to calculate the proportion K of the gravel initially supplied by the pixel that reaches the catchment outlet as gravel[20,23]:

$$K = e^{-\lambda\alpha} \quad (1)$$

where λ is the percentage of gravel (or pebble) mass loss per kilometre and $K = M/M_0$, where M_0 represents the mass of gravel initially supplied by the pixel and M the remaining mass of gravel after a transport distance α. We assume that all products of abrasion are sand and finer sediment[23]. We made the calculation for three erodibility coefficients representative of Himalayan lithologies for both a trans-Himalayan catchment (Kosi River, maximum stream length about 600 km, drainage area about 50,000 km^2) and a foothill catchment (Bakeya River, maximum stream length about 50 km, drainage area about 350 km). Maps were generated with constant erodibility coefficients across the whole catchments for illustrative purposes (Fig. 4), using coefficients of 0.2%, 2% and 20% mass loss per kilometre, representative of the hardest, most common, and weakest lithologies exposed in the catchments, respectively[20,23]. We note that spatial variations in erosion rates could affect the absolute gravel flux supplied from different parts of the catchment and therefore the relative proportions of a given lithology on gravel bars. For example, higher erosion rates are expected in areas supplying Greater Himalaya lithologies[20,22], which should lead to a relatively higher abundance of gravel from these lithologies compared to a scenario with uniform erosion. However, this does not affect the maps shown in Fig. 4 because they relate the fraction of gravel remaining after transport to the outlet to the fraction of gravel initially supplied by a given pixel, irrelevant of the absolute volume (or flux) supplied. Similarly, some lithologies may contribute a relatively greater amount of gravel than others[20], but again this does not affect the maps shown in Fig. 4.

Determination of pebble lithology in the field. The four major structural units running broadly parallel from west to east across the Himalayan orogen are, from north to south: the Tethyan Himalayan Sequence, the Greater Himalayan metamorphic unit, the Lesser Himalayan Sequence and the Siwalik Group[21,33]. The Tethyan Sequence contains marine sedimentary to low-grade meta-sedimentary rocks. The Greater Himalayan metamorphic unit consists largely of medium to high-grade schist, paragneiss and orthogneiss[34]. The Lesser Himalayan Sequence comprises lower-grade metasedimentary rocks including phyllite, quartzite, marble and dolostone[21,34]. The Siwalik Group contains Neogene sandstones, conglomerates and shales, formed by the erosional products of the Lesser and Greater Himalaya[35].

Between six and eleven gravel bars located between up to approximately 100 km upstream of the mountain front and the gravel–sand transition were surveyed along each river. At each site, two 25-m-long lines were positioned near the centre of the bar, parallel to the river, and the lithology of each pebble was recorded every 0.5 m (ref. 20). The percentage lithology numbers obtained from this survey are directly comparable to volumetric proportions, with surface and sub-surface samples typically yielding comparable results[20]. In terms of lithological identification, quartzite is sourced from all across the Himalayan mountains and, as such, it is not possible to distinguish the quartzite pebble source region from visual inspection. Therefore, quartzite pebbles were grouped into a separate lithology category. Low- to medium-grade metamorphic rocks were grouped as Lesser Himalayan, while medium- to high-grade metamorphic and igneous rocks were grouped as Greater Himalayan. No pebble that could definitively be related to the Tethyan Himalayan lithologies was found, though some quartzite pebbles are likely to be sourced from this unit. Similarly, limestone, dolostone or even very low-grade metasedimentary clasts may derive from either Tethyan or Lesser Himalayan successions. Siwalik lithologies included Neogene non-metamorphosed sedimentary rocks such as sandstone, mudstones and conglomerates that were easily distinguishable in the field. Proportions of the different lithologies at each site are shown in Extended Data Fig. 1. Only the sites downstream of the mountain front were used to produce the data in Fig. 3b.

Data availability. All data used in the production of this paper and figures are listed in the text, Methods or Extended Data Figs 1–3 and Extended Data Tables 1–3. Data presented in Fig. 2 were generated using the values listed in Extended Data Tables 1–3 and as discussed in Methods.

30. Leier, A. L., DeCelles, P. G. & Pelletier, J. D. Mountains, monsoons, and megafans. *Geology* **33,** 289–292 (2005).
31. Chakraborty, T., Kar, R., Ghosh, P. & Basu, S. Kosi megafan: historical records, geomorphology and the recent avulsion of the Kosi River. *Quat. Int.* **227,** 143–160 (2010).
32. Turowski, J. M., Rickenmann, D. & Dadson, S. J. The partitioning of the total sediment load of a river into suspended load and bedload: a review of empirical data. *Sedimentology* **57,** 1126–1146 (2010).
33. Gansser, A. *The Geology of the Himalayas* 289 (Wiley Interscience, 1964).
34. DeCelles, P. G. *et al.* Neogene foreland basin deposits, erosional unroofing, and the kinematic history of the Himalayan fold-thrust belt, western Nepal. *Geol. Soc. Am. Bull.* **110,** 2–21 (1998).
35. Kumar, R., Sangode, S. J. & Ghosh, S. K. A multistorey sandstone complex in the Himalayan Foreland Basin, NW Himalaya, India. *J. Asian Earth Sci.* **23,** 407–426 (2004).
36. Narula, P. L., Acharyya, S. K. & Banerjee, J. *Seismotectonic Atlas of India and its Environs: Calcutta* 12–26 (The Geological Survey of India, 2000).
37. Sinclair, H. D. & Naylor, M. Foreland basin subsidence driven by topographic growth versus plate subduction. *Geol. Soc. Am. Bull.* **124,** 368–379 (2012).

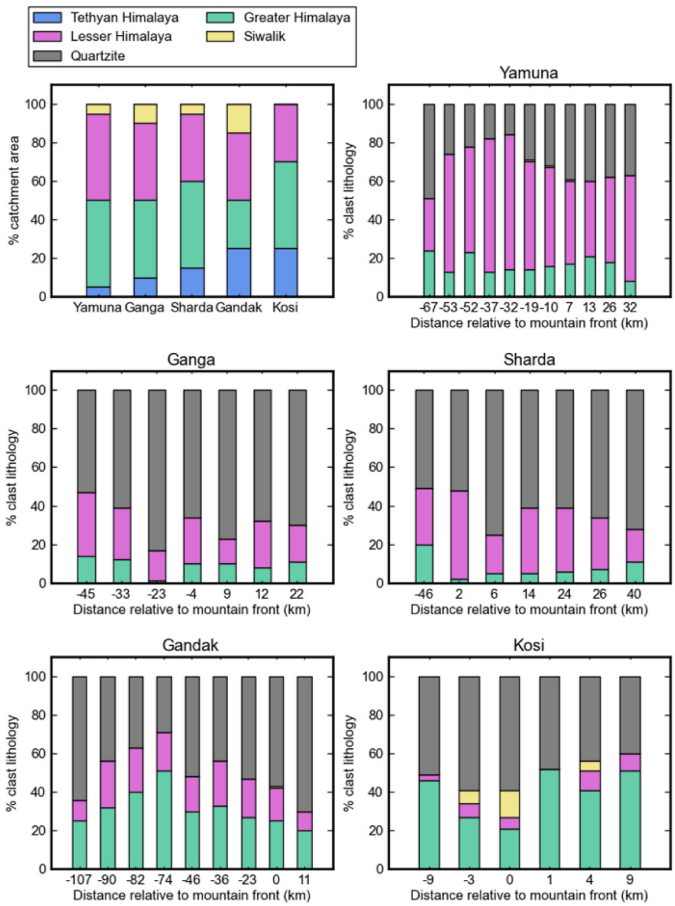

Extended Data Figure 1 | Details of pebble lithologies documented on exposed gravel bars along trans-Himalayan rivers upstream of the gravel–sand transition. Data in Fig. 3b represent an average of the sites downstream of the mountain front for each river. Note that Siwalik lithologies were found on bars sampled along the Kosi River, despite no Siwalik units being mapped in the catchment geology[21]; this is probably due to the coarse nature of the Himalayan scale geological map[21], where small outcrops may have been omitted. Distances are relative to the mountain front, so negative distances are upstream of the mountain front.

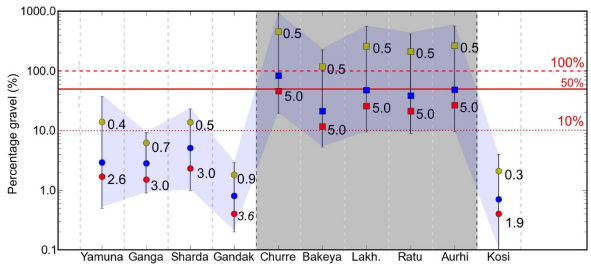

Extended Data Figure 2 | Sensitivity of gravel proportions to the position of the gravel–sand transition. Gravel proportions were calculated for instances where the gravel–sand transition was 5 km further downstream and upstream of the mapped position to test the effect on the results presented in Fig. 2b; these changes are reflected by the increased length of error bars associated with each river, but the overall patterns remain unchanged. As in Fig. 2b, gravel percentage values are estimated by dividing the flux of gravel calculated based on fan geometry and location of the gravel–sand transition by the total sediment flux from (1) catchment-averaged ^{10}Be derived erosion rates for trans-Himalayan catchments[18], and (2) a range of possible catchment-averaged erosion rates for the foothill-fed catchments[19]. Foothill-fed catchments are shaded in grey. Red, blue and yellow data points correspond to maximum, average and minimum total sediment flux scenarios, respectively, with corresponding erosion rates (in mm yr^{-1}) indicated next to data points for maximum and minimum flux scenarios for reference. Error bars reflect differences in accommodation space generated under maximum and minimum subsidence rates[17].

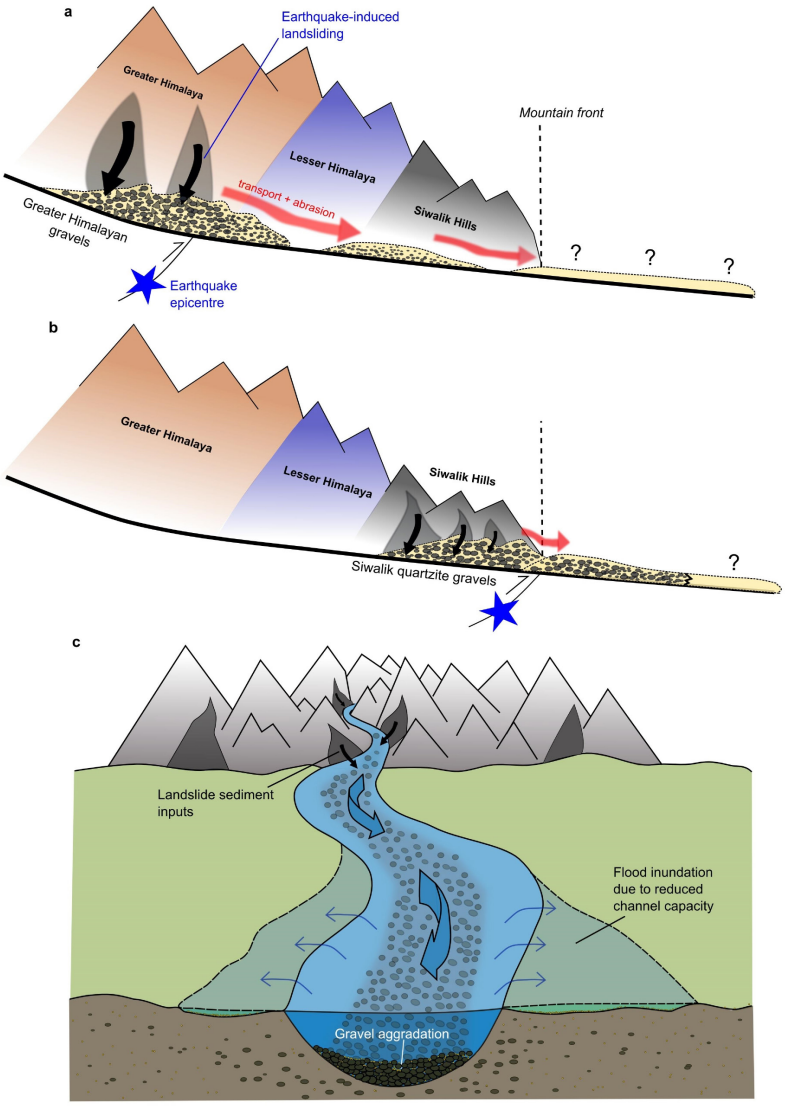

Extended Data Figure 3 | Schematic of gravel abrasion and sediment pulse delivery from the interior of the Himalayan mountains into the Ganga Plain. Schematic comparison of the evolution of coarse sediment pulses generated in the Greater Himalayas and Siwalik Hills, as a result of earthquake-induced landsliding. The magnitude and extent of the pulses as they travel downstream is unknown, as is the timescales over which the pulses migrate[27]. **a**, As the sediment pulse is translated and dispersed downstream[27], a combination of abrasion of weaker lithologies sourced in the Higher Himalayas and greater transport distances minimizes the gravel flux reaching the Ganga Plain, downstream of the mountain front. **b**, In contrast, stronger quartzite pebbles sourced from the Siwalik Hills undergo much less abrasion and, when combined with shorter transport distances, a larger gravel flux survives into the Ganga Plain when landsliding is focused closer to the mountain front. A large fraction of this gravel will probably remain trapped upstream of the gravel–sand transition, whereas more mobile sand and finer sediment (generated by the landslide inputs themselves and from the abrasion of coarser sediments) can be transported and deposited further downstream; where and when this finer sediment is deposited between the mountain front and the tip of the Bengal fan is less well understood. **c**, Where gravel flux downstream of the mountain front is enhanced, gravel aggradation could reduce channel capacity and enhance over-bank flooding. The extent of flooding is exacerbated by the low-relief topography that characterizes sedimentary basins downstream of large mountain ranges.

Extended Data Table 1 | Subsidence and fan geometries used to calculate gravel flux

Catchment	Catchment area (km^2)	Distance to transition (km)	Fan width (km)	Maximum subsidence rate (m/yr)	Average subsidence rate (m/yr)	Minimum subsidence rate (m/yr)
Yamuna	9,419	38	37	0.0007	0.0003	0.0001*
Ganga	19,666	28	44	0.0010	0.0008	0.0006
Sharda	13,182	45	51	0.0006	0.0004	0.0002
Gandak	31,460	20	18	0.0018	0.0014	0.0010
Churre	35	14	3.8	0.0022	0.0015†	0.0010
Bakeya	350	16	8.5	0.0022	0.0015†	0.0010
Lakhandei	70	11	5.5	0.0022	0.0015†	0.0010
Ratu	90	14	4.5	0.0022	0.0015†	0.0010
Aurhi	25	11	2	0.0022	0.0015†	0.0010
Kosi	50,079	13	16.5	0.0022	0.0016	0.0010

Shown is the data used to calculate gravel fluxes for each catchment. Catchment areas are derived from a 90-m Shuttle Radar Topography Mission Digital Elevation Model, while distances to the gravel–sand transition are taken from previously published works[16,17]. Fan widths were determined as outlined in Methods. Maximum, average and minimum total (tectonic plus sediment-load induced) subsidence rates beneath the mountain front were taken from ref. 17, based on depth-to-basement data derived from seismic surveys[36], and horizontal shortening rates between the Ganga Plain and the Himalaya. Given the short distances to the gravel–sand transition relative to the full width of the flexural profile that defines the basin, we do not expect a substantial decrease in subsidence rate downstream over the lengths considered[37] and therefore have not incorporated it into our calculations.

*Where the subsidence rate beneath the Yamuna was $0.3 \pm 0.4\,mm\,yr^{-1}$ (ref. 17), a minimum subsidence rate of $0.1\,mm\,yr^{-1}$ was used, given that the basin is actively subsiding.

†Where the subsidence rates beneath the adjacent Gandak and Kosi rivers were given as $1.4\,mm\,yr^{-1}$ and $1.6\,mm\,yr^{-1}$ (ref. 17), respectively, an average rate of $1.5\,mm\,yr^{-1}$ was applied to the foothill-fed catchments that lie in in the interfan region of these two trans-Himalayan systems. The maximum and minimum rates reflect the maximum and minimum subsidence estimates of the Gandak and Kosi rivers combined.

Extended Data Table 2 | Subsidence and fan geometries used to calculate gravel flux

Catchment	Minimum accommodation space (m^3/yr)	Average accommodation space (m^3/yr)	Maximum accommodation space (m^3/yr)	Minimum gravel flux (Mt/yr)	Average gravel flux (Mt/yr)	Maximum gravel flux (Mt/yr)
Yamuna	140,600	421,800	984,200	0.37	1.12	2.61
Ganga	739,200	985,600	1,232,000	1.96	2.61	3.26
Sharda	459,000	918,000	1,377,000	1.22	2.43	3.65
Gandak	360,000	504,000	648,000	0.95	1.34	1.72
Churre	53,200	79,800	117,040	0.14	0.21	0.31
Bakeya	136,000	204,000	299,200	0.36	0.54	0.79
Lakhandei	60,500	90,750	133,100	0.16	0.24	0.35
Ratu	63,000	94,500	138,600	0.17	0.25	0.37
Aurhi	22,000	33,000	48,400	0.06	0.09	0.13
Kosi	214,500	343,200	471,900	0.57	0.91	1.25

The accommodation space created per year represents the product of the fan width, distance between mountain front and gravel–sand transition, and the subsidence rate. These accommodation space values should be considered as a maximum, given that we assume that subsidence rate does not decrease with distance downstream of the mountain front, and that the entire surface of the fan is available to receive sediments (see Methods). Minimum, average and maximum gravel fluxes (in megatonnes per year) are calculated by multiplying the accommodation space generated by a density of 2.65 tonnes m^{-3}, reflecting the quartzite and quartz sand (about 15%)[17] nature of sediments trapped upstream of the gravel–sand transition.

Extended Data Table 3 | Sediment fluxes and gravel ratios

Catchment	Maximum sediment flux (Mt/yr) and erosion rate (mm/yr) in parentheses	Average sediment flux (Mt/yr) and erosion rate (mm/yr) in parentheses	Minimum sediment flux (Mt/yr) and erosion rate (mm/yr) in parentheses	Maximum gravel proportion (%)	Average gravel proportion (%)	Minimum gravel proportion (%)
Yamuna	64 (2.6)	39 (1.6)	8 (0.4)	32.6	2.9	0.6
Ganga	176 (3.0)	93 (1.8)	42 (0.7)	7.8	2.8	1.1
Sharda*	107 (3.0)	47 (1.3)	18 (0.5)	20.5	5.1	1.1
Gandak	299 (3.6)	159 (1.9)	75 (0.9)	2.3	0.8	0.3
Churre	0.46 (5.0)	0.25 (2.75)	0.05 (0.5)	668.8	82.9	30.4
Bakeya	4.55 (5.0)	2.50 (2.75)	0.46 (0.5)	171.0	21.2	7.8
Lakhandei	0.91 (5.0)	0.50 (2.75)	0.09 (0.5)	380.3	47.1	17.3
Ratu	1.17 (5.0)	0.64 (2.75)	0.12 (0.5)	308.0	38.2	14.0
Aurhi	0.33 (5.0)	0.18 (2.75)	0.03 (0.5)	387.2	48.0	17.6
Kosi	242 (1.9)	130 (1.0)	43 (0.3)	2.9	0.7	0.2

Sediment fluxes, catchment-averaged erosion rates and gravel-to-total-sediment-load proportions. Gravel-to-total-sediment-load proportions (shown as percentage of gravel proportion) were calculated using the gravel fluxes shown in Extended Data Table 2 and the total sediment fluxes are taken from the literature[17,18]. The maximum gravel proportion here reflects the scenario with the lowest total sediment flux and the highest subsidence rate or maximum accommodation space. Conversely, the minimum gravel proportion represents the scenario with the highest sediment flux and the lowest subsidence rate or minimum accommodation space.

*Erosion rate data were not available for the Sharda catchment; instead, the catchment-averaged erosion rates for the adjacent trans-Himalayan Karnali catchment[18] were used to generate sediment fluxes.

Appendix C

Appendix C

Temporal variability in detrital ^{10}Be concentrations in a large Himalayan catchment

Elizabeth H. Dingle[1], Hugh D. Sinclair[1], Mikael Attal[1], Ángel Rodés[2], and Vimal Singh[3]

[1]School of GeoSciences, University of Edinburgh, Drummond Street, Edinburgh, EH8 9XP, United Kingdom
[2]Scottish Universities Environmental Research Centre (SUERC), Rankine Avenue, Scottish Enterprise Technology Park, East Kilbride, G75 0QF, United Kingdom
[3]Department of Geology, University of Delhi, Delhi 110007, India

Correspondence to: Elizabeth Dingle (elizabeth.dingle@ed.ac.uk)

Abstract. Accurately quantifying sediment fluxes in large rivers draining tectonically active landscapes is complicated by the stochastic nature of sediment inputs. Cosmogenic ^{10}Be concentrations measured in modern river sands have been used to estimate 10^2-10^4 year sediment fluxes in these types of catchments, where upstream drainage areas are often in excess of 10,000 km^2. It is commonly assumed that within large catchments, the effects of stochastic sediment inputs are buffered such that ^{10}Be concentrations at the catchment outlet are relatively stable in time. We present eighteen new ^{10}Be concentrations of modern river and dated Holocene terrace and floodplain deposits from the Ganga River near to the Himalayan mountain front (or outlet). We demonstrate that ^{10}Be concentrations measured in modern Ganga River sediments display a notable degree of variability, with concentrations ranging between ∼9,000-19,000 atoms g^{-1}. We propose that this observed variability is driven by two factors. Firstly, by the nature of stochastic inputs of sediment (e.g. the dominant erosional process, surface production rates, depth of landsliding, degree of mixing) and, secondly, by the evacuation timescale of individual sediment deposits which buffer their impact on catchment-averaged concentrations. Despite intensification of the Indian Summer Monsoon and subsequent doubling of sediment delivery to the Bay of Bengal between ∼11-7 ka, we also find that Holocene sediment ^{10}Be concentrations documented at the Ganga outlet have remained within the variability of modern river concentrations. We demonstrate that in certain systems, sediment flux cannot be simply approximated by converting detrital concentration into mean erosion rates and multiplying by catchment area as it is possible to generate larger volumetric sediment fluxes whilst maintaining comparable average ^{10}Be concentrations.

1 Introduction

The quantity of sediment exported from large mountainous catchments is a fundamental control on downstream river morphology (Sinha and Friend, 1994; Dade and Friend, 1998; Church, 2006; Allen et al., 2013), the advance and retreat of coastlines (Syvitski et al., 2005) and the growth of deltas (Orton and Reading, 1993; Goodbred and Kuehl, 1999; Galy et al., 2007). How sediment flux varies over thousand year times scales reflects changes in upstream landscape evolution which is set by climatic and tectonic conditions in active orogenic settings (Whipple and Tucker, 2002). Quantification of sediment flux from large, tectonically active catchments is challenged by the nature of the river channels (e.g. size and access), the stochastic nature of

sediment inputs (Benda and Dunne, 1997; Kirchner et al., 2001), and highly variable water discharge regimes (e.g. Collins and Walling, 2004; Singh et al., 2005; Gitto et al., 2017). Constraining sediment fluxes at intermediate timescales of 10^2-10^4 years has been significantly improved through the development of detrital ^{10}Be cosmogenic radionuclide (CRN) analysis (e.g. Brown et al., 1995; Granger et al., 1996; Niedermann, 2002; Kirchner et al., 2001; Vance et al., 2003; Von Blanckenburg, 2005). The concentration of ^{10}Be recorded in quartz-rich river sediments is assumed to reflect the rate of upstream landscape lowering, assuming steady-state denudation averaged over the entire upstream catchment. Based on this approach, catchment-averaged denudation rates can be calculated, and converted into CRN-derived sediment fluxes which are typically averaged over hundred to thousand year timescales (Kirchner et al., 2001; Lupker et al., 2012). These timescales are a function of the landscape denudation rate (i.e. the time taken to erode to a depth equivalent to the cosmic ray attenuation length in that landscape) (Lal, 1991).

Sediment production, delivery and transport out of large mountain catchments is heavily influenced by stochastic inputs such as hillslope mass wasting generated by earthquakes or intense storms, or glacial lake outburst floods (Benda and Dunne, 1997; Hovius et al., 2000). In small catchments ($<$100 km^2) that are susceptible to such events, stochastic controls on sediment release may significantly perturb the ^{10}Be signal measured in sediment samples at the catchment outlet (Niemi et al., 2005; Yanites et al., 2009; West et al., 2014). In particular, deep-seated landslides excavate sediment from depths greater than the attenuation length of cosmic rays. This addition of ^{10}Be-poor landslide material dilutes ^{10}Be concentrations recorded in fluvial sediments sampled at the catchment outlet (Niemi et al., 2005; West et al., 2014) resulting in an over-estimation of the long-term erosion rate (Yanites et al., 2009). The timescales over which these stochastic inputs influence downstream ^{10}Be concentrations is related to the time taken to evacuate the sediment input from the impacted reach, and also depends on patterns of intermediate sediment storage and release (recycling) upstream of the sampling locality (Granger et al., 1996; Yanites et al., 2009; Blöthe and Korup, 2013; Scherler et al., 2014; Schildgen et al., 2016). However, even in regions dominated by high rates of landslide occurrence, it is commonly assumed that given sufficiently large catchment areas and sufficient sediment mixing, the imprint of mass wasting processes on ^{10}Be concentrations measured at the outlet should be negligible (Niemi et al., 2005; Yanites et al., 2009).

The gross sediment flux from the Himalaya is the largest out of any mountain range on the planet and provides fertile soils for $\sim$10 % of the global population. The vast majority of this sediment flux is sequestered in the Indus and Ganga-Brahmaputra delta and submarine fans (Lupker et al., 2011). Sediment volumes in the Ganga-Brahmaputra delta imply that overall sediment flux from these two major Himalayan river systems has halved due to the reduction in monsoon rainfall since the early Holocene (Goodbred and Kuehl, 2000; Fleitmann et al., 2007). Our current understanding of how sediment flux from tributaries of the Ganga River into the Himalayan foreland basin varies is primarily from suspended sediment and detrital ^{10}Be concentration data collected over the last 20 years (Ghimire and Uprety, 1990; Jha et al., 1993; Sinha and Friend, 1994; Vance et al., 2003; Andermann et al., 2012; Lupker et al., 2012). Suspended sediment data are generally based on a single daily measurement and are difficult to scale up spatially and temporally. Under these circumstances, ^{10}Be concentrations in modern river sands can be used to generate sediment flux estimates with the advantage of temporal and spatial averaging. However, substantial variations in ^{10}Be concentrations from repeat river sand samples at the catchment outlets of major Himalayan rivers

have been documented (Vance et al., 2003; Lupker et al., 2012). Concentrations measured on the Ganga River close to the mountain front (near Rishikesh) vary from 9.2±1.0 to 19.5±4.1 $\times 10^3$ atoms g^{-1} over a 13 year time period based on three samples (Vance et al., 2003; Lupker et al., 2012); at the Kosi River near Chatara, measurements vary between 26.7±3.4 to 54.4±2.9 $\times 10^3$ atoms g^{-1} for three samples collected in August 2007 and November 2009, respectively (Lupker et al., 2012). Measurement uncertainty on Ganga River samples record a 1σ of around 10-20 % of the measured concentration, whereas the measured variability from the repeat samples is >100 %. Similar observations were made along main stem samples on the Yamuna River, where discrepancies of up to ∼60 % between samples were observed (Scherler et al., 2014, 2015). This degree of variability could suggest that stochastic controls on sediment release may influence the ^{10}Be signal, yet this is at odds with previous modelling and analysis of large catchments which has proposed that catchments of this size should be buffered against variations in detrital ^{10}Be concentrations induced by individual hillslope events (Niemi et al., 2005).

Well preserved and dated river terraces (Srivastava et al., 2003, 2008; Sinha et al., 2010; Wasson et al., 2013) associated with the Ganga River in the west Ganga Plain present a unique opportunity to test for variations in ^{10}Be concentrations in both ancient (i.e. independently dated terrace and floodplain deposits) and modern fluvial sediments at the Himalayan mountain front. The half-life of ^{10}Be (∼1.36 Myr) implies that any post-burial decay during the last 0.01 Myr is minimal and can be accounted for, making it the ideal technique for this approach. We analyse eighteen samples of river sands from near the outlet of the Ganga River as it crosses the mountain front. Samples are taken from modern river gravel bars, recent sand deposits of the 2013 Alaknanda floods (Dobhal et al., 2013; Durga-Rao et al., 2014; Devrani et al., 2015), and dated terrace and floodplain deposits ranging in age from ∼200 to 23,500 years. Using these data, we evaluate the short-term variability in ^{10}Be concentrations and test for longer-term changes that are expected to reflect variations in the strength of the Indian Summer Monsoon (ISM) (Sirocko et al., 1993; Gupta et al., 2005; Fleitmann et al., 2007; Clift et al., 2008; Dixit et al., 2014). Motivated by the results, we examine the impact of stochastic inputs of sediment from the upstream mountain catchment on ^{10}Be concentrations close to the mountain front (herein referred to as the Ganga outlet). We conclude by combining field observations, data and numerical analyses results to synthesise potential drivers of CRN concentration variability in large tectonically active catchments.

2 Study area and context

The Ganga River is a glacially-fed perennial river rising in the High Himalaya (Fig. 1). The Ganga has two major tributaries, the Bhagirathi and Alaknanda, which join near the village of Devprayag. Further downstream, the Ganga flows through the eastern end of the Dehra Dun, an intermontane valley in the Sub-Himalaya, prior to passing through the Mohand Anticline, exiting the mountains at Haridwar before reaching the Ganga Plain (Fig. 1). This study focuses on the portion of the Ganga catchment upstream of the Himalayan mountain front, the most downstream extent of which we also term the catchment outlet. The Ganga catchment, like other Himalayan rivers such as the Marsyandi River in Nepal (Godard et al., 2012), is characterised by a number of broad geomorphic process domains. These process domains can be related to the spatial distribution of tectonic structures, glacial cover, topographic relief and climatic influences which vary across the catchment (Fig. 2).

Upstream of the mountain front, down cutting by the Ganga River has left behind a series of strath terraces cut into Lesser Himalayan or Siwalik rocks, and cut and fill terraces in Quaternary alluvial fan deposits (Sinha et al., 2010). A number of these terraces have been dated using optically stimulated luminescence (OSL) to reveal terrace ages of up to ∼14 ka (Sinha et al., 2010). During the transition from the Late Pleistocene to the Holocene, an intensification of the ISM is observed in a number of proxy records (Goodbred and Kuehl, 2000; Fleitmann et al., 2003; Dixit et al., 2014), which is believed to have driven a period of intense fluvial incision across much of the Himalaya (Sinha et al., 2010; Dixit et al., 2014). Erosion of pre-Holocene sedimentary records during this period of intensified monsoon is proposed as one mechanism to explain the notable absence of older terraces (Pandey et al., 2014). Further changes in the intensity of the ISM during the Holocene have been inferred from marine sediments in the Bay of Bengal and Arabian Sea, and speleothems from Oman and China (Denniston et al., 2000; Goodbred and Kuehl, 2000; Gupta et al., 2005; Clift et al., 2008; Dixit et al., 2014). Limited terrestrial records from the Indian subcontinent (Dixit et al., 2014) suggest a period of intensified ISM during the early Holocene in response to changes in summer insolation forcing, which is consistent with terrace formation driven by enhanced fluvial incision during the early Holocene (Gupta et al., 2005; Srivastava et al., 2008; Sinha et al., 2010; Ray and Srivastava, 2010). Mean sediment flux to the lower Ganga Plains during the period 11-7 ka is estimated to have increased by over two fold (Goodbred and Kuehl, 2000; Sinha and Sarkar, 2009), which is in good agreement with stalagmite δ^{18}O profiles in Oman which indicate a rapid increase in ISM precipitation between ∼10.6 and 9.2 ka (Fleitmann et al., 2007). Arabian Sea records further indicate an earlier period of monsoon intensification at ∼13 ka, representing the major transition between the glacial and Holocene periods, although smaller magnitude changes in climate are observed even earlier (Sirocko et al., 1993). These phases of incision during the early Holocene are punctuated by minor depositional events that form sequences of fill terraces close to the mountain front. Slip on the underlying Himalayan Frontal Thrust (HFT) produces vertical displacement rates of 4 to 6.9 mm yr^{-1} and may result in terrace abandonment (Sinha et al., 2010). During the mid-Holocene, stalagmite records in Oman and Yemen suggest that the ISM has been gradually weakening since ∼7.6 ka in response to a progressive decrease in summer insolation (Fleitmann et al., 2007). Evidence presented by Gupta et al. (2005) suggests that the ISM entered a more arid phase at ∼5 ka, although a number of abrupt events punctuate the mid to late Holocene record. For example, speleothem evidence from caves in central Nepal has suggested that between 2300-1500 yr BP there was a significant drop in monsoon precipitation (Denniston et al., 2000; Fleitmann et al., 2007). In general however, the ISM appears to have been relatively stable over the last 1.5-2 ka.

2.1 Sample information

A number of slack water and flood deposits in the Ganga valley record rapid sediment accumulation over the Ganga floodplain during high flow events in the late Holocene (Wasson et al., 2013). Seven of these flood units have been dated between ∼280 and 600 years old by OSL and calibrated with ^{14}C ages from preserved charcoal fragments (Wasson et al., 2013). These deposits are preserved in a slightly wider part of the bedrock gorge upstream of the mountain front, where flood waters would have backed up as the river enters the narrower gorge immediately downstream. Additional deposits were studied by Wasson et al. (2013) at Devprayag and Raiwala (Fig. 1) although they recorded small flood couplets as opposed to single flood event deposits. Stacked sand-silt couplets representing phases of persistent flooding were also identified between 2,500-1,200 and

320-209 yr BP at Devprayag and were attributed to changes in the spatial extent of the ISM based on geochemical evidence (Srivastava et al., 2008).

During 2013, heavy rainfall between the 15th and 17th June was centred over the Alaknanda and Bhagirati catchments and generated significant flash flooding and numerous landslides, causing notable damage to the Kedarnath region in the Alaknanda catchment (Fig. 1). A moraine dammed lake (Chorabari) had formed north west of the Kedarnath region in response to the elevated levels of snow-melt runoff in the preceding month, which is also understood to have burst on the morning of 17th June 2013, releasing water with a peak discharge estimated at 783 m^3 s^{-1} into the Alaknanda valley (Durga-Rao et al., 2014). Flash flooding is not an uncommon phenomenon in the Ganga basin; other large magnitude events were documented in 1894 and 1970 (Rana et al., 2013). Both of these flood events were attributed to the breaching of dams created by landslides on the tributaries of the Alaknanda River, following unusually high rainfall events. Sediment deposited following the 2013 floods upstream of Devprayag (Fig. 1) over-topped the 1970 flood sediment deposits (thought to be the largest flood during the last 600 years), suggesting that the 2013 flood water levels were the highest in the Alaknanada valley during at least the last 600 years (Rana et al., 2013; Wasson et al., 2013), and possibly since the Last Glacial Maximum (Devrani et al., 2015). The 2013 event also presents a rare opportunity to re-sample ^{10}Be concentrations following an extreme flood event in the modern Ganga River, to compare against pre-event concentrations as documented by Lupker et al. (2012).

3 Methods

3.1 Sample collection

Quartz-rich sand samples were taken from modern gravel bars (herein termed modern samples) and independently dated terrace and floodplain deposits (Fig. 3). ^{10}Be concentrations measured from floodplain samples are thought to accurately reflect upstream basin-averaged denudation rates if sediment residence time in the floodplain is sufficiently short to avoid additional ^{10}Be accumulation prior to burial (Gosse and Phillips, 2001; Lupker et al., 2012). In the instance of thick event beds (>2 m), sediment at the base of each bed is assumed to have been rapidly buried to a depth greater than the penetration range of cosmic rays, so will have remained shielded since burial and therefore should have accumulated minimal post-depositional ^{10}Be. In order to reduce the impact of ^{10}Be accumulation after deposition of dated terraces, sediment samples were collected from the base of thick beds (> 1 m) that record individual flood events either as overbank fines, or as channel braid bars (Wasson et al., 2013). At least 2 kg of quartz-rich sand was sieved from the base of event beds. All samples were collected following horizontal digging for ∼1 m into steep cuts through the deposits to minimise post-burial CRN production. CRN concentrations from terrace and floodplain samples were corrected for post-depositional ^{10}Be accumulation by considering that the samples had been exposed to cosmic radiation since deposition at the same depth as they were sampled from. For the slower, long-term sedimentation rates of ∼2 mm yr^{-1} in the older early Holocene terraces, only samples from the base of very thick-bedded (>1-2 m) gravels were used to minimise post-depositional effects, where it is assumed that samples would have been largely shielded from further CRN production. Sample depths and post-depositional corrections are presented in Table 1. Sand was taken from

the base of several metre thick sand deposits (RFLO and DV2013) abandoned following the summer 2013 Alaknanda flood event to evaluate the degree of mixing of sand during a single extreme event.

3.2 Sample preparation and analysis

Floodplain, terrace and modern river sand samples were first dried before sieving into a number of grain size fractions. The main grain size fraction of interest in this study is 250-500 μm. Samples with sufficient material in the 250-500 μm fraction were then passed through a horizontal Frantz to remove magnetic minerals. Samples were also supplemented with material from the 125-250 μm grain size fraction where there was insufficient material in the 250-500 μm fraction. Following this procedure, samples were put through repeated dissolutions in aqua regia and diluted HF and HNO_3 solutions to remove mineral phases other than quartz. Quartz samples were then etched with HF to remove between 30 and 50 % of their volume. The purity of the clean quartz cores were then tested by ICP-OES. All the Al concentrations in the quartz cores were below 300 ppm. Between 7 and 30 g of quartz cores were dissolved in concentrated HF. Samples were spiked with c. 220 μg of a ^{9}Be carrier produced in the cosmogenic isotope analysis facility at the Scottish Universities Environmental Research Centre (SUERC) from phenakite crystals. The ^{10}Be carrier concentration is c. 9 $\times 10^{-16}$ ^{10}Be/^{9}Be. A procedural blank was prepared together with each group of samples. Be was isolated from the solutions following routine column chemistry (Darvill et al., 2015). ^{10}Be/^{9}Be ratios of the produced BeO targets were measured with the 5 MV Pelletron AMS at the SUERC (Xu et al., 2010). ^{10}Be data were calibrated against the National Institute of Standards and Technology standard reference material NIST SRM 4325. The activity of NIST SRM 4325 corresponds to a nominal ^{10}Be/^{9}Be ratio of 2.79 $\times 10^{-11}$ for a ^{10}Be half-life of 1.36 $\times 10^{6}$ years. The processed blank ratios ranged between 4 and 54 % of the sample ^{10}Be/^{9}Be ratios. The uncertainty of this correction is included in the stated standard uncertainties.

3.3 Denudation rate calculations

Catchment-averaged denudation rates were calculated for each sample using the CAIRN method (Mudd et al., 2016), which estimates production and shielding factors on a pixel-by-pixel basis, rather than a catchment-averaged shielding factor as in more commonly used CRN analysis packages such as CRONUS (Balco et al., 2008). Snow shielding was determined for the Ganga catchment using data downloaded from the Global Land Ice Measurements from Space (GLIMS) Glacier Database (Armstrong et al., 2005); production rates beneath snow covered areas were assumed to be zero. The GLIMS data suggest that $\sim$14 % of the Ganga catchment is glaciated (Fig. 1), which is $\sim$12 % higher than estimates in Lupker et al. (2012) which were produced prior to the completion of the GLIMS database in this region. The proportion of catchment glacier cover is likely to have been notably higher during the early Holocene, and as such, production rates may have been lower when averaged over the full catchment. We therefore consider the production and erosion rates calculated for ancient deposits as maximum values.

4 Results

The ^{10}Be concentrations of the two modern samples near the mountain front (GAPUB and RAEM) are 17.70 and 15.53 $\times 10^3$ at g^{-1}, respectively. When combined with sample BR924 from (Lupker et al., 2012) which was similarly collected near the mountain front, an average concentration of 14.1 $\times 10^3$ at g^{-1} is estimated for modern samples. The concentration of modern sample BGM taken from further upstream of the Alaknanda-Bhagirathi confluence is 13.56 $\times 10^3$ at g^{-1} which is comparable to the average modern concentration of samples close to the mountain front which integrates the full Bhagirathi catchment. ^{10}Be concentrations of the majority of samples, both from ancient terraces and recent flood deposits, largely fall within the error of modern detrital samples (Fig. 4 and Table 1). Only three samples (BG1.8, DVDF and CDT4) display ^{10}Be concentrations considerably greater than the upper error bound (19.1 $\times 10^3$ at g^{-1}) of modern river samples; the average concentrations of these terrace samples are in excess of 20 $\times 10^3$ at g^{-1}. Only one sample, DVTT2, has an average concentration (6.66 $\times 10^3$ at g^{-1}) notably below the lower error bound of the modern samples (8.20 $\times 10^3$ at g^{-1}). Samples taken from flood deposits associated with the 2013 Alaknanda flood (DV2013 and RFLO) reveal concentrations of 16.06 and 12.85 $\times 10^3$ at g^{-1}, respectively, which fall well within the error of modern river sediment samples.

In a frequency-histogram of ^{10}Be concentration data (Fig. 5a), the three samples with the highest concentrations (BG1.8, DVDF and CDT4) produce a positively skewed distribution. These samples represent a fine grained ∼300 year flood deposit (Wasson et al., 2013), ∼10,000 year old terrace fill (Srivastava et al., 2008) and ∼11,000 year old terrace fill (Sinha et al., 2010), respectively (See Appendix B for further sample details). With the removal of samples BG1.8 and CDT4 from the frequency-histogram, the ^{10}Be concentration data generate a near-normal distribution (Fig. 5a).

Results from CAIRN modelling of all concentrations suggest that catchment-averaged denudation rates for each sample largely lie within the error of modern detrital samples (Fig. 5b). Based on the measured concentrations, these samples correspond to integration timescales of ∼500 years, representing the average time period when the erosion rate is considered to be constant, based on the time needed to erode one mean attenuation path length (approximately 60 cm/erosion rate) (Lal, 1991). There does not appear to be a spatial trend between ^{10}Be concentration and upstream catchment area, even downstream of large tributary confluences (Fig. 6). The impact of high CRN concentration samples on the frequency-histogram of erosion rates calculated using CAIRN modelling is less apparent (Fig. 5b), but the distribution shows significant spread. Calculating sediment flux estimates from a single erosion rate at the upper end of the distribution could result in sediment flux estimate being up to seven times larger than one based on a sample at the lower end of the distribution.

5 Impact of stochastic inputs on CRN variability and sediment flux estimates

5.1 CRN sample interpretation

Possible explanations for the high concentration measurement at BG1.8 may include insufficient shielding since deposition, resulting in ^{10}Be enrichment of the deposit. Unlike other samples analysed here, the event bed associated with this sample was only ∼0.5 m thick so burial (and therefore complete shielding) was unlikely to be instantaneous. Whilst a number of

additional samples were taken from this exposure to try and produce depth-concentration profiles, their grain size was too fine for CRN analysis. However, the maximum CRN enrichment at the site during burial is likely to only be $\sim$1650 atoms g^{-1} based on local CRN production rates and sample depth, which is less than the measurement uncertainty. With respect to the two terrace deposits (DVDF and CDT4), high concentrations could also have been produced if the samples were overwhelmed by locally derived, high concentration hillslope sediment which was not well mixed. Samples with the largest CRN concentration variability also seem to focus around 10-15 ka (Fig. 4), which may represent a period of post-glacial conditions where a combination of low CRN concentration material (generated by glacial erosion) and high CRN concentration sediment (due to lower precipitation rates and therefore slower erosion of non-glaciated landscapes) generated during the Last Glacial Maximum may have been mobilised as the ISM intensified during the early Holocene.

5.2 Impact of landslides on CRN variability

A range of processes are likely to drive temporal variability in CRN concentrations in sand sampled close to the outlet of large Himalayan catchments. The most obvious process is stochastic inputs generated by mass wasting of hillslopes, which generate large quantities of sediment with relatively low CRN concentrations. Frequency-histograms presented in Figure 5 suggest that such stochastic processes may form part of the natural background variability, as low concentration values tend not to skew the distributions. More samples would be needed to draw a clearer picture on this. Below, we examine how different erosional processes may drive the types of temporal variability in CRN concentrations measured close to the Ganga outlet. This is approached using a numerical analysis of catchment-averaged CRN concentrations derived under varying background erosion rates, landslide depth, surface CRN production rates and degrees of event buffering (i.e. varying proportions of 'event' sediments are mixed into the fluvial network). Given the complexity of this type of landscape (e.g. multiple geomorphic process domains, climatic variability), we do not attempt to mimic these processes and reproduce measured concentrations or erosion rates (e.g. Niemi et al., 2005). Neither do we use this analysis to determine the relative contributions required from stochastic processes (e.g. area and depth of landsliding) to produce our observed concentrations. Instead, this numerical analysis is used to explore the sensitivity of outlet CRN concentrations to a range of parameters and scenarios that may drive variability. The analysis considers the impact of a single sediment generating event, as opposed to the evolution of catchment-averaged concentrations which occur in response to a distribution of landslides occuring over timescales of hundreds to thousands of years across a landscape (e.g. Niemi et al., 2005; Yanites et al., 2009).

The relative ^{10}Be contribution by landsliding can be approximated to first-order by calculating the volume of material generated by the event, and the average concentration of that material. The concentration of landslide material is strongly controlled by the local surface CRN production rate and depth of the landslide. CRN production rates rapidly diminish in the upper few metres of the Earth's surface (Lal, 1991; Stone, 2000; Niedermann, 2002) following:

$$P(z) = P_0 e^{(\frac{-z\rho}{\Lambda})} \quad (1)$$

where z is the depth below the surface (cm), Λ is the attenuation length (g cm^{-2}), ρ is rock density (g cm^{-3}), and P_0 is the surface nuclide production rate (atoms g^{-1} yr^{-1}). At depths greater than $\sim$2 m the CRN production rate (by spallation reactions) is negligible, as is muon production, as atoms generated by muon interactions represents a small proportion relative to those produced by spallation reactions in the upper 1-2 m of the Earth's surface (e.g. Niedermann, 2002). Here, we calculate the average concentration of landslide material by integrating the surface production rate within the upper 2 m; we find that the depth-averaged production rate of the upper 2 m (P_d) is $\sim$30 % of P_0. This was converted into a ^{10}Be concentration (C) in atoms g^{-1} using:

$$C = \frac{(P_d \Lambda)}{\rho(\epsilon + \Lambda\lambda/\rho)} \tag{2}$$

from Niedermann (2002), where we assume that the CRN decay constant (λ) is equal to 0 over the timescales we are concerned with ($<10^3$ years) relative to the half-life of ^{10}Be. We use ρ = 2.7 g cm^{-3} and Λ = 160 g cm^{-2}. We also assume a steady-state erosion-rate (ϵ) across the upstream catchment. For landslide depths of less than 2 m, the average concentration was calculated based on the production rate integral specific to that depth. For simplicity, we initially assume that the rest of the catchment is eroding uniformly at a background erosion rate, with a catchment average CRN production rate of 35 atoms g^{-1} yr^{-1} which is comparable to the catchment-averaged production rate calculated for the Ganga catchment in CAIRN. The concentrations calculated at the Ganga outlet also assume complete sediment mixing. The CRN concentration at the catchment outlet ($\alpha_{event+uniform}$) is then calculated using:

$$\alpha_{event+uniform} = \frac{(\alpha_{uniform}\phi_{uniform}) + (\alpha_{event}\phi_{event})}{\alpha_{uniform} + \alpha_{event}} \tag{3}$$

where $\phi_{uniform}$ and $\alpha_{uniform}$ are the background sediment flux and ^{10}Be concentration, respectively. ϕ_{event} and α_{event} are the event or landslide generated sediment flux and ^{10}Be concentration, respectively. A series of sub-catchments were then selected to examine the influence of spatial variability in surface production rates across the Ganga basin, to provide a realistic range of values in the numerical analysis (Fig. 7). Average shielding factors (snow and topographic shielding) were first calculated for each of these sub-catchments using the CAIRN method (Mudd et al., 2016), which were then used in the online CRONUS v2.3 calculator (Balco et al., 2008) to calculate production rates, using a constant production rate model with a Lal/Stone scaling scheme for spallation (Fig. 7 and Table 2). The default landslide surface production rates were initially set to the same as the catchment-average production rate. The landslide surface production rates were then varied based on realistic production rates derived from sub-catchments across the Ganga catchment (Table 2). Earthquake-induced landsliding datasets from the 1999 Chi-Chi (Taiwan) and 2015 Gorkha (Himalaya) earthquakes (Lin and Tung, 2004; Martha et al., 2017; Roback et al., 2018), state that the total landslide areas were $\sim$128 and 87-90 km^2, respectively. Areas of these sizes represent approximately 0.5 % of the Ganga catchment area. We therefore use the value of 0.5 % as an approximation of the proportion of the hypothetical catchment to have been impacted by landsliding. In the analysis, the average depth of the landslides was varied from 0.5 to 5 m, the average background erosion rate from 0.2 to 2.0 mm yr^{-1}, and the average landslide surface production rate from

10 to 60 atoms g^{-1} yr^{-1}. We use an average landslide depth where in reality, the depths of individual landslides occurring in response to an earthquake or intense storm are likely to fit a power-law distribution (Hovius et al., 1997). However, at any point in time it is unlikely that the full power-law distribution of landslide depths is sampled or integrated into the catchment wide signal, due to the recurrence interval and amount of time taken to evacuate larger and deeper co-seismic landslides. Sediment generated by inter-seismic landsliding is assumed to be represented in the background erosion rate imposed across the catchment, whilst the sediment generated by the landslide event is assumed to reflect a large co-seismic event (i.e. the tail-end of landslide-frequency distribution). We also assume that the CRN concentration profile in the upper 2 m of the landscape is in steady-state before landsliding. This assumption is more important in slowly eroding landscapes, where it may take tens of thousands of years to reach secular equilibrium (Dunai, 2010). This may result in over-estimated landslide CRN concentrations in our analysis, if the CRN concentration profile is not in equilibrium. Similarly, landsliding is more likely to occur in parts of the landscape undergoing faster erosion rates where above a certain hillslope gradient, erosion rate becomes less closely correlated (to hillslope gradient) as the main mechanism of erosion changes from transport-limited to detatchment-limited processes (Binnie et al., 2007). It might therefore be expected that these regions have initially lower CRN concentrations. By varying the landslide surface production rates in our analysis, we indirectly assess the importance of such effects.

We calculate 'volumetric sediment flux' by combining the flux derived from background erosion rates with the calculated landslide flux, and compared these to sediment flux estimates derived from the ^{10}Be concentration at the catchment outlet (which we term the 'CRN-derived sediment flux'). For a catchment eroding at a uniform rate (ϵ in mm yr^{-1}), the CRN-derived sediment flux is the product of the erosion rate, catchment area (A in km^2) and average rock density (ρ in kg m^{-3}).

In this analysis, we assume that sediment storage between the region affected by landslides and the outlet is small relative to the total sediment flux of the catchment. Unlike the eastern and western Himalaya, the central Himalaya (which is largely drained by tributaries of the Ganga River) is comparatively void of large valley fills (Blöthe and Korup, 2013), which is likely to limit large volumes of sediment storage and sediment residence times. Recent modelling has also suggested that approximately 50 % of coarse material generated by post-seismic landsliding is evacuated within 5 to 25 years (Croissant et al., 2017). In our scenarios, we initially assume complete evacuation of material to the outlet within a year. We then run additional analysis where much smaller proportions of the event material are mixed into the fluvial network in this first year (3, 5, 10 and 20% of the event sediment). The default and range of values tested for each parameter in the analysis are shown in Table 3.

Based on the above calculations, our results suggest that increasing the average landslide depth results in a marked decrease in outlet ^{10}Be concentration, most notably between depths of 0.5-3 m (Fig. 8a). This can be explained through the exponential decay in ^{10}Be production rates in the upper 2 m of the landslide (Lal, 1991; Stone, 2000; Niedermann, 2002). This reduction in concentration is greatest under lower background erosion rates. Increasing background erosion rates from 0.2-2.0 mm yr^{-1} also reduces the effect of landsliding on outlet ^{10}Be concentrations (Fig. 3b). Under lower background erosion rate, landslide material represents a greater proportion of the total sediment flux, so the system has less capacity to buffer the landslide input and the ^{10}Be concentration is more sensitive to deeper landslides. We also find that outlet ^{10}Be concentrations are sensitive to the average landslide surface production rate. Where the average surface production rate of the landsliding is increased (e.g. comparable to that expected in high altitude sub-catchments of the Ganga - see Table 2), predicted outlet ^{10}Be concentrations

also increase relative to scenarios with otherwise identical parameter values (Fig. 8c). Interestingly, we also find that volumetric sediment flux estimates are consistently higher than CRN-derived fluxes (Fig. 8d). Increasing background erosion rates increases both CRN-derived and volumetric sediment flux estimates, but increasing average landslide depth or landslide CRN production rate can reduce CRN-derived sediment flux estimates to a much greater degree than volumetric flux estimates.

By reducing the landslide surface production rate to mimic the effects of faster erosion rates in regions more prone to landsliding and landscapes without steady-state concentration profiles, the absolute range of outlet CRN concentration variability in notably reduced from a maximum of $\sim$70,000 (in Fig. 8a) to 20,000 atoms g^{-1} under the lowest background erosion rate scenarios (Fig. 9a). This range of outlet CRN variability is more comparable to that observed at the Ganga outlet. Furthermore, the difference in volumetric and CRN-derived sediment fluxes is also reduced (Fig. 9b). By reducing the proportion of event sediment mixed into the fluvial network, similar reductions in the amount of CRN concentration variability generated at the outlet are also observed (Fig. 10a). Under faster background erosion rates (2.0 mm yr^{-1}, the variability generated by events of all depths can be effectively masked by background variability where only 10% of the event sediment is mixed in (i.e. such that the outlet concentration lies within 100% of the maximum value). Similarly, under lower background erosion rates of 0.6 mm yr^{-1}, the fraction of event sediment needed to generate variability within 100% of the highest concentration is slightly lower at 3%.

Our analysis generates variability in CRN concentrations that is considerably larger than what we document in the Ganga catchment (Fig. 4), suggesting that buffering of stochastic inputs must occur (Croissant et al., 2017). The evacuation time of fine-grained sediment (sand and finer) is likely to be fast relative to the coarse fraction, as the fine-grained fraction is annually entrained and transported downstream during months impacted by the ISM. This is supported by grain size analysis (Dingle et al., 2016) along a number of exposed gravel bars within the Ganga catchment, which demonstrate that the channel bed is comprised largely of grain sizes $>$1 mm, even beneath the surface armour layer. Typically, grain sizes $<$1 mm represent less than $\sim$15 % of the grain size distribution (Fig. 11) which is also observed across other catchments of the Ganga River. This suggests that there is relatively little in-channel storage (or mixing) of finer grained sediments relative to the large fluxes of these river systems, which on entering the Ganga Plain, are thought to be largely dominated ($>$90 %) by sand-sized (and finer) sediments (Dingle et al., 2017). However, the majority of landslide deposits are likely to be made of coarser material (Attal and Lavé, 2006; Attal et al., 2015) which will take longer to be evacuated or abraded into smaller and more easily transportable grain sizes. Whilst landsliding may generate the quantities and ^{10}Be concentrations of sediment required to drive significant changes in concentration at the outlet, the evacuation timescales of these event sediments buffers their impact. Evacuation of event deposits over decadal to centennial timescales will reduce the ratio of background to event sediment fluxes (Croissant et al., 2017), and likely limit the impact on ^{10}Be concentrations documented at the outlet.

5.3 Other potential sources of variability in CRN concentration

Whilst landsliding with different depths and from different parts of the Ganga catchment is likely to represent a key component in CRN variability, a number of other factors may also contribute, which are discussed below. Firstly, spatially variable distributions of quartz-rich lithologies across the Ganga catchment may lead to over and under-estimation of denudation rates

in specific lithological settings. However, potential variations in sediment quartz content have been assessed by Vance et al. (2003) in the Ganga catchment, who concluded that the correction due to the dilution of quartz from sediments sourced from carbonate-rich series in the catchment is of a similar magnitude (maximum of ∼9 % change in erosion rate for sub-catchments in the High Himalaya) to the production rate estimates and analytical errors. Recent studies have also highlighted the effect of grain-size dependent ^{10}Be enrichment, where coarser gravel-sized fractions have been documented to yield higher apparent denudation rates than the medium sand-sized fraction which is typically sampled (Puchol et al., 2014; Schildgen et al., 2016; Lukens et al., 2016) as a result of the process through which the different grain size fractions are generated (e.g. reworked hillslope material, landsliding), or differing sediment source elevations. Similarly, downstream lags in ^{10}Be denudation rate spikes have been observed along the Tsangpo-Brahmaputra River in the eastern Himalayan syntax (Lupker et al., 2017), due to the distance which sediment generated in the rapidly uplifting Namche Barwa-Gyala Peri massif must travel before being abraded into the grain size fraction used for sampling. However, modern samples collected close to the Ganga outlet are not likely to be influenced by either process, as the majority of sediment has already been abraded into sand by this point (Dingle et al., 2017). Similarly, a number of the floodplain and terrace deposits sampled were entirely sand. Exceptions to this include terrace deposits CDT3, CDT4, DVDF, DVMT2, DVTT2 and RLB, where sand samples were taken from poorly consolidated fluvial deposits containing imbricated and well-rounded quartzite cobbles and pebbles. However, additional CRN samples were not run on individual clasts in these deposits to determine whether the coarser fraction yielded higher apparent denudation rates.

Glacial lake outburst floods (GLOFs) are not uncommon across the Himalaya (e.g. Cenderelli and Wohl, 2003; Kattelmann, 2003), and have the potential to generate and mobilise large quantities of sediment. Geomorphic analysis following the 1977 and 1985 GLOFs in the Mount Everest region (Cenderelli and Wohl, 2003) suggested that much of the sediment eroded from the upper 10-16 km of the GLOF route was unconsolidated sediment (glacial till, colluvium, glacio-fluvial terraces). Erosion was typically found to be limited in valleys with resistant bedrock or consolidated side walls. Similarly, the availability of unconsolidated material is also thought to be a key limiting factor in the volume of debris flows triggered following GLOFs, which can limit the erosive potential of the flow (Breien et al., 2008). In the absence of existing studies which document ^{10}Be concentrations in proglacial lake sediments, we cannot infer how sediment released from the glacial lake may contribute to downstream variations in ^{10}Be concentration. Geomorphological evidence in reaches downstream of GLOFs suggests that much of the sediment eroded by the flood is largely unconsolidated (glacially-influenced) material from relatively shallow depths (<3 m; Cenderelli and Wohl, 2003) which is likely to have a complex exposure history. Given the relatively short length of the reach impacted downstream of the GLOF (relative to the full length of a system such as the Ganga), and the likely CRN enriched nature of surface deposits reworked by GLOFs, it seems unlikely that these types of events drive significant change in outlet ^{10}Be concentrations. This is supported by work in the Marsyandi River catchment in Nepal, which suggested that localised erosion in the upper glaciated catchment is almost an order of magnitude lower than fluvial incision rates in the upper Marsyandi River (Heimsath and McGlynn, 2008). An analysis of the evolution of detrital ^{10}Be concentrations along the Marsyandi River suggested that low concentration ^{10}Be inputs from glaciated tributaries dilute main stem ^{10}Be concentrations (Godard et al., 2012). In this instance, glacial erosion was averaged at ∼5 mm yr^{-1} in the High and Tethyan Himalayan portions

of the catchment, suggesting that glacially derived sediments may complicate detrital CRN concentrations and interpretation of catchment-averaged denudation rates.

Extreme monsoonal storms, such as the one that generated the 2013 Alaknanda flooding, also have the potential to generate CRN variability if hillslope runoff mobilises large quantities of unconsolidated sediment on valley sides and initiates mass-wasting of hillslopes (Dobhal et al., 2013; Devrani et al., 2015). Sample DV2013 was collected from a thick sand unit at the Ganga channel margins (∼18 m above the modern channel) near Devprayag, known locally to have been deposited following the 2013 Alaknanda flood. We find that the ^{10}Be concentration of this deposit (16.06 $\times 10^3$ at g^{-1}) also lies within the error of modern samples at the outlet. One interpretation is that the sediment generated by this event was sufficiently well mixed: on reaching the Ganga outlet it had minimal impact on the outlet CRN concentration. Material mobilised by the Alaknanda flooding was largely unconsolidated, surficial hillslope material (Dobhal et al., 2013). As such, the ^{10}Be concentration of these sediments will reflect their local production rate (∼50 atoms g^{-1} yr^{-1} - see Table 2) and background erosion rate. If erosion in the Alaknanda valley is driven primarily by large storm and flood events, unconsolidated surface sediments could have been accumulating ^{10}Be since as early as the LGM (Devrani et al., 2015), with very low background erosion rates. As such, this type of erosive event may have generated sediment with a higher than expected CRN concentration (given the depth of material removed) as a result of this CRN-enriched surface layer.

Annual monsoonal storms may also contribute to the observed variability where storms tap into localised parts of the catchment. The hillslope sediments and reworked deposits these storms mobilise could vary in ^{10}Be concentration in the different geomorphic process domains, as they will have variable CRN production rates (which is a function of elevation), background erosion rates and deposit characteristics (e.g. deep-seated landslide). Background erosion rates in particular are likely to vary dramatically across the Ganga catchment as a result of spatially variable rock uplift, lithology, rainfall and vegetation cover (Vance et al., 2003; Anders et al., 2006; Bookhagen and Burbank, 2006). Earthquake-induced landsliding, GLOFs and extreme storm events are all likely to generate large quantities of sediment with ^{10}Be concentrations that would be sufficient to drive significant change in the ^{10}Be concentration recorded at the Ganga outlet. However, the impact that these processes have is limited by the ability of the river to entrain and transport this sediment out of the catchment. The evacuation timescales of sediment generated by these processes will likely vary as a function of the frequency and magnitude of localised storm events which mobilise mass-flow deposits from hillslopes into rivers sediment.

If this sediment is sourced close to the sampling location, it is also unlikely to be fully homogenised. The distance required to fully mix localised hillslope or tributary inputs has been shown to be as much as several kilometres (Binnie et al., 2006), which may induce variability in ^{10}Be concentrations recorded at the outlet. In terms of modern river samples, a number of small ephemeral streams drain directly in the main Ganga channel near the outlet. During the monsoon season when these channels are active, sediment of differing ^{10}Be concentrations will be transported to the main channel and may not be sufficiently mixed on reaching the outlet sampling locations. High concentration samples documented close to the Ganga outlet could therefore represent locally derived and poorly mixed sediments, which reflect the erosional processes specific to a small frontal region of the catchment.

5.4 Suitability of CRN as a proxy for sediment flux in large catchments

Our analysis of outlet CRN concentrations suggests that the observed doubling in sediment delivery to the Bengal fan during the early Holocene may have been masked by the natural variability in palaeo-erosion rate or CRN concentration data preserved close to the Himalayan mountain front. Whilst changes in the amount of sediment being delivered into the fluvial network may have occurred, the natural variability in CRN concentrations delivered to the mountain front is sufficiently high that a doubling in volumetric flux (and therefore catchment-averaged erosion rate) cannot be clearly identified using detrital sampling.

Our results suggest that, for ^{10}Be concentrations within a natural degree of system variability, the volumetric sediment flux could theoretically differ from that calculated directly from ^{10}Be concentrations (Fig. 8d and Table 3). Similar outlet CRN concentrations could be derived from landscapes dominated by different erosional processes within large catchments. For example, our analysis suggests that a 'fast eroding' landscape experiencing a background erosion rate of 2.0 mm yr^{-1} and 1 m deep landslides over 0.5 % of the catchment (e.g. a landscape dominated by shallow landsliding or debris flows) could produce comparable outlet CRN concentrations to a 'slow eroding' landscape experiencing 0.4 mm yr^{-1} background erosion and 5.0 m deep landslides over the same area (e.g. a landscape experiencing deep earthflows) (Fig. 12). The CRN-derived sediment fluxes between these two landscapes may be comparable, but the volumetric flux from the landscape with lower background erosion (and deeper landsliding) is considerably larger than from the landscape with higher background erosion (and shallower landsliding). Halving the area affected by landsliding in only the lower background erosion scenario (with deeper landsliding) still yields comparable CRN-derived fluxes (within 15 % of each other, rather than 6 %), but the volumetric flux is double that generated under higher background erosion rates (with shallower landsliding over a larger area) . These types 'slow eroding' landscapes which experience episodes of mass wasting are exemplified by arid parts of the northwest Himalaya, which generally only experience high intensity rainstorms during abnormal monsoon years where the ISM can penetrate north of the orographic barrier formed by the Higher Himalaya (Bookhagen et al., 2005) (Fig. 2). Similarly, slow moving earthflows in parts of the Eel River catchment in California which is characterised by long and low-gradient hillslopes mobilise huge quantities of sediment which contribute to the majority of the suspended sediment flux from the catchment (Mackey and Roering, 2011). The two end-member models presented in Figure 12 suggest that under different geomorphic process domains, comparable mean CRN concentrations can be produced through different CRN concentration populations.

CRN-derived sediment fluxes are based on an average landscape lowering rate, and thus fail to incorporate the effects of spatially limited deeper inputs of sediment which are characterised by much lower CRN concentrations. Lower rates of background erosion means that sediment eroded off the surface is enriched in CRN (as sediment residence times in the upper 1-2 m of the Earth's surface are longer as a function of lower background erosion rates). This effectively averages out the influence of lower concentration input from deeper inputs, and results in near identical CRN concentrations at the mountain front to a system undergoing only a slightly faster (or more uniform) rate of background erosion. Thus, considerably different volumetric fluxes can be obtained for the same CRN concentration. However our analysis has also shown that spatially variable erosion rates and event buffering can alter this relationship, such that CRN-derived and volumetric sediment fluxes can be comparable. Furthermore, under particular conditions it is possible to generate systems where the effects of large sediment

generating events are lost within the natural variability of the system. This may explain the absence of a ^{10}Be concentration signature of Holocene climate change.

6 Conclusions

We present CRN analysis from a variety of modern and Holocene sedimentary deposits in a large trans-Himalayan catchment spanning more than 7000 m in relief, where sediment production is heavily influenced by stochastic inputs. We find a natural degree of variability in ^{10}Be concentrations documented in the modern channel and Holocene flood deposits preserved near the catchment outlet. These concentrations appear insensitive to regional intensification of the ISM, thought to have occurred ∼11-7 ka. We suggest that the observed variability is driven by 1) the nature of the stochastic inputs of sediment (e.g. the type of hillslope process, surface CRN production rates, degree of mixing), and 2) the evacuation timescales of these sediment deposits. Sediment deposits generated by processes such as earthquake-induced landsliding, GLOFs or storm events, are typically large in volume and low in ^{10}Be concentration, but the time taken to mobilise this sediment out of the catchment limits its impact on catchment-averaged concentrations. We suggest that in landscapes characterised by high topographic relief, spatially variable climate and multiple geomorphic process domains, the use of ^{10}Be concentrations to generate sediment flux estimates may not be truly representative, as comparable mean catchment CRN concentrations can be derived through dramatically different erosional processes. For a given CRN concentration, volumetric sediment flux estimates may vary and under certain conditions, CRN concentrations may under-estimate actual erosion rates and hence sediment flux.

Code and data availability. The CAIRN software used to calculate erosion rates is available at the LSDTopoTools Github wesite ($http://github.com/LSDtopotools$) with accompanying documentation ($http://lsdtopotools.github.io/LSDTT\_book/$). The DEM used in this analysis (Shuttle Radar Topography Mission 30 m resolution) is freely available from the United States Geological Survey digital globe website ($http://earthexplorer.usgs.gov/$). Full CRN sample details are provided in Table 1 and text within the manuscript. The equations and parameter values used in the numerical analysis are available in the manuscript text and as a python script at $http://github.com/LizzieDingle/CRN_landslides$.

Author contributions. E.H.D., H.S., M.A. and V.S. collected the samples used in the cosmogenic radionuclide analysis, which A.R. and E.H.D. prepared for analysis at SUERC. E.H.D. designed and carried out the numerical analysis. E.H.D. produced the figures and wrote the manuscript with discussions and contributions from H.D.S., M.A., and A.R.

Competing interests. The authors declare that they have no conflict of interest.

Acknowledgements. Elizabeth Dingle is funded under a NERC PhD Studentship (NE/L501566/1) and CRN analysis was undertaken at the SUERC CIAF (under grant application 9150.1014). We would like to thank the International Association of Sedimentologists, British Society of Geomorphology and the Edinburgh University Club of Toronto for their financial support of the fieldwork, and Konark Maheswari for his assistance in the field. We thank Shasta Marerro and Simon Mudd for helpful discussions during the writing of this manuscript. We are also grateful to Maarten Lupker and an anonymous reviewer for comments that have greatly improved this manuscript.

References

Allen, P. A., Armitage, J. J., Carter, A., Duller, R. A., Michael, N. A., Sinclair, H. D., Whitchurch, A. L., and Whittaker, A. C.: The Qs problem: sediment volumetric balance of proximal foreland basin systems, Sedimentology, 60, 102–130, 2013.

Andermann, C., Crave, A., Gloaguen, R., Davy, P., and Bonnet, S.: Connecting source and transport: Suspended sediments in the Nepal Himalayas, Earth and Planetary Science Letters, 351, 158–170, 2012.

Anders, A. M., Roe, G. H., Hallet, B., Montgomery, D. R., Finnegan, N. J., and Putkonen, J.: Spatial patterns of precipitation and topography in the Himalaya, Geological Society of America Special Papers, 398, 39–53, 2006.

Armstrong, R., Raup, B., Khalsa, S., Barry, R., Kargel, J., Helm, C., and Kieffer, H.: GLIMS glacier database, National Snow and Ice Data Center, Boulder, Colorado, USA, 2005.

Attal, M. and Lavé, J.: Changes of bedload characteristics along the Marsyandi River (central Nepal): Implications for understanding hillslope sediment supply, sediment load evolution along fluvial networks, and denudation in active orogenic belts, vol. 398, pp. 143–171, Geological Society of America, 2006.

Attal, M., Mudd, S., Hurst, M., Weinman, B., Yoo, K., and Naylor, M.: Impact of change in erosion rate and landscape steepness on hillslope and fluvial sediments grain size in the Feather River basin (Sierra Nevada, California), Earth Surface Dynamics, 3, 201, 2015.

Balco, G., Stone, J. O., Lifton, N. A., and Dunai, T. J.: A complete and easily accessible means of calculating surface exposure ages or erosion rates from 10 Be and 26 Al measurements, Quaternary geochronology, 3, 174–195, 2008.

Benda, L. and Dunne, T.: Stochastic forcing of sediment routing and storage in channel networks, Water Resources Research, 33, 2865–2880, https://doi.org/10.1029/97WR02387, http://adsabs.harvard.edu/abs/1997WRR....33.2865B, 1997.

Binnie, S. A., Phillips, W. M., Summerfield, M. A., and Fifield, L. K.: Sediment mixing and basin-wide cosmogenic nuclide analysis in rapidly eroding mountainous environments, Quaternary Geochronology, 1, 4–14, 2006.

Binnie, S. A., Phillips, W. M., Summerfield, M. A., and Fifield, L. K.: Tectonic uplift, threshold hillslopes, and denudation rates in a developing mountain range, Geology, 35, 743–746, 2007.

Blöthe, J. H. and Korup, O.: Millennial lag times in the Himalayan sediment routing system, Earth and Planetary Science Letters, 382, 38–46, 2013.

Bookhagen, B. and Burbank, D. W.: Topography, relief, and TRMM-derived rainfall variations along the Himalaya, Geophysical Research Letters, 33, 2006.

Bookhagen, B., Thiede, R. C., and Strecker, M. R.: Abnormal monsoon years and their control on erosion and sediment flux in the high, arid northwest Himalaya, Earth and Planetary Science Letters, 231, 131–146, 2005.

Breien, H., De Blasio, F. V., Elverhøi, A., and Høeg, K.: Erosion and morphology of a debris flow caused by a glacial lake outburst flood, Western Norway, Landslides, 5, 271–280, 2008.

Brown, E. T., Stallard, R. F., Larsen, M. C., Raisbeck, G. M., and Yiou, F.: Denudation rates determined from the accumulation of in situ-produced 10Be in the Luquillo Experimental Forest, Puerto Rico, Earth and Planetary Science Letters, 129, 193–202, 1995.

Cenderelli, D. A. and Wohl, E. E.: Flow hydraulics and geomorphic effects of glacial-lake outburst floods in the Mount Everest region, Nepal, Earth Surface Processes and Landforms, 28, 385–407, 2003.

Church, M.: Bed material transport and the morphology of alluvial river channels, Annu. Rev. Earth Planet. Sci., 34, 325–354, 2006.

Clift, P. D., Giosan, L., Blusztajn, J., Campbell, I. H., Allen, C., Pringle, M., Tabrez, A. R., Danish, M., Rabbani, M., Alizai, A., et al.: Holocene erosion of the Lesser Himalaya triggered by intensified summer monsoon, Geology, 36, 79–82, 2008.

Collins, A. L. and Walling, D. E.: Documenting catchment suspended sediment sources: problems, approaches and prospects, Progress in Physical Geography, 28, 159–196, 2004.

Croissant, T., Lague, D., Steer, P., and Davy, P.: Rapid post-seismic landslide evacuation boosted by dynamic river width, Nature Geoscience, 10, ngeo3005, 2017.

Dade, W. B. and Friend, P. F.: Grain-size, sediment-transport regime, and channel slope in alluvial rivers, The Journal of Geology, 106, 661–676, 1998.

Darvill, C. M., Bentley, M. J., Stokes, C. R., Hein, A. S., and Rodés, Á.: Extensive MIS 3 glaciation in southernmost Patagonia revealed by cosmogenic nuclide dating of outwash sediments, Earth and Planetary Science Letters, 429, 157–169, 2015.

Denniston, R. F., González, L. A., Asmerom, Y., Sharma, R. H., and Reagan, M. K.: Speleothem evidence for changes in Indian summer monsoon precipitation over the last 2300 years, Quaternary Research, 53, 196–202, 2000.

Devrani, R., Singh, V., Mudd, S., and Sinclair, H.: Prediction of flash flood hazard impact from Himalayan river profiles, Geophysical Research Letters, 42, 5888–5894, 2015.

Dingle, E. H., Sinclair, H. D., Attal, M., Milodowski, D. T., and Singh, V.: Subsidence control on river morphology and grain size in the Ganga Plain, American Journal of Science, 316, 778–812, 2016.

Dingle, E. H., Attal, M., and Sinclair, H. D.: Abrasion-set limits on Himalayan gravel flux, Nature, 544, 471–474, 2017.

Dixit, Y., Hodell, D. A., Sinha, R., and Petrie, C. A.: Abrupt weakening of the Indian summer monsoon at 8.2 kyr BP, Earth and Planetary Science Letters, 391, 16–23, 2014.

Dobhal, D., Gupta, A. K., Mehta, M., and Khandelwal, D.: Kedarnath disaster: facts and plausible causes, Current Science, 105, 171–174, 2013.

Dunai, T. J.: Cosmogenic Nuclides: Principles, concepts and applications in the Earth surface sciences, Cambridge University Press, 2010.

Durga-Rao, K., Venkateshwar-Rao, V., Dadhwal, V., and Diwakar, P.: Kedarnath flash floods: a hydrological and hydraulic simulation study, Current Science, 106, 598–603, 2014.

Fleitmann, D., Burns, S. J., Mudelsee, M., Neff, U., Kramers, J., Mangini, A., and Matter, A.: Holocene forcing of the Indian monsoon recorded in a stalagmite from southern Oman, Science, 300, 1737–1739, 2003.

Fleitmann, D., Burns, S. J., Mangini, A., Mudelsee, M., Kramers, J., Villa, I., Neff, U., Al-Subbary, A. A., Buettner, A., Hippler, D., et al.: Holocene ITCZ and Indian monsoon dynamics recorded in stalagmites from Oman and Yemen (Socotra), Quaternary Science Reviews, 26, 170–188, 2007.

Galy, V., France-Lanord, C., Beyssac, O., Faure, P., Kudrass, H., and Palhol, F.: Efficient organic carbon burial in the Bengal fan sustained by the Himalayan erosional system, Nature, 450, 407–410, 2007.

Ghimire, G. and Uprety, B.: Causes and effects of siltation on the environment of Nepal, Environmentalist, 10, 55–65, 1990.

Gitto, A., Venditti, J., Kostaschuk, R., and Church, M.: Representative point-integrated suspended sediment sampling in rivers, Water Resources Research, 53, 2956–2971, 2017.

Godard, V., Burbank, D., Bourlès, D., Bookhagen, B., Braucher, R., and Fisher, G.: Impact of glacial erosion on 10Be concentrations in fluvial sediments of the Marsyandi catchment, central Nepal, Journal of Geophysical Research: Earth Surface, 117, 2012.

Goodbred, S. L. and Kuehl, S. A.: Holocene and modern sediment budgets for the Ganges-Brahmaputra river system: Evidence for highstand dispersal to flood-plain, shelf, and deep-sea depocenters, Geology, 27, 559–562, 1999.

Goodbred, S. L. and Kuehl, S. A.: Enormous Ganges-Brahmaputra sediment discharge during strengthened early Holocene monsoon, Geology, 28, 1083–1086, 2000.

Gosse, J. C. and Phillips, F. M.: Terrestrial in situ cosmogenic nuclides: theory and application, Quaternary Science Reviews, 20, 1475–1560, 2001.

Granger, D. E., Kirchner, J. W., and Finkel, R.: Spatially averaged long-term erosion rates measured from in situ-produced cosmogenic nuclides in alluvial sediment, The Journal of Geology, 104, 249–257, 1996.

Gupta, A. K., Das, M., and Anderson, D. M.: Solar influence on the Indian summer monsoon during the Holocene, Geophysical Research Letters, 32, 2005.

Heimsath, A. M. and McGlynn, R.: Quantifying periglacial erosion in the Nepal high Himalaya, Geomorphology, 97, 5–23, 2008.

Hovius, N., Stark, C. P., and Allen, P. A.: Sediment flux from a mountain belt derived by landslide mapping, Geology, 25, 231–234, 1997.

Hovius, N., Stark, C. P., Hao-Tsu, C., and Jiun-Chuan, L.: Supply and removal of sediment in a landslide-dominated mountain belt: Central Range, Taiwan, The Journal of Geology, 108, 73–89, 2000.

Jha, P., Vaithiyanathan, P., and Subramanian, V.: Mineralogical characteristics of the sediments of a Himalayan river: Yamuna River—a tributary of the Ganges, Environmental Geology, 22, 13–20, 1993.

Kattelmann, R.: Glacial lake outburst floods in the Nepal Himalaya: a manageable hazard?, Natural Hazards, 28, 145–154, 2003.

Kirchner, J. W., Finkel, R. C., Riebe, C. S., Granger, D. E., Clayton, J. L., King, J. G., and Megahan, W. F.: Mountain erosion over 10 yr, 10 ky, and 10 my time scales, Geology, 29, 591–594, 2001.

Lal, D.: Cosmic ray labeling of erosion surfaces: in situ nuclide production rates and erosion models, Earth and Planetary Science Letters, 104, 424–439, 1991.

Lin, M.-L. and Tung, C.-C.: A GIS-based potential analysis of the landslides induced by the Chi-Chi earthquake, Engineering Geology, 71, 63–77, 2004.

Lukens, C. E., Riebe, C. S., Sklar, L. S., and Shuster, D. L.: Grain size bias in cosmogenic nuclide studies of stream sediment in steep terrain, Journal of Geophysical Research: Earth Surface, 121, 978–999, 2016.

Lupker, M., France-Lanord, C., Lavé, J., Bouchez, J., Galy, V., Métivier, F., Gaillardet, J., Lartiges, B., and Mugnier, J.-l.: A Rouse-based method to integrate the chemical composition of river sediments: Application to the Ganga basin, Journal of Geophysical Research: Earth Surface, 116, 2011.

Lupker, M., Blard, P.-H., Lave, J., France-Lanord, C., Leanni, L., Puchol, N., Charreau, J., and Bourlès, D.: 10 Be-derived Himalayan denudation rates and sediment budgets in the Ganga basin, Earth and Planetary Science Letters, 333, 146–156, 2012.

Lupker, M., Lavé, J., France-Lanord, C., Christl, M., Bourlès, D., Carcaillet, J., Maden, C., Wieler, R., Rahman, M., Bezbaruah, D., et al.: 10 Be systematics in the Tsangpo-Brahmaputra catchment: the cosmogenic nuclide legacy of the eastern Himalayan syntaxis, Earth Surface Dynamics, 5, 429–449, 2017.

Mackey, B. H. and Roering, J. J.: Sediment yield, spatial characteristics, and the long-term evolution of active earthflows determined from airborne LiDAR and historical aerial photographs, Eel River, California, Geological Society of America Bulletin, 123, 1560–1576, 2011.

Martha, T. R., Roy, P., Mazumdar, R., Govindharaj, K. B., and Kumar, K. V.: Spatial characteristics of landslides triggered by the 2015 Mw 7.8 (Gorkha) and Mw 7.3 (Dolakha) earthquakes in Nepal, Landslides, 14, 697–704, 2017.

Mudd, S. M., Hurst, M. D., Grieve, S. W., and Marrero, S. M.: The CAIRN method: automated, reproducible calculation of catchment-averaged denudation rates from cosmogenic nuclide concentrations, Earth Surface Dynamics, 4, 655, 2016.

Niedermann, S.: Cosmic-ray-produced noble gases in terrestrial rocks: dating tools for surface processes, Reviews in Mineralogy and Geochemistry, 47, 731–784, 2002.

Niemi, N. A., Oskin, M., Burbank, D. W., Heimsath, A. M., and Gabet, E. J.: Effects of bedrock landslides on cosmogenically determined erosion rates, Earth and Planetary Science Letters, 237, 480–498, 2005.

Orton, G. and Reading, H.: Variability of deltaic processes in terms of sediment supply, with particular emphasis on grain size, Sedimentology, 40, 475–512, 1993.

Pandey, A. K., Pandey, P., Singh, G. D., and Juyal, N.: Climate footprints in the Late Quaternary–Holocene landforms of Dun Valley, NW Himalaya, India, Curr. Sci, 106, 245–253, 2014.

Puchol, N., Lavé, J., Lupker, M., Blard, P.-H., Gallo, F., France-Lanord, C., Team, A., et al.: Grain-size dependent concentration of cosmogenic 10 Be and erosion dynamics in a landslide-dominated Himalayan watershed, Geomorphology, 224, 55–68, 2014.

Rana, N., Singh, S., Sundriyal, Y., and Juyal, N.: Recent and past floods in the Alaknanda valley: causes and consequences, Current Science, 105, 1209–1212, 2013.

Ray, Y. and Srivastava, P.: Widespread aggradation in the mountainous catchment of the Alaknanda–Ganga River System: timescales and implications to Hinterland–foreland relationships, Quaternary Science Reviews, 29, 2238–2260, 2010.

Roback, K., Clark, M. K., West, A. J., Zekkos, D., Li, G., Gallen, S. F., Chamlagain, D., and Godt, J. W.: The size, distribution, and mobility of landslides caused by the 2015 Mw7. 8 Gorkha earthquake, Nepal, Geomorphology, 301, 121–138, 2018.

Scherler, D., Bookhagen, B., and Strecker, M. R.: Tectonic control on 10Be-derived erosion rates in the Garhwal Himalaya, India, Journal of Geophysical Research: Earth Surface, 119, 83–105, 2014.

Scherler, D., Bookhagen, B., Wulf, H., Preusser, F., and Strecker, M. R.: Increased late Pleistocene erosion rates during fluvial aggradation in the Garhwal Himalaya, northern India, Earth and Planetary Science Letters, 428, 255–266, 2015.

Schildgen, T. F., Robinson, R. A., Savi, S., Phillips, W. M., Spencer, J. Q., Bookhagen, B., Scherler, D., Tofelde, S., Alonso, R. N., Kubik, P. W., et al.: Landscape response to late Pleistocene climate change in NW Argentina: Sediment flux modulated by basin geometry and connectivity, Journal of Geophysical Research: Earth Surface, 121, 392–414, 2016.

Singh, P., Haritashya, U. K., Ramasastri, K., and Kumar, N.: Diurnal variations in discharge and suspended sediment concentration, including runoff-delaying characteristics, of the Gangotri Glacier in the Garhwal Himalayas, Hydrological Processes, 19, 1445–1457, 2005.

Sinha, R. and Friend, P. F.: River systems and their sediment flux, Indo-Gangetic plains, Northern Bihar, India, Sedimentology, 41, 825–845, 1994.

Sinha, R. and Sarkar, S.: Climate-induced variability in the Late Pleistocene–Holocene fluvial and fluvio-deltaic successions in the Ganga plains, India: a synthesis, Geomorphology, 113, 173–188, 2009.

Sinha, S., Suresh, N., Kumar, R., Dutta, S., and Arora, B.: Sedimentologic and geomorphic studies on the Quaternary alluvial fan and terrace deposits along the Ganga exit, Quaternary International, 227, 87–103, 2010.

Sirocko, F., Sarnthein, M., Erlenkeuser, H., Lange, H., Arnold, M., and Duplessy, J. C.: Century-scale events in monsoonal climate over the past 24,000 years, Nature, 364, 322–324, 1993.

Srivastava, P., Singh, I., Sharma, M., and Singhvi, A.: Luminescence chronometry and Late Quaternary geomorphic history of the Ganga Plain, India, Palaeogeography, Palaeoclimatology, Palaeoecology, 197, 15–41, 2003.

Srivastava, P., Tripathi, J. K., Islam, R., and Jaiswal, M. K.: Fashion and phases of late Pleistocene aggradation and incision in the Alaknanda River Valley, western Himalaya, India, Quaternary Research, 70, 68–80, 2008.

Stone, J. O.: Air pressure and cosmogenic isotope production, Journal of Geophysical Research: Solid Earth, 105, 23 753–23 759, 2000.

Syvitski, J. P., Vörösmarty, C. J., Kettner, A. J., and Green, P.: Impact of humans on the flux of terrestrial sediment to the global coastal ocean, Science, 308, 376–380, 2005.

Vance, D., Bickle, M., Ivy-Ochs, S., and Kubik, P. W.: Erosion and exhumation in the Himalaya from cosmogenic isotope inventories of river sediments, Earth and Planetary Science Letters, 206, 273–288, 2003.

Verma, N.: Geomorphic and morphometric investigation of the Ganga River, Ph.D. thesis, Department of Geology, University of Delhi, 2016.

Von Blanckenburg, F.: The control mechanisms of erosion and weathering at basin scale from cosmogenic nuclides in river sediment, Earth and Planetary Science Letters, 237, 462–479, 2005.

Wasson, R., Sundriyal, Y., Chaudhary, S., Jaiswal, M. K., Morthekai, P., Sati, S., and Juyal, N.: A 1000-year history of large floods in the Upper Ganga catchment, central Himalaya, India, Quaternary Science Reviews, 77, 156–166, 2013.

West, A. J., Hetzel, R., Li, G., Jin, Z., Zhang, F., Hilton, R. G., and Densmore, A. L.: Dilution of 10 Be in detrital quartz by earthquake-induced landslides: Implications for determining denudation rates and potential to provide insights into landslide sediment dynamics, Earth and Planetary Science Letters, 396, 143–153, 2014.

Whipple, K. X. and Tucker, G. E.: Implications of sediment-flux-dependent river incision models for landscape evolution, Journal of Geophysical Research: Solid Earth, 107, 2002.

Xu, S., Dougans, A. B., Freeman, S. P., Schnabel, C., and Wilcken, K. M.: Improved 10 Be and 26 Al-AMS with a 5MV spectrometer, Nuclear Instruments and Methods in Physics Research Section B: Beam Interactions with Materials and Atoms, 268, 736–738, 2010.

Yanites, B. J., Tucker, G. E., and Anderson, R. S.: Numerical and analytical models of cosmogenic radionuclide dynamics in landslide-dominated drainage basins, Journal of Geophysical Research: Earth Surface, 114, 2009.

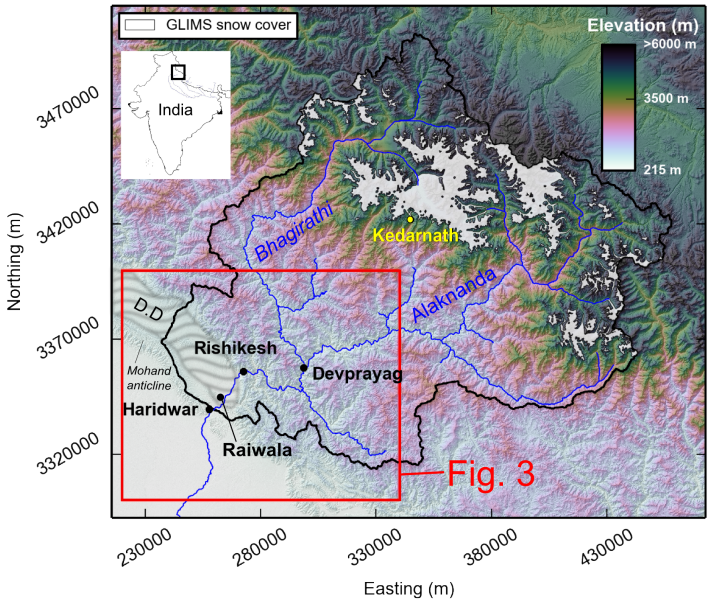

Figure 1. 30m Shuttle Radar Topography Mission (SRTM) Digital Elevation Model (DEM) of the Ganga catchment. Coordinates are projected in UTM Zone 44N. Glacier coverage as documented in the Global Land Ice Measurements from Space (GLIMS) database is also shown in white. The red box represents the spatial area shown in more detail in Fig. 3. D.D refers to the Dehra Dun region which is delineated by the grey striped area.

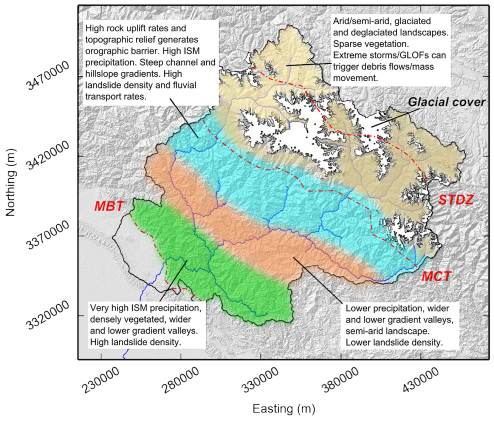

Figure 2. Broad distribution of geomorphic process domains across the Ganga catchment. The approximate positions of the Main Boundary Thrust (MBT), Main Central Thrust (MCT) and South Tibetan Detachment Zone (STDZ) are shown by red dashed lines following Ray and Srivastava (2010). Relative landslide density was determined by manual mapping of >400 landslides across the Ganga catchment using GoogleEarth imagery, where landslides in glacially influenced parts of the catchment were excluded. ISM denotes the Indian Summer Monsoon.

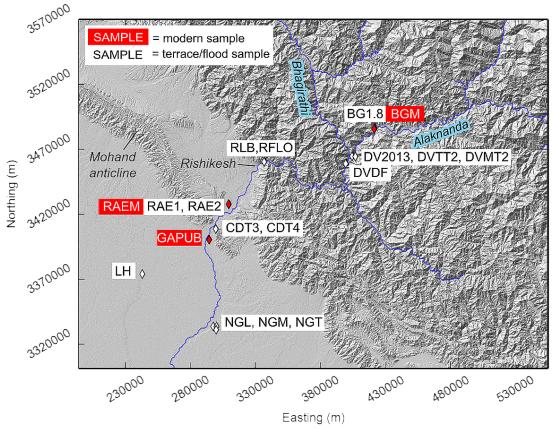

Figure 3. Modern (red) and terrace/floodplain/flood (white) sample locations and names in the lower Ganga catchment. See Table 1 for full description of samples.

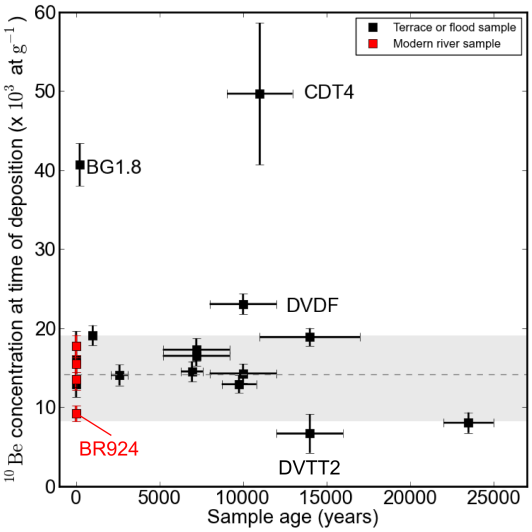

Figure 4. Measured modern river (red) and terrace or flood/floodplain (black) ^{10}Be concentrations relative to their depositional age. Horizontal error bars represent the published age error associated with the independently dated deposit, and vertical error bars represent error in ^{10}Be concentrations determined in this study. Sample BR924 from Lupker et al. (2012) is also included and labelled.

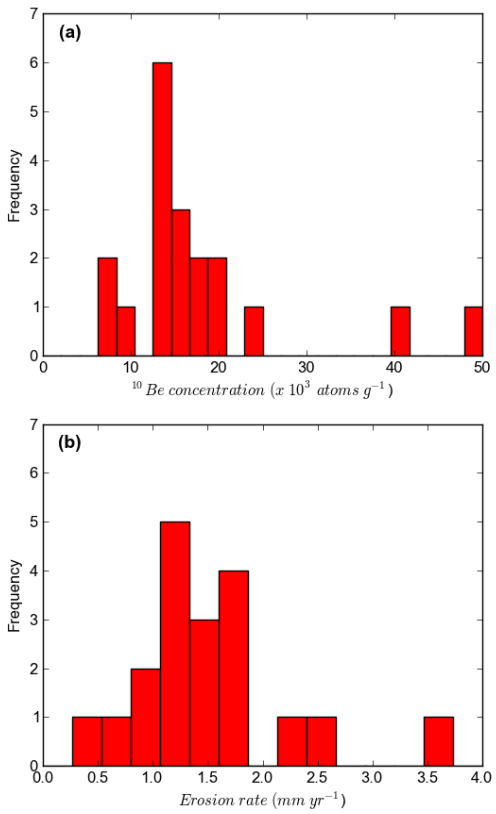

Figure 5. (a) Frequency histogram of mean ^{10}Be concentrations shown in Fig. 4. (b) Frequency histogram of mean erosion rates calculated using the CAIRN method.

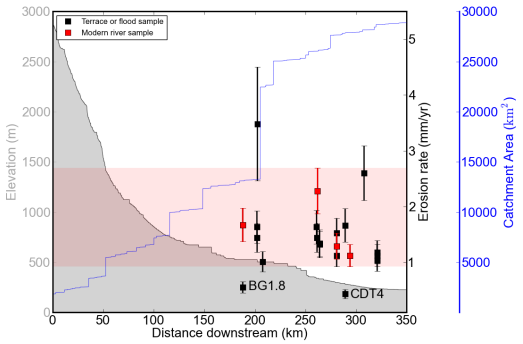

Figure 6. Modern river (red) and terrace or flood/floodplain (black) catchment-averaged erosion rates with respect to distance downstream, sample elevation (grey shaded region) and upstream catchment area (blue line). Vertical error bars represent error associated with the modelled erosion rate and propagated ^{10}Be concentration errors used to derive the erosion rate. The red shaded area represents erosion rates within the error of modern samples. Outliers BG1.8 and CDT4 are labelled.

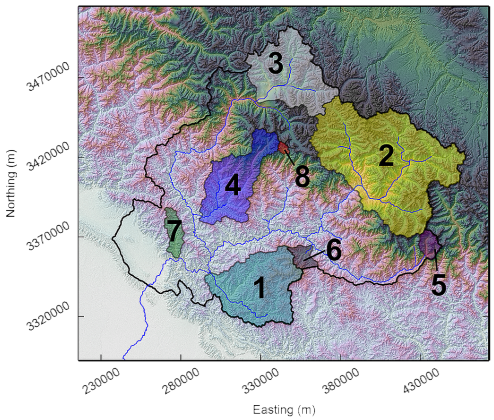

Figure 7. Location of sub-catchments used to determine the variability in production rate across the Ganga catchment (presented in Table 2).

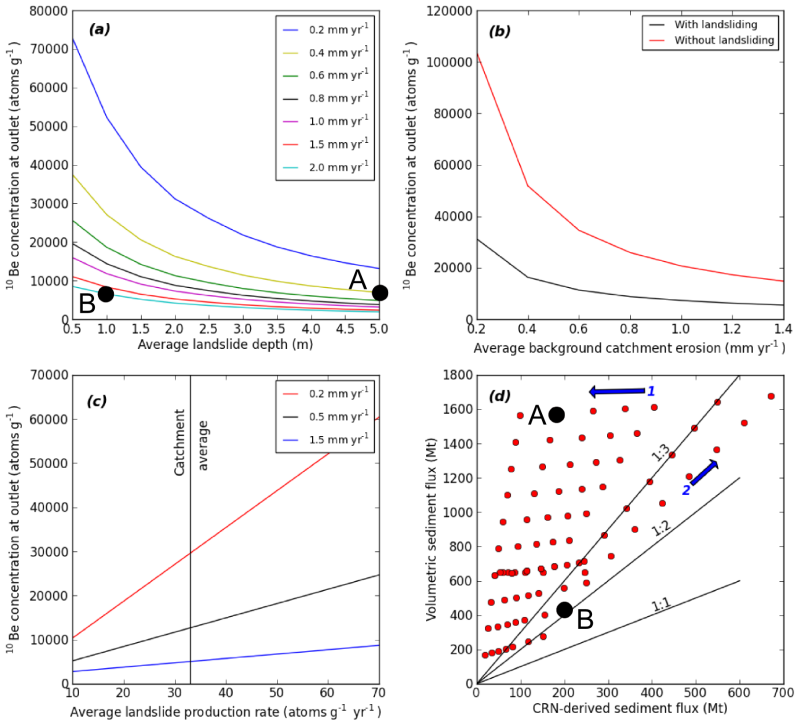

Figure 8. (a) Variations in ^{10}Be concentration predicted at the outlet in response to increasing landslide depth and as a function of background erosion rates (represented by coloured lines). (b) Outlet ^{10}Be concentration as a function of background erosion rate (where all other parameters are constant at default values - see Table 3), for a system undergoing no landsliding (red line - where erosion is driven purely by background erosion) and another with 2 m deep landsliding over 0.5 % of the catchment area (black line). (c) Outlet ^{10}Be concentration under varying average landslide ^{10}Be surface production rates (based on Table 2) and background erosion rates (coloured lines). The black vertical line represents the whole Ganga catchment-averaged production rate of ∼33 atoms g^{-1} yr^{-1}. (d) Comparison of volumetric and CRN-derived sediment fluxes from analysis in Figures 8a-c. The blue arrow labelled 1 shows the effect of decreasing background erosion rate, and the blue arrow labelled 2 shows the effect of increasing landslide depth and/or landslide CRN production rate . The black dots in (a) and (d) represent scenarios A and B which are discussed in more detail later and in Fig. 12.

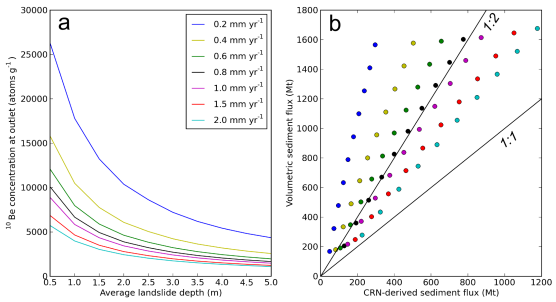

Figure 9. (a) Effect of lowering landslide surface production rate to 10 atoms g^{-1} yr^{-1} on outlet CRN concentrations in response to varying landslide depths and catchment background erosion rates. The overall range in outlet concentrations is notably lower than in Fig. 8a. (b) Comparison of volumetric and CRN-derived sediment fluxes for the same model conditions, where marker colour corresponds to background erosion rate shown in part (a). The difference in volumetric and CRN-derived fluxes is much less than scenarios shown in Fig. 8d. In scenarios with higher background erosion rates, volumetric fluxes are only marginally higher than CRN-derived fluxes.

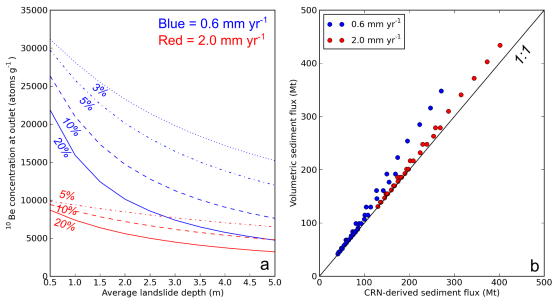

Figure 10. (a) Effect of event buffering on outlet CRN concentrations, where smaller fractions (3, 5, 10 and 20%) of the event sediment are mixed into the fluvial network based on two background erosion rates of 0.6 and 2.0 mm yr^{-1} shown in blue and red, respectively. The event proportions are represented by the different dashed lines. The landslide surface production rate is set to 10 atoms g^{-1} yr^{-1}, whilst the rest of the catchment is set to 35 atoms g^{-1} yr^{-1}. Under faster background erosion rates, the effect of larger landsliding events are more easily buffered in outlet CRN concentrations. (b) Comparison of volumetric and CRN-derived sediment fluxes for event buffering scenarios. Under these conditions, volumetric and CRN-derived sediment flux estimates are much more comparable. In landscapes with lower background erosion, volumetric fluxes are still slightly larger with higher event inputs.

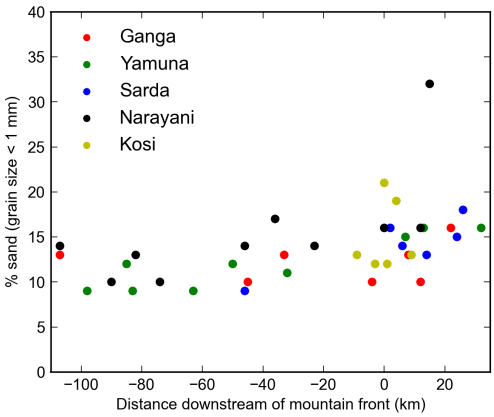

Figure 11. Volumetric sand (grain sizes $<$1 mm) proportions in sub-surface sediment samples along major tributaries of the Ganga River from Dingle et al., 2016.

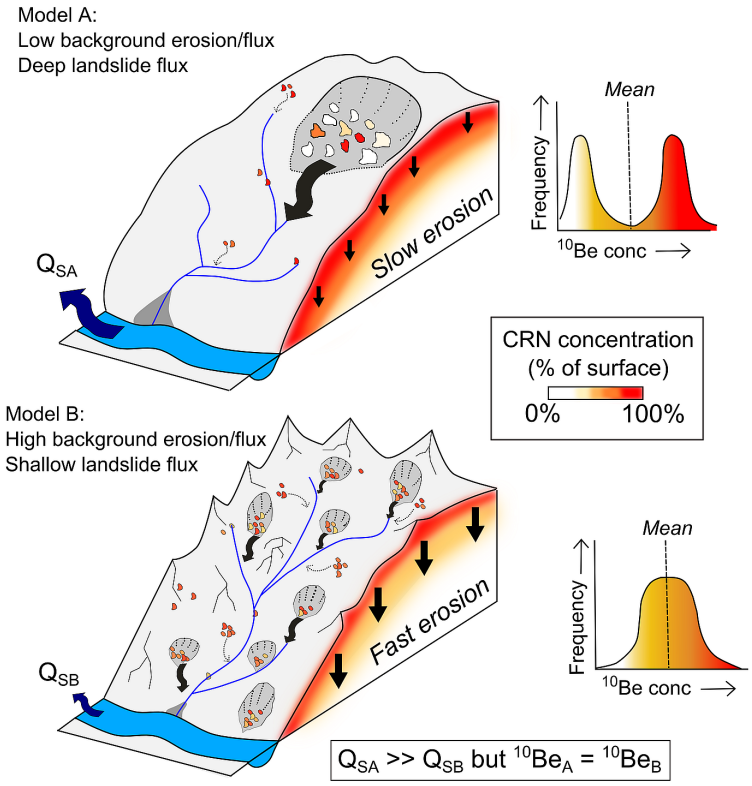

Figure 12. Schematic of how comparable mean CRN concentrations in river sand can be derived under two different end-member erosion scenarios with different volumetric sediment fluxes. In these instances, slow background erosion rates and deep landsliding (Model A) result in comparable CRN concentrations to landscapes domianted by faster background erosion rates and shallow landsliding (Model B). If Model A is set with a background erosion rate of 0.4 mm yr^{-1} and 5 m deep landsliding over 0.5 % of the catchment, and Model B with 2 mm yr^{-1} background erosion rates and 1 m deep landsliding (over the same area), comparable CRN concentrations (see black dots marked on Fig. 8a) and CRN-derived sediment fluxes are generated, but volumetric sediment fluxes are over three times larger in Model A. This is due to the relative enrichment of ^{10}Be in the upper 2 m of the landscape with low background erosion rates, which when combined with low CRN concentration material from depth, results in two distinct CRN concentration populations. Where erosion is generally more homogeneous (Model B) and CRN concentrations are distributed more uniformly, comparable mean CRN concentrations are derived between the two models. Both scenarios assume complete mixing of the event sediment, hence why these are considered end-member or extreme scenarios.

Table 1. CRN sample details, ^{10}Be concentrations and modelled erosion rates. Full sample details are given in Appendix A.

Sample	Locality	Sampling date	Lat.	Lon.	Basin area (km^2)	Mean basin elevation (m)	Sample age (years)	Age reference	Sample elevation (m, from DEM)	Average shielding factor*	Sample depth (cm)	Sample ^{10}Be concentration ($\times 10^3$ at g^{-1})	^{10}Be concentration at time of deposition ($\times 10^3$ at g^{-1})	CAIRN-derived erosion rate (mm yr^{-1})
BGM	Bagwan - modern	06-Oct-2014	30.2255	78.6823	10,920	3,825	Modern	n/a	498	0.862	0	13.57±1.40	13.56±1.40	1.67±0.30
BG1.8	Bagwan - terrace	06-Oct-2014	30.2253	78.6812	10,920	3,825	217±76	Wasson et al. (2013) - OSL	504	0.862	500	40.70±2.69	40.69±2.69	0.55±0.10
DV2013	Devprayag - 2013 flood	05-Oct-2014	30.1499	78.6136	11,052	3,805	1	n/a	492	0.868	0	16.07±3.55	16.06±3.55	1.44±0.26
DVTT2	Devprayag - terrace	05-Oct-2014	30.1508	78.6107	11,052	3,805	14,000±2,000	Srivastava et al. (2008) - OSL	530	0.868	600	7.09±2.45	6.66±2.45	3.48±1.02
DVMT2	Devprayag - terrace	05-Oct-2014	30.1508	78.6153	11,052	3,805	10,000±2,000	Ray and Srivastava (2010) - OSL	517	0.868	650	14.69±1.22	14.27±1.22	1.63±0.29
DVDF	Devprayag - terrace	06-Oct-2014	30.1253	78.5905	18,716	3,870	10,000±2,000	Ray and Srivastava (2010) - OSL	559	0.868	1,300	23.19±1.28	23.04±1.28	1.01±0.18
RLB	Rishikesh - terrace	03-Oct-2014	30.1305	78.3322	21,675	3,670	6,940±650	Sinha et al. (2010) - OSL	393	0.879	300	15.61±1.27	14.52±1.27	1.45±0.26
RFLO	Rishikesh - 2013 flood	03-Oct-2014	30.1328	78.3342	21,675	3,670	1	n/a	370	0.879	20	12.86±1.58	12.85±1.58	1.63±0.30
RAE1	Raewalla - terrace	08-Oct-2014	30.0053	78.2195	23,030	3,580	2,600±500	Wasson et al. (2013) - OSL	308	0.877	100	17.51±1.04	14.07±1.31	1.52±0.27
RAE2	Raewalla - terrace	08-Oct-2014	30.0053	78.2195	23,030	3,580	1,000±200	Wasson et al. (2013) - OSL	308	0.877	80	20.76±1.09	19.08±1.28	1.12±0.20
RAEM	Raewalla - modern	08-Oct-2014	30.0054	78.2227	23,030	3,580	Modern	n/a	303	0.885	0	15.53±1.07	15.52±1.07	1.29±0.23
CDT3	Chandi Devi - terrace	03-Oct-2014	29.9461	78.1757	23,221	3,560	9,760±1,040	Sinha et al. (2010) - OSL	309	0.877	320	14.19±1.11	12.91±1.12	1.66±0.30
CDT4	Chandi Devi - terrace	03-Oct-2014	29.9398	78.1788	23,221	3,560	11,080±1,960	Sinha et al. (2010) - OSL	389	0.877	1,000	49.72±8.96	49.65±8.96	0.43±0.08
GAPUB	Haridwar - modern	11-Oct-2014	29.9067	78.1635	23,221	3,560	Modern	n/a	271	0.886	0	17.70±1.42	17.70±1.42	1.12±0.20
LH	Landhaura - terrace	07-Oct-2014	29.8105	77.9460	23,941	3,510	23,500±1,500	Verma (2016) - OSL	256	0.879	220	15.65±1.21	8.06±1.31	2.60±0.49
NGL	Nagal - terrace	07-Oct-2014	29.6698	78.1786	23,941	3,510	14,000±3,000	Sinha et al. (2010) - OSL	249	0.889	1260	19.07±1.13	18.86±1.13	1.03±0.19
NGM	Nagal - terrace	07-Oct-2014	29.6652	78.1850	23,941	3,510	7,200±2,000	Sinha et al. (2010) - OSL	258	0.889	850	16.67±1.28	16.49±1.28	1.18±0.21
NGL	Nagal - terrace	07-Oct-2014	29.6649	78.1859	23,941	3,510	7,200±2,000	Sinha et al. (2010) - OSL	259	0.889	250	18.96±1.36	17.27±1.44	1.12±0.20
BR924**	Rishikesh - modern	11-Aug-2009	30.127	78.330	21,690	3,150	Modern	n/a	357	0.879	0	9.20±1.0	n/a	2.28±0.41

* Average shielding factor is the average of the combined shielding factors; topographic, snow and self-shielding values. These were calculated using a depth integrated approach (see Mudd et al., 2016).

** Details for this sample (BR924) are from Table 1 in Lupker et al. (2012). We have recalculated the erosion rate using the CAIRN method (Mudd et al., 2016).

Table 2. Catchment area, average elevation and average ^{10}Be surface production rate for sub-catchments in the Ganga catchment

	Catchment area (km^2)	Catchment-average elevation (m)	Surface production rate (atoms g^{-1} yr^{-1})
Sub-catchment 1	1,955	1,606	11.08
Sub-catchment 2	4,635	4,716	56.02
Sub-catchment 3	1,801	5,033	70.51
Sub-catchment 4	1,449	1,642	24.28
Sub-catchment 5	169	4,483	49.13
Sub-catchment 6	181	1,868	12.82
Sub-catchment 7	253	1,404	9.57
Sub-catchment 8*	39	4,806	49.61
Ganga (whole)	23,038	3,560	33.16

*This sub-catchment represents the area upstream of Kedarnath during the 2013 Alaknanda flooding

Table 3. Default and range of parameter values used in numerical analysis

Parameter	Default value	Range of modelled values
Landslide depth (m)	2	0.5 - 5.0
Catchment area (km^2)	23,000	-
% of catchment impacted by landsliding	0.5	-
Catchment-averaged surface production rate (atoms g^{-1} yr^{-1})	35	-
Background erosion rate (mm yr^{-1})	0.5	0.2-2.0
Landslide surface production rate (atoms g^{-1} yr^{-1})	35	10-60
Proportion of event sediment mixed into fluvial network (%)	100	3-20

*This sub-catchment represents the area upstream of Kedarnath during the 2013 Alaknanda flooding